Gut Microbial-Host Metabolic Interactions Following Bariatric Surgery

A thesis submitted by

JUTAROP PHETCHARABURANIN

For the Degree of Doctor of Philosophy of

Imperial College London

Division of Computational and Systems Medicine

Department of Surgery and Cancer

Faculty of Medicine

Imperial College London

2018

Abstract

Obesity has emerged as one of the major global socioeconomic healthcare burdens at present. Bariatric surgery, especially Roux-en-Y gastric bypass (RYGB) has been largely utilised to treat individual suffering from morbid obesity. In the current study, a hyperinsulinemic obese Zucker rat model was employed to study two different weight loss approaches, RYGB and caloric restriction. To understand the host metabolic-microbial cross-talk, the two major analytical platforms including nuclear magnetic resonance (NMR) spectroscopy and 16S rRNA gene Illumina MiSeq sequencing were used in companion with multivariate statistical analysis to extract useful information from data with high complexity. The aim of this study was to 1) characterise the genotype-associated metabolic and microbial fingerprints; 2) investigate the dynamic changes in biofluids from RYGB-treated or caloric restriction-treated obese Zucker rats; 3) investigate genotype-related, RYGB-induced or caloric restriction-induced metabolic profiles and microbial shifts of the luminal contents; and 4) investigate the statistical correlation between metabolites and gut microbiota following either of the weight loss treatment.

Metabolic observations of portal vein and peripheral blood plasma profiles in both obese and lean Zucker rats indicated the phenotype-independent absorption of short-chain fatty acids (SCFAs), choline and trimethylamine (TMA). However, phenotype-specific urinary host-microbial co-metabolites were revealed, suggesting distinct gut microbial metabolic activities in lean and obese Zucker rats. Furthermore, metabolic alterations induced by the RYGB surgery included the enhanced production of neuroactive metabolites, branched-chain amino acid (BCAA) catabolism, aromatic amino acid metabolism with lower lipogenesis and SCFA production. Even though caloric restriction demonstrated some health benefit-related biochemical and microbial markers, its effectiveness as a resolution for metabolic syndrome, especially type-2 diabetes mellitus has not been observed in this study in spite of the significant weight reduction.

“I dedicate this thesis to my family for their support, love and care.”

Acknowledgements

I would like to acknowledge my supervisor Dr. Jia Li for her great help, constant support, delightful encouragement and remarkable supervision in my studies during the past four years. I am also very grateful to Prof. Julian Marchesi for his supervision and microbiome perspectives. I would also like to express my acknowledgement to Prof. Jeremy Nicholson and Prof. Elaine Holmes for the financial support (STRATiGRAD scholarship) and for providing access to spectroscopic facilities and valuable scientific advice. I am also very grateful to Dr. Florian Seyfried for his help on animal gastric bypass experiment.

I would like to thank Dr. Antony Dona, Dr. Maria Gomez Romeo, Dr. Panagiotis Vorkas and Dr. Elizabeth Want who have given me a lot of laboratory and technical help on my experiments. I would also like to thank all STRATiGRAD cohorts for their support and friendship.

I would like to extend my acknowledgements to Prof. Paiboon Sithithaworn, Prof. Puangrat Yongvanit, Assoc. Prof. Watcharin Loilome and Assoc. Prof. Nisana Namwat for their support and care. I would also like to thank the Department of Biochemistry, Faculty of Medicine at Khon Kaen University (KKU) for the financial support. I am grateful to my colleagues at the Department of Biochemistry, Faculty of Medicine, KKU that helped cover my workload during my four years of study.

Last but not least, I would like to deeply thank my dear mother Asst. Prof. Penprapa Phetcharaburanin, my grandmother Mrs. Umpai Phetcharaburanin as well as all my family members, and all my dear friends, to name but a few, Ms. Ancheera Lerttana, Ms. Jutharat Tongprasert and Mr. Bhumipat Dhanakitwiwatana for giving me constant strength, courage and love.

Statement of originality

I certify that this thesis (except for measurements of body weight, food intake, OGTT glucose and insulin in Chapters 3 and 4, and 16S rRNA gene sequencing in Chapter 5), and the research it which it refers, are the product of my own work, and that any ideas or quotations from the work of other people, published or otherwise, are fully acknowledged in accordance with the standard referencing practices of the discipline.

Copyright declaration

The copyright of this thesis rests with the author and is made available under a Creative Commons Attribution Non-Commercial No Derivatives licence. Researchers are free to copy, distribute or transmit the thesis on the condition that they attribute it, that they do not use it for commercial purposes and that they do not alter, transform or build upon it. For any reuse or redistribution, researchers must make clear to others the licence terms of this work.

Table of contents

Abstract…….. 2

Acknowledgments……...3

Statement of originality…….....4

Copyright declaration…….. 5

List of figures……... 13

List of tables……..... 18

List of abbreviations…….. 19

Chapter 1 Introduction…….22

1.1 Introduction to obesity: prevalence, causes and treatments…….. 22
1.2 Studies of obesity on Zucker rat model…….. 23
1.3 Effectiveness of obesity treatments…….. 24

1.3.1 Caloric restriction…….. 25

1.3.2 Bariatric surgery……..27

1.4 Gut microbiota…….. 30

1.4.1 Function of gut microbiota……..31

1.4.2 Host and microbiota co-metabolism and signalling in obesity……..32

1.4.3 Gut microbiota in relation to obesity, caloric restriction and bariatric surgery…….... 33

1.5 Metabonomics…….. 36

1.5.1 Outline of metabolic profiling methods……..36

1.5.2 Basic principles of NMR spectroscopy…….37

1.5.3 Basic principles of mass spectrometry……..38

1.5.4 Multivariate statistical analysis……..... 40

1.5.4.1 Principal component analysis (PCA) ……..40

1.5.4.2 Projection to latent structures (PLS) and orthogonal signal correction PLS (O-PLS) ……...42

1.5.4.3 Projection to latent structures-discriminant analysis (PLS-DA) and O-PLS-DA..... 42

1.6 16S ribosomal RNA (rRNA) sequencing……..……43

1.7 Research aims and objectives……..……..…44

Chapter 2 Methodology……...……45

2.1 Study design ……..……..……45

2.2 Body weight and food intake measurement……..……..……46

2.3 Measurement of oral glucose tolerance, glucose and fasting insulin…….……46

2.4 Measurement of pH……..…….…….. 47

2.5 Sample preparation for ^{1}H NMR analysis, pre-processing and statistical analysis of ^{1}H NMR spectral data…… 47

2.5.1 ^{1}H NMR spectroscopy-based metabolic profiling of faecal water…….… 47

2.5.2 ^{1}H NMR spectroscopy-based metabolic profiling of urine samples……...48

2.5.3 ^{1}H NMR spectroscopy-based metabolic profiling of plasma samples…..…..…49

2.5.4 Pre-processing of ^{1}H NMR spectra……..……..49

2.5.5 Multivariate statistical analysis of ^{1}H NMR spectral data……..…..……50

2.5.6 Univariate statistical analysis of selected ^{1}H NMR metabolites……..50

2.5.6 Univariate statistical analysis of selected ^{1}H NMR metabolites……...……. 51

2.6 Ultra-performance liquid chromatography mass-spectrometry……..…..……51

2.6.1 Aqueous and organic metabolite extraction……...……..……51

2.6.2 HILIC-UPLC-MS analysis of aqueous extracts……..……..……52

2.7 Community analysis of microbiota contained in the intestinal contents of stomach, duodenum, upper-jejunum, lower-jejunum, ileum and colon together with faeces using 16S rRNA gene Illumina MiSeq sequencing……...……53

2.7.1 Isolation of DNA from gastrointestinal content and faecal samples……..…53

2.7.2 Illumina MiSeq sequencing……..……...…… 54

2.7.3 Phylogenetic identification and data analysis……..……54

Chapter 3 Global metabolic profiling of peripheral and portal vein plasma, urine and faecal water in the lean and obese Zucker rats……..…….55

3.1 Aim…….……55

3.2 Materials and methods……..……..55

3.3 Results……...……55

3.3.1 Differences in body weight, food intake, oral glucose tolerance test and fasting insulin between Zucker obese (*fa/fa) and lean (fa/+)* rats……..……..55

3.3.2 Urinary metabolic profiles of obese (fa/fa) and lean (fa/+) Zucker rats…..…..57

3.3.3 Faecal metabolic profiles of Zucker obese and lean rats……..…… 61

3.3.4 Metabolic profiles of systemic and portal vein blood plasma from Zucker obese and lean rats…… 61

3.3.5 Intercompartmental correlation analysis of biofluid metabolites……..……. 62

3.4 Discussion……...…… 64

3.4.1 Muscle and adipose tissue metabolism……...…… 64

3.4.2 Microbial metabolism and host-microbial co-metabolism in obesity……... 66

3.4.3 Branched chain amino acid metabolism……..……. 68

3.4.4 Energy metabolism in obese rats……..…… 69

3.5 Summary……70

Chapter 4 ^{1}H NMR-based metabolic profiling of peripheral and portal vein plasma, urine and faecal water in the obese Zucker rats treated with Roux-en-Y gastric bypass or caloric restriction……..71

4.1 Aim…….……..…….…… 71

4.2 Materials and methods……..……..71

4.3 Results……71

4.3.1 Differences in body weight, food intake, oral glucose tolerance test and fasting insulin between RYGB and caloric restriction groups in comparison with obese control……71

4.3.2 Caloric restriction effects on faecal, urinary, peripheral and portal vein plasma metabolic profiles of obese Zucker rats……... 73

4.3.3 Effects of Roux-en-Y gastric bypass on faecal metabolic profiles of obese Zucker rats……..78

4.3.4 Urinary metabolic differences between Roux-en-Y gastric bypass-treated and obese Zucker rats……84

4.3.5 Peripheral and portal vein plasma metabolic differences between Roux-en-Y gastric bypass-treated and obese Zucker rats…….. 86

4.3.6 Faecal metabolic differences between Roux-en-Y gastric bypass- and caloric restriction-treated obese Zucker rats……89

4.3.7 Urinary metabolic differences between Roux-en-Y gastric bypass-treated and caloric restriction-treated obese Zucker rats……90

4.3.8 Peripheral and portal vein plasma metabolic differences between Roux-en-Y gastric bypass-treated and caloric restriction-treated obese Zucker rats……92

4.4 Discussion……94

4.4.1 Increased microbially-derived neuroactive intermediates……95

4.4.2 Altered microbial activity on aromatic amino acid metabolism and biosynthesis of host-microbial co-metabolites following RYGB…… 96

4.4.3 Beneficial effects associated with altered SCFA production……...97

4.4.4 Effects of RYGB on BCAA metabolism……98

4.4.5 Effects of caloric restriction on metabolic alteration in comparison with RYGB operation……... 99

4.5 Summary…….. 101

Chapter 5 UPLC-MS-based metabolic profiling and 16S rRNA gene sequencing of gastrointestinal contents obtained from obese Zucker rats-treated with RYGB or caloric restriction……. 102

5.1 Aim……..…….. 102

5.2 Materials and methods……..…….. 102

5.3 Results……..……... 102

5.3.1 Changes in pH after caloric restriction or RYGB operation……..…. 102

5.3.2 Genotype-related metabolic profiles of gastric and intestinal contents of obese and lean Zucker rats…….……..……... 103

5.3.3 Effects of caloric restriction on metabolic profiles of gastric and intestinal contents……..……... 109

5.3.4 Effects of RYGB on metabolic profiles of gastric and intestinal contents….. 114

5.3.5 Gastrointestinal microbial shifts following RYGB surgery and caloric restriction…… 123

5.3.6 Caloric restriction-induced bacterial alteration along gastrointestinal tract....127

5.3.7 Gastrointestinal bacterial shifts following RYGB operation……..…… 129

5.3.8 Gastrointestinal bacterial differences between RYGB and caloric restriction…… 132

5.3.9 Correlation analysis of metabolome and microbiome data……..…… 134

5.4 Discussion…….……..…… 137

5.4.1 An obese phenotype-related gastrointestinal metabolic and microbial fingerprints……..…… 137

5.4.2 Caloric restriction reverses metabolome and microbiome of obese Zucker rats to leaner phenotype…….…….…… 140

5.4.3 RYGB-related effects improve gastrointestinal health of obese Zucker rats……..142

5.5 Summary…… 146

Chapter 6 Summary and future work…….…..…… 147

6.1 Summary and general discussion……147

6.1.1 Summary of animal randomisation and sham-operation……147

6.1.2 Summary of energy metabolism……148

6.1.3 Summary of BCAA metabolism……149

6.1.4 Summary of polyamine catabolism……150

6.1.5 Summary of gut microbiota-related metabolisms……150

6.1.6 Summary of hepatic succinate metabolism……152

6.1.7 Implications……153

6.2 Future work……153

References……155

Appendix I……173

Appendix II……174

Appendix III……175

List of figures

Figure 1-1. Three main approaches for obesity treatment……...25

Figure 1-2. Most common types of bariatric surgery……29

Figure 2-1. Schematic diagrams illustrate (A) study design and (B) sample collection…..46

Figure 3-1. (A) Measurement of body weight; (B) food intake, data are shown as mean ± SD (****p < 0.0001) and statistical differences determined by two-way ANOVA and (C) oral glucose tolerance test (OGTT) of lean and obese Zucker rats (n=12 per group). OGTT glucose (solid line) and insulin (dashed line) measurements of Zucker rats. Data are shown as mean ± SD (*p < 0.05; ****p < 0.0001 of OGTT glucose and ++p < 0.01; +++p < 0.001; ++++p < 0.0001 of OGTT insulin by two-way ANOVA)……56

Figure 3-2. Principal component analysis of urinary (A), faecal (B) metabolic profiles of obese and lean Zucker rats over 4-week period and of obese peripheral, lean peripheral, obese portal vein and lean portal vein blood plasma (C) metabolic profiles at week 4. PCA trajectory scores plot of urinary and faecal data sets obtained from the average scores of PC1 against PC2 of each strain of rat at a particular time point and error bars are expressed by the standard error of mean of PC1 and PC2 of each time point. Percentage on each PC represents variation explained by each principal component and Q2 represents predictive ability of the model……57

Figure 3-3. Inter-compartmental correlation map of plasma (red), urinary (green) and faecal (black) metabolites from Zucker obese and lean rats with p-value < 0.05. Red denotes positive correlation, blue denotes negative correlation, and blank denotes no significant correlation. Key: 3-HPPA, 3-hydroxyphenyl propionic acid. Dashed-line box indicates different metabolic structures, where-as solid-line box indicates similar metabolic structures between lean and obese rats……63

Figure 3-4. Schematic illustration of systemic changes observed in biofluids from obese Zucker rats. Red indicates higher relative concentration, whereas blue indicates lower relative concentration of metabolites in obese rats compared with lean animals. Key: IPA, indole-3-propionic acid; NNMT: nicotinamide *N*-methyltransferase; PAG, phenylacetylglycine; PEP, phosphoenolpyruvate. * indicates that these metabolites are higher in portal vein blood plasma in contrast to peripheral blood plasma independent of the animal genotypes……64

Figure 4-1. (A) Measurement of body weight; (B) food intake, data are shown as mean ± SD (***p < 0.001) and statistical differences determined by two-way ANOVA and (C) oral glucose tolerance test (OGTT) of RYGB (n=11), sham-BWM (n=5) and sham-obese Zucker rats (n=5). OGTT glucose (solid line) and insulin (dashed line) +measurements of Zucker rats. Data are shown as mean ± SD (OGTT glucose: +p < 0.05 (sham-BWM vs. sham-obese); ^^p < 0.01, ^^^ p < 0.001 (RYGB vs. Sham-BWM); *** p < 0.001 (RYGB vs. sham-obese) and OGTT inulin: ! p < 0.05, !!! p < 0.001 (Sham-BWM vs. sham-obese); ## p < 0.01 (RYGB vs. sham-obese) by two-way ANOVA)……72

Figure 4-2. A PCA trajectory scores plot of faecal water ^{1}H NMR spectral data set obtained from RYGB (blue), sham-BWM (green) and sham-obese (red) Zucker rats at pre-operation (square), 1-week (triangle), 2-week (diamond) and 4-week (circle) post-operations. Each dot represents the average scores of the first principal component (PC1) against the second principal component (PC2) of the spectral data from each group and the error bars are expressed by the standard error of the mean of PC1 and PC2 of each time point…..73

Figure 4-3. A PCA trajectory scores plot of urinary ^{1}H NMR spectral data set obtained from RYGB (blue), sham-BWM (green) and sham-obese (red) Zucker rats at pre-operation (square), 1-week (triangle), 2-week (diamond) and 4-week (circle) post-operations. Each dot represents the average scores of the first principal component (PC1) against the second principal component (PC2) of the spectral data from each group and the error bars are expressed by the standard error of the mean of PC1 and PC2 of each time point…...74

Figure 4-4. PCA scores plots (left panel) and O-PLS-DA cross-validated scores plots (right panel) of the faecal metabolic profiles between sham-BWM (green) and sham-obese (red) Zucker rats at pre-operation (square), 1-week (star), 2-week (inverted triangle) and 3-week (dot) post-operations. Percentage on each PC represents variation explained by each principal component and Q^2 represents predictability of the model……75

Figure 4-5. PCA scores plots (left panel) and O-PLS-DA cross-validated scores plots (right) of the urinary metabolic profiles between sham-BWM (green) and sham-obese (red panel) Zucker rats at pre-operation (square), 1-week (star), 2-week (inverted triangle) and 3-week (dot) post-operations. Percentage on each PC represents variation explained by each principal component and Q^2 represents predictability of the model……..76

Figure 4-6. PCA scores plots (left panel) and O-PLS-DA cross-validated scores plots (right panel) of peripheral (dot) and portal vein (triangle) plasma metabolic profiles between sham-BWM (green) and sham-obese (red) Zucker rats. Percentage on each PC

represents variation explained by each principal component and Q^2 represents predictability of the model……..77

Figure 4-7. PCA scores plots (left panel) and O-PLS-DA cross-validated scores plots (right panel) of faecal metabolic profiles between RYGB (blue) and sham-obese (red) Zucker rats at pre-operation (square), 1-week (star), 2-week (inverted triangle) and 3-week (dot) post-operations. Percentage on each PC represents variation explained by each principal component and Q^2 represents predictability of the PCA model……..78

Figure 4-8. PCA scores plots (left panel) and O-PLS-DA cross-validated scores plots (right panel) of urinary metabolic profiles between RYGB (blue) and sham-obese (red) Zucker rats at pre-operation (square), 1-week (star), 2-week (inverted triangle) and 3-week (dot) post-operations. Percentage on each PC represents variation explained by each principal component and Q^2 represents predictive ability of the PCA model……84

Figure 4-9. PCA scores plots (left) and O-PLS-DA cross-validated scores plots (right) of peripheral (dot) and portal vein (triangle) plasma metabolic profiles of RYGB (blue) and obese (red) Zucker rats. Percentage on each PC represents variation explained by each principal component and Q^2 represents predictive ability of the PCA model……86

Figure 4-10. PCA scores plots (left) and O-PLS-DA cross-validated scores plots (right) of faecal metabolic profiles of RYGB (blue) and sham-BWM (red) rats at pre-operation (square), 1-week (star), 2-week (inverted triangle) and 3-week (circle) post-operations. Percentage on each PC represents variation explained by each principal component and Q^2 represents predictive ability of the PCA model……90

Figure 4-11. PCA scores plots (left) and O-PLS-DA cross-validated scores plots (right) of urinary metabolic profiles between RYGB (blue) and sham-BWM (red) rats at pre-operation (square), 1-week (star), 2-week (inverted triangle) and 3-week (circle) post-operations. Percentage on each PC represents variation explained by each principal component and Q^2 represents predictive ability of the PCA model……....91

Figure 4-12. PCA scores plots (left) and O-PLS-DA cross-validated scores plots (right) of peripheral (circle) and portal vein (triangle) plasma metabolic profiles of RYGB (blue) and sham-BWM (green) Zucker rats. Percentage on each PC represents variation explained by each principal component and Q^2 represents predictive ability of the PCA model…….92

Figure 4-13. Schematic illustration of systemic changes observed in biofluid from RYGB-treated obese Zucker rats in comparison with either sham-obese or sham-BWM rats…...94

Figure 5-1. Measurement of pH in different gastrointestinal contents of sham-obese, sham-BWM and RYGB groups. Data are shown as mean ± SEM (* $p < 0.05$; ** $p < 0.01$ and *** $p < 0.001$) and statistical differences determined by one-way ANOVA……103

Figure 5-2. PCA scores plots of HILIC-UPLC-MS data sets of the luminal content from stomach (A), duodenum (B), upper-jejunum (C), lower-jejunum (D), ileum (E) and colon (F) of lean (black) and obese (red) Zucker rats at 3-week post-operation. Left and right panels represent positive (1) and negative (2) modes……107

Figure 5-3. PCA scores plots of GI content data set including stomach (A), duodenum (B), upper-jejunum (C), lower-jejunum (D), ileum (E) and colon (F) contents of sham-BWM (green) and sham-obese (red) Zucker rats at 3-week post-sham-operation analysed using HILIC-UPLC-MS positive (1) and negative (2) modes……110

Figure 5-4. PCA scores plots of GI content data set including stomach (A), duodenum (B), upper-jejunum (C), lower-jejunum (D), ileum (E) and colon (F) contents of RYGB (blue) and sham-obese (red) Zucker rats at 3-week post- operation analysed using HILIC-UPLC-MS positive (1) and negative (2) modes……115

Figure 5-5. PCA scores plots of GI content data set including stomach (A), duodenum (B), upper-jejunum (C), lower-jejunum (D), ileum (E) and colon (F) contents of RYGB (blue) and sham-BWM (green) Zucker rats at 3-week post- operation analysed using HILIC-UPLC-MS positive (1) and negative (2) modes……119

Figure 5-6. Non-metric dimensional scaling (NMDS) plots of the weighted UniFrac distances of bacterial community data obtained from different gastrointestinal contents including stomach (A), duodenum (B), upper-jejunum (C), lower-jejunum (D), ileum (E) and colon (F) contents of RYGB (blue), sham-BWM (green) and sham-obese (red) rats……124

Figure 5-7. Pie charts representing the percentages of the mean relative abundances of bacteria at the phylum level in different luminal regions along the gastrointestinal tract of obese hyperinsulinemic (sham-obese), RYGB-operated (RYGB) and diet restriction-treated (sham-BWM) Zucker rats. Data was shown in percentage of relative abundance ± SD……126

Figure 5-8. PCA scores plots of bacterial profiles from GI contents including gastric (A), duodenal (B), upper-jejunal (C), lower-jejunal (D), ileal (E) and colonic (F) contents between sham-BWM (green) and sham-obese (red) rats using 16S rRNA gene sequencing analysis……127

Figure 5-9. Box plots of the significantly altered gut microbiota between sham-BWM (green) and sham-obese (red) rats at the genus level. Two-sided non-parametric t-test with Welch's correction was performed. Asterisks indicate significant differences: * P<0.05 and ** P<0.01……128

Figure 5-10. PCA scores plots of bacterial profiles from GI contents including gastric (A), duodenal (B), upper-jejunal (C), lower-jejunal (D), ileal (E) and colonic (F) contents between RYGB (blue) and sham-obese (red) rats using 16S rRNA gene sequencing analysis……...129

Figure 5-11. Box plots show the significantly altered gut microbiota between RYGB (blue) and sham-obese (red) rats at the genus level. Two-sided non-parametric t-test with Welch's correction was performed. Asterisks indicate significant differences: * P<0.05 and ** P<0.01……131

Figure 5-12. PCA scores plots of bacterial profiles from GI contents including gastric (A), duodenal (B), upper-jejunal (C), lower-jejunal (D), ileal (E) and colonic (F) contents between RYGB (blue) and sham-BWM (green) rats using 16S rRNA gene sequencing analysis……..…….132

Figure 5-13. Box plots show the significantly altered gut microbiota between RYGB (blue) and sham-BWM (green) rats at genus level. Two-sided non-parametric t-test with Welch's correction was performed. Asterisks indicate significant differences: * P<0.05 and ** P<0.01……133

Figure 5-14. O-PLS regression analysis of the selected significantly altered metabolites detected using HILIC-UPLC-MS against discriminatory bacterial genera; A, O-PLS scores plots and B, corresponding S-line plots showing the correlated features to either increased or decreased relative abundance of bacteria……..……134

Figure 6-1. Schematic illustration of the suggested metabolic alterations based on altered metabolites found in obese, caloric restriction and RYGB groups of this study. Abbreviations: BCAA, branched-chain amino acid; GI, gastrointestinal; SCFA, short-chain fatty acid……..……..149

List of tables

Table 1-1. Classification of obesity in adults……..22

Table 3-1. Summary of metabolic changes in urinary (u) and faecal (f) ^{1}H NMR profiles..59

Table 3-2. Summary of metabolic changes in plasma ^{1}H NMR profiles……60

Table 4-1. Summary of O-PLS-DA statistical parameters for all pairwise comparison models demonstrated in Chapter 4. Significant models are bold……79

Table 4-2. Summary of O-PLS-DA metabolic changes in urinary (U) and faecal km (F) ^{1}H NMR profiles……81

Table 4-3. Summary of O-PLS-DA metabolic changes in peripheral plasma (P_s) and portal vein plasma (P_p) ^{1}H NMR profiles……88

Table 5-1. Summary of O-PLS-DA statistical parameters for all pairwise comparison models demonstrated in Chapter 5……104

Table 5-2. List of metabolites found in different gastrointestinal contents obtained from pairwise O-PLS-DA analysis between Zucker obese and lean rats……108

Table 5-3. List of metabolites found in different gastrointestinal contents obtained from pairwise O-PLS-DA analysis between caloric restriction-treated and obese Zucker rats.112

Table 5-4. List of metabolites found in different gastrointestinal contents obtained from pairwise O-PLS-DA analysis between RYGB-treated and obese Zucker rats……116

Table 5-5. List of metabolites found in different gastrointestinal contents obtained from pairwise O-PLS-DA analysis between RYGB-treated and caloric-restricted obese Zucker rats……..120

List of abbreviations

2-OG	2-oxoglutarate
3-HB	3-hydroxybutyrate
3-HPPA	3-hydroxypropionate
5-HIAA	5-hydroxyindole-3-acetate
5-HT	5-hydroxytryptamine
5-HTP	5-hydroxytryptophan
AGB	adjustable gastric band
BCAA	branched-chain amino acid
BMI	body mass index
BWM	body weight-matched
CE	capillary electrophoresis
CoA	coenzyme A
DMA	dimethylamine
EC	endochromaffin cell
ESI	electrospray ionisation
GABA	gamma-amino-N-butyrate
GAD	glutamate decarboxylase
GI	gastrointestinal
GLP-1	glucagon-like peptide-1
GPCR	G-protein-coupled receptor
IS	indoxyl sulfate
L-AADC	L-amino acid decarboxylase
LC	liquid chromatography

LoA	level of assignment
LPS	lipopolysaccharide
MS	mass spectrometry
NAD	nicotinamide adenine dinucleotide
NMR	nuclear magnetic resonance
OGTT	oral glucose tolerance test
O-PLS	orthogonal signal correction partial-least square
O-PLS-DA	orthogonal signal correction partial-least square-discriminant analysis
OSC	orthogonal signal correction
OUT	operational taxonomic unit
PAR	pareto
PAG	phenylacetylglycine
PC	phosphorylcholine
PEP	phosphoenolpyruvate
PLP	pyridoxal-5'-phosphate
IPA	indole-3-propionate
PS	phosphatidylserine
PCA	principal component analysis
PCR	polymerase chain reaction
PLS	projection to latent structures
PLS-DA	projection to latent structures-discriminant analysis
RNA	ribonucleic acid
rRNA	ribosomal ribonucleic acid
RYGB	Roux-en-Y gastric bypass

SCFA	short-chain fatty acid
SG	sleeve gastrectomy
STOCSY	statistical total correction spectroscopy
T2DM	type-2 diabetes mellitus
TCA	tricarboxylic acid
TMA	trimethylamine
TMAO	trimethylamine-*N*-oxide
TRH	tryptophan hydroxylase
TSP	3-(trimethylsilyl)-propionate-2,2,3,3-d_4
UPLC	ultra high performance liquid chromatography
UV	unit variance
VLDL	very low-density lipoprotein
WHO	World Health Organisation

1. Introduction

1.1 Introduction to obesity: prevalence, causes and treatments

Obesity is an epidemic medical health condition, in which fat accumulation increases to the extent that health is adversely affected through the development of comorbidities. Approximately 1.5 billion adults over the age of 20 and 43 million children under the age of five are over-weight (Body Mass Index [BMI], a measure of weight relative to height ≥25 kg/m^2) and 500 million are clinically obese (BMI≥30 kg/m^2) (World Health Organization [WHO], 2014) (Table 3-1).

Table 1-1. Classification of obesity in adults

BMI (kg/m^2)	Classification
25 – 29.9	Overweight
30 – 34.9	Obesity class I
35 – 39.9	Obesity class II
40 and over	Obesity class III

(Source: The World Health Organisation, 2014)

Obesity has emerged as one of the major global socioeconomic healthcare burdens of the 21st century (World Health Organization, 2014). The WHO estimates a rising prevalence of approximately seven million per year, associated with a concomitant rise in obesity-related co-morbidities such as diabetes, metabolic syndrome, heart disease, sleep apnoea and cancer that may result in significantly increased healthcare cost and consumption of medical resources (Li *et al.*, 2011a). In the United Kingdom, obesity rates are the highest in Europe and have increased remarkably over the past few years (World Health Organization, 2014). It has been reported that about 20% of the population are obese and costs the UK about £3 billion per year.

High energy is derived from energy-dense food intake, in combination with markedly low physical activity, leading to excess energy storage and ultimately obesity (Zhang *et al.*, 2008a). Although lifestyle modification is commonly used to reduce weight among obese

individuals, it has not yet to be reported for substantial long-term outcomes – insufficient weight reduction and inadequate reduction in obesity-associated complications (Mutch *et al.*, 2009). Instead, bariatric surgery provides dramatic and sustained weight reduction in morbid obese patients and resolution of type 2 diabetes mellitus (Monte *et al.*, 2012). Of three most common types of bariatric surgery including the Roux-en-Y gastric bypass (RYGB), Adjustable Gastric Band (AGB) and the Sleeve Gastrectomy (SG), RYGB has been largely employed as the gold standard procedure for the severe form of obesity (BMI ≥ 40 kg/m^2 or BMI ≥ 35 kg/m^2 with comorbidities). The idea of this treatment is to interfere with the ingestion and/or absorption of food. The RYGB operation results in changes in acid exposure to gastric remnant and proximal small bowel and restricts the amount and types of foods that can be ingested. Hence, it induces modest degree of nutrient malabsorption by shortening the length of small bowel resulting in intestinal dysmobility and altered gut microbiota (Aron-Wisnewsky, Dore & Clement, 2012).

1.2 Studies of obesity on Zucker rat model

Although numerous obesity studies have been performed in humans, animal models remain valuable for providing complementary insights into disease mechanisms (Oana *et al.*, 2005). The Zucker (fa/fa) rat has been one of the most commonly used rat models to study obesity over the last three decades (Oana *et al.*, 2005). Obesity in these rats is caused by a mutation in a single recessive gene (*fa*) of the leptin receptor and is characterized by hyperphagia, hyperlipidaemia, hypercholesterolemia, leptin resistance, hyperinsulinemia, and development of adipocyte hypertrophy and hyperplasia (Unger, 1997).

A ^{1}H NMR spectroscopy-based metabonomics study by Waldram *et al*. (Waldram *et al.*, 2009) reported higher levels of plasma lipids, choline and branched chain amino acids (BCAAs) and higher urinary concentrations of propionate, acetate and 3-methylglutarate

in Zucker obese (fa/fa) compared with the Zucker lean (fa/+) or (+/+) phenotype. Although many of the metabolic features that characterize the obese Zucker rat relate to energy metabolism, a core component of the phenotype suggests a differential signature in the obese phenotype arising from the gut microbiota. The role of the gut microbiota in creating an obesogenic environment is supported by many studies (Zhao *et al.*, 2010). However, another previous analysis of the faecal microbial composition of lean and obese Zucker rats carried out by Lees *et al*. (Lees *et al.*, 2014) found no significant phenotypic difference, with variation attributed to age and animal husbandry. Given the disagreement in findings between Waldram and Lees' studies with regards to microbial composition of lean and obese Zucker rats, it is worth noting the different animal housing strategies employed: animals housed according to a single or mixed strains. In our study, we address this issue by housing animals individually. These previous studies suggested that a shift from investigation of biochemical composition to the metabolic functionality of the gut microbiota in obesity could be of great benefit.

1.3 Effectiveness of obesity treatments

According to WHO (2014), the broad principles to overcome overweight and obesity including lifestyle modification, pharmacotherapy and surgery have been largely employed depending on the BMI and comorbidities considered as the decision-making criteria for the appropriate approach: long-term behaviour modification (dietary change, enhanced physical activity, reduced sedentary behaviours and developed sleep patterns) and/or long-term weight maintenance strategies; and consideration of the use of pharmacotherapy, more intensive dietary therapies and bariatric surgery (Figure 1-1) (World Health Organization, 2014).

Throughout this research project, the focus has been drawn on caloric restriction as part of life style modification and bariatric surgery, especially Roux-en-Y gastric bypass which

is the widely used gold standard procedure causing the most metabolic changes compared with other bariatric surgical types.

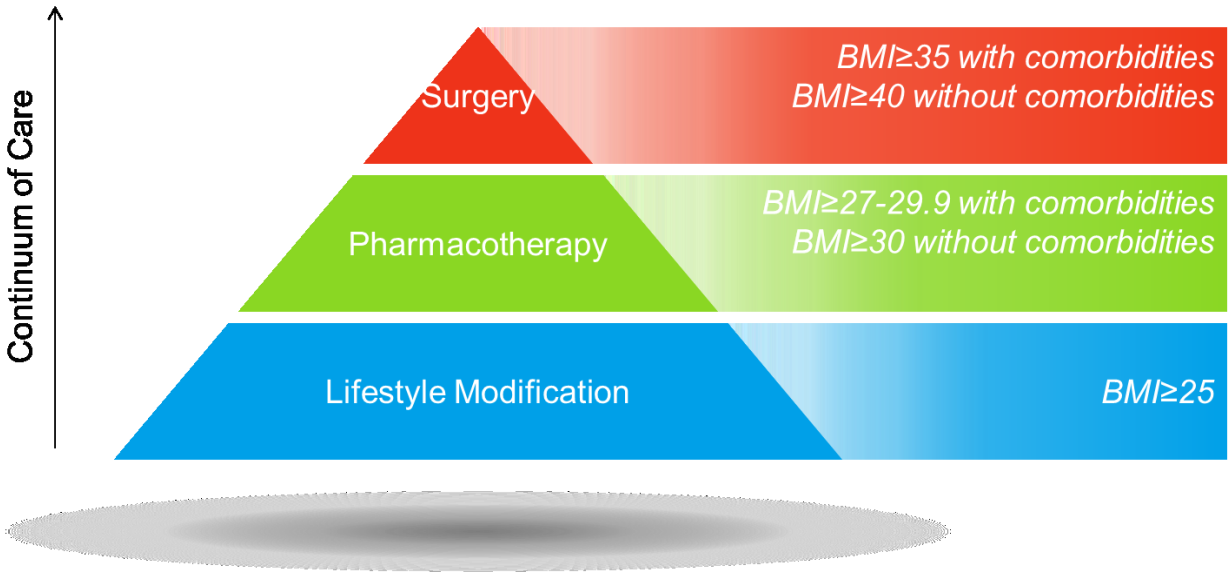


Figure 1-1. Three main approaches for obesity treatment

1.3.1 Caloric restriction

Caloric restriction or energy restriction is a dietary regimen that promotes the reduction of calorie intake without incurring malnutrition or reduced essential nutrients. Caloric restriction was experimentally verified to possess beneficial health and lifespan effects in rodents over eight decades ago (Speakman & Mitchell, 2011). The concept of limiting calorie intake, which has the beneficial effects on lifespan, was first discovered by McCay and colleagues in 1935 so that this strategy for weight loss has been long known (McCay, Crowell & Maynard, 1935). Despite a long history of caloric restriction, the underlying mechanisms are still not well understood.

When animals are on energy restriction, their hunger increases and they show remarkable increase in physical activity at some certain time, which probably reflect food anticipatory activity and food-seeking behavior. This is consistent with the neuropeptide profile in the hypothalamus that indicates hunger, together with elevated neuropeptide Y (NPY) and Agouti-regulated peptide (AgRP) levels in response to diminished leptin

(Minor, Chang & de Cabo, 2009). A previous study by Hambly *et* al (2007) showed the normalisation of hypothalamic neuropeptide pattern took place after the post-restriction hyperphagia, validating the level of hyperphagia as an indicator of the hunger during restriction (Hambly, Mercer & Speakman, 2007a). It was demonstrated that when mice were placed on 20% caloric restriction for between 50 and 100 days, the magnitude of the hyperphagic response they showed was independent of the previously given length of caloric restriction. Hyperphagia ended when body mass was normalised relative to the *ad libitum* fed controls. Hunger, therefore, did not diminish in mice under caloric restriction even when they were restricted for 100 days, which is equivalent to about 11 years in humans (Hambly, Mercer & Speakman, 2007b).

In regard to insulin resistance and metabolic syndrome, aging is accompanied by a noticeable increase in hepatic resistance to the action of insulin. In rats, 18 month-caloric restriction restores hepatic insulin sensitivity to the same levels observed in young rats aged 4-months-old (Barzilai *et al.*, 1998a). Similarly to rats selectively bred for low aerobic running capacity, there is an age related development of the metabolic syndrome, including hyperinsulinemia, insulin resistance, visceral obesity and dyslipidaemia, and they further reported that hyperinsulinemia in these rats was related to impaired hepatic insulin clearance (Bowman *et al.*, 2010). Following the 3-month 30% caloric restriction, the aforementioned metabolic abnormalities were reversed (Bowman *et al.*, 2010). It was additionally shown that the age-related insulin resistance could be related with fat mass, especially visceral fat, elevation (Catalano, Stefanovski & Bergman, 2010). Both fat mass and visceral fat were decreased to about one-third, while lean body mass was not altered under caloric restriction condition and more importantly, a remodelling of body composition away from visceral fat in the calorie-restricted animals (Barzilai *et al.*, 1998b). However, there are some contrasting data showing that individuals who lost least fat under caloric restriction survived the longest that is commonly known as the age and obesity paradox (Bertrand *et al.*, 1980). Cao and colleagues (2001) showed that a key metabolic alteration during caloric restriction was

a shift from carbohydrate metabolism to fat metabolism and this is consistent with the work conducted by Kuhla and co-workers (2008) showing that the lifelong caloric restriction in mice induces a metabolic adaptation with reduced lipogenesis and enhanced lipolysis and ketogenesis (Cao *et al.*, 2001; Kuhla *et al.*, 2014).

In parallel, it has been revealed that the beneficial effects of caloric restriction were exerted *via* the inhibition or stimulation of a relatively small number of metabolic pathways that interacted with and modulate a few key processes, such as oxidative stress and autophagy (Sanz, Caro & Barja, 2004; Ash & Merry, 2011). Studies in non-human primates, and a limited amount of work in humans under relatively short-term restriction, have provided prominent results that caloric restriction provides similar beneficial effects (Fontana *et al.*, 2004; Masoro, 2005).

1.3.2 Bariatric surgery

Despite the effectiveness of some extent of caloric restriction, patients who are severely obese with or without co-morbidities do require more meaningful and sustained weight loss. A non-surgical weight loss remedies that yields such effects do not exist. Therefore, it is not a surprise that the field of bariatric surgery has remarkably expanded from its modest beginning in the 1950s.

The first jejuno-ileal bypass was performed in dogs by the three surgeons, Drs. Kremen, Linner and Nelson in 1954, which demonstrated the significant malabsorption of fat and weight loss (Kremen, Linner & Nelson, 1954), thus leading to the origin of bariatric surgery. A number of different operative procedures have been developed over time. Some proved as having high risk or harmful effects to patients have been abandoned while some have been evolved into safer and more effective variants.

Roux-en-Y gastric bypass (Figure 1-2A) is the most common weight loss procedure performed in the United States and the United Kingdom and is considered as a combined approach of restrictive and malabsorptive procedures (Schmidt *et al.*, 2013). It has been

reported that patients can lose more than 50% of their excess weight (MacLean *et al.*, 1993; MacLean, Rhode & Nohr, 2000; Pories *et al.*, 1995). The mortality ranges from 0.3% to 1.6% of which its thirty-day mortality is less than 1% (Suter *et al.*, 2011; Lanyon & Maxwell, 2007; MacLean, Rhode & Nohr, 2000; Pories *et al.*, 1995). However, there are some serious complications including deep venous thrombosis, pulmonary embolism, gastrointestinal leak, and long-term complications, such asanaemia, vitamin and mineral deficiencies (Khoursheed *et al.*, 2011). In RYGB procedure, a small stomach pouch is generated and subsequently anastomosed to the jejunum. Bypass is then achieved by anastomosing the stomach remnant to a segment of jejunum, which creates an alimentary limb. The small intestine continues from the larger stomach remnant and is anastomosed to the jejunum *via* jejunojejunostomy to produce a biliopancreatic limb, which constructs the 'Y' configuration of the Roux-en-Y bypass (Bower *et al.*, 2015; Mason & Ito, 1969).

Adjustable gastric band (Figure 1-2B) is an reversible procedure that the adjustable silicone band is placed around the upper stomach, generating a 15 – 20 mL pouch and thus limiting food intake (Belachew *et al.*, 1995). Approximately 40 – 60% of excess weight can be lost following the operation (Vella & Galloway, 2003; O'Brien, 2003). As this weight loss approach is solely restrictive, anaemia and vitamin deficiencies are concerned (Kothari *et al.*, 2002). In addition to restriction-related complications, band slippage (2 – 4% risk), erosion into the stomach (1 – 2% risk) are also reported as common complications (Vella & Galloway, 2003).

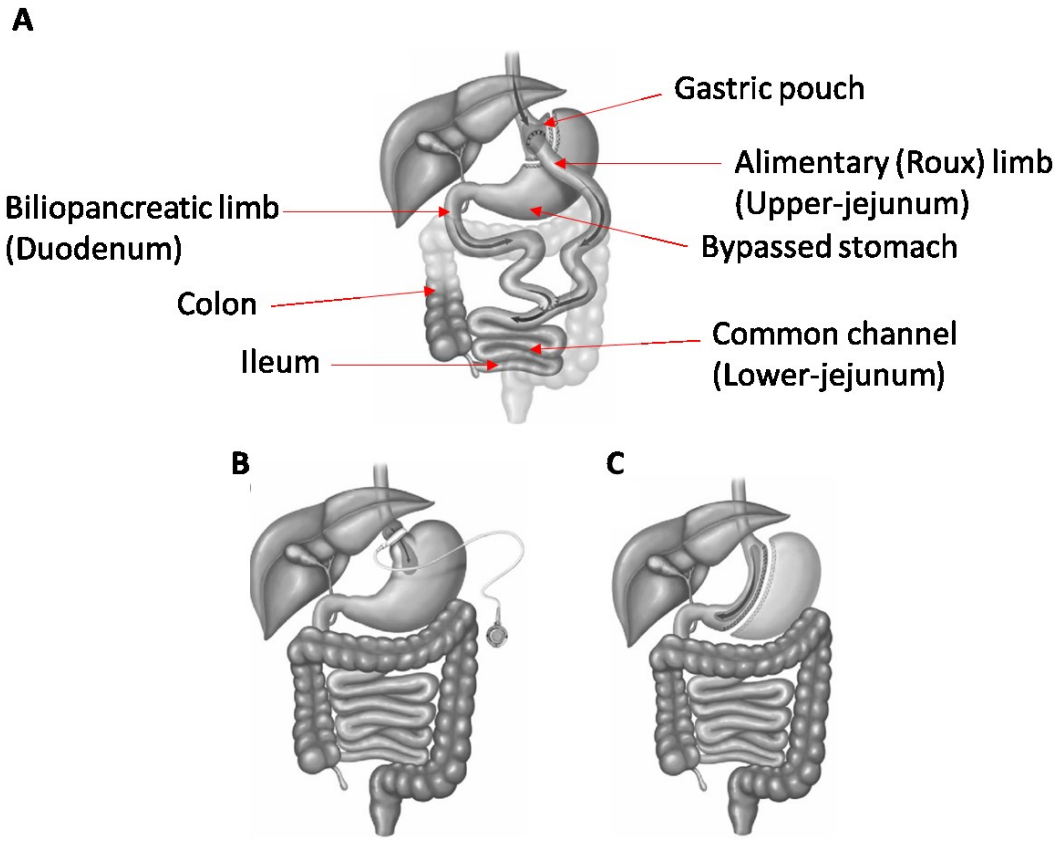


Figure 1-2. Most common types of bariatric surgery. (A) Roux-en-Y gastric bypass, (B) laparoscopic adjustable banding, and (C) vertical sleeve gastrectomy. [Modified from original figure of Marihart *et al* (2014) (Marihart, Brunt & Geraci, 2014)].

Sleeve gastrectomy (Figure 1-2C) involves the excision of the greater curvature of the stomach leaving tubular section along the lesser curvature and leading to early satiety and reduced appetite as a result of gastric restriction (Trelles & Gagner, 2007). A number of previous studies have shown that the results and complications of the sleeve procedure is between the band and RYGB. Although sleeve gastrectomy results in positive outcomes in weight loss, as a concern, the remaining stomach may dilate with time, potentially leading to weight loss failure and requiring the second bariatric procedure to be performed (Ser *et al.*, 2010).

The degree of weight loss related to bariatric surgery is dependent on the type of operation used. According to Swedish Obese Subjects (SOS) trial, the greatest total weight loss was associated with RYGB, followed by vertical banded gastroplasty (VBG) and laparoscopic adjustable gastric banding (LAGB) accounting for 25%, 17% and 13%, respectively (Sjöström *et al.*, 2007a). Moreover, the meta-analysis results reported by

Buchwald (2015) stated that the degree of weight loss is lowest for restrictive procedures and highest for malabsorptive procedures (Buchwald & Oien, 2013). Another meta-analysis conducted by Maggard and co-workers further showed that excessive weight loss was higher for patients who underwent RYGB (61.6%) or VGB (68.2%) compared with patients received LAGB which accounts for 47.5% (Maggard *et al.*, 2005).

Diabetes, hypertension and hyperlipidaemia are the most common co-morbidities contributing towards the devastating medical conditions of people worldwide. These three co-morbidities along with visceral obesity are the characteristics of the metabolic syndrome, acting as strong risk factors for cardiovascular mortality (Grundy, 2008). However, these co-morbidities could be improved following RYGB with the resolution rate of 82% for diabetes, 70% for hypertension, 63% for hyperlipidaemia (Schauer *et al.*, 2000). The results obtained from SOS study further demonstrated that surgically treated patients showed significant reductions in hypertension (25%) and diabetes (75%) cases, and 43% improvement in levels of high density lipoprotein (Sjöström *et al.*, 2007b). Moreover, non-alcoholic fatty liver disease (NAFLD) is improved by weight loss surgery (Klein *et al.*, 2006). Despite the beneficial effects of bariatric surgery, faecal water from RYGB surgery rats was shown to be highly cytotoxic to mouse lymphoma cell line (Li *et al.*, 2011b). This has raised our attention to investigating the factors, e.g. toxic microbial metabolites, which could contribute to the high cytotoxicity following RYGB.

1.4 Gut microbiota

Gut microbiota is composed of considerable numbers and species of microorganisms making up a bacterial community in the mammalian gastrointestinal tract (Sender, Fuchs & Milo, 2016). There are several hundred species available in the gut and the composition of the gut microbiota is relatively stable, comprising of *Bacteroidetes* and *Firmicutes* as the two most predominant bacterial phyla, followed by *Actinobacteria*,

Proteobacteria, *Verrucomicrobiota* and others (Eckburg *et al.*, 2005; Lozupone, Hamady & Knight, 2006).

1.4.1 Function of gut microbiota

The gut microbiota is thought as the metabolically active organ providing the metabolic products that are beneficial for host (Lyra *et al.*, 2010). Over the last decades, previous studies demonstrated the several main functions of gut microbiota, such as production of short-chain fatty acids (SCFA), production of vitamins, drug metabolism and other metabolic activity (Jandhyala *et al.*, 2015).

Short-chain fatty acids such as acetate, propionate and butyrate can be produced by the intestinal microbiota from undigested dietary carbohydrates (*e.g.* oligosaccharides) and endogenous substrates (*e.g.* mucin). These SCFAs have been shown to contribute to approximately 10% of the total caloric requirements of humans (Yuan *et al.*, 2006; McNeil, 1984). Butyrate is the most preferred substrate, serving as a fuel for colonic mucosa. It has been shown to possess the inhibitory effect on histone deacetylases, resulting in hyperacetylation of chromatin and altered gene expression (Davie, 2003). Butyrate has also been reported to inhibit inflammation and carcinogenesis and reduce oxidative stress (Canani *et al.*, 2011). Propionate, instead, is mostly delivered to the liver and serves as a substrate in gluconeogenesis (Verbrugghe *et al.*, 2012). In contrast, acetate acts as a *de novo* lipogenesis substrate in hepatocytes and adipocytes (Zambell, Fitch & Fleming, 2003).

Food-related lactic acid bacteria (LAB) along with some other human gut microbiota such as bifidobacteria are involved in the *de novo* synthesis and supply of vitamins. This is vital as humans are incapable of biosynthesizing most vitamins; therefore, they must be provided exogenously (LeBlanc *et al.*, 2013). Previous studies have also shown that fermented milks with high levels of B-group vitamins, such as, folate and riboflavin, can be produced by LAB-promoted and possibly *Bifidobacterium*-promoted biosynthesis.

Moreover, certain strains of LAB produce the complex vitamin cobalamin (or vitamin B12). Vitamin K is fat-soluble and essential micronutrient for vitamin K-dependent protein modification and activation that is involved in regulation of calcification, energy metabolism, and inflammation (Booth, 2009). Vitamin K contains a naphthoquinone ring structure and there are two major forms, namely phylloquinone (vitamin K1) and menaquinone (vitamin K2), which can be biosynthesized by the intestinal bacteria (Kindberg *et al.*, 1987; Fujita, Kakuya & Ito, 1993).

Intestinal microbiota has been reported to be capable of metabolizing drugs (Wilson & Nicholson, 2009). For example, digoxin, which is a widely used drug for treating a number of heart diseases, can undergo a significant metabolic conversion into cardio-inactive metabolites by the activity of a common colonic microbiota in human, namely, *Eggerthella lenta* with the presence of arginine (Saha *et al.*, 1983). The gut microbiota is also known to be able to degrade proteins releasing ammonia, sulfur-containing compounds, amines, indoles, *p*-cresol and phenol (Hughes, Magee & Bingham, 2000). Bioactive compounds produced by gut microbiota affect host physiology and hence metabolism so that understanding and controlling the composition as well as metabolic activity of the gut microbiota are of researchers' interests.

1.4.2 Host and microbiota co-metabolism and signalling in obesity

Gut microbiota is composed of a diverse range of symbiotic gut bacteria and other microorganisms that coevolved with human and other coelomate animals. The colonization by gut microbiota is established soon after birth and the composition of core gut microbiota is essentially stable throughout adulthood even though the composition in early life varies (Nicholson *et al.*, 2012). Human gastrointestinal (GI) tract harbours more than 1014 different species, 90% of which belong to two main phyla, namely, *Bacteroidetes* and *Firmicutes*. Different locations along GI tract harbour different number and species of the microbiota depending on variations in the environmental niche. Their

composition and activity depend on host genome, early life exposure to the microbiota, nutrition, lifestyle, medication and so on (Holmes *et al.*, 2012). They are involved in the multiple host metabolic pathways giving rise to evolutionary fitness of host (Hamady & Knight, 2009). Host and microbiota co-metabolism and signalling involve a vast array of small molecules from food and xenobiotics. These molecules play vital roles in shuttling information between host cells and microbial symbionts. For example, dietary fibre or complex carbohydrate are digested and fermented by gut microbes in order to yield SCFAs. These SCFAs are essential for host health and disease risks and can be sensed by G-protein coupled receptors expressed by gut enteroendocrine cells (Tang *et al.*, 2011; Kimura *et al.*, 2014). Another example of the gut microbial functions is bile acid metabolism. Glycine- or taurine-conjugated bile acids can be deconjugated by gut bacteria that possess bile salt hydrolases (Ridlon, Kang & Hylemon, 2006). Turnbaugh *et al.* (2006) showed the role of the gut microbiota in weight regulation in a mouse model. The same publication also reported that the gut microbiota in obese individuals was more efficient than that of lean individuals in extracting energy from diet and promoting fat storage in adipose tissue (Turnbaugh *et al.*, 2006).

1.4.3 Gut microbiota in relation to obesity, caloric restriction and bariatric surgery

Previous studies show that gut microbiota exert metabolic effects on host through several different mechanisms in order to interact with host and regulate energy metabolism (Jandhyala *et al.*, 2015). Ley and co-workers (2005) have reported the difference between lean and obese animals and humans and further reported that the *Bacteroidetes/Firmicutes* ratio was lower in obese subjects than lean individuals (68). The *Bacteroidetes/Firmicutes* ratio of obese individuals who lost weight following 1-year carbohydrate-restricted and fat-restricted diets was found to be more similar to lean individuals and this phenomenon also occurred in an animal experiment (69). Turnbaugh and colleagues (2006) showed that mice receiving microbiota from obese donors gained more weight compared with the lean-type microbiota in spite of the equal food intake. In

contrast to mice with lean-type microbiota, the *Bacteroidetes/Firmicutes* ratio of mice receiving obese-type microbiota was lower with increased concentrations of fermentation end products and lower calories remaining in the faeces, indicating the transmissible obese-type energy extraction capabilities (Turnbaugh *et al.*, 2006). Furthermore, rural African children demonstrated significantly higher proportion of *Bacteroidetes* compared with European children who usually had higher calorie intake (De Filippo *et al.*, 2010). In line with the previous study mentioned above, fasted mice had greater the *Bacteroidetes/Firmicutes* ratio compared with the non-fasted mice (Crawford *et al.*, 2009). However, Ley and co-workers (2010) showed the inconsistent proportion of *Bacteroidetes* in obese and lean humans suggesting the inter-individual variation that may affect the composition of the gut microbiota (Ley, 2010).

Mice treated with caloric restriction showed increased abundance of *Proteobacteria* and *Verrucomicrobia* in their faeces compared with *ad libitum* group and percentage body weight loss was related to *Proteobacteria* abundance (Bartley *et al.*, 2017). Caloric restriction-induced changes in microbiota in animal experiments have also been observed in humans. After long-term caloric restriction, distinct alteration in the microbiota compared with obese adolescents was clearly seen in the treatment group and this approach has been demonstrated to induce shifts in total and β-galactosidase (βGAL)-containing microbiota, decreasing the *Firmicutes/Bacteriodetes* ratio, and thus enhancing the growth of *Bacteroides, Roseburia, Faecalibacterium* and *Clostridium* XIVa that possess some beneficial effects, evidenced by the similar structure and composition to lean adolescents (Ruiz *et al.*, 2017). A previous study demonstrated that the abundance of *Akkermansia muciniphila* was inversely associated to fat mass and glucose intolerance in mice (Shin *et al.*, 2014). In line with the animal study mentioned above, a study based on 49 overweight or obese adults who were calorie-restricted for 6 weeks showed that the baseline *Akkermansia muciniphila counts* was inversely related to fasting glucose, waist-to-hip ratio, and adipocyte diameter in subcutaneous white adipose tissue (Dao *et al.*, 2016). Individuals showing greater microbial gene richness

and *Akkermansia muciniphila* had the healthiest metabolic status, particularly in fasting glucose, triglycerides and body composition. In other words, higher abundance of baseline *Akkermansia muciniphila* was associated with greater improvement in insulin sensitivity and other clinical parameters after caloric restriction (Dao *et al.*, 2016).

Some studies in human and rodents have demonstrated that bariatric surgery resulted in a marked shift in the composition of the gut microbiota, from predominantly *Firmicutes*- and *Bacteroidetes*-dominated toward *Gammaproteobacteria*-dominated community (Zhang *et al.*, 2008b; Li *et al.*, 2011a). This significant change in microbial profiles post RYGB is believed to contribute to postoperative weight loss. Liou *et al*. showed a reduction in body adiposity of animals transplanted with RYGB-microbiome compared with ones with Sham-microbiome (Liou *et al.*, 2013). In addition, RYGB induces both metabolic alterations in energy metabolism and urinary excretion of host-gut microbial co-metabolites such as 4-cresyl sulfate, phenylacetateglycine and choline degradation products (Smith & Macfarlane, 1996). Another study showed that the higher levels of trimethylamine, hippurate and trigonelline in urine of RYGB-operated mice indicate the microbial disturbance caused by RYGB surgery (Seyfried *et al.*, 2013). In addition to the changes in gut microbiota composition and metabolic effects, it has been found that faecal water of rat undertaken RYGB surgery is highly cytotoxic to rodent cells compare to sham-operated control (Li *et al.*, 2011b). Prolonged cytotoxic loads could cause long-term inflammation to host cells, potentially resulting in cancer risk, which is in agreement with a human study where obesity surgery was reported to be associated with an increased risk of colorectal cancer over time (Derogar *et al.*, 2013).

Collectively, metabolic activity and the composition of gut microbiota play significant roles in regulating host metabolism. In order to monitor the alteration of host-microbial co-metabolism, metabonomics, which is one of the omics methodologies, has been developed to accommodate the drive to express an organism's behaviour at the global systems biology level.

1.5 Overview of metabonomics

Metabonomics, defined as “the quantitative measurement of the dynamic multiparametric metabolic response of living systems to pathophysiological stimuli or genetic modification”, is able to reflect the metabolic fingerprints of biofluids and tissues (Nicholson, Lindon & Holmes, 1999). Metabonomics or metabolic profiling is underpinned by various high resolution spectroscopic analytical platforms in combination with multivariate data analyses to monitor the complex biological conditions and elucidate a map of host-microbial metabolic interaction (Nicholson *et al.*, 2012).

1.5.1 Outline of metabolic profiling methods

Metabonomics involves several steps comprising of sample collection and preparation, analysis of biochemical composition, multivariate data analysis for biomarker identification and statistical model validation (Nicholson & Lindon, 2008). A wide spectrum of samples can be analysed with metabolic phenotyping such as urine, faeces, serum, plasma, tissues, saliva, sweat, breath culture media and cell extract using the high-throughput instruments, of which the main analytical platforms include nuclear magnetic resonance (NMR) spectroscopy and mass spectrometry (MS). Sample preparation is simple and straightforward in the case of NMR. For liquid chromatography-MS, the extraction method is dependent on the nature of samples and the chosen analytical assays (Lenz & Wilson, 2007). Several studies have shown the effects of sample preparation on metabolic profiling, suggesting that appropriate protocols are essential (Yin, Lehmann & Xu, 2015; Gong *et al.*, 2017). Data obtained from these technologies are considered as data-rich data sets with high complexity. Therefore, computer-based analytical tools, specifically pattern recognition, is required in order to extract significant information from large and complex data sets. Pattern recognition helps simplify huge and complex data and provide easy data visualisation of the similarities and differences between observations. These spectroscopic can also be

correlated with other clinical parameters such as body mass index and histological grade of pathology that need both statistical and biological validation for potential biomarkers before the applications in clinical diagnosis and surgical or therapeutic decision-making (Yong Chan, Mal & Pasikanti, 2012).

1.5.2 Basic principles of NMR spectroscopy

NMR spectroscopy, a very robust and highly reproducible platform, exploits the spin property of nuclei, which is a physical phenomenon where nuclei can absorb and re-emit electromagnetic radiation in a magnetic field. ^{1}H and ^{13}C are the most commonly used in metabonomics, particularly ^{1}H, because of its great abundance in biological samples and also high sensitivity to NMR. When the nuclei are excited by a strong and short radiofrequency pulse, the NMR absorption spectra are received for the spin-active nuclei and reflect the electronic and chemical environment of each nucleus in a time domain space that require Fourier transformation for the transformation into the frequency domain, enabling the NMR spectra interpretation based on the chemical shift scale (ppm: part per million), the number of the splitting pattern of peaks (peak multiplicity) and the distance between split peaks (coupling constant, ***J***). The external magnetic field and the shielding effects of the electron cloud determine the resonance frequency of a nucleus, but a reference chemical shift scale is routinely used, allowing the comparison of spectral data obtained from instruments with different strengths of external magnetic field. Peak multiplicity and spin-spin couplings are due to the neighbouring nuclei interaction through electron bonds. NMR spectroscopy is quantitative; the peak integral area is proportional to the metabolite concentration. In the current thesis, the peak integral areas are considered as relative abundance to allow the comparison of the metabolite abundances between different samples. Another advantage of NMR spectroscopy is generation of macromolecule or lower-molecular weight molecule profiles by diffusion-edited spectroscopy, without the need of pre-separating process of the samples. This is very useful for profiling biochemical composition of blood plasma, which contains both small

molecules (*e.g.* amino acid and glucose) and macromolecules (*e.g.* lipids and lipoproteins).

^{1}H NMR spectra are typically acquired on a high-field NMR spectrometer using a standard one-dimensional (1-D) pulse sequence with water resonance suppression. A typically used standard sequence is [recycle delay (RD)-90˚-t_1-90˚- t_m-90˚-acquire free induction decay (FID)]. The water signal is suppressed by a selective irradiation during recycle delay and the mixing time (t_m) allowing the better visualisation of other biochemical components. Two-dimensional (2-D) NMR spectroscopy, providing more detailed structural information, can be used for molecular identification. Typically, a small set of representative samples are chosen for the 2-D analysis as the acquisition time is much longer than for 1-D experiment. ^{1}H-^{1}H correlation spectroscopy (COSY) and ^{1}H-^{1}H total correlation spectroscopy (TOCSY) give information on the connectivities of proton. For example, they indicate which proton is adjacent to which cluster of protons. ^{1}H-^{13}C heteronuclear single-quantum correlation and ^{1}H-^{13}C heteronuclear multiple-bond correlation spectroscopy indicate correlation between protons and carbons in a molecule (Wishart, 2008; Markley *et al.*, 2017).

1.5.3 Basic principles of mass spectrometry

Mass spectrometry, usually coupled with a separation system such as liquid chromatography (LC), gas chromatography (GC) or capillary electrophoresis (EC) to reduce the complexity of the biological sample, has been widely employed for both targeted and untargeted metabolic profiling experiments. Amongst the available separation techniques at present, ultra-performance liquid chromatography (UPLC) is often chosen since it reduces the experimental running time by approximately ten-fold compared with the conventional LC system. Another benefit of UPLC system is the reduction of ion suppression problem by the higher resolution of peak separation. Hydrophilic interaction LC (HILIC)-UPLC-MS has good retention of polar compounds and

has begun to be widely used in metabonomic study (Want *et al.*, 2013; Vinaixa *et al.*, 2012). GC is appropriate for volatile compounds and has the advantage of well-developed database for metabolite identification. Derivatisation is a prerequisite stage that becomes the limitation of this technique. GC-MS is, however, the preferred method for measuring SCFAs, hence a useful tool for characterising the functionality of gut microbiota in terms of energy production (Mulat & Feilberg, 2015). Capillary electrophoresis (CE)-MS is another analytical platform that is becoming more popular because of its low instrument cost and easy establishment. CE separates metabolites based on charge-to-mass ratios and is appropriate for analysing polar and charged compounds. However, this technique is still not suitable for high-throughput analysis and biomarker identification can be difficult as it requires other confirmation approach such as tandem MS or running standard chemicals (Ramautar, Somsen & de Jong, 2009).

Following the separation system, a mass spectrometer produces multiple ions from the sample under investigation, it then separates them according to their specific mass-to-charge ratio (m/z), and then records the relative abundance of each ion type. The first step in the mass spectrometric analysis of compounds is the generation of gas phase ions of the compound, basically by electron ionization. This molecular ion undergoes fragmentation. Each primary product ion derived from the molecular ion, in turn, undergoes fragmentation, and so on. The ions are separated in the mass spectrometer based on their m/z ratio, and are detected in proportion to their abundance. A mass spectrum of the molecule is thus created. It illustrates the result in the form of a plot of ion abundance against mass-to-charge ratio. Ions provide information concerning the nature and the structure of their precursor molecule. In the spectrum of a pure compound, the molecular ion, if present, appears at the highest value of m/z (followed by ions containing heavier isotopes) and the molecular mass of the compound is then obtained (Hoffmann & Stroobant, 2007).

1.5.4 Multivariate statistical analysis

Multivariate statistical analysis, in metabonomics, comprises of both unsupervised and supervised multivariate statistical methods. Unsupervised approach such as principal component analysis (PCA) and hierarchical cluster analysis are used to generate a model that indicates the intrinsic similarities or differences without prior class membership information. The other type is supervised technique, for example, projection to latent structures (PLS) and projection to latent structures-discriminant analysis (PLS-DA) that generate the statistical model involving the information of class membership which is used to optimise the separation between different classes and thus requiring the model validation (Worley & Powers, 2012).

1.5.4.1 Principal component analysis (PCA)

Principal component analysis is a commonly used unsupervised method. PCA can reduce the complexity of the metabolic information, identify outliers and detect pattern in data. Spectral data can simply be defined as an X matrix containing N rows (observations) and K columns (variables). Samples can be plotted in K dimensional space and usually be mean-centred, which means the average value of each variable is calculated and subtracted from data, improving the interpretability of the models. However, without proper scaling methods, it may highlight the variation in the prominent features, for instance, signals from metabolites present at high concentrations. A feature with a wide numerical range can contain a large variance while features present at low concentrations could possess smaller variance. To avoid the dominance of the variables with a large variance on the models, scaling is therefore essential in pre-processing of spectral data and optimising information recovery. There are several widely used scaling methods, for example, scaling to unit variance (UV) and Pareto scaling (PAR). For UV scaling method, each variable is divided by its standard deviation, such that the weight of a variable with a large variance will become smaller whilst a small variance of a

variable will be stretched. Therefore, all the variables have equal variance and no domination of some variables is seen, giving rise to small variations in the levels of low concentration signals in the spectral data to be detected. This scaling method is very useful when variables have a broad range of variance and are not directly comparable. However, scaling to unit variance could sometimes make models prone to artefacts generated by noise. Therefore, it is not typically used for UPLC-MS data. Instead, PAR scaling method is normally used for UPLC-MS data. In PAR scaling method, each variable is divided by the square root of its standard deviation. This method is compromising between no scaling and UV scaling. PCA compresses a large data set by reducing dimensionality without much loss of information. It defines an axis of the first principal component (PC1) through the mean centre of the data and minimises the square of the distance of each point to that axis, which is also called the coordinate value, or scores represented by t_b where b is the number of the component. The first component, in other words, expresses the maximum variation in the data. Then, the second principal component (PC2) must meet three criteria; 1) it must pass through the centre point; 2) it must be orthogonal to the first component; and 3) it must best describe the data set using the remaining variables. The subsequent components in the same model follow the same rules and it is hence that all components occur in an order of significance. In case that a 2-D plane is defined by PC1 and PC2, all data points representing all observations are projected onto this plane and the resulting diagram is called scores plot, where the points in the same cluster sharing the similarity. The corresponding loading plot ($p_{b,}$ where b is the number of the component) illustrates variables influencing the score plot, revealing information on the relationship between the patterns of similarities or differences in the scores plot and suggesting the discriminatory metabolites between the two discrete conditions (Worley & Powers, 2012; Abdi & Williams, 2010).

1.5.4.2 Projection to latent structures (PLS) and orthogonal signal correction PLS (O-PLS)

PLS, extensively used regression modelling, comprises X matrix (*e.g.* NMR spectral data) and Y matrix, representing quantitative values or some sorts of measurement of responses. PLS model indicates the linear connection between data set X and the corresponding response Y. The systematic variation in matrix X, which are not related to matrix Y, however, introduces some noise into the model and may compromise the strong and distinct correlation between the two matrices, resulting in concealing the metabolite biomarkers. O-PLS is an optimized method based on PLS. It applies the data filtering algorithm to the data set before conducting PLS analysis. The orthogonal signal correction is a mathematical tool, which can remove or suppress the systematic variations from matrices X and Y that are non-relevant to the correlation of X and Y. O-PLS helps separate the systematic variation in matrix X into a linear correlation to Y, and a non-correlation to Y by adding orthogonal components (Trygg & Wold, 2002).

1.5.4.3 Projection to latent structures-discriminant analysis (PLS-DA) and O-PLS-DA

PLS-DA is a special case of PLS and it addresses the separation between the discrete classes by the use of class membership indicator in matrix Y. Y contains quantitative values defining two or more classes encoded in discrete fashion. PLS-DA method gives a maximum separation of observations in matrix X based on the classification information in matrix Y. O-PLS-DA is the extension of PLS-DA approach and the O-PLS-DA models remove or suppress the variations that is uncorrelated to classification indicated in Y (Cloarec *et al.*, 2005).

1.6 16S ribosomal RNA (rRNA) sequencing

The microbiota have been shown to play an important role in diverse biological processes including immunity, metabolism, and digestion. Assessing the exact composition of the microbiota has proven challenging due to the unknown growth specificities of its members, and culture-based approaches typically fail to capture the complete diversity of microorganisms. 16S ribosomal RNA (rRNA) sequencing is a common amplicon sequencing approach used to identify and compare bacteria within a given sample. 16S rRNA gene sequencing is a well-established method for studying phylogeny and taxonomy of samples from complex microbiomes or environments such as gastrointestinal tract (Shah *et al.*, 2011).

Ribosomes are complex organelle found in all living cells, which is involved in protein synthesis machinery. Ribosome consists of two subunits, each of which is composed of protein and a type of RNA, known as ribosomal RNA (Anon, 1972). Prokaryotic ribosomes consist of 30S subunit (small sub unit) and 50S subunit (large sub unit), where S stands for Svedberg unit, a non-SI unit for sedimentation rate. 30S subunit is composed of 16S ribosomal RNA and 21 polynucleotide chains, while 50S subunit is composed of two rRNA species, the 5S and 23S rRNAs (Malhotra, 2002). The presence of hypervariable regions in the 16S rRNA gene gives a species-specific signature sequence, which is useful for bacterial identification process. As a result, 16S rRNA gene sequencing has become prevalent in microbiology and microbial ecology as a rapid and accurate alternative to phenotypic methods of bacterial identification (Janda & Abbott, 2007).

The 16S rRNA sequencing experiment is typically carried out using 454 pyrosequencing, specifically 454 Genome Sequencer FLX machine, amplicons (sequence reads) of one or two tandem variable 16S rRNA gene regions are quantified and subsequently assigned to microbial phylogenies and hence to taxonomies. The Illumina genome analyzer instruments could routinely produce more than ten times the number of reads per run compared with the 454 Genome Sequencer FLX platform, albeit of much shorter

lengths, typically between 100 and 150 bp. Briefly, by extracting the entire DNA content of a microbiota sample and performing a targeted high-throughput sequencing of the 16S rRNA gene, a phylogenetic marker for prokaryotes, prediction of the composition of the entire bacterial community is made possible (Rapin *et al.*, 2017).

1.7 Research aims and objectives

The overall aim is to investigate the host-microbial interactions in obesity, bariatric surgery and caloric restriction using a Zucker obese rat model.

Objectives are as below:

1) To investigate obese phenotype- and lean phenotype-specific metabolic profiles in biofluids (urine, faecal extracts, peripheral and portal vein plasma) of Zucker rat model (Chapter 3);

2) To investigate metabolic profile alterations in biofluids (urine, faecal extracts, peripheral and portal vein plasma) post-RYGB surgery or caloric restriction in hyperinsulinemic obese Zucker rat model (Chapter 4);

3) To investigate metabolic profile alterations in gastrointestinal contents (gastric, duodenal, upper-jejunal, lower-jejunal, ileal and colonic contents) post RYGB surgery or caloric restriction (Chapter 5);

4) To investigate changes in gut microbial composition of gastrointestinal contents (gastric, duodenal, upper-jejunal, lower-jejunal, ileal and colonic contents) post RYGB surgery or caloric restriction in hyperinsulinemic obese Zucker rats (Chapter 5);

5) To integrate the key metabolites with the microbial profiles to investigate mammalian-microbial interactions following RYGB surgery (Chapter 5).

2. Methodology

This chapter describes study design and standard procedures for sample collection for ^{1}H NMR spectroscopy analysis and ultra-performance liquid chromatography mass-spectrometry, together with general parameters availed in multivariate statistical analysis of spectroscopic data. Furthermore, 16S rRNA gene Illumina MiSeq sequencing of intestinal content samples are also mentioned in this chapter.

2.1 Study design

Thirty-one obese (*fa/fa*) and five lean (*fa/+*) male Zucker rats were housed individually and maintained under standard housing conditions of a 12h/12h light/dark cycle provided access to standard chow and water *ad libitum*. All experiments complied with the Animal (Scientific Procedure) Act 1986. Preoperatively, all animals were acclimatised for 2 weeks. Thirty one obese Zucker (fa/fa) rats were randomised into four groups: (1) RYGB-operated rats (RYGB, n =11); (2) sham-operated rats on *ad libitum* feeding (sham-obese, n = 5); (3) sham-operated with food restriction to match the body weight of the RYGB group (sham-BWM, n = 5); and five lean Zucker rats were also included as lean control. All operation procedures were performed by Dr Florian Seyfried (Department of Surgery, University of Wuerzburg, Germany). In brief, rats were anaesthetized using isoflurane (4% for induction, 3% for maintenance). The abdomen was shaved and a midline laparotomy was performed. The Sham-surgery comprised a gastrectomy (7mm) on the anterior wall of the stomach, which was subsequently closed, followed by a jejunotomy (7mm) which was subsequently closed. The RYGB procedure consisted of creating a small gastric pouch from the stomach and bypassing the remaining stomach and the duodenum (termed the 'biliopancreatic' limb) to form a Y-shaped structure. This structure was completed through the attachment of the biliopancreatic and alimentary limbs with a 10 cm common channel. Urinary and faecal samples were collected at pre-operation and 1,2 and 3 weeks post-operation and directly stored at -80 °C. At 3-week post-operation, the peripheral and portal vein blood were collected into lithium heparin vials

and centrifuged at ~2,400 x *g* for 20 minutes to obtain plasma which was snap-frozen at -80°C. In addition, gastrointestinal (GI) contents obtained from stomach, duodenum, upper-jejunum, lower-jejunum, ileum and colon were collected, snap-frozen and stored at -80°C.

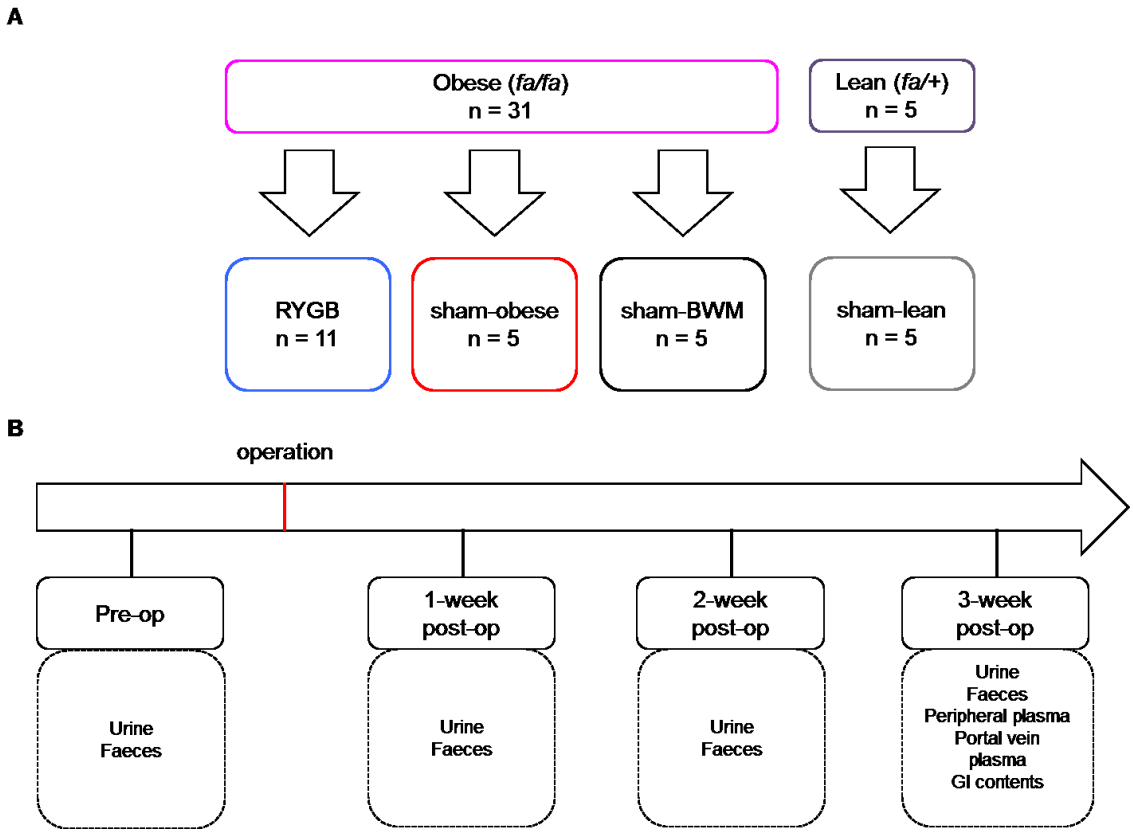


Figure 2-1. Schematic diagrams illustrate (A) study design and (B) sample collection.

2.2 Body weight and food intake measurement

Animals and food were weighed on a daily basis during the experiment, using a Mettler balance with an accuracy of 0.1 g (Im Langacher, Switzerland).

2.3 Measurement of oral glucose tolerance, glucose and fasting insulin

An oral glucose tolerance test (OGTT) was performed at the beginning of the dark cycle in all animals. In order to avoid oral gavage and therefore to reduce discomfort and pressure on the upper anastomosis, animals were trained to drink 10 ml/kg body weight of a 25% glucose solution within 10 min after an overnight fast on two occasions before the OGTT was performed. After an 8 hour overnight fast, blood glucose was measured

(Breeze 2® glucometer, Bayer, Zurich, Switzerland) in conscious rats at baseline, and 15, 30, 60 and 120 minutes after glucose ingestion. Blood was obtained from the tail vein by a small incision. A drop of blood (approximately 1 µL) was applied directly to a glucometer and 100 µl were collected at each time point in tubes containing EDTA and a dipeptidyl peptidase-4 inhibitor. The plasma fraction was separated by centrifugation at 4°C, 8000 rpm and stored at -80°C. Total insulin was measured using the Ultrasensitive Rat Insulin ELISA (Merodia AB, Sweden 10-1251-10).

2.4 Measurement of pH

pH of gastrointestinal samples were measured using a pH meter (Thermo Scientific Orion) connected with a microprobe. The pH meter was calibrated for pH 4 – pH 10. Following the calibration, the microprobe was placed in the sample until the measure was obtained. The probe was then rinsed with deionised water before using with the subsequent sample.

2.5 Sample preparation for ^{1}H NMR analysis, pre-processing and statistical analysis of ^{1}H NMR spectral data

During sample preparation and ^{1}H NMR spectral data acquisition, samples were randomised in order to reduce the confounding effect of any potential systemic time-related variation in experimental factors, for example variation in room temperature. The sample preparation steps for ^{1}H NMR analysis used throughout the study are all validated in-house protocols (Beckonert *et al.*, 2007a; Dona *et al.*, 2014).

2.5.1 ^{1}H NMR spectroscopy-based metabolic profiling of faecal water

Approximately 250 mg of homogenised faecal samples were mixed with 500 µL HPLC-grade water in 1.5 mL microtubes. The mixtures were sonicated for 3 x 10 minutes at 25°C and vortexed when each sonication cycle is completed. The mixtures were centrifuged at 16,000 x *g* for 10 min at 4°C. A total of 400 µL faecal water extract was transferred into a clean 1.5 mL microtubes and mixed with 250 µL of 0.2 M sodium

phosphate buffer (100% D_2O, 0.01% TSP (3-(trimethylsilyl)propionic-2,2,3,3-d_4 acid sodium salt) as a chemical shift reference, and 3 mM sodium azide (NaN_3) as a bacteriostatic reagent, pH 7.4). The mixture was vortexed and centrifuged at 16,000 x *g* for 10 min at 4°C and 600 µL of supernatant was transferred into NMR tube with an outer diameter of 5 mm.

^{1}H NMR spectra of all faecal samples were acquired using a 600 MHz spectrometer (Bruker Avance III, Bruker Biospin, Germany) with 5 mm broadband inverse configuration probe with a z axis magnetic field-gradient capability operating at 600.13 Mhz for proton. D_2O solvent in the sample buffer was used to lock the magnetic field. A standard 1-dimensional (1-D) NMR pulse [recycle delay (RD)-90°-t_1-90°-t_m-90°-acquire free induction decay (FID)] was employed at 300 K for the acquisition of faecal water spectra. A total of 128 scans were recorded into 64 k data points with a spectral width of 20 ppm.

2.5.2 ^{1}H NMR spectroscopy-based metabolic profiling of urine samples

Urine samples were prepared by combining 400 µL of urine with 250 µL of 0.2 M sodium phosphate buffer (100% D_2O, 0.01% TSP, and 3 mM sodium azide (NaN_3), pH 7.4). The mixture was vortexed and centrifuged at 16,000 x *g* for 10 min at 4°C and 600 µL of supernatant was transferred into NMR tube with an outer diameter of 5 mm pending for NMR analysis.

^{1}H NMR spectra of all urinary samples were acquired using a 600 MHz spectrometer (Bruker Avance III, Bruker Biospin, Germany) with 5 mm broadband inverse configuration probe with a z axis magnetic field-gradient capability operating at 600.13 MHz for proton. D_2O solvent in the sample buffer was used to lock the magnetic field. A standard 1-dimensional (1-D) NMR pulse [recycle delay (RD)-90°-t_1-90°-t_m-90°-acquire free induction decay (FID)] was employed at 300 K for the acquisition of urine spectra. A total of 128 scans were recorded into 64 k data points with a spectral width of 20 ppm.

2.5.3 ^{1}H NMR spectroscopy-based metabolic profiling of plasma samples

Plasma samples were first vortexed before 400 µL was combined with 250 µL of saline solution (0.9% NaCl w/v, 20% D_2O). The mixture was vortexed and centrifuged at 16,000 x *g* for 10 min at 4 °C before 600 µL of the supernatant was transferred to a 5 mm outer diameter NMR tube. A Carr−Purcell−Meiboom−Gill (CPMG) pulse sequence [RD−90°−(ƭ−180°−ƭ)n−acquisition] was applied to plasma samples at 310 K (2ƭn=76.8 ms) in order to improve the visualization of signals generated from low molecular weight metabolites. A total of 32 scans were recorded into 72 k data points with a spectral width of 20 ppm.

2.5.4 Pre-processing of ^{1}H NMR spectra

^{1}H NMR spectra obtained from the rat samples were automatically pre-processed in TopSpin 3.1 software which included phasing, baseline correction and referencing to TSP peak in urinary and faecal spectra at δ^{1}H 0 or the anomeric proton from α-glucose at δ^{1}H 5.223 in plasma spectra.

The high resolution integration of peaks in the spectra creates huge data matrices which require powerful software; MATLAB (MathWorks) has been employed in this study. The NMR spectra were subsequently transferred into MATLAB software and digitised into 20 k data points with a resolution of 0.0005 ppm using a script developed in-house by Dr Olivier Cloarec at Imperial College London. The water peak was excised from urinary (δ^{1}H 4.72 and 4.90), faecal (δ^{1}H 4.50 and 5.10) and plasma (δ^{1}H 4.50 and 5.10) spectra in order to minimise the effect of the remaining baseline distortion caused by imperfect water suppression. In addition, regions between δ^{1}H 5.45 and 6.15 containing urea signals were removed from urinary spectra. Citrate (δ^{1}H 2.48 and 2.70) was removed from plasma spectra. If these regions of the spectra were not removed it would confound the multivariate statistical analysis.

Following the import of acquired and pre-processed spectra into MATLAB and the removal of uninformative regions, the spectral peaks were aligned to adjust for shifts in peak position due to small pH differences between samples.

2.5.5 Multivariate statistical analysis of ^{1}H NMR spectral data

The resulting NMR spectra were imported into SIMCA 14.0 (Umetrics) to conduct principal component analysis (PCA) with a unit variance (UV) scaling method, followed by an orthogonal signal correction-projection to latent structures-discriminant analysis (O-PLS-DA) in MATLAB (R2014a) environment using in-house developed scripts. MATLAB was used to generate O-PLS-DA coefficient plots, with a colour visualization of correlation values (r2) of each variable. Red colour indicates higher correlation whilst blue indicates lower correlation of the variables with the classification. The fitness and predictability of the models obtained from OPLS-DA were determined by the R2 and Q2 values, respectively. The O-PLS-DA models in the current study were established based on one PLS component and one orthogonal component using mean-centred and UV-scaled spectral data sets. Metabolic profiles of urine, faeces at all time points and peripheral plasma at the last time point from both lean and obese Zucker rats were correlated with body weight using O-PLS regression analysis. Fasting insulin levels from all groups were statistically correlated with urinary and faecal profiles at the last time point, and the portal vein and peripheral plasma profiles using O-PLS regression analysis. The validation of all O-PLS-DA and O-PLS models involved in this study was assessed using 1,000-times permutation test. To assist metabolite assignment, J-resolved spectroscopy (JRES) was carried out along with the use of in-house and public databases (Wishart *et al.*, 2018) and previously published literatures (Beckonert *et al.*, 2007b; Foxall *et al.*, 1993; Nicholson *et al.*, 1984). Further assignment of metabolites was also accomplished with the use of statistical total correction spectroscopy (STOCSY) on 1-D spectra.

2.5.6 Univariate statistical analysis of selected ^{1}H NMR metabolites

Selected metabolites were integrated using an in-house MATLAB script written by Dr Jake Thomas Midwinter Pearce (Imperial College London). Resonances to be integrated were carefully selected such that no other peaks overlapped with the peak of interest. In addition, variation in integral width and baseline between samples was avoided so as not to confound the relative spectral intensities obtained.

Univariate statistical analysis was performed on the integral values using R 3.1.0. When data from two groups were compared, a two-tailed heteroscedastic t-test with Benjamini-Hochberg FDR correction was used to identify the statistical significance of differences between the groups.

2.6 Ultra-performance liquid chromatography mass-spectrometry

2.6.1 Aqueous and organic metabolite extraction

Aqueous and organic metabolite extraction in this study was performed based on the optimized standard procedure previously developed by Dr Panagiotis Vorkas (Imperial College London). In brief, approximately 150 mg of intestinal contents obtained from stomach, duodenum, upper-jejunum, lower-jejunum, ileum and colon, along with faeces were weighed out and individually loaded into bead beating tubes (Percellys) filled with zirconia beads. A prechilled methanol (MeOH)/water solution (1:1) was added to the samples. The volume of the solution was adjusted according to weight of the sample starting up to a maximum weight with 1.5 mL, and reduced proportionally to sample weight (100 µL of solvent/28 mg of sample). Aqueous metabolite extraction was performed using a bead beater (Bertin Technologies) after freezing on dry ice. The bead beater was set to 6500 Hz for 40 s with another 2 cycles were performed separated by freezing of the samples on dry ice. Bead beating was followed by centrifugation (Eppendorf, Centrifuge 5417R, Germany) at 13000g for 20 min, at 4°C. Aliquots of 100 µL (25 mg of tissue/100 µL of aliquot) of the supernatant were obtained into

microcentrifuge tubes. Samples were spun in a vacuum concentrator for 3 h at 45°C (Eppendorf Concentrator Plus, V-AQ mode) until dry and stored at -40°C.

Following aqueous extraction, a solution of prechilled dichloromethane (DCM)/MeOH (3:1) was added to the residual pellet. The volume of the solution was proportional to the sample weight as described in previous paragraph. Samples were frozen on dry ice and reloaded into the bead beater (2 cycles, 6500 Hz, 40 s). Samples were centrifuged at 13000g for 20 min, and 100 µL (25 mg of tissue/100 µL of aliquot) of organic phase supernatant was subsequently aliquoted into glass vials. Samples were allowed to evaporate at room temperature in extractor hood overnight and stored at -40°C prior to analysis.

2.6.2 HILIC-UPLC-MS analysis of aqueous extracts

The aqueous extracts were reconstituted in 200 µL of water and 150 µL of mixture was transferred into the capillary individually placed in the glass vial and 40 µL was transferred into the Total Recovery vials (Waters Corp, USA) after centrifugation for 20 min at 13000g, 4°C.

UPLC separation was conducted using an Acquity UPLC System (Waters Corp, USA). An Acquity UPLC BEH HILIC 2.1 X 100 mm, 1.8 µm, column (Waters Corp, USA) was used. Column temperature was set at 35°C. Mobile phase A consisted of acetonitrile (ACN)/water (95:5) and mobile phase B CAN/water (50:50). In both solutions ammonium acetate was diluted to 10 mM and formic acid to 0.1%. The elution gradient was set as follows: 99% A (0.0-2.0 min; 0.4 mL/min), 99-45% A (2.0-8.0 min; 0.4 mL/min), 45-1% A (8.0-9.0 min; 0.4 mL/min), 1% A (9.0-9.1 min; 0.4-0.8 mL/min), 1% A (9.1-11.0 min; 0.8 mL/min), 1-99% A (11.0-11.1 min; 0.8 mL/min), 99% A (11.1-19.0 min; 0.8 mL/min), 99% A (19.0-19.1 min; 0.8-0.4 mL/min), 99% A (19.1-23.0 min; 0.4 mL/min). An injection volume of 5 µL was used for both positive and negative ionisation polarity modes. The autosampler was set at 4°C. Mass spectrometry was performed using a Xevo G2 QTof (Waters MS Technologies, U.K.) with an electrospray ionisation (ESI) source. Scans

were acquired with scan time of 0.2 s and interscan time of 0.02 s. Leucine enkephalin (0.25ng/μL, 50% ACN, 0.1% FA) was used for lock mass correction. Lock mass data were collected with scan time of 0.20 s and scan frequency of 30 s. Conditions in positive mode: m/z range: 50-1000, cone voltage 30C, capillary voltage 3KV, source temperature 120°C. desolvation temperature 400°C, desolvation gas Flow 800L/h. Conditions in negative mode: m/z range: 50-1000, cone voltage 30C, capillary voltage 2.5KV, source temperature 120°C, desolvation temperature 350°C, desolvation gas 800L/h.

A standard QC strategy was used for UPLC-MS analysis. In brief, a pooled sample (Quality Control Sample, QC) of the reconstituted extracts was prepared. This sample was injected 10 times prior to initiating the run, in order to condition the column. The sample was reinjected once at the beginning, every 10 sample injections, and at the end of the run to assess instrument stability and analyte reproducibility. In addition, the extraction blank sample was also reconstituted in the same manner as other samples and run in order to assess the constituents and impurity of the extraction solvent.

Metabolite assignments were performed based on five levels of assignment: 1) accurate mass matched to database, 2) accurate mass matched to database and tandem MS spectrum matched to *in silico* fragmentation pattern, 3) tandem MS spectrum matched to database or literature, 4) retention time and the molecular mass matched to standard compound, and 5) MS/MS spectrum matched standard compound.

2.7 Community analysis of microbiota contained in the intestinal contents of stomach, duodenum, upper-jejunum, lower-jejunum, ileum and colon together with faeces using 16S rRNA gene Illumina MiSeq sequencing

2.7.1 Isolation of DNA from gastrointestinal content and faecal samples

Bacterial genomic DNA was isolated from gastrointestinal content and faecal samples using a PowerFecal® DNA isolation kit (MOBIO Laboratories, Inc., USA). A total weight of approximately 0.25 g was transferred to the prefilled-dry bead tube followed by the

addition of 750 µL of bead solution and 60 µL of solution C1 containing sodium dodecyl sulphate (SDS) prior to homogenisation and cell lysis. The mixture was heated at 65 °C for 10 minutes and subsequently bead-beaten at 5500 Hz for 2 cycles x 20 seconds. The mixture was centrifuged at 13,000 x g for 1 minute and approximately 400 µL of supernatant was transferred to a clean 2 ml collection tube.

2.7.2 Illumina MiSeq sequencing

DNA sequencing was undertaken by Research and Testing Laboratory (Austin, Tex) using the Illumina MiSeq. In brief, to determine the diversity and structure of the bacterial communities in different samples, the protocol as previously described by Caporaso et al (2011) was used. PCR amplifications were performed with the primers 515F (5-GTGCCAGCMGCCGCGGTAA-3') and 806R (5-GGACTACHVGGGTWTCTAAT-3'), which contains a 6-bp error-correcting barcode unique to each sample, for the V4 region of the 16S rRNA gene. The PCR products from different samples were quantified using a Qubit 2.0 fluorometer (Invitrogen, Carlsbad, CA) and mixed accordingly to achieve the equal concentration in the final mixture, which was used to construct PCR amplicon libraries. To minimize the impact of potential early round PCR errors, twenty independent PCR products for each sample were combined to construct PCR amplicon libraries. Sequencing was performed on an Illumina MiSeq platform.

2.7.3 Phylogenetic identification and data analysis

The 16S rRNA gene sequences were analyzed using the bioinformatics software package Mothur and the MiSeq SOP Pipeline. 16S rRNA gene sequence reads were quality checked and normalized to the lowest number of reads in Mothur. To maintain normalization and minimize artifacts, singletons and any Operational Taxonomic Units (OTUs), which were not found on more than 454 occasions in any sample, were collated as OTU singletons and OTU_rare phylotypes. Using the Vegan package of the R

statistical package, analysis was performed on the data sets contained within the files generated by Mothur (all OTUs were defined using a cutoff value of 97%). The Unifrac-weighted distance matrix was analyzed in R using nonmetric multidimensional scaling ordination and the shared OTU file was used to determine the number of times that an OTU was observed in multiple samples, and was used for multivariate analysis in R. Operational Taxonomic Unit taxonomies (from phylum to genus) were determined using the RDP MultiClassifier script to generate the RDP taxonomy. Alpha and beta indices were calculated from these datasets with Mothur and R using the Vegan package.

3. Global Metabolic Profiling of Peripheral and Portal Vein Plasma, Urine and Faecal Water in the Lean and Obese Zucker Rats

3.1 Aim

The global aim of this study was to 1) monitor dynamic changes in urinary and faecal water profiles obtained from obese and lean Zucker rats over 4 weeks; 2) characterise the biochemical composition of the portal vein and peripheral blood, for the first time in Zucker obese animals; and 3) investigate the uptake of the gut microbial metabolites and their systemic circulation and metabolism in the host using ^{1}H NMR spectroscopy in combination with multivariate statistical analyses.

3.2 Materials and methods

Male Zucker obese (fa/fa) and lean control (fa/+) rats (n = 12, per group) were housed individually, maintained under standard animal housing conditions (a 12h/12h light/dark cycle, ambient humidity and 22 °C), and provided access to standard chow and water ad libitum. Animals were acclimatised for two weeks prior to the onset of the experiment. Urinary and faecal samples were collected weekly using metabolic cages (Techniplast®) during the dark cycle (12 hours) over a 4-week period and directly stored at -80 °C. At week 4, the peripheral and portal vein blood were collected into a sodium heparin-coated tube and spun at 4 °C at 3600 g for 10 mins to obtain plasma, which was snap-frozen and stored at -80 °C. Measurement of body weight, food intake, oral glucose tolerance test and fasting insulin, preparation for ^{1}H NMR spectroscopy analysis and spectroscopic data analyses have been described in Chapter 2.

3.3 Results

3.3.1 Differences in body weight, food intake, oral glucose tolerance test and fasting insulin between Zucker obese (*fa/fa) and lean (fa/+)* rats

The difference for all the phenotypic traits between lean and obese Zucker rats were measured. The mean body weight of obese rats (fa/fa) was significantly higher than that of lean rats (obese: 499.5 ± 40.9 g vs. lean: 379.5 ± 21.2 g, $p < 0.0001$) as obese rats consumed higher amount of food compared to lean animals over the 4-week study period (obese: 32.5 ± 0.9 g vs. lean: 24 ± 0.5 g, $p < 0.0001$, using two-way ANOVA) (Figures 3-1A and 3-1B). Fasting glucose levels measured in serum of obese and lean Zucker rats were remarkably different (obese: 105.8 ± 8.7 mg/dL vs lean: 80.8 ± 3.9 mg/dL, $p = 0.0033$).

Similarly, both glucose and insulin levels were significantly greater in obese rats compared with lean rats during the OGTT (at 15, 30 and 60 mins). At 120 min, the glucose level normalized in obese rats and was comparable with lean rats, the insulin levels, nonetheless, remained higher. The glucose level of obese rats persisted at a high concentration for 1 hour after feeding, whilst in lean rats it started to decrease at 15 min (Figure 3-1C). Obese Zucker rats demonstrated significantly higher fasting insulin levels (1334.0 ± 134.2 pmol/L) than lean rats (135.7 ± 17.6 pmol/L, $p < 0.001$) (Figure 3-1C).

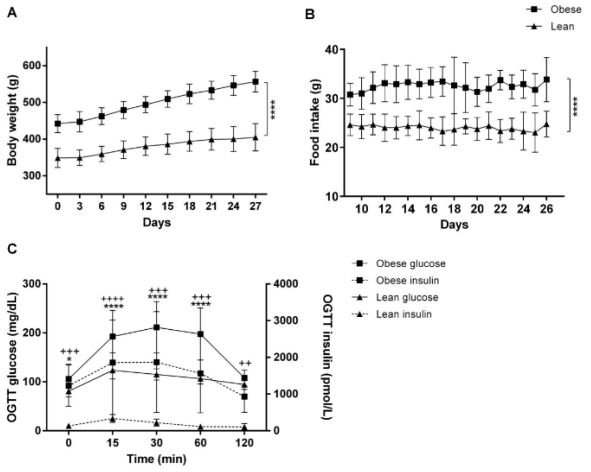


Figure 3-1. Measurements of body weight, food intake, and OGTT glucose and insulin levels. (A) Measurement of body weight; (B) food intake, data are shown as mean ± SD (**p < 0.0001) and statistical differences determined by two-way ANOVA and (C) oral glucose tolerance test (OGTT) of lean and obese Zucker rats (n=12 per group). OGTT glucose (solid line) and insulin (dashed line) measurements of Zucker rats. Data are shown as mean ± SD**

(*p < 0.05; ****p < 0.0001 of OGTT glucose and ++p < 0.01; +++p < 0.001; ++++p < 0.0001 of OGTT insulin by two-way ANOVA).

3.3.2 Urinary metabolic profiles of obese (fa/fa) and lean (fa/+) Zucker rats

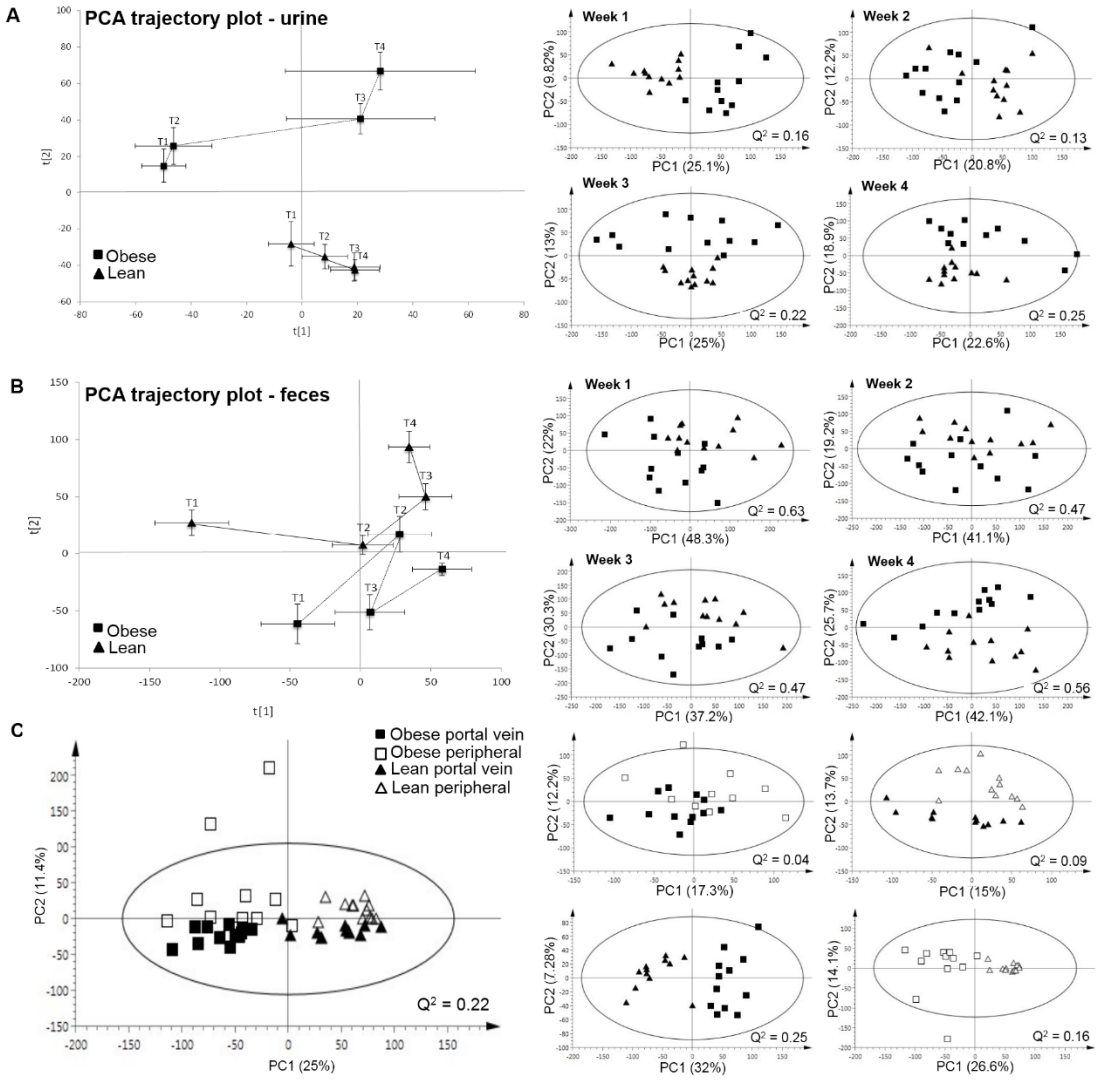


Figure 3-2. Principal component analysis of biofluid metabolic profiles. Principal component analysis of urinary (A), faecal (B) metabolic profiles of obese and lean Zucker rats over 4-week period and of obese peripheral, lean peripheral, obese portal vein and lean portal vein blood plasma (C) metabolic profiles at week 4. PCA trajectory scores plot of urinary and faecal data sets obtained from the average scores of PC1 against PC2 of each strain of rat at a particular time point and error bars are expressed by the standard error of mean of PC1 and PC2 of each time point. Percentage on each PC represents variation explained by each principal component and Q2 represents predictive ability of the model.

A global urinary metabolite profile shift of both lean and obese rats was observed over a 4-week period, revealing in the PCA trajectory scores plot as a time-related shift along the first principal component (PC1) and a separation of obese rats from lean rats along the second principal component (PC2) (Figure 3-2A). PCA scores plots based on each

discrete time point illustrated distinct clustering of the two groups of rats along PC1 or PC2 (Figure 3-2A). This indicates that the two strains could be discriminated from the first time point and the metabolic difference persisted over the entire period of the study. O-PLS-DA analysis was employed to investigate the discriminatory metabolites between the obese and lean classes at each time point (Table 3-1). The loadings of the pairwise O-PLS-DA models identified significantly higher concentrations of urinary 2-hydroxyvalerate, 2-hydroxybutyrate, 2-ketoisocaproate, methylmalonate, *N*-epsilon-acetyllysine, *N*-acetylcysteine, 4-cresyl glucuronide, creatinine, proline, allantoin, indoxyl sulfate (IS) and unknown 3 (δ^1H 8.08 (s); δ^1H 8.57 (s)) in the lean Zucker rats, while higher concentrations of 1-methylnicotinamide, unknown 1 (δ^1H 0.91 (s); δ^1H 1.73 (t)) and unknown 4 (δ^1H 8.32 (d, ***J***=2.65)) levels were found in urinary samples of obese rats. The relative concentrations of 2-hydroxybutyrate, methylmalonate, creatinine, proline and phenylacetylglycine (PAG) were consistently lower in obese rats over a 4-week period, whilst other metabolites such as 2-hydroxyvalerate, 2-ketoisocaproate were discriminating features at two or three time points. The O-PLS regression model of urinary profiles against insulin levels was invalid (R^2X=7.91%; Q^2Y=0.11, CV-ANOVA p=0.102). However, O-PLS regression analysis (R^2X=24.8%, Q^2Y=0.66, CV-ANOVA p<0.001) of urinary metabolic profiles against body weight demonstrated that 1-methylnicotinamide was positively correlated with body weight, whereas metabolites such as 4-cresyl glucuronide, creatinine, PAG and IS were inversely correlated with body weight (Table 3-1).

Table 3-1. Summary of metabolic changes in urinary (u) and faecal (f) ^{1}H NMR profiles

Metabolites	Chemical shift	O-PLS-DA models of obese and lean Zucker rats								O-PLS regression
		Week 1 (u):R^2X=32.9%, Q^2Y=0.92, p = 0.001 (f):R^2X=69.2%, Q^2Y=0.48, p = 0.001		Week 2 (u):R^2X=30%, Q^2Y=0.59, p = 0.001 (f):R^2X=54.8%, Q^2Y=0.38, p = 0.005		Week 3 (u):R^2X=30.3%,Q^2Y=0.65, p = 0.001 (f):R^2X=60%, Q^2Y=0.39, p = 0.018		Week 4 (u):R^2X=33.5%,Q^2Y=0.85, p = 0.001 (f):R^2X=66%, Q^2Y=0.71, p = 0.001		Body weight[b] (u):R^2X=24.8%,Q^2Y=0.66, p = 0.001 (f):R^2X=75.3%, Q^2Y=0.57, p = 0.001
2-hydroxyvalerate	0.84 (t)	-0.9057 (u)	****	-0.7163 (u)	***					
2-hydroxybutyrate	0.86 (t); 1.60 (m); 1.71 (m)	-0.9201 (u)	****	-0.7458 (u)	***	-0.6820 (u)	**	-0.7903 (u)	***	-0.6461 (u)
Butyrate	0.90 (t); 1.56 (m); 2.16 (t)	+0.8140 (f)	****	+0.6433 (f)	**			+0.6218 (f)	**	
Unknown1	0.91 (s); 1.73 (t)	+0.8330 (u)	***	+0.8093 (u)	***	+0.5626 (u)	**	+0.9016 (u)	****	+0.6234 (u)
2-ketoisocaproate	0.94 (d); 2.08 (m); 2.60 (d)	-0.7609 (u)	**			-0.7675 (u)		-0.7728 (u)		-0.6544 (u);
Leucine	0.96 (t); 1.71 (m)									-0.4898 (f)
Isoleucine	1.00 (d); 0.92 (t)									-0.5066 (f)
Valine	0.99 (d); 1.02 (d)					-0.6779 (f)				-0.5208 (f)
Propionate	1.06 (t); 2.19 (q)							+0.8248 (f)	****	+0.5425 (f)
Methylmalonate	1.26 (d)	-0.7644 (u)	****	-0.633 (u)	**	-0.7353 (u)	***	-0.8301 (u)	**	-0.6991 (u)
Lactate	1.33 (d); 4.11 (q)					+0.7036 (f)	**	+0.6808 (f)	***	
Acetate	1.92 (s)					+0.6865 (f)	**	+0.7308 (f)	****	
N-epsilon-acetyllysine	1.99 (s)		***	-0.6556 (u)	*			-0.7728 (u)	****	-0.6013 (u)
N-acetylcysteine[a]	2.05 (s)	-0.8774 (u)		-0.7045 (u)				-0.9080 (u)	***	-0.786 (u)
N-acetylglucosamine	2.06 (s); 5.21 (d)	-0.7761 (f)	**							
4-cresyl glucuronide	2.30 (s); 7.05(d); 7.2 (d)	-0.7002 (u)	***	-0.7132 (u)	**			-0.7848 (u)	****	-0.537 (u)
3-hydroxyphenyl propionic acid	2.47 (t); 2.84 (t); 7.25 (t); 6.76 (dd); 6.8 (s); 6.88 (d)							+0.7289 (f)	****	
Creatinine	3.04 (s); 4.05 (s)	-0.9108 (u)	****	-0.7776 (u)	****	-0.7739 (u)	****	-0.9007 (u)	****	-0.6284 (u)
Glycine	3.57 (s)	-0.6152 (f)						-0.6299 (f)		
Glycerol	3.58 (dd); 3.65 (dd)	0.6814 (f)				+0.6814 (f)	**	+0.7366 (f)	***	
Proline	4.14(d); 2.33 (m); 2.02 (m); 3.32 (m); 3.42 (m)	-0.8475 (u)	*	-0.8074 (u)	*	-0.6930 (u)	**	-0.7479 (u)	**	
1-methylnicotinamide	4.48 (s); 8.19 (t); 8.90 (d); 8.96 (d); 9.28 (s)	+0.8902 (u)	****	+0.8106 (u)	****			+0.7993 (u)	****	+0.5188 (u)
Allantoin	5.40 (s)					-0.7194 (u)		-0.8457 (u)		-0.6842 (u)
Unknown2	5.64 (d); 8.57 (s)	-0.7663 (f)	**							-0.5252 (f)
Cytosine	5.97 (d); 7.51 (d)							+0.8190 (f)	****	+0.5498 (f)
Phenylacetylglycine	7.42 (m); 7.35 (m); 3.66 (s); 3.74 (d)	-0.6697 (u)	**	-0.6723 (u)	**	-0.5228 (u)	*	-0.7809 (u)	****	-0.5421 (u)
Indoxyl sulfate	7.36 (s); 7.50 (d); 7.69 (d); 7.21 (t); 7.27 (t)	-0.8275 (u)	***	-0.7128 (u)	*			-0.7515 (u)	****	-0.6746 (u)
Unknown3	8.08 (s); 8.57 (s)							-0.7812 (u)	***	
Unknown4	8.32 (d, *J*=2.65 Hz)	+0.8806 (u)	****	+0.7187 (u)	*	0.6871 (u)	**	+0.8683 (u)	****	+0.592 (u)

"+" indicates higher correlation in obese Zucker rats, whereas "–" indicates higher correlation in lean Zucker rats. Abbreviations: s, singlet; d, doublet; dd, double of doublets; t, triplet; bs, broad singlet; m, multiplet; q, quartet. [a]Database in Chenomx. [b]"+" indicates higher correlation of metabolites with increasing body weight, whereas "– "indicates higher correlation with decreasing body weight. *, **, * and **** indicate significant levels of metabolite differences between lean and obese Zucker rats of each time point at p<0.05, p<0.01, p<0.001 and p<0.0001, respectively using two-tailed heteroscedastic t-test with Benjamini-Hochberg correction. P values of all models were derived from permutation tests (n=1000).**

Table 3-2. Summary of metabolic changes in plasma ^{1}H NMR profiles

Metabolites	Chemical shift	O-PLS-DA models								O-PLS regression models	
		obese peripheral (+)[a] vs. obese portal vein (-) (R^2X=25.7%, Q^2Y=0.71, p = 0.001)		lean peripheral (+) vs. lean portal vein (-) (R^2X=19.9%, Q^2Y=0.79, p = 0.001)		lean peripheral (+) vs. obese peripheral (-) (R^2X=37.8%, Q^2Y=0.88, p = 0.001)		lean portal vein (+) vs. obese portal vein (-) (R^2X=32%, Q^2Y=0.83, p = 0.001)		Peripheral plasma with Body weight[b] (R^2X=37.4%, Q^2Y=0.73, p = 0.001)	Peripheral plasma with Fasting insulin[c] (R^2X=37.2%, Q^2Y=0.63, p = 0.001)
Valine	0.99 (d); 1.02 (d)					-0.6779	*				
Isoleucine	1.00 (d); 0.92 (t)					-0.6462	*	-0.8221			
Propionate	1.06 (t); 2.19 (q)	-0.7762	***	-0.6460	****						
D-3-hydroxybutyrate	1.19 (d); 2.31 (dd); 2.41 (dd)			+0.8581	**						
Lactate	1.33 (d); 4.11 (q)					-0.7229	***				
Alanine	1.48 (d)					+0.8294				-0.5752	
Acetate	1.92 (s)	-0.7003	**	-0.7786	***						
Glutamine	2.14 (m); 2.46 (m)					+0.8759	****	+0.6807	****	-0.7962	-0.8046
Proline	4.14(d); 2.33 (m); 2.02 (m); 3.32	-0.9053		-0.8688							
Pyruvate	2.38 (s)	-0.8901	**	-0.8122	***						
Succinate	2.41 (s)			-0.8920	****			+0.8098	****		-0.5918
Trimethylamine	2.89 (s)	-0.8850	****	-0.7965	****						
Creatine	3.04 (s); 3.93 (s)					+0.6881	***	+0.7818	****		
Malonate	3.12 (s)	-0.7522	****	-0.9043	****	+0.7442	***	+0.7346	**	-0.713	
Phenylalanine	3.13 (dd); 3.28 (dd); 3.39 (m); 4.00 (dd); 7.39 (m)			-0.8606	****						-0.6763
choline	3.17 (s)	-0.8497	****	-0.8878	***					-0.7368	
2-deoxycytidine	6.03 (d); 6.25 (t); 7.83 (d)					+0.7613	****				
Fumarate	6.53 (s)	-0.8308	*	-0.7770	****						
Tyrosine	3.06 (dd); 3.26 (dd); 3.94 (dd); 6.90 (d); 7.19 (d)			-0.6701	*	+0.7676	****	+0.8388	****	-0.7134	-0.6126
Lipids CH_3-	0.84 (bs)					-0.8515	****	-0.9285	****	+0.8287	+0.749
Lipids $(CH_2)_n$	1.25 (bs)					-0.9319	****	-0.9032	**	+0.8067	+0.7879
Lipids CH_2C=C	2.00 (bs)					-0.7925	***	-0.6962	***	+0.6251	+0.8243
Lipids =C-CH_2-C=	2.76 (bs)					-0.8531	****	-0.9402	****	+0.7805	+0.766
Lipids CH=CH	5.29 (bs)					-0.847	****	-0.914	****		+0.8102

"+" or "–" indicates higher correlation in either group of O-PLS-DA pairwise comparison models. Abbreviations: s, singlet; d, doublet; dd, double of doublets; t, triplet; bs, broad singlet; m, multiplet; q, quatet. [b,c]"+" indicates higher correlation of metabolites with increasing body weight or fasting insulin whereas "– "indicates higher correlation with decreasing body weight or fasting insulin. *, **, * and **** indicate significant levels of metabolite differences between lean and obese Zucker rats of each pairwise comparison at p<0.05, p<0.01, p<0.001 and p<0.0001, respectively using two-tailed heteroscedastic t-test with Benjamini-Hochberg correction. P values of all models were derived from permutation tests (n=1000).**

3.3.3 Faecal metabolic profiles of Zucker obese and lean rats

Clustering of faecal water profiles from obese compared with lean Zucker rats was observed along the PC2 in both the time-related PCA trajectory plot and PCA scores plots at each individual time point (Figure 3- 2B). Faecal profiles of lean and obese rats exhibited a similar degree of variation in the PCA plot that is different from the urinary PCA trajectory. Faecal concentrations of lactate, short chain fatty acids (SCFAs including propionate, acetate, and butyrate), cytosine, and 3-hydroxyphenylpropionic acid (3-HPPA) and glycerol, and lower levels of N-acetylglucosamine, valine and glycine were found in obese rats compared with lean animals (Table 3-1). As with the urinary data, correlation between the faecal metabolites and insulin levels was not robust (O-PLS regression model: R^2X=13.23%, Q^2Y<0, CV-ANOVA p=0.192). However, animal body weight was found to be directly correlated with faecal metabolites including propionate and cytosine, and inversely correlated with BCAAs (*e.g.* leucine, isoleucine and valine) and an unknown metabolite 2 (δ^1H 5.64 (d), 8.57 (s)) (Table 3-1) based on the O-PLS regression analysis.

3.3.4 Metabolic profiles of systemic and portal vein blood plasma from Zucker obese and lean rats

The metabolic differences between obese and lean rats were greater than metabolic changes observed between portal and peripheral blood with the genotypes separating along the PC1 and the peripheral versus portal vein plasma separating along the PC2 (Figure 3-2C). Within the lean or obese group, the peripheral and portal vein plasma metabolite profiles separated, with more distinct clustering observed in lean genotype along the PC2 (Figure 3-2C). A stronger class differentiation between the genotypes in either peripheral or portal vein blood was observed along PC1, with portal vein lean rat plasma samples clustering much tighter. SCFAs (*e.g.* propionate and acetate), metabolites involved in the tricarboxylic acid (TCA) cycle (*e.g.* pyruvate and fumarate), proline, choline, trimethylamine (TMA) and malonate were observed in higher concentrations in portal vein blood compared with the peripheral blood of both obese

and lean animals. Moreover, the portal vein blood of lean rats was shown to carry higher succinate, phenylalanine and tyrosine than the peripheral blood, but these metabolites were not found to differentiate peripheral and portal blood in obese rats. On the contrary, D-3-hydroxybutyrate was significantly higher in peripheral blood plasma compared with portal vein blood in the lean genotype. Both portal and peripheral blood plasma from obese Zucker rats showed higher lipids and isoleucine and lower glutamine, creatine, malonate and tyrosine in contrast to the lean animals. In obese animals, circulating blood plasma BCAAs including valine and isoleucine, and lactate were higher, and 2-deoxycytidine was lower, compared to lean animals. Succinate was found to be higher in the portal vein blood of the lean, compared to obese rats (Table 3-2). O-PLS regression analysis was performed to probe the association between the plasma metabolic phenotype and the concentration of fasting insulin and body weight so the peripheral plasma metabolite profiles were correlated with body weight and fasting insulin levels separately. Both body weight and fasting insulin concentrations were directly correlated with plasma lipid concentrations, whilst glutamine and tyrosine were inversely correlated. Alanine, malonate and choline were inversely correlated with body weight, whereas succinate and phenylalanine were found to inversely correlate with fasting insulin levels.

3.3.5 Inter-compartmental correlation analysis of biofluid metabolites

To probe the inter-correlation among metabolites from three biofluid compartments including urine, faeces and plasma and uncover the differences in these correlation structures between lean and obese rats, correlation matrices were constructed for lean and obese animals separately without clustering to allow the direct comparison between two genotypes (Figure 3-3). The strong inter-correlations of lipid signals and their significantly positive correlation with glycolysis end products including pyruvate, lactate and alanine, 2-ketoisocaproate derived from leucine metabolism, and 4-cresyl glucuronide in the obese rats were the most prominent observations, whereas in lean

animals, only the correlation between lactate and all lipid signals was observed. Furthermore, BCAAs such as valine and isoleucine were positively correlated in obese rats, which were inversely correlated with alanine, pyruvate, IS and PAG and positive correlations between plasma acetate and propionate, and between urinary PAG, IS and 4-cresyl glucuronide were observed in both groups. Nevertheless, these two urinary host-microbial co-metabolites were positively correlated with metabolites, for instance 4-cresyl glucuronide and creatinine in obese rats, and inversely correlated with faecal valine, propionate and acetate in lean animals.

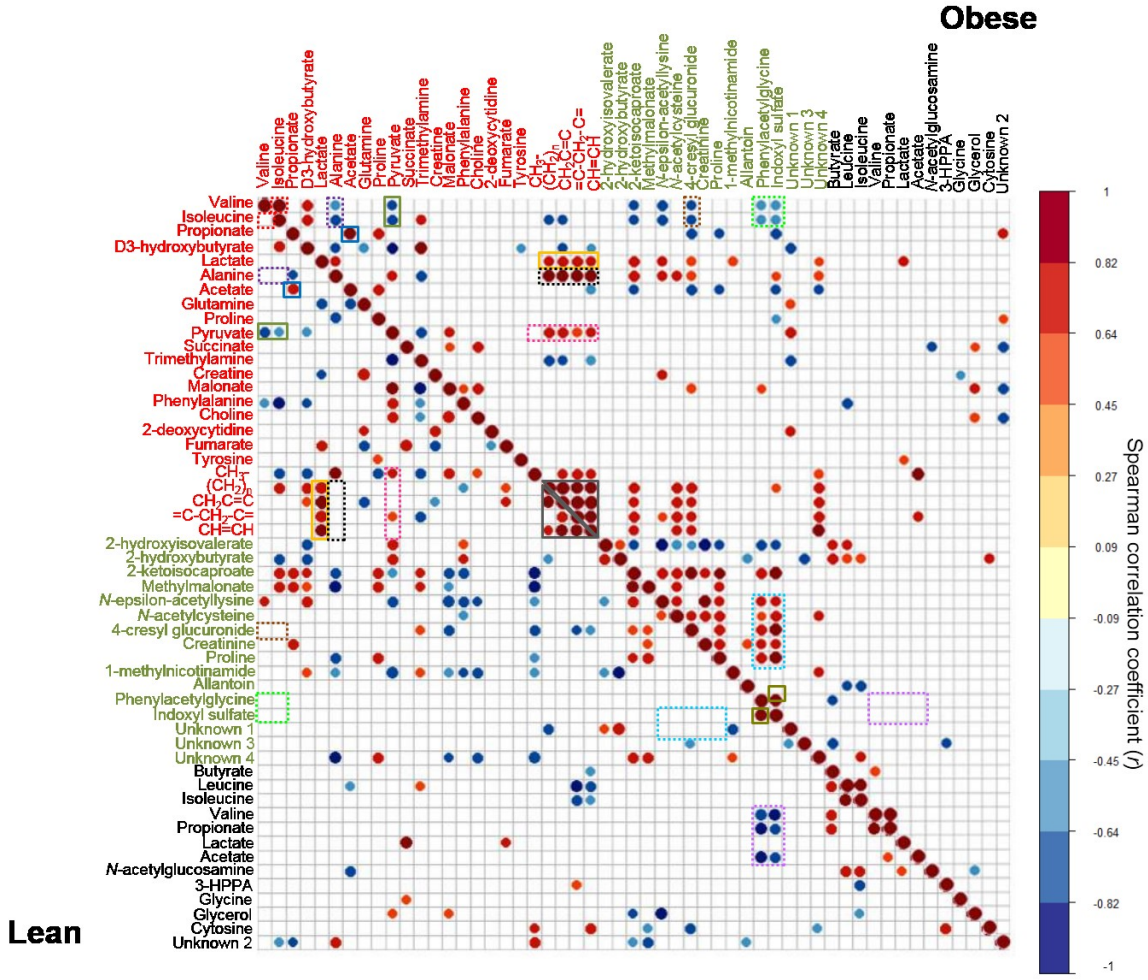


Figure 3-3. Inter-compartmental correlation analysis of biofluids. Inter-compartmental correlation map of plasma (red), urinary (green) and faecal (black) metabolites from Zucker obese and lean rats with p-value < 0.05. Red denotes positive correlation, blue denotes negative correlation, and blank denotes no significant correlation. Key: 3-HPPA, 3-hydroxyphenyl propionic acid. Dashed-line box indicates different metabolic structures, whereas solid-line box indicates similar metabolic structures between lean and obese rats.

3.4 Discussion

Obese (*fa*/*fa*) and lean (*fa*/+) Zucker rats were phenotypically different in all biological matrices measured using a ^{1}H NMR spectroscopy-based metabolic profiling approach and the global metabolic profiles of portal vein plasma of hyperinsulinemic obese Zucker rats in this study were reported for the first time providing the baseline metabolic information to further understand this particular type of obese animal model. Obese Zucker rats were significantly hyperphagic compared to lean controls as expected (Figurte S1), resulting in a greater food intake and body weight (Morton, Meek & Schwartz, 2014).

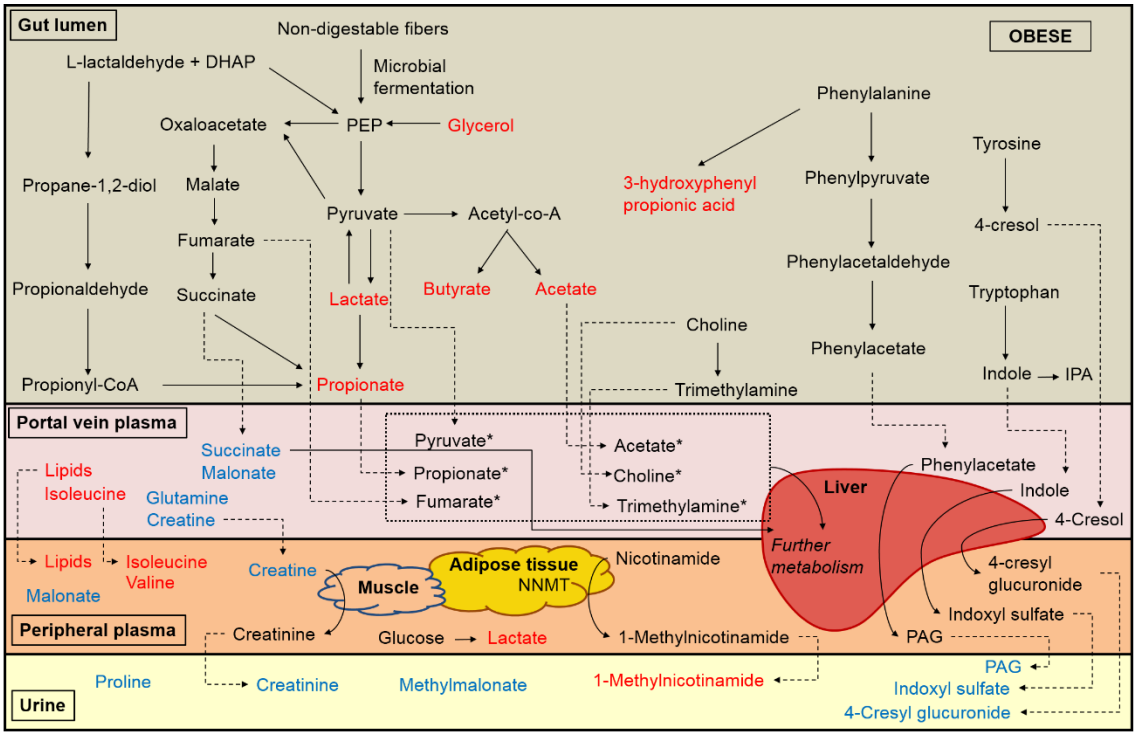


Figure 3-4. Schematic illustration of systemic changes observed in biofluids from obese Zucker rats. Red indicates higher relative concentration, whereas blue indicates lower relative concentration of metabolites in obese rats compared with lean animals. Key: IPA, indole-3-propionic acid; NNMT: nicotinamide *N*-methyltransferase; PAG, phenylacetylglycine; PEP, phosphoenolpyruvate. * indicates that these metabolites are higher in portal vein blood plasma in contrast to peripheral blood plasma independent of the animal genotypes.

3.4.1 Muscle and adipose tissue metabolism

Urinary creatinine and plasma creatine were observed in higher levels in the lean Zucker rats as compared to their obese counterparts, which is consistent with a previous study

in Zucker rats (Waldram *et al.*, 2009). Higher levels of creatine in the white adipose tissue of lean Zucker rats compared with that of obese Zucker rats at two months old was previously reported, but such a change was not observed in rats at six months old (de Castro *et al.*, 2013). Creatinine is obtained from creatine phosphate in muscle and creatinine formation results from the loss of a water molecule from creatine (Peters *et al.*, 2014). Creatinine is delivered to kidney through the blood and removed from the body by glomerular filtration and partial tubular excretion (Bennett, Bevington & Walls, 1992). Twenty four-hour urinary excretion of creatinine was shown to be significantly correlated with fat-free mass (Peters *et al.*, 2014). A cohort of 170 healthy individuals also demonstrated that the association of higher muscle mass with higher levels of physical activity, and the positive correlation of serum and urinary creatinine with the muscle mass and body weight, with a greater degree of correlation with muscle mass (Baxmann *et al.*, 2008). In the current study, the excretion of lower levels of urinary creatinine in the obese rats indicates of lower lean mass, compared with the lean rats.

Elevated levels of urinary 1-methylnicotinamide were observed in the obese Zucker rats, which is in accord with previous findings in high fat diet (HFD)-induced male C57BL/6N obese mice (Riederer *et al.*, 2009). 1-methylnicotinamide is a catalysis product of nicotinamide *via* nicotinamide N-methyltransferase (NNMT) which is found in both liver and adipose tissue (Trammell & Brenner, 2015). It has been found that levels of NNMT activity were highly expressed in 3T3-L1 adipocytes and murine adipose tissue, resulting in production of 1-methylnicotinamide, which is excreted into urine, and S-adenosyl-l-homocysteine, which is further metabolized into homocysteine by S-adenosyl-l-homocysteine hydrolase (Riederer *et al.*, 2009). Although high NNMT expression in liver was shown to improve lipid parameters through sirtuin 1 stabilisation (Hong *et al.*, 2015), Kraus et al (2014) reported that high NNMT expression in adipose tissue correlates with adiposity in both humans and mice (Kraus *et al.*, 2014). Nicotinamide can be salvaged for via NAD^+ re-synthesis that is essential for the fuel oxidation. When NNMT is highly expressed, nicotinamide may not be salvageable, limiting fuel oxidation and promoting

the storage of fat (Kraus *et al.*, 2014). Hence, the higher level of 1-methylnicotinamide is indicative of a rich pool of NNMT in the adipose tissue of the obese rats.

3.4.2 Microbial metabolism and host-microbial co-metabolism in obesity

Faecal concentrations of SCFAs were found to be significantly higher in obese Zucker rats compared with lean rats, potentially resulting from the increased fermentation substrate bioavailability from higher food intake and/or increased microbial non-digestible carbohydrate fermentation by the gut microbiota in the obese rats. Higher cecal concentrations of SCFAs have been reported in genetically obese C57BL/6J (ob/ob) mice, indicating the greater energy extraction ability of microbiota from obese mice (Turnbaugh *et al.*, 2006). Higher levels of propionate and acetate, but not butyrate, were found in the portal vein blood compared with peripheral blood in both lean and obese animals. This could be attributed to the fact that colonocytes utilise a large part of butyrate as an important energy source. Acetate and propionate are, by contrast, absorbed and further utilised in the liver for cholesterol and long-chain fatty acid synthesis, and hepatic gluconeogenesis (den Besten *et al.*, 2013). Concentrations of acetate and propionate in the portal vein blood plasma between the lean and obese animals did not significantly differ given the elevated faecal SCFAs, suggesting that the acetate and propionate absorption through hepatic portal vein circulation may not directly contribute to the obese phenotype in Zucker rats. Propionate production occurs *via* three known bacterial fermentation pathways (Figure 4) including the succinate pathway, where fumarate and succinate are produced as intermediates; the acrylate pathway, where pyruvate and lactate are intermediates; and the propanediol pathway, where propane-1,2-diol is an intermediate (Reichardt *et al.*, 2014). Fumarate and pyruvate were shown to be absorbed into the hepatic portal circulation in both obese and lean animals in this study. Moreover, higher levels of hepatic portal succinate in the lean animals were detected compared with obese animals, but its level in the peripheral blood did not differ between the two phenotypes. This finding indicates an elevated uptake of succinate and

enhanced hepatic succinate metabolism (*e.g.* TCA cycle and adenosine triphosphate generation in mitochondria) in the lean animals. In lean Zucker rats, the previously mentioned succinate pathway for producing propionate could be suppressed, resulting in increased succinate availability in the intestinal lumen, leading to its increased portal vein blood concentrations.

The relatively high faecal acetate concentrations of the obese animals suggest an imbalance of lactate-producing (*e.g*. *Bifidobacteria*) and lactate-utilizing bacteria (*e.g. Eubacterium hallii* or *Anaerostipes caccae*) in the gastrointestinal tract. A previous study reported the highest abundance of lactate-producing bacteria in T2DM, followed by obese and lean participants orderly (Remely *et al.*, 2014). A positive correlation between faecal SCFAs and faecal lactate, an intermediate metabolite of SCFAs was observed in the current study. Lactate is found in low concentrations (<5 mmol/L) in faecal samples from healthy individuals, but it may accumulate in concentrations up to 90 mmol/L in patients with ulcerative colitis as previously reported (Vernia *et al.*, 1988), which could be attributed to curtailment of lactate utilization at pH of 5.2.

Higher levels of choline and TMA were detected in the portal vein blood compared with peripheral blood of the genotypes of the animals. Choline, a common dietary component, can be metabolized into TMA by the gut microbiota (Dumas *et al.*, 2006). The unmetabolized choline and resulting TMA are absorbed and the latter is known to be further oxidised in the liver to trimethylamine-*N*-oxide involving flavin-containing monooxygenases (FMO) (Myers & Zatman, 1971). Although the strain-specific and genetically determined selections of the gut microbiota of high fat diet-fed animals were reported to be associated with choline metabolism (Dumas *et al.*, 2006), TMA and choline were similar between two genotypes, indicating that the obesity phenotype of the Zucker rats could be independent of the microbial metabolism of choline.

Microbial metabolism of aromatic amino acids (*e.g.* phenylalanine and tyrosine) and tryptophan were altered in obese Zucker rats, evidenced by lower urinary concentrations of host-microbial co-metabolites including 4-cresyl glucuronide, IS and PAG, and higher

faecal 3-HPPA compared to lean animals. 4-Cresol is metabolized from tyrosine *via* 4-hydroxyphenylacetate by the gut microbiota and further metabolized into 4-cresyl glucuronide or 4-cresyl sulfate in the liver (Figure 3-4). PAG, a conjugation product of glycine and phenylacetate, is produced by microbiota from phenylalanine, and 3-HPPA is also a product from phenylalanine metabolism (Delaney *et al.*, 2004). Indoxyl sulfate is produced in the liver from indole derived from the microbial metabolism of dietary tryptophan (Yokoyama & Carlson, 1979). Our findings are indicative of lower microbial activity for producing the precursors of these urinary host-microbial co-metabolites. 4-Cresyl sulfate and phenylacetylglutamine (equivalent to phenyacetylglycine in rodents) was found to be inversely associated with BMI in UK and USA cohorts of the INTERMAP (International Study of Macro- and Micronutrients and Blood Pressure) epidemiologic study (Wijeyesekera *et al.*, 2012), which are in line with our findings. A Roux-en-Y gastric bypass surgical model in rats also exhibited increased urinary IS, PAG, 4-cresyl glucuronide and 4-cresyl sulfate concentrations after weight loss (Li *et al.*, 2011). Our results indicate that conversion of phenylalanine to 3-HPPA is greater in the obese Zucker rats, whereas in lean animals, production of phenylacetate from phenylalanine is likely to be enhanced and excreted as urinary PAG. Higher levels of tyrosine were also delivered into the portal vein blood in lean, compared to obese rats. A positive correlation of IS with PAG was observed in both genotypes. Moreover, a positive correlation between 4-cresyl glucuronide and PAG or IS was only seen in obese rats, suggesting that in obese animals the metabolism of tyrosine, phenylalanine and tryptophan could be closely inter-connected, whereas in lean rats, 4-cresol production from tyrosine may be disproportionally up-regulated in comparison to phenylacetate and indole.

3.4.3 Branched chain amino acid metabolism

Systemic circulating BCAAs - valine and isoleucine were higher and faecal BCAAs were lower in the obese compared with lean rats. Elevated plasma BCAAs in obese humans and animals have been previously reported (Wijekoon *et al.*, 2004). Wijekoon and

colleagues (2004) (Wijekoon *et al.*, 2004) demonstrated the significantly increased concentrations of plasma BCAAs in the Zucker obese rat compared to lean rat. Although a correlation between BCAAs and fasting insulin levels was not observed, a gradual increase in plasma BCAAs of obese and diabetic individuals was reported by Adeva et al (2012) (Adeva *et al.*, 2012) and the study suggested that the metabolism of BCAAs is particularly responsive to the inhibitory insulin action on amino acid released by skeletal muscle and their metabolism is profoundly altered in conditions featuring insulin resistance, insulin deficiency, or both.

3.4.4 Energy metabolism in obese rats

Obese Zucker rats showed higher levels of lipids in both portal vein and peripheral blood plasma and higher concentrations of lactate peripheral blood plasma compared with lean rats, which are expected and in agreement with previous studies (Waldram *et al.*, 2009; Llado, Palou & Pons, 1998; Serkova *et al.*, 2006; Zhao *et al.*, 2011). Glucose is oxidised to pyruvate and the latter is catalysed by lactate dehydrogenase, yielding lactate and NAD+ which is further required for the oxidation 3-phosphoglyceraldehyde during production of pyruvate from glucose (Phypers and Pierce, J.M., 2006). Lipid signals (CH2C=C and CH=CH) in the obese animals were, furthermore, observed to be negatively associated with D-3-hydroxybutyrate, a ketone body produced in the liver mainly from the oxidation of fatty acids that is exported to peripheral tissues for use as an energy source (Mitchell *et al.*, 1995). Change in the body's fuel from carbohydrate to fat results in ketosis that has a significant effect on suppressing hunger (Dashti *et al.*, 2004). The more prominent inter-correlation among the metabolites involved in energy metabolism was observed in obese animals, evidenced by strong positive correlation between lipid signals and pyruvate, alanine or lactate. Alanine can be produced from pyruvate *via* alanine transaminase and a positive correlation between alanine and pyruvate was detected in obese rats, not in lean rats. Alanine can also be produced by BCAAs, contributing approximately 60% of the nitrogen for alanine synthesis (Haymond

& Miles, 1982). A negative correlation between alanine and valine and isoleucine was also observed in this study, indicating a down-regulated synthesis of alanine from BCAAs in obese animals.

3.5 Summary

This study has systematically demonstrated for the first time the metabolic profiles of urine, portal vein and peripheral blood plasma and faecal water of hyperinsulinemic obese Zucker rats. Metabolic observations of portal vein and peripheral blood plasma profiles in both obese and lean Zucker rats indicated the phenotype-independent absorption of SCFAs, choline and TMA. However, phenotype-specific urinary host-microbial co-metabolites such as PAG, IS and 4-cresyl glucuronide were revealed, suggesting distinct gut microbial metabolic activities in lean and obese Zucker rats. The study also provided a baseline picture of metabolic profiles of a genetically obese rat model in order to further our understanding of utilising this animal model for future obesity studies.

4. ^{1}H NMR-Based Metabolic Profiling of Peripheral and Portal Vein Plasma, Urine and Faecal Water in the Obese Zucker Rats Treated with Roux-en-Y Gastric Bypass or Caloric Restriction

4.1 Aim

The aim of this study was to 1) monitor dynamic changes in urinary and faecal water profiles obtained from obese Zucker rats with Roux-en-Y (RYGB) gastric bypass or caloric restriction; 2) characterise the biochemical composition of the portal vein and peripheral blood, for the first time in obese Zucker rats treated with RYGB or caloric restriction; and 3) investigate the uptake of the gut microbial metabolites and their systemic circulation and metabolism in the different group of rats using ^{1}H NMR spectroscopy in combination with multivariate statistical analyses.

4.2 Materials and methods

Experimental design, animal experiment, sample collection, preparation for ^{1}H NMR spectroscopy analysis and spectroscopic data analyses have been described in Chapter 2.

4.3 Results

4.3.1 Differences in body weight, food intake, oral glucose tolerance test and fasting insulin between RYGB and caloric restriction groups in comparison with obese control

The differences in body weight, food intake, oral glucose tolerance test and fasting insulin between RYGB, sham-BWM and sham-obese rats were measured. The mean body weight of sham-obese rats was significantly higher than that of RYGB and sham-BWM rats observed on Day 6 onwards (sham-obese: 504.3 g ± 40.87 g; RYGB: 427.4

g ± 11.63 g; sham-BWM: 424.6 g ± 13.66 g) as obese rats consumed higher amount of food while RYGB and sham-BWM rats were prone to consume less despite the different weight loss strategies (sham-obese: 31.4 g ± 1.67 g; RYGB: 21.3 g ± 1.6 g; sham-BWM: 19.8 g ± 2.5 g) (Figure 4-1A and 4-1B).

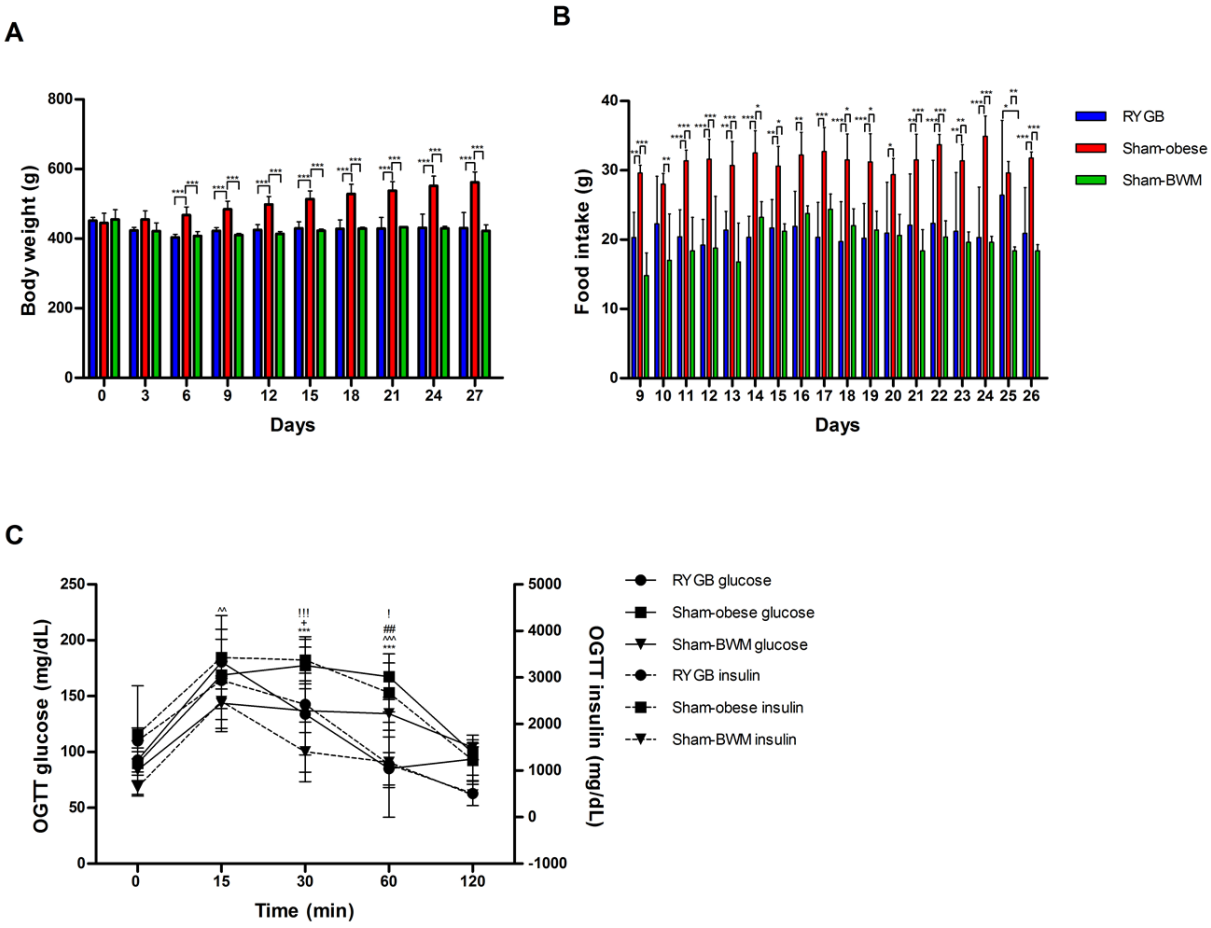


Figure 4-1. (A) Measurement of body weight; (B) food intake, data are shown as mean ± SD (*p < 0.001) and statistical differences determined by two-way ANOVA and (C) oral glucose tolerance test (OGTT) of RYGB (n=11), sham-BWM (n=5) and sham-obese Zucker rats (n=5). OGTT glucose (solid line) and insulin (dashed line) +measurements of Zucker rats. Data are shown as mean ± SD (OGTT glucose: +p < 0.05 (sham-BWM vs. sham-obese); ^^p < 0.01, ^^^ p < 0.001 (RYGB vs. Sham-BWM); *** p < 0.001 (RYGB vs. sham-obese) and OGTT inulin: ! p < 0.05, !!! p < 0.001 (Sham-BWM vs. sham-obese); ## p < 0.01 (RYGB vs. sham-obese) by two-way ANOVA).**

Fasting glucose level (at 30 and 60 mins) and insulin level (at 60 min) were significantly lower in RYGB compared with sham-obese rats (Figure 4-1C). Similarly, sham-BWM rats showed significantly lower levels of both glucose level at 30 min and insulin level at 60

min in comparison with sham-obese rats. At 15 and 60 mins, glucose levels were significantly lower in caloric restriction group compared with RYGB group (Figure 4-1C).

4.3.2 Caloric restriction effects on faecal, urinary, peripheral and portal vein plasma metabolic profiles of obese Zucker rats

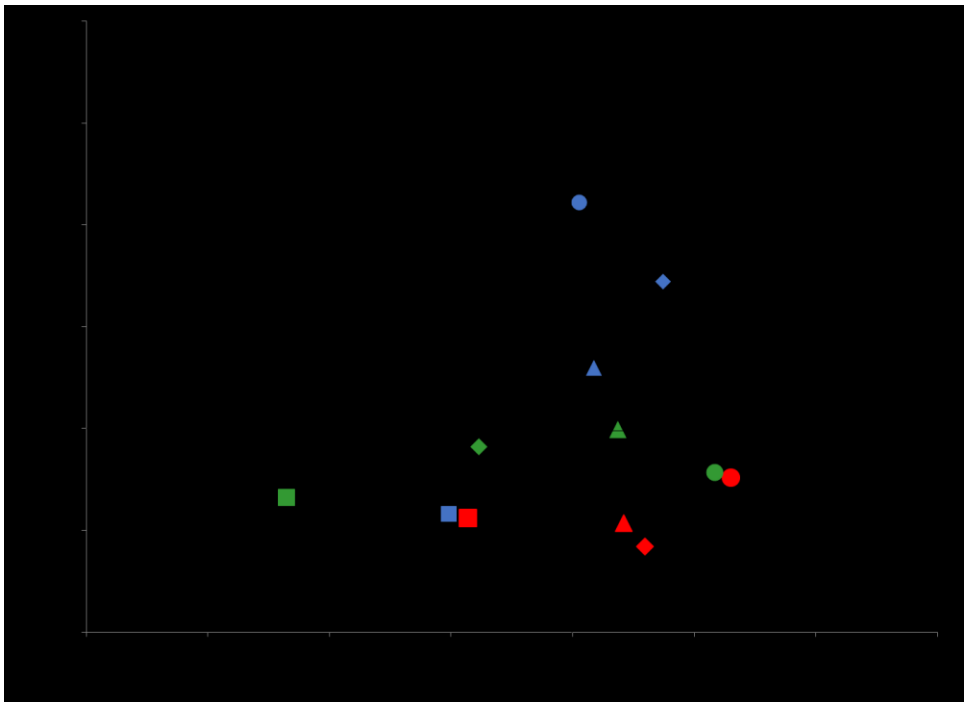


Figure 4-2. A PCA trajectory scores plot of faecal water ^{1}H NMR spectral data set obtained from RYGB (blue), sham-BWM (green) and sham-obese (red) Zucker rats at pre-operation (square), 1-week (triangle), 2-week (diamond) and 4-week (circle) post-operations. Each dot represents the average scores of the first principal component (PC1) against the second principal component (PC2) of the spectral data from each group and the error bars are expressed by the standard error of the mean of PC1 and PC2 of each time point.

A high degree of shift in faecal metabolic profiles of RYGB, sham-obese and sham-BWM rats was observed (Figure 4-2). The pre- and post-operation time points (time-related shift) are separated along the first principal component (PC1), whilst differentiation between RYGB- and sham-obese rats is along the second principal component (PC2). The sham-obese and sham-BWM rats showed similar degree of variation.

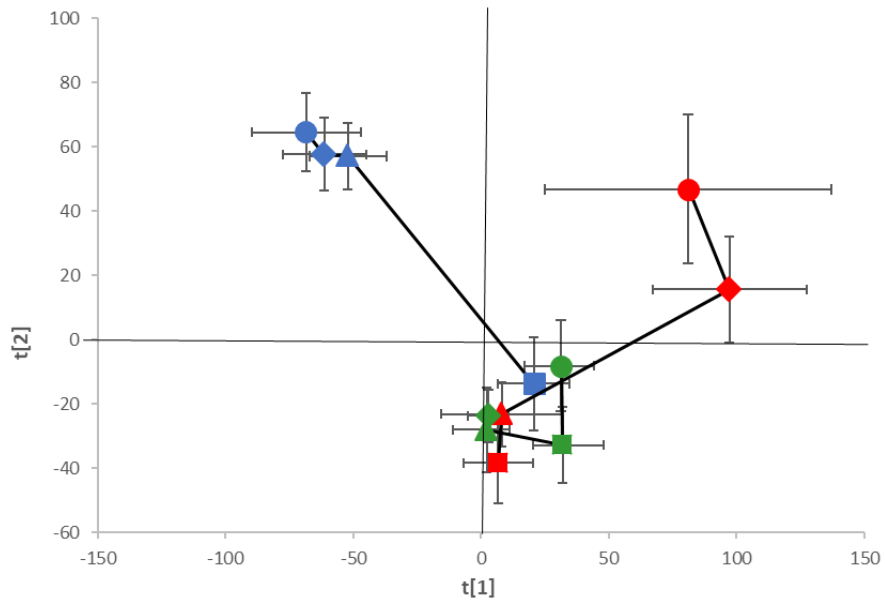


Figure 4-3. A PCA trajectory scores plot of urinary ^{1}H NMR spectral data set obtained from RYGB (blue), sham-BWM (green) and sham-obese (red) Zucker rats at pre-operation (square), 1-week (triangle), 2-week (diamond) and 4-week (circle) post-operations. Each dot represents the average scores of the first principal component (PC1) against the second principal component (PC2) of the spectral data from each group and the error bars are expressed by the standard error of the mean of PC1 and PC2 of each time point.

The PCA trajectory scores plot (Figure 4-3) demonstrated a significant shift in global urinary metabolic profiles of RYGB rats compared with sham-obese and sham-BWM rats as the surgery-related shift is shown along PC1 and the time-related shift is along PC2. A tight clustering of sham-BWM and a different trajectory of the sham-rats compared with RYGB rats were observed in the PCA trajectory scores plot.

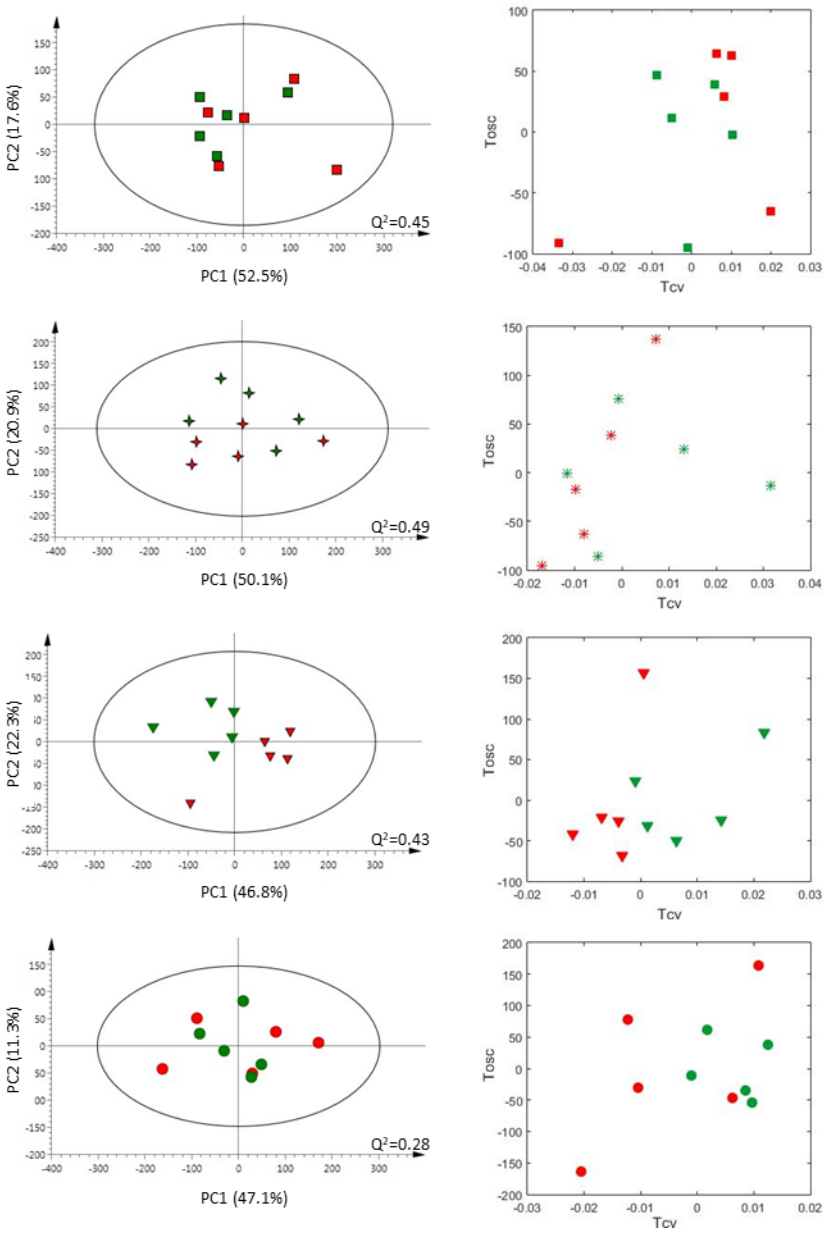


Figure 4-4. PCA scores plots (left panel) and O-PLS-DA cross-validated scores plots (right panel) of the faecal metabolic profiles between sham-BWM (green) and sham-obese (red) Zucker rats at pre-operation (square), 1-week (star), 2-week (inverted triangle) and 3-week (dot) post-operations. Percentage on each PC represents variation explained by each principal component and Q^2 represents predictability of the model.

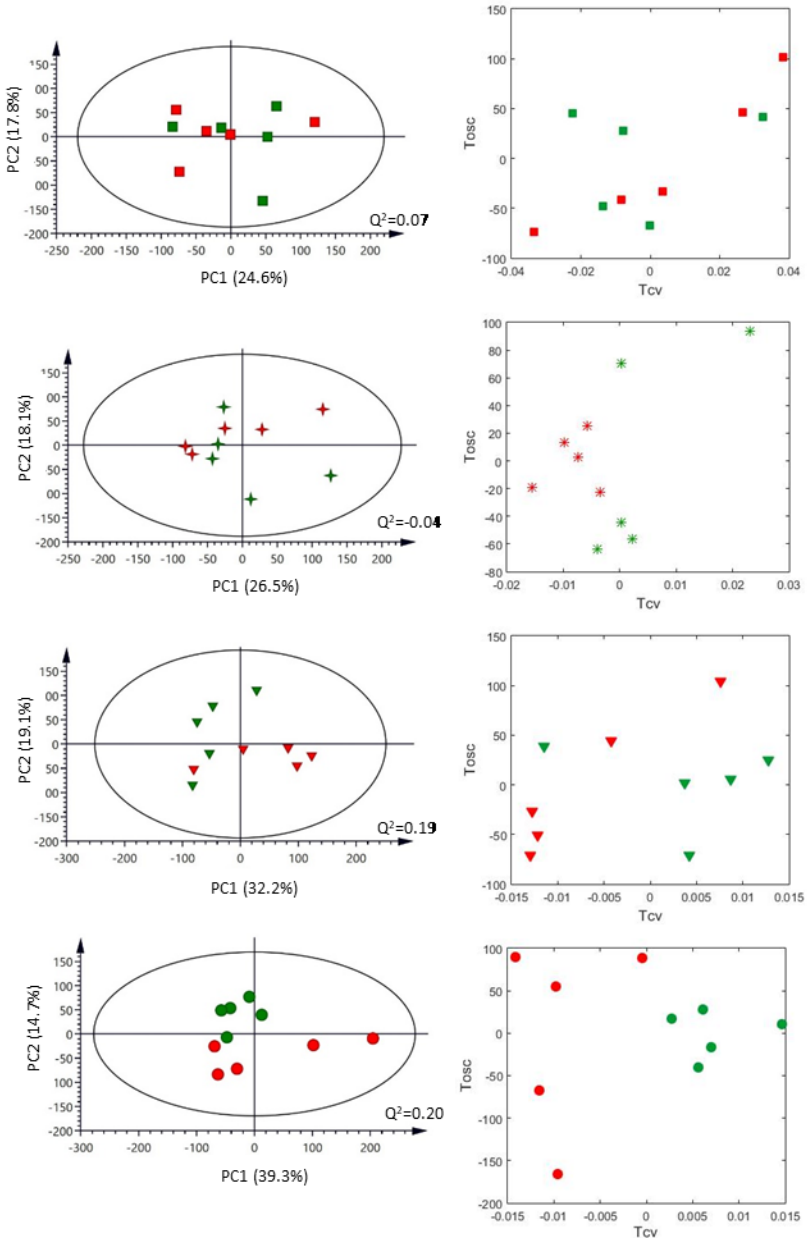


Figure 4-5. PCA scores plots (left panel) and O-PLS-DA cross-validated scores plots (right) of the urinary metabolic profiles between sham-BWM (green) and sham-obese (red panel) Zucker rats at pre-operation (square), 1-week (star), 2-week (inverted triangle) and 3-week (dot) post-operations. Percentage on each PC represents variation explained by each principal component and Q^2 represents predictability of the model.

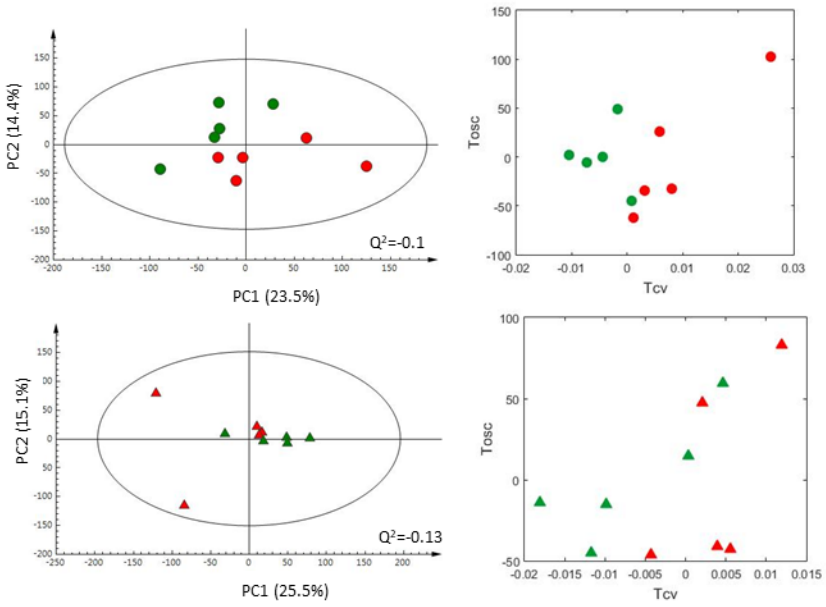


Figure 4-6. PCA scores plots (left panel) and O-PLS-DA cross-validated scores plots (right panel) of peripheral (dot) and portal vein (triangle) plasma metabolic profiles between sham-BWM (green) and sham-obese (red) Zucker rats. Percentage on each PC represents variation explained by each principal component and Q^2 represents predictability of the model.

PCA and O-PLS-DA analyses demonstrated that faecal metabolic profiles obtained from sham-BWM were not significantly different from sham-obese (Figure 4-4 and Table 4-1). Moreover, urinary metabolic profiles of sham-BWM were compared with those of sham-obese and the results showed that no distinct urinary metabolic difference was observed at pre-sham operation, 1- and 2-week post-sham operation (Figure 4-5 and Table 4-1). Although O-PLS-DA model comparing urinary metabolic profiles between sham-BWM and sham-obese at week 3 displayed valid statistical parameters (Table 4-1), there was no significant discriminatory metabolite obtained after Benjamini-Hochberg FDR correction. PCA and O-PLS-DA models comparing peripheral plasma and portal vein plasma between sham-BWM and sham-obese revealed the non-robust models, suggesting no metabolic differences between these groups (Figure 4-6 and Table 4-1).

4.3.3 Effects of Roux-en-Y gastric bypass on faecal metabolic profiles of obese Zucker rats

Pairwise comparison including RYGB vs. sham-obese and RYGB vs. sham-BWM were carried out using PCA and O-PLS-DA in order to extract the detailed faecal metabolic alterations exerted through the two different weight loss strategies – RYGB and caloric restriction.

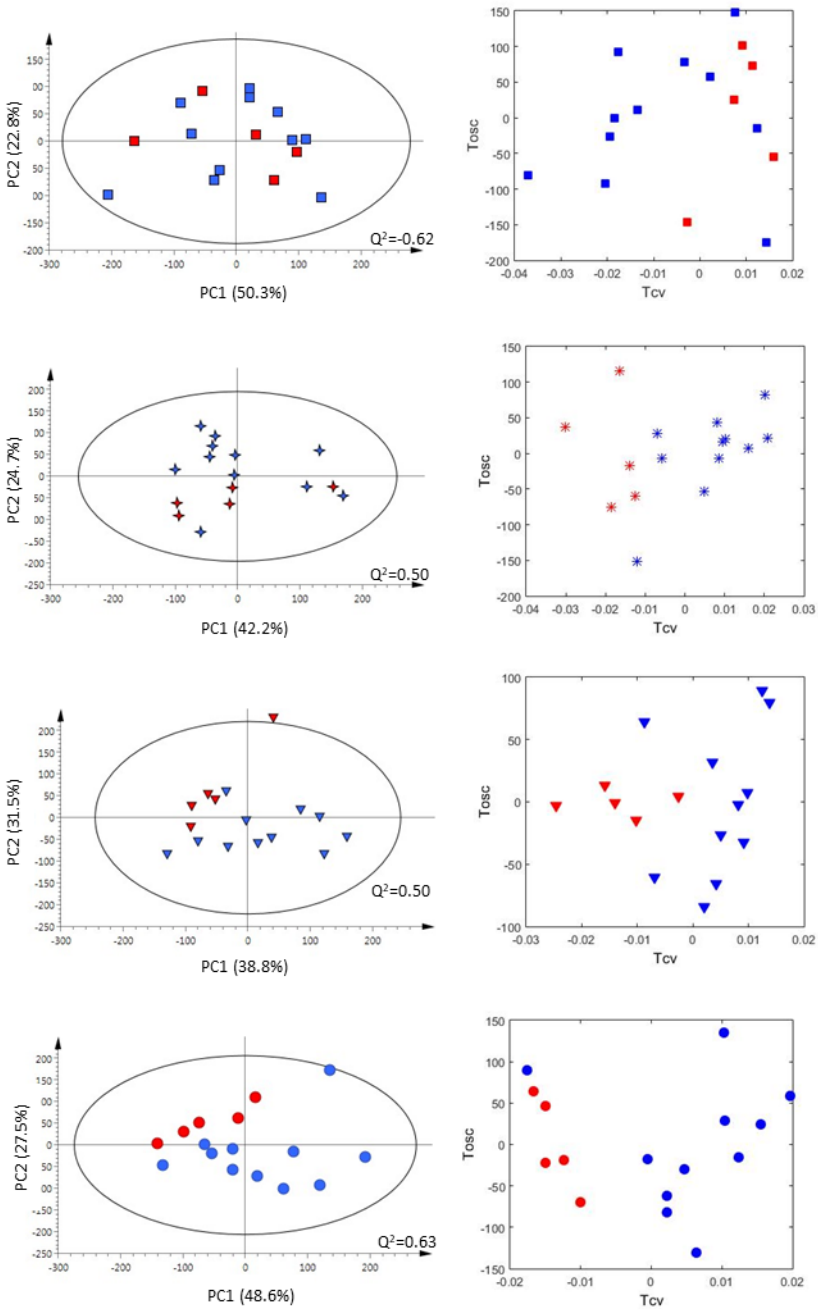


Figure 4-7. PCA scores plots (left panel) and O-PLS-DA cross-validated scores plots (right panel) of faecal metabolic profiles between RYGB (blue) and sham-obese (red) Zucker rats at pre-operation (square), 1-week (star), 2-week (inverted triangle) and 3-week (dot) post-operations. Percentage on each PC represents variation explained by each principal component and Q^2 represents predictability of the PCA model.

Table 4-1. Summary of O-PLS-DA statistical parameters for all pairwise comparison models demonstrated in Chapter 4. Significant models are bold.

Biofluid	Models	Time point	O-PLS-DA statistical parameters		
			R^2X	Q^2Y	Permutation p value
Faeces	RYGB vs. Sham-obese	Pre-op	55.40%	-0.61	0.802
	RYGB vs. Sham-obese	**1-week post-op**	**47.10%**	**0.65**	**0.001**
	RYGB vs. Sham-obese	**2-week post-op**	**55.40%**	**0.67**	**0.001**
	RYGB vs. Sham-obese	**3-week post-op**	**68.80%**	**0.58**	**0.001**
	RYGB vs. Sham-BWM	Pre-op	55.70%	-0.57	0.864
	RYGB vs. Sham-BWM	**1-week post-op**	**49.30%**	**0.8**	**0.001**
	RYGB vs. Sham-BWM	**2-week post-op**	**61.90%**	**0.72**	**0.001**
	RYGB vs. Sham-BWM	**3-week post-op**	**64.70%**	**0.56**	**0.001**
	Sham-BWM vs. Sham-obese	Pre-op	60.60%	-0.37	0.856
	Sham-BWM vs. Sham-obese	1-week post-op	64.20%	0.29	0.454
	Sham-BWM vs. Sham-obese	2-week post-op	67.80%	-0.63	0.114
	Sham-BWM vs. Sham-obese	3-week post-op	56.10%	0.28	0.265
Urine	RYGB vs. Sham-obese	Pre-op	34.80%	-1.26	0.994
	RYGB vs. Sham-obese	**1-week post-op**	**35.50%**	**0.65**	**0.002**
	RYGB vs. Sham-obese	**2-week post-op**	**40.40%**	**0.67**	**0.001**
	RYGB vs. Sham-obese	**3-week post-op**	**42.90%**	**0.81**	**0.002**
	RYGB vs. Sham-BWM	Pre-op	33.80%	-0.57	0.864
	RYGB vs. Sham-BWM	**1-week post-op**	**32.40%**	**0.76**	**0.002**
	RYGB vs. Sham-BWM	**2-week post-op**	**35.40%**	**0.74**	**0.002**
	RYGB vs. Sham-BWM	**3-week post-op**	**64.70%**	**0.65**	**0.001**
	Sham-BWM vs. Sham-obese	Pre-op	60.60%	-0.37	0.855
	Sham-BWM vs. Sham-obese	1-week post-op	64.20%	0.29	0.252
	Sham-BWM vs. Sham-obese	2-week post-op	67.80%	0.33	0.294
	Sham-BWM vs. Sham-obese	**3-week post-op**	**53.00%**	**0.66**	**0.014**
Plasma	**RYGB (P_s) vs. RYGB (P_p)**	**3-week post-op**	**27.63%**	**0.43**	**0.006**
	Sham-BWM (P_s) vs. Sham-BWM (P_p)	3-week post-op	32.85%	0.51	0.106
	RYGB (P_s) vs. Sham-obese (P_s)	**3-week post-op**	**32.50%**	**0.65**	**0.001**
	RYGB (P_p) vs. Sham-obese (P_p)	**3-week post-op**	**29.40%**	**0.63**	**0.001**
	RYGB (P_s) vs. Sham-BWM (P_s)	**3-week post-op**	**31.10%**	**0.75**	**0.001**
	RYGB (P_p) vs. Sham-BWM (P_p)	**3-week post-op**	**28.30%**	**0.82**	**0.001**
	Sham-BWM (P_s) vs. Sham-obese (P_s)	3-week post-op	34.90%	0.42	0.158
	Sham-BWM (P_p) vs. Sham-obese (P_p)	3-week post-op	34.90%	0.35	0.272

Abbreviations: P_s, peripheral plasma; P_p, portal vein plasma; Pre-op, pre-operation; Post-op, post-operation. P values of all models were derived from permutation tests (n=1000).

Prior to RYGB or sham surgery, there was no significant differences in the metabolic profiles of faeces between the two groups (Figure 4-7 and Table 4-1). A clear and significant separation between RYGB and sham-obese Zucker rats was observed at 1-, 2- and 3-week post-operation along the PC2 in PCA scores plots (Figure 4-7, left panel). O-PLS-DA analysis was applied to investigate the metabolites that were discriminant between the RYGB and sham-obese classes at each time point (Table 4-1). The loadings of the pairwise O-PLS-DA models between RYGB and sham-obese rats identified relatively higher concentrations of faecal γ-amino butyric acid (GABA) and trimethylamine (TMA) over 3-week period after operation with relatively higher levels of faecal nicotinate at 1-week post-operation and faecal uracil at 2- and 3-week post-operations in RYGB rats, whereas faecal levels of lactate, succinate, cytosine, tyrosine, γ-hydroxybutyrate, *N*-acetylglucosamine, 3-hydroxyphenyl propionic acid (3-HPPA) and short-chain fatty acids (SCFAs; e.g. propionate and acetate) were found in relatively lower concentrations in RYGB rats over the 3-week period after operation with lower relative level of *N*-acetylhistamine at only 1- and 2-week post-operations (Table 4-2).

Table 4-2. Summary of O-PLS-DA metabolic changes in urinary (U) and faecal (F) ^{1}H NMR profiles

Metabolite	Chemical shift	Biofluid	O-PLS-DA models					
			1-Week Post-op		2-Week Post-op		3-Week Post-op	
			RYGB (+) vs. Sham-obese (-)	RYGB (+) vs. sham-BWM (-)	RYGB (+) vs. Sham-obese (-)	RYGB (+) vs. sham-BWM (-)	RYGB (+) vs. Sham-obese (-)	RYGB (+) vs. sham-BWM (-)
Butyrate	0.90 (t); 1.56 (m); 2.16 (t)	F					-0.6661	-0.7469*
Isoleucine	0.94 (t); 1.01 (d); 1.26 (m);	F		-0.6275		-0.8011*	-0.7221	
Propionate	1.06 (t); 2.19 (q)	F	-0.6703		-0.7097*	-0.6873	-0.7718**	-0.6055
3-Hydroxybutyrate	1.21 (d); 2.28 (m); 2.37 (m)	F		-0.7745		-0.7995		
Methylmalonate	1.25 (d); 3.17 (q)	F		-0.7469				-0.7773
Valerate	1.30 (m)	F		-0.7987		-0.9091		-0.6197
Lactate	1.33 (d); 4.11 (q)	F	-0.6729*		-0.8276****	-0.895**	-0.611**	
γ-Hydroxybutyrate	1.82 (s)	F	-0.6051*		-0.8572*	-0.9185*	-0.8871**	-0.8239*
γ-amino-butyric acid	1.91 (q); 2.30 (t); 3.02 (t)	F	0.7083	0.7745	0.7344	0.6973	0.804	0.8065**
Acetate	1.92 (s)	F	-0.6601		-0.9107****	-0.8752**	-0.9248****	-0.8735**
Proline	2.03 (m); 2.35 (m); 3.38 (m); 4.16 (dd)	F		-0.8009		-0.8917		
N-acetyl-L-aspartate	2.03 (s); 2.70 (dd)	F			-0.8349****	-0.9643***	-0.899**	-0.8867*
N-acetylglucosamine	2.06 (s); 5.22 (d)	F	-0.7426**	-0.797**	-0.6805***	-0.5971**	-0.8857****	-0.6858****
Succinate	2.41 (s)	F	-0.784	-0.5721	-0.75	-0.702	-0.829	-0.8575
α-Ketoglutarate	2.45 (t)	F		-0.8237		-0.7752		-0.8371
3-Hydroxyphenyl propionic acid	2.47 (t); 2.84 (t); 7.25 (t); 6.76 (dd); 6.8 (s); 6.88 (d)	F	-0.8006**		-0.971****	-0.7879*	-0.9639****	-0.9013***
Pyridoxal	2.49 (s); 5.12 (dd); 6.58 (s); 7.61 (s)	F				-0.8721		-0.7293**
N-acetylhistamine	2.84 (t); 3.45 (m); 7.03 (s); 7.95 (s)	F	-0.7283*		-0.949****	-0.767		-0.7766***
Trimethylamine	2.89 (s)	F	0.6903***	0.6631***	0.6778**	0.6939**	-0.8668*	0.6226
Xylose	3.21 (dd); 3.42 (t); 3.51 (dd); 3.63 (m); 3.91 (dd); 4.57 (d); 5.21 (d)	F		-0.7644	-0.633	-0.717*		
Arabinose	3.51 (dd); 3.68 (m); 3.82 (dd); 3.90 (m); 3.95 (m); 4.02 (m); 4.52 (d); 5.31 (d)	F				-0.8769		
Uracil	5.81 (d); 7.53 (d)	F		0.6199	0.6289***	0.6005***	0.6522	0.6146*
Cytosine	5.97 (d); 7.51 (d)	F	-0.841**	-0.8927**	-0.9336**	-0.9652***	-0.9399***	0.9679***
Urocanate	6.38 (d); 7.31 (d); 7.41 (s); 7.89 (s)	F				-0.9205		-0.8685****

Tyrosine	7.19 (d); 6.91 (d)	F	-0.7683*	-0.678	-0.632	-0.7263**	-0.6453***	-0.6328**
Nicotinate	7.53 (dd); 8.25 (dt); 8.61 (dd); 8.95 (d)	F	0.6643	0.6864		0.6856**		0.6439
Xanthine	7.79 (s)	F				-0.8399****		
Formate	8.46 (s)	F				-0.8121		
3-Methyl-2-oxovalerate	0.90 (t); 1.12 (d); 1.46 (m); 1.70 (m); 2.93 (m)	U	-0.7369*		-0.7694**	-0.6358	-0.778	-0.6859**
Unknown 1	0.91 (s); 1.73 (t)	U	-0.8216		-0.675		-0.859	
α -Ketoisocaproate	0.94 (d); 2.08 (m); 2.60 (d)	U				-0.7384		
Propionate	1.06 (t); 2.19 (q)	U			0.6708***	0.6527***		
α-Ketoisovalerate	1.14 (d); 3.02 (m)	U	0.753		0.762	0.6183		
Caproate	1.30 (m); 1.57 (m)	U	-0.738					
Lactate	1.33 (d); 4.11 (q)	U	-0.9764		-0.7017	-0.8446		-0.8171
Arginine	1.66 (m); 1.73 (m); 1.92 (m) 3.25 (t); 3.77 (t)	U				0.6639****		
N_{ε}-acetyllysine	1.99 (s)	U	-0.8048					
N-acetylalanine	2.01 (s)	U	-0.8048*					
N_{α}-acetyllysine	2.03 (s); 3.01(t)	U	-0.898**		-0.8938**	-0.8806**	-0.8647	-0.8819*
N-acetylcysteine	2.05 (s)	U	-0.6635					
Methionine	2.14 (s); 2.65 (t)	U			0.7428**	0.6889***		
Acetoacetate	2.29 (s); 3.45 (s)	U						0.7707***
4-Cresyl glucuronide	2.30 (s); 7.05(d); 7.2 (d)	U			0.7183***	0.7806****		
Malate	2.40 (dd); 2.69 (dd); 4.31 (dd)	U			-0.8302**	-0.7655*		-0.8778****
Succinate	2.41 (s)	U						-0.9548****
2-Oxoglutarate	2.45 (t); 3.02 (t)	U	-0.8208****		-0.9034****	-0.8211*	-0.8678****	-0.8861***
Pyridoxal	2.49 (s); 5.19 (dd); 6.58 (s); 7.61 (s)	U						-0.865
Citrate	2.54 (d); 2.69 (d)	U	-0.6872*		-0.9249***	-0.8754**	-0.7269*	-0.8056**
Hypotaurine	2.66 (t); 3.36 (t)	U				0.9062****		0.7378****
HPHPA	2.68 (m); 6.97 (d); 6.91 (s); 6.84 (dd); 5.01 (dd); 7.03 (t)	U						0.8424****
Dimethylamine	2.72 (s)	U			-0.7555*			
Biliverdin	2.80 (bs)	U	-0.9049					
4-Hydroxyphenylacetate	2.81 (dd); 3.02 (dd); 4.22 (dd); 6.86 (d); 7.19 (d)	U			0.7897	0.7567	0.7422*	0.814*
Phenylalanine	3.13 (dd); 3.28 (dd); 4.00 (dd); 7.39 (m)	U					-0.6764	**

Choline	3.20 (s)	U		0.6674***	0.6741***		
5-Hydroxytrptophan	3.23 (dd); 3.41 (dd); 4.03 (dd); 6.87 (d); 6.88 (d); 7.14 (s); 7.28 (s); 7.41 (d);	U	0.855**	0.8916***	0.8214***	0.8085****	0.7614***
Glycine	3.57 (s)	U			0.6363*		
Glycerol	3.58 (dd); 3.65 (dd)	U		0.844*			
5-Hydroxyindole-3-acetate	3.59 (s)	U			0.8189***		
Glyceraldehyde	3.62 (m); 3.79 (dd)	U					0.7294**
Uridine	3.81 (dd); 3.92 (dd); 4.14 (q); 4.24 (t); 4.36 (t); 5.9 (s); 5.92 (d); 7.87 (d)	U		0.8421***	0.7762***		
β-glucose	4.67 (d)	U		0.702***			
Pyridoxal-5-phosphate	4.94 (d); 5.16 (d); 2.50 (s); 7.77 (s)	U	-0.8576				
α-Glucose	5.25 (d)	U		0.7318****			
Allantoin	5.40 (s)	U		0.7251			-0.8292****
Urocanate	6.38 (d); 6.44 (d)	U	-0.7982*				
Fumarate	6.53 (s)	U		-0.664*			-0.7184**
Tyrosine	7.16 (d); 6.86 (d)	U	0.7826****	0.6427***		0.6817***	0.7526***
Indoxyl sulfate	7.21 (t); 7.36 (s); 7.50 (d); 7.69 (d); 7.27 (t)	U	0.7538**	0.6761**		0.6546***	0.6136**
Phenylacetylglycine	7.42 (m); 7.35 (m); 3.66 (s); 3.74 (d)	U	0.6636	0.6663***		0.8069	0.7785****
Unknown 2	8.08 (s); 8.57 (s)	U					0.8456
NAD	9.36 (s); 9.15 (d); 8.83 (d); 8.40 (s); 8.20 (m); 8.14 (s); 6.12 (d); 6.08 (d)	U	-0.7472**				

"+" indicates higher correlation, whereas "-" indicates higher correlation in either group of O-PLS-DA pairwise comparison models. Abbreviations: s, singlet; d, doublet; dd, double of doublets; t, triplet; bs, broad singlet; m, multiplet; q, quartet; F, faeces; U, urine; P_s, peripheral plasma; P_p, portal vein plasma; HPHPA, 3-(3-hydroxyphenyl)-3-hydroxypropionic acid; NAD, nicotinamide adenine dinucleotide. *, **, * and **** indicate significant levels of metabolite differences between pairwise groups of each time point at p<0.05, p<0.01, p<0.001 and p<0.0001, respectively using two-tailed heteroscedastic t-test with Benjamini-Hochberg correction.**

4.3.4 Urinary metabolic differences between Roux-en-Y gastric bypass-treated and obese Zucker rats

Pairwise comparison of RYGB vs. sham-obese, and RYGB vs. Sham-BWM were constructed to investigate RYGB-induced metabolic changes.

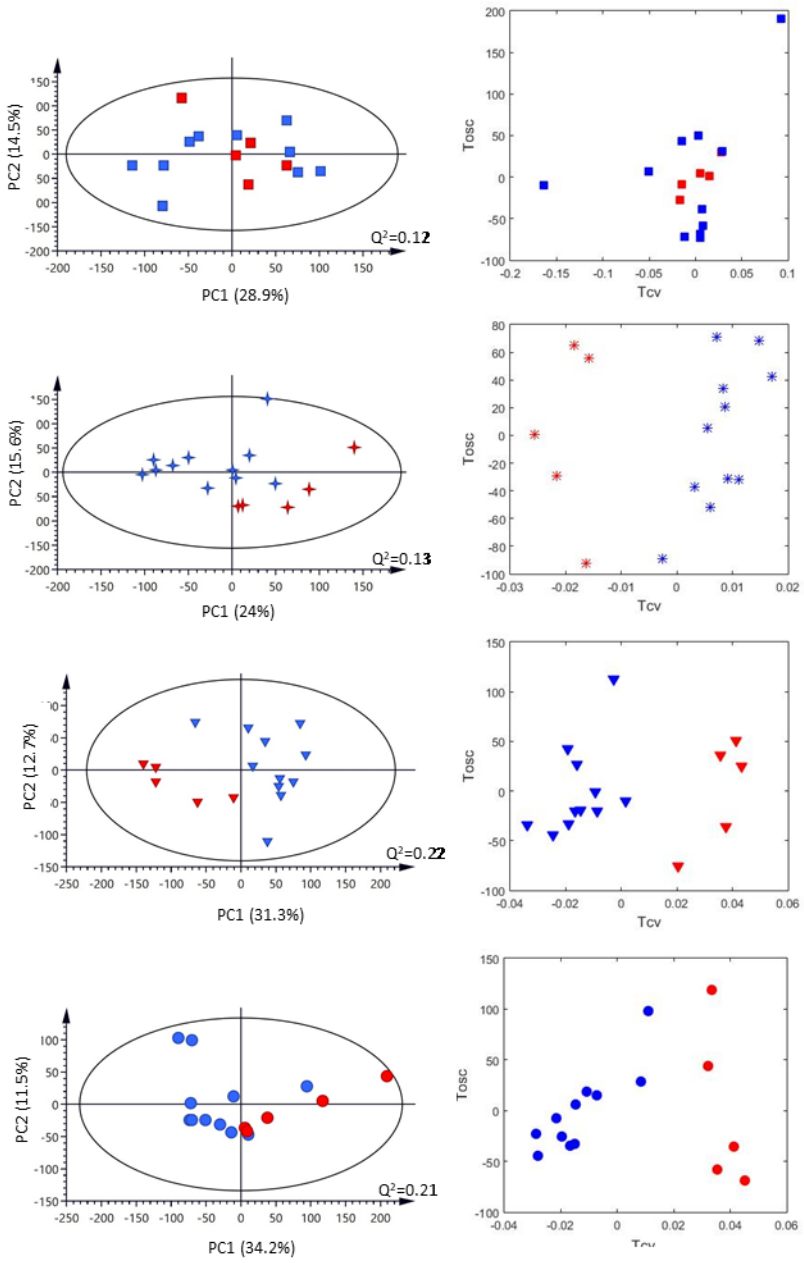


Figure 4-8. PCA scores plots (left panel) and O-PLS-DA cross-validated scores plots (right panel) of urinary metabolic profiles between RYGB (blue) and sham-obese (red) Zucker rats at pre-operation (square), 1-week (star), 2-week (inverted triangle) and 3-week (dot) post-operations. Percentage on each PC represents variation explained by each principal component and Q^2 represents predictive ability of the PCA model.

Urinary metabolic profiles of RYGB and sham-obese rats at pre-operation were not significantly different, evidenced by poor clustering in PCA scores plot and a negative Q^2Y value of the O-PLS-DA model (Figure 4-8 and Table 4-1). In contrast, PCA scores plots (Figure 4-8) showed the class separation between RYGB and sham-obese along PC1 at all post-operation time points (1, 2 and 3 weeks). Likewise, O-PLS-DA cross-validated scores plots clearly demonstrated the differentiation between these two groups post-operatively (Figure 4-8). The relative concentrations of urinary 5-hydroxytryptophan, tyrosine, indoxyl sulfate (IS) and phenylacetylglycine (PAG) increased in RYGB compared with sham-obese rats over the 3-week post-operation period (Table 4-2). Moreover, higher relative concentrations of propionate, 4-cresyl glucuronide, methionine, choline, glycerol, uridine, α-glucose, β-glucose, and allantoin were only observed at 2-week post-operation (Table 4-2). In comparison to sham-obese rats, urinary concentrations of α-ketoisovalerate and 4-hydroxyphenylacetate was only found to be higher in RYGB rats at 1-week post-operation, and 2- and 3-week post-operations, respectively (Table 4-2). In contrast, relative concentrations of urinary 3-methyl-2-oxovalerate, unknown 1 (δ^1H 0.91 (s); δ^1H 1.73 (t)), N_α-acetyllysine, 2-oxoglutarate and citrate were found to be significantly lower in RYGB compared with sham-obese rats throughout the 3-week period of post-operation (Table 4-2). Some discriminatory metabolites were significantly altered at a particular post-operation time point. For instance, urinary levels of caproate, N_ε-acetyllysine, *N*-acetylalanine, *N*-acetylcysteine, biliverdin, pyridoxal-5-phosphate, urocanate and nicotinamide adenine dinucleotide (NAD) were relatively lower in RYGB rats at 1-week post-operation, whereas urinary relative concentrations of malate, dimethylamine and fumarate were shown to be lower in RYGB rats at 2-week post-operation only (Table 4-2). Additionally, the urinary level of lactate significantly decreased during the first two weeks post-operation (Table 4-2).

4.3.5 Peripheral and portal vein plasma metabolic differences between Roux-en-Y gastric bypass-treated and obese Zucker rats

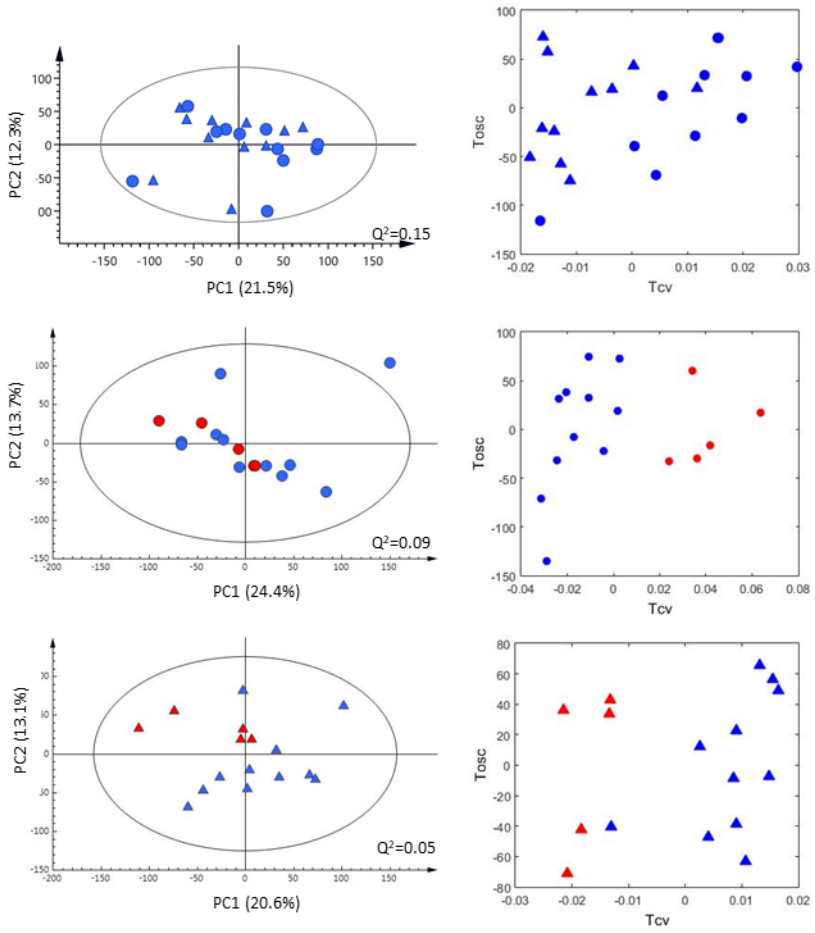


Figure 4-9. PCA scores plots (left) and O-PLS-DA cross-validated scores plots (right) of peripheral (dot) and portal vein (triangle) plasma metabolic profiles of RYGB (blue) and obese (red) Zucker rats. Percentage on each PC represents variation explained by each principal component and Q^2 represents predictive ability of the PCA model.

Clustering between peripheral and portal vein plasma obtained from RYGB rats at 3-week post-operation was not clearly seen on PCA scores plot. O-PLS-DA cross-validated scores plot showed the significant separation between them (Figure 4-9). Relative concentrations of *N,N,N*-trimethyllysine, propionate and succinate were found to be significantly higher in portal vein plasma than peripheral plasma of RYGB rats (Table 4-3).

Distinct class differentiation was not observed on PCA scores plots when comparing either the peripheral plasma profiles or the portal vein plasma profiles between RYGB and sham-obese rats (Figure 4-9, left panel). However, the corresponding O-PLS-DA

models were significant and identified the discriminatory metabolites as relatively lower levels of BCAAs (e.g. leucine and valine) in both peripheral and portal vein plasma in RYGB compared with sham-obese (Table 4-3). However, higher relative concentration of creatine accompanied with lower relative levels of 5-hydroxytryptophan, isoleucine, threonine, creatinine, very low-density lipoprotein (VLDL) and lipids (=C-CH_2-) in RYGB compared with sham-obese rats were observed in peripheral plasma only (Table 4-3). Portal vein plasma concentrations of 3-hydroxybutyrate and malate of RYGB decreased, whereas the relative concentration of creatinine was found to be significantly higher in RYGB compared with the sham-obese control (Table 4-3).

Table 4-3. Summary of O-PLS-DA metabolic changes in peripheral plasma (P_s) and portal vein plasma (P_p) ^{1}H NMR profiles

Metabolite	Chemical shift	O-PLS-DA models					
		RYGB (P_s) vs. Sham-obese (P_s)	RYGB (P_p) vs. Sham-obese (P_p)	RYGB (P_s) vs. Sham-BWM (P_s)	RYGB (P_p) vs. Sham-BWM (P_p)	RYGB (P_s) vs. RYGB (P_p)	Sham-BWM (P_s) vs. Sham-BWM (P_p)
3-Hydroxybutyrate	1.20 (d); 2.31 (m); 2.41 (m)		-0.6564				
5-Hydroxytrptophan	7.42 (d); 3.12 (t); 3.31 (t); 6.90(dd); 7.12 (d); 7.3 (s)	-0.6932		-0.8757*	-0.9284		
Creatine	3.04 (s); 3.93 (s)	0.7003**		0.7103***			
Creatinine	3.05 (s)	-0.802**	0.7753*		-0.908**		
Dimethylamine	2.72 (s)						-0.9051**
Formate	8.45 (s)						-0.9501
Isoleucine	0.94 (t); 1.01(d); 1.26 (m); 1.48 (m); 1.98 (m)	-0.7837****		-0.91**	-0.9648****		
Leucine	0.96 (t); 1.71 (m);	-0.8774**	-0.7851	-0.9103**	-0.9471*		
Lipids (CH2)n	1.28 (bs)			0.7882	0.7773		
Lipids =C-CH2-	2.75 (bs)	-0.7321		-0.72**	-0.8325*		
Lipids CH3-	0.86 (bs)			0.8057**	0.7416**		
Malate	2.39 (dd); 2.69 (dd); 4.28 (dd)		-0.8274				
N,N,N-Trimethyllysine	3.12 (s); 3.35 (m); 3.76 (t)					-0.8526**	-0.9321*
Proline	2.35 (m)						-0.9475*
Propionate	1.06 (t); 2.19 (q)					-0.7561**	-0.9557***
Pyruvate	2.37 (s)				0.7499*		-0.9429
Succinate	2.41 (s)					-0.8399****	
Threonine	1.32 (d); 3.59 (d); 4.24 (m)	-0.7369***					
Valine	0.99 (d); 1.04 (d); 3.57 (d)	-0.727**	-0.665	-0.8034**	-0.9434**		
VLDL	0.88 (bs)	-0.8007		-0.8598	-0.8976		

"+" indicates higher correlation in RYGB group, whereas "–" indicates higher correlation in sham-BWM group of O-PLS-DA pairwise comparison models. Abbreviations: s, singlet; d, doublet; dd, double of doublets; t, triplet; bs, broad singlet; m, multiplet; q, quatet. *, **, * and **** indicate significant levels of metabolite differences between RYGB and sham-BWM groups of each pairwise comparison at p<0.05, p<0.01, p<0.001 and p<0.0001, respectively using two-tailed heteroscedastic t-test with Benjamini-Hochberg correction. P values of all models were derived from permutation tests (n=1000).**

4.3.6 Faecal metabolic differences between Roux-en-Y gastric bypass- and caloric restriction-treated obese Zucker rats

Faecal metabolic profiles of RYGB and sham-BWM (calorie-restricted group) at pre-operation were similar as indicated in both the PCA scores plot and the O-PLS-DA cross-validated scores plot with a very low Q^2Y (-0.57) and a large p value (p=0.864) (Figure 4-10 and Table 1). The group clustering on the PCA scores plots had become clearer over the 3-week post-operation period. The group separation along PC2 was observed at 2- and 3-week post-operation (Figure 4-10). O-PLS-DA analysis revealed the relatively higher concentrations of faecal GABA, TMA, uracil and nicotinate in RYGB rats compared with sham-BWM rats (Table 4-2). These findings were similar to the metabolic differences between RYGB and sham-obese rats. Metabolic differences between RYGB and sham-BWM rats included faecal uracil concentration that was present in RYGB faeces since the first week post-operation, and faecal nicotinate concentration that prolonged until the terminal time point.

Concentrations of faecal *N*-acetylglucosamine, succinate, cytosine and tyrosine were relatively lower in RYGB compared with sham-BWM throughout post-operation period and relative concentrations of faecal propionate, *N*-acetyl-L-aspartate, 3-HPPA, *N*-acetylhistamine were also lower in RYGB at either 1- and 2-week post-operation or 2- and 3-week post-operation (Table 4-2). Interestingly, RYGB rats showed lower relative levels of faecal valerate and α-ketoglutarate at 1-, 2- and 3-week post-operation, accompanied with lower relative concentrations of 3-hydroxybutyrate and proline after the first two weeks post-operation, decreased relative levels of methylmalonate at 1- and 3-week post-operation and lower levels of xanthine and formate at 2-week post-operation that were only observed when comparing RYGB vs. sham-BWM but not RYGB vs. sham-obese (Table 4-2).

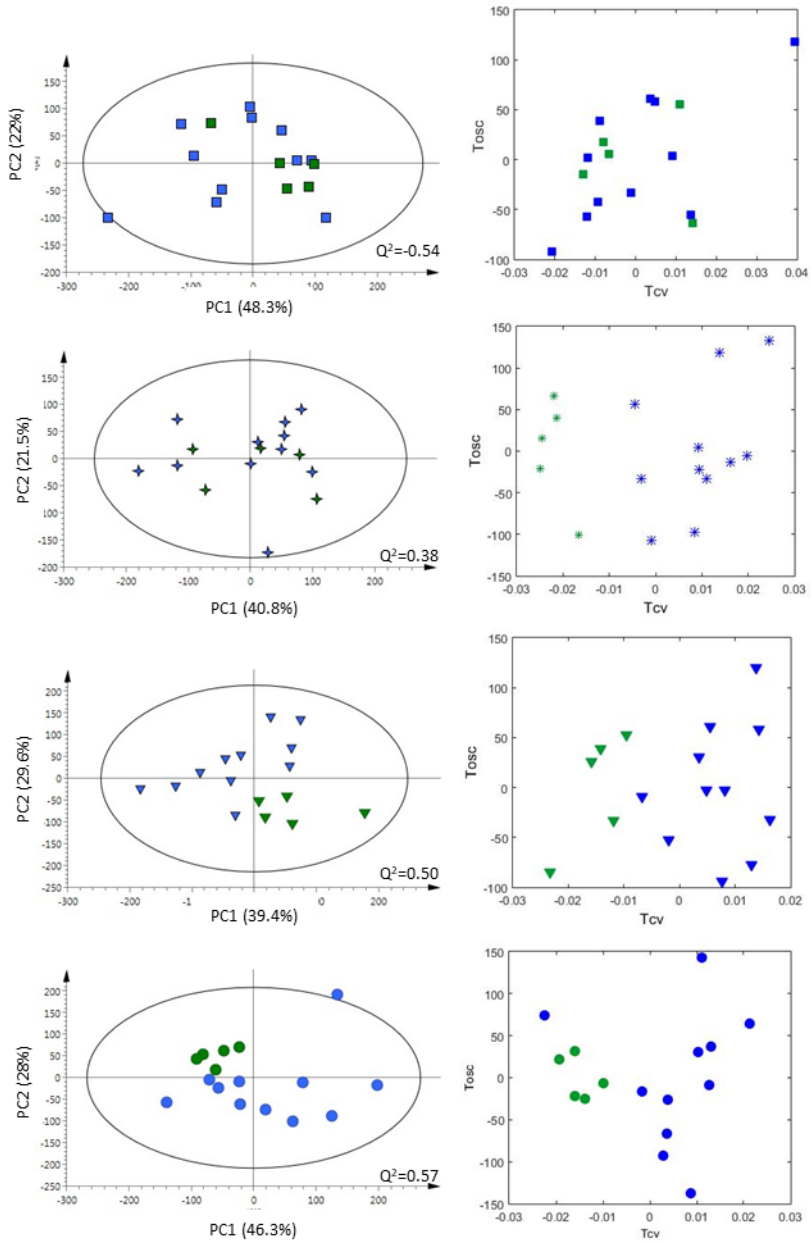


Figure 4-10. PCA scores plots (left) and O-PLS-DA cross-validated scores plots (right) of faecal metabolic profiles of RYGB (blue) and sham-BWM (red) rats at pre-operation (square), 1-week (star), 2-week (inverted triangle) and 3-week (circle) post-operations. Percentage on each PC represents variation explained by each principal component and Q^2 represents predictive ability of the PCA model.

4.3.7 Urinary metabolic differences between Roux-en-Y gastric bypass-treated and caloric restriction-treated obese Zucker rats

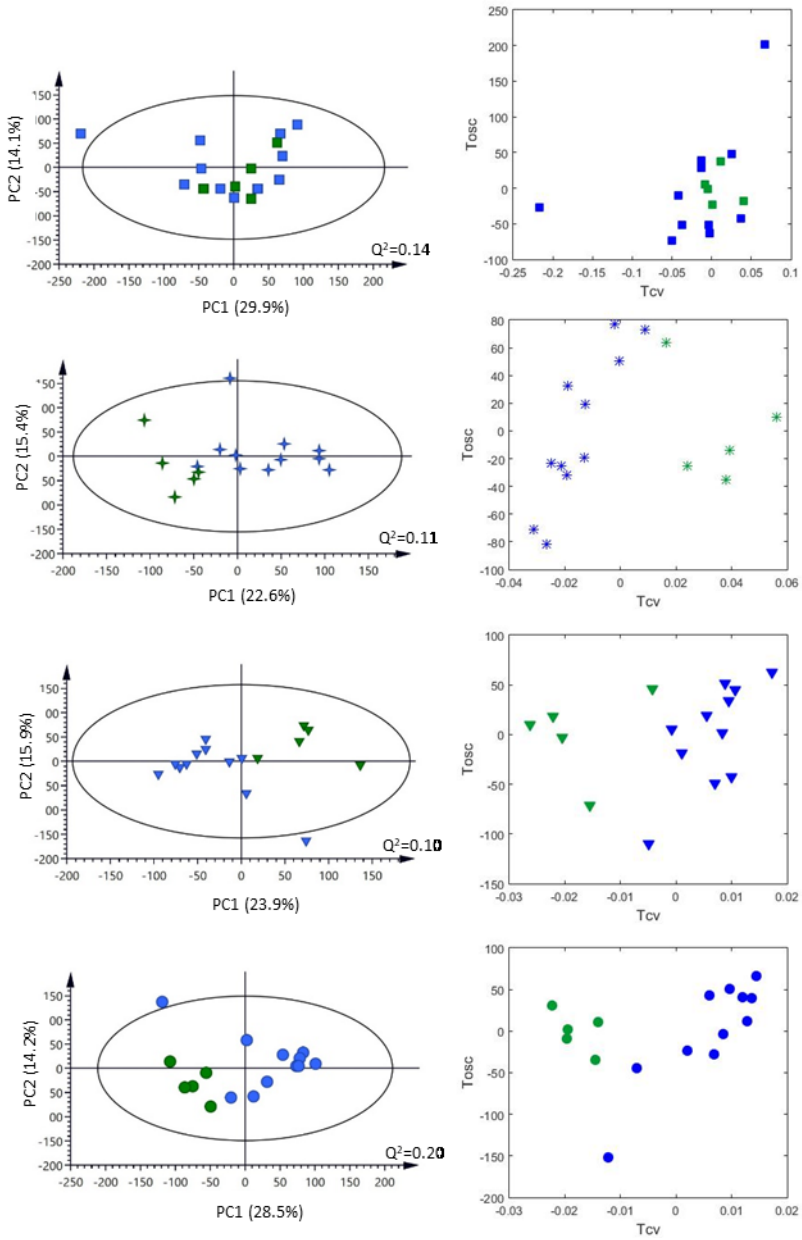


Figure 4-11. PCA scores plots (left) and O-PLS-DA cross-validated scores plots (right) of urinary metabolic profiles between RYGB (blue) and sham-BWM (red) rats at pre-operation (square), 1-week (star), 2-week (inverted triangle) and 3-week (circle) post-operations. Percentage on each PC represents variation explained by each principal component and Q^2 represents predictive ability of the PCA model.

PCA scores and O-PLS-DA cross-validated scores plots of the pairwise comparison between RYGB and sham-BWM at pre-operation suggested the similar urinary metabolic profiles of both groups (Figure 4-11). A clear class separation between RYGB and sham-BWM along PC1 was observed at 1-week post-operation onwards (Figure 4-11). O-PLS-DA analysis determined that higher relative concentrations of propionate, α-ketoisovalerate, arginine, methionine, 4-cresyl glucuronide, choline, glycine, glycerol, 5-hydroxyindole-3-acetate and uridine at only 2-week post-operation, together with

elevated levels of urinary hypotaurine, 4-hydroxyphenylacetate and 5-hydroxytryptophan at 2- and 3-week post-operation in RYGB (Table 4-2). Furthermore, relative concentrations of glyceraldehyde, tyrosine, IS, PAG and unknown 2 (δ^{1}H 8.08 (s); δ^{1}H 8.57 (s)) were found to be higher in RYGB at 3-week post-operation only. Relative concentrations of urinary 3-methyl-2-oxovalerate, lactate, N_{α}-acetyllysine, 2-oxoglutarate and citrate were, however, found to be elevated in sham-BWM during 2- and 3-week post-operation (Table 4-2). In addition, sham-BWM showed higher relative concentrations of urinary 2-ketoisocaproate at only 2-week post-sham operation and phenylalanine, allantoin and fumarate at only 3-week post-sham operation in contrast to RYGB rats (Table 4-2).

4.3.8 Peripheral and portal vein plasma metabolic differences between Roux-en-Y gastric bypass-treated and caloric restriction-treated obese Zucker rats

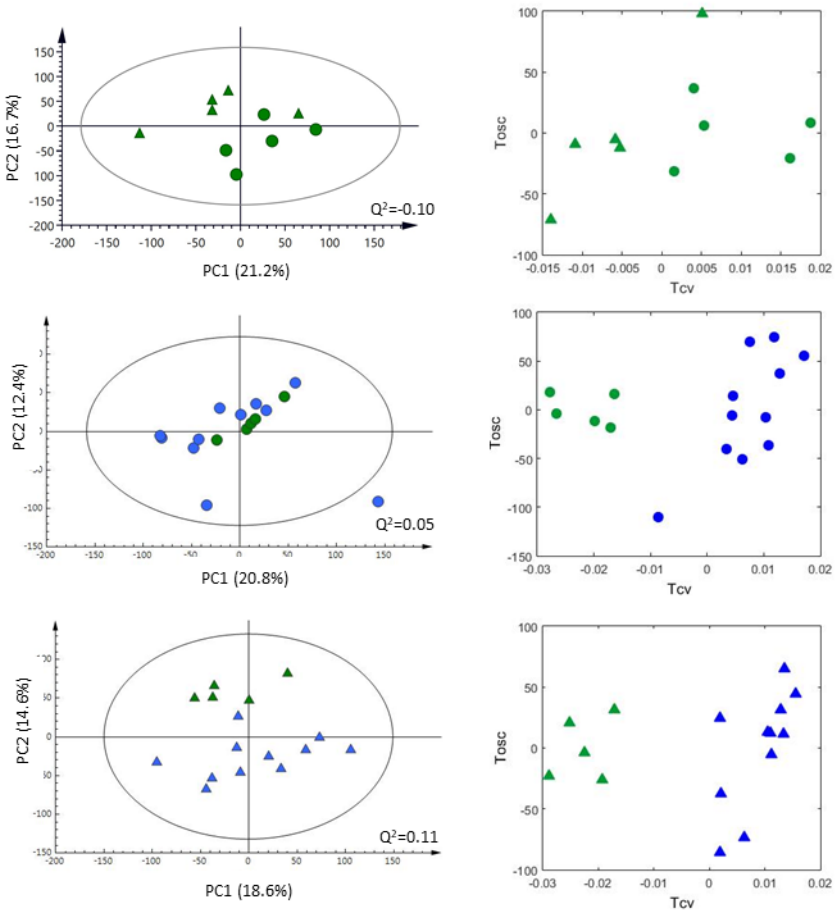


Figure 4-12. PCA scores plots (left) and O-PLS-DA cross-validated scores plots (right) of peripheral (circle) and portal vein (triangle) plasma metabolic profiles of RYGB (blue) and sham-BWM (green) Zucker rats. Percentage on each PC represents variation explained by each principal component and Q^2 represents predictive ability of the PCA model.

Metabolic profiles obtained from peripheral and portal vein plasma of sham-BWM were mildly separated along PC2 as indicated on PCA scores plot and such a separation was also observed on O-PLS-DA cross-validated scores plot (Figure 4-12). O-PLS-DA analysis revealed the significantly higher relative concentrations of *N,N,N*-trimethyllysine and propionate in the portal vein plasma compared with peripheral plasma in the sham-BWM and RYGB rats. More interestingly, portal vein plasma carried higher relative levels of dimethylamine, formate, proline and pyruvate compared with the peripheral plasma in sham-BWM that were quite different from the RYGB rats (Table 4-3).

4.4 Discussion

Roux-en-Y gastric bypass was found to systemically change the metabolic profiles of hyperinsulinemic obese (*fa/fa*) Zucker rats as indicated in the significant alteration of metabolites measured using ^{1}H NMR spectroscopy-based metabolic profiling. This study revealed, for the first time, the global metabolic profiles of all biological matrices including portal vein plasma, peripheral plasma, faeces and urine obtained from RYGB- or caloric restriction-treated hyperinsulinemic obese Zucker rats (Figure 4-12).

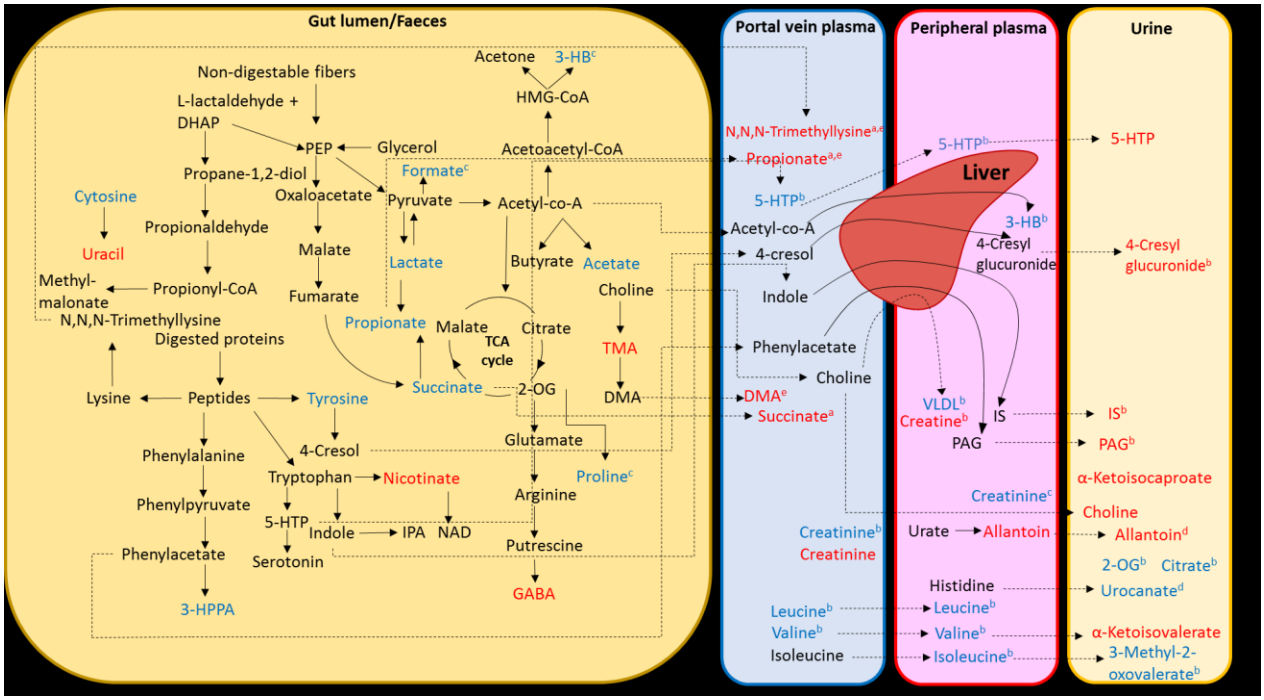


Figure 4-13. Schematic illustration of systemic changes observed in biofluid from RYGB-treated obese Zucker rats in comparison with either sham-obese or sham-BWM rats. Red indicates higher relative concentrations, whereas blue indicates lower relative concentrations of metabolites in RYGB group compared with either sham-obese or sham-BWM rats. [a] indicates the metabolites obtained from comparison model between portal vein plasma or peripheral plasma within the RYGB group; [b] indicates metabolites obtained from the comparison model of RYGB vs. sham-BWM only; [c] indicates metabolites obtained from the comparison model of RYGB vs. sham-obese only; [d] indicates metabolites obtained from comparison model between portal vein plasma or peripheral plasma within the sham-BWM group. Key: 3-HB, 3-hydroxybutyrate; 3-HPPA, 3-hydroxypropionate; PEP, phosphoenolpyruvate; IPA, indole-3-propionate; 5-HTP, 5-hydroxytryptophan; 2-OG, 2-oxoglutarate; TMA, trimethylamine; GABA, γ-amino butyrate; PAG, phenylacetylglycine; IS, indoxyl sulfate; VLDL, very low density lipoprotein.

4.4.1 Increased microbially-derived neuroactive intermediates

Higher concentrations of GABA were found in RYGB group compared with sham-obese rats and sham-BWM rats (Figure 4-13) that may result from the dramatic microbial changes in the GI tract following RYGB (data will be shown in Chapter 5). GABA, a neuroactive peptide has been demonstrated to derive from the microbial processing of putrescine and higher concentrations of GABA in post-RYGB faecal samples have been shown in the previous studies (Kurihara *et al.*, 2010; Li *et al.*, 2011a). GABA can also be produced by the decarboxylation of glutamate catalysed by glutamate decarboxylase (GAD) and cofactor, pyridoxal-5'-phosphate (PLP) (Ueno, 2000). GABA was shown to have hypotensive, tranquilising, diuretic, and anti-diabetic effects (Adeghate & Ponery, 2002). GABA stimulates Glucagon-like peptide-1 (GLP-1) secretion from enterocytes and raises the level of GLP-1, which in turn promotes GABA formation from pancreatic islet of Langerhans β-cells to exert the autocrine and paracrine effects, for instance, regulation of Islet of Langerhans α-cell to inhibit glucagon secretion (Okafor *et al.*, 2015). In addition to GLP-1 regulatory effect, GABA was found to inversely correlate with cell survival in the cytotoxic assay of which mouse lymphoma cell line was treated with RYGB-operated faecal water (Li *et al.*, 2011b). The presence of GABA could indicate the altered intestinal microenvironment that is more favourable towards the GABA-producing bacteria following the RYGB operation.

Relative concentration of 5-HTP was found to be lower in portal vein and peripheral plasma of RYGB when comparing RYGB vs. sham-BWM only but higher in urine when comparing RYGB with both sham-obese and sham-BWM (Figure 4-13). 5-HTP is a precursor of 5-hydroxytryptamine (5-HT) or serotonin which is a critical signalling molecule in the brain-gut-microbial axis (Yano *et al.*, 2015; O'Mahony *et al.*, 2015). Higher relative concentration of 5-HTP in urine could indicate that serotonin was lower in the tissue. The synthesis of 5-HT begins with the conversion of tryptophan, a precursor for both host serotonin and bacterial tryptamine biosynthesis, to 5-HTP and then 5-HT

catalysed by tryptophan hydroxylase (TRH) and aromatic L-amino acid decarboxylase (L-AADC) in the host, respectively. The newly synthesised 5-HT in the enterochromaffin (EC) cells is contained in the vesicle prior to secretion following mechanical or chemical stimulation of the mucosa (Nzakizwanayo *et al.*, 2015). 5-HTP acts on G-protein-coupled receptor (GPCR) within the GI tract to modulate gut motility (Dale, Hollingworth & McKenna, 2011).

4.4.2 Altered microbial activity on aromatic amino acid metabolism and biosynthesis of host-microbial co-metabolites following RYGB

Microbial metabolism of aromatic amino acids (e.g. phenylalanine, tryptophan and tyrosine) was altered in obese Zucker rats-treated with RYGB, as evidenced by lower level of faecal 3-HPPA, higher levels of PAG in portal vein plasma and urine, and urinary IS in RYGB compared with either sham-obese or sham-BWM (Figure 4-13).

With respect to the results previously reported in Chapter 3, faecal relative concentration of 3-HPPA was found to be higher in faeces obtained from obese Zucker rats compared with lean Zucker rats. However, the faecal level of this microbial polyphenol metabolite decreased post-RYGB operation (Figure 4-13). 3-HPPA is a keto-acid intermediate derived from phenylalanine which is metabolised by gut microbiota *via* phenylacetate (Diaz *et al.*, 2001; Teufel *et al.*, 2010) (Figure 4-13). In this study, the urinary concentration of PAG in RYGB rats was shown to be higher than that of sham-obese and sham-BWM rats. PAG is a host-microbial co-metabolite that results from the microbial metabolism of phenylalanine to phenylacetate, which is conjugated with glycine in the rat liver to produce PAG or with glutamine in the human liver to produce phenylacetylglutamine (Dinan & Cryan, 2017). Higher urinary PAG level post-RYGB found in this study is consistent with the previous study (Li *et al.*, 2011a). Our findings indicate that RYGB results in the greater conversion of phenylalanine to PAG rather than

3-HPPA while in the sham-obese and sham-BWM rats' production of phenylacetate from phenylalanine seems to be enhanced and excreted as 3-HPPA in faeces.

Higher relative concentrations of urinary IS in RYGB rats, compared with sham-obese or sham-BWM rats, was observed in this study. Indoxyl sulfate is derived from the bacterial metabolite indole through hepatic biotransformation (Shimizu *et al.*, 2012). Aerobic gut microbes such as *Escherichia coli* are mainly responsible for the indole pool which arises from dietary tryptophan metabolism (Li *et al.*, 2011a). This metabolite is also considered a uremic toxin associated with atherosclerosis (Shimizu *et al.*, 2012). The results in the current study may indicate the adverse effect of bariatric surgery on both the heart and the kidneys to act on the cardiorenal syndrome.

Intestinal bacteria have been shown to be able to metabolise dietary tyrosine to 4-cresol that, upon the absorption from the gut, is glucuronidated in the liver to yield 4-cresyl glucuronide as a host-microbial co-metabolite and an end product of tyrosine biotransformation by anaerobic intestinal bacteria (Poesen *et al.*, 2016) (Figure 4-13). In this study, the elevated concentration of 4-cresyl glucuronide, accompanied with higher levels of PAG and IS, further suggested increased microbial activity producing precursors of these urinary host-microbial co-metabolites.

4.4.3 Beneficial effects associated with altered SCFA production

SCFA production occurs in the distal small intestine and colon where non-digestible carbohydrates, such as resistant starch, dietary fibre, and other low-digestible polysaccharides, are fermented by the saccharolytic bacteria including the phyla *Bacteroidetes*, *Firmicutes* and *Actinobacteria* (den Besten *et al.*, 2013). Lower concentrations of faecal SCFAs (e.g. acetate and propionate) were found in RYGB-treated obese Zucker rats compared with sham-obese rats, which could result from the decreased bioavailability of the fermentation substrates due to a lower amount of food

intake and/or decreased microbial fermentation of non-digestible carbohydrates by the potent gut microbiota in the RYGB rats.

Propionate stimulates the secretion of both GLP-1 and PYY from L-cells in the mucosa of gastrointestinal tract (Byrne *et al.*, 2015). It has previously been found to inhibit cholesterol synthesis, thereby antagonizing the cholesterol-increasing action of acetate, and to inhibit the expression of resistin, an adipose tissue-specific secretory factor (ADSF) in adipocytes. It is, furthermore, known that propionate is a gluconeogenic substrate and inhibits the utilisation of acetate for lipid and cholesterol synthesis (Demigne *et al.*, 1995; Byrne *et al.*, 2015). A previous study reported that mice which received the caecal content from RYGB-operated animals showed greater production of propionate and lower production of acetate compared with the recipients with the caecal content from sham-operated mice (Liou *et al.*, 2013). In this study, relative propionate concentration was found to be lower in faeces but higher in portal vein plasma of RYGB, accompanied with lower concentration of faecal acetate. These observations indicate that RYGB rats could exhibit greater production of propionate and lower production of acetate via microbial fermentation when comparing with sham-obese or sham-BWM rats. Luminal propionate could subsequently be taken to the liver through the portal vein blood in the RYGB animals, which resulted in lower faecal levels of propionate. The reduced faecal levels of acetate may affect the acetate bioavailability in the liver and adipose tissue and therefore decrease lipogenesis. The elevated levels of propionate may also assist the inhibition of acetate conversion into lipid in the liver and adipose tissue.

4.4.4 Effects of RYGB on BCAA metabolism

Peripheral plasma levels of BCAA were shown to be higher in obese Zucker rats compared with their lean counterparts as reported in Chapter 3. In the current study, BCAAs such as leucine and valine were lower in peripheral plasma of RYGB compared with sham-obese or sham-BWM rats (Figure 4-13). Moreover, leucine, valine and

isoleucine were found to be lower in portal vein plasma of RYGB rats (Figure 4-13). In addition to the decreased levels of BCAAs in both peripheral and portal vein plasma, higher level of α-ketoisovalerate, along with lower levels of α-ketoisocaproate and 3-methly-2-oxovalerate were found to be excreted in urine of RYGB rats (Figure 4-13). α-Ketoisovalerate, α-ketoisocaproate and 3-methly-2-oxovalerate are the breakdown products of valine, leucine and isoleucine, respectively (Karlsson, Ko & Blomstrand, 2006). Increases in plasma BCAAs and their C3 and C5 acylcarnitine metabolites have been reported to be involved in the pathogenesis of insulin resistance (Newgard *et al.*, 2009). The findings in the current study suggested that RYGB–induced improvement in insulin sensitivity decreases plasma BCAA concentrations by reducing skeletal muscle protein breakdown and the release of BCAA into the circulation. This is supported by previous studies showing that insulin infusion resulted in a marked decrease in total plasma BCAA concentrations (Magkos *et al.*, 2013; Chen *et al.*, 2011).

4.4.5 Effects of caloric restriction on metabolic alteration in comparison with RYGB operation

Urinary level of 5-hydroxyindole-3-acetate (5-HIAA) was only found to be higher in RYGB when compared with sham-BWM rats in the current study (Figure 4-13). 5-HIAA is a breakdown product of serotonin that transmits signals between nerve cells and is excreted in the urine. 5-HIAA was reported to be significantly associated with four metabolic syndrome components including central obesity, raised triglycerides, raised blood pressure, and raised fasting plasma glucose (Afarideh *et al.*, 2015). This means that, despite the similar weight loss, caloric restriction provides lower risk of developing the aforementioned metabolic conditions compared with RYGB approach.

Sham-BWM rats exhibited lower levels of hypotaurine in urine compared with RYGB only (Figure 4-12). Hypotaurine is a product of the enzyme cysteine dioxygenase (CDO) that catalyses the conversion of cysteine to cysteine sulfonate which, in turn, can be

converted into hypotaurine catalysed by cysteinesulfonate decarboxylase (CSAD) (Cummins *et al.*, 2014). In addition, hypotaurine, a taurine precursor, can act as a hydroxyl radical scavenger and inhibit lipid peroxidation, and therefore prevent iron (Fe^{2+}) self-oxidation (De Carvalho *et al.*, 2017). Furthermore, taurine is proposed to generate several physiological effects, for example, regulation of calcium homeostasis in both skeletal muscle and cardiac tissue (Huxtable, 1992), increased muscle force (Schaffer *et al.*, 2010), improved lipid metabolism (Murakami, 2015), and increased insulin sensitivity (Cappelli *et al.*, 2014). In addition, taurine may improve carbohydrate metabolism and favour glycogen re-synthesis (Ito *et al.*, 2009). Higher relative concentration of urinary hypotaurine in RYGB rats may contribute to the profound resolution of metabolic syndrome in the obese Zucker rats, whereas lower urinary hypoxanthine level in sham-BWM rats may result from the impacts of caloric restriction that enhances catabolism of stored energy source such as glycogen. Hypoxanthine is a purine-based organic compound. It is formed during the purine catabolism as a product of xanthine oxidase action on xanthine. It is also a reaction intermediate in adenosine metabolism and in formation of nucleic acids by the salvage pathway (Robillard, Bone & Hammond, 2008).

Urinary concentration of 3-hydroxybutyrate (3-HB) was found to be lower in sham-BWM compared with RYGB but this is not observed when comparing RYGB with sham-obese rats (Figure 4-13). When blood glucose is low, ketones are produced through fatty acid β-oxidation in the liver and disseminated via the blood stream. This glucose replacement ensures sufficient energy support for the body, especially the brain (Nehlig, 2004). 3-HB is synthesized in the liver from acetyl-CoA and can be, therefore, used as an energy source by the brain when blood glucose is low. Gut microbiota play a key role in enhancing 3-HB production during starvation and moderating the steady-state ketogenic profile. It is thought to be a consequence of the enhanced stored energy afforded by gut microbial SCFA production (Crawford *et al.*, 2009). A previous study has demonstrated that when either colonic SCFA or 3-HB production is enhanced, gut microbial-regulated metabolites in the circulation are capable of directly mediating effects on host cells *via*

GPCR signalling (Selkrig *et al.*, 2014). Results in the current study demonstrate that caloric restriction approach may not be powerful enough to exert the metabolic changes despite the similar weight loss and restricted amount of food compared with RYGB.

4.5 Summary

Collectively, metabolic alterations induced by the RYGB operation include the enhanced production of neuroactive metabolites including GABA and 5-HTP that can exert their effects on hormonal regulation and gut motility, respectively. Many microbial metabolites and host-microbial co-metabolites were altered in the faecal, urinary and plasma metabolic profiles following the RYGB surgery. Even though caloric restriction demonstrates some metabolic changes that represent the health benefits, its effectiveness as a resolution for metabolic syndrome, especially T2DM has not been observed in this study in spite of the significant weight reduction. However, the underlying mechanisms of gut-brain-microbe axis after the weight loss surgery should be further addressed.

5. UPLC-MS-Based Metabolic Profiling and 16S rRNA Gene Sequencing of Gastrointestinal Contents Obtained from Obese Zucker Rats-treated with RYGB or Caloric Restriction

5.1 Aim

The aim of this study was to (1) investigate genotype-related metabolic profiles of the luminal contents obtained from Zucker obese and lean rats; (2) examine effects of caloric restriction on the luminal content of obese Zucker rats; (3) investigate RYGB-induced metabolic alteration in the luminal contents; (4) assess the gut microbial shifts caused by either caloric restriction or RYGB operation along the gastrointestinal tract; and (5) investigate the statistical correlation between the metabolites and the gut bacteria, which are significantly changed by either caloric restriction or RYGB operation.

5.2 Materials and methods

Experimental design, animal experiment, sample collection, preparation for UPLC-MS spectrometry analysis, UPLC-MS data analyses along with DNA isolation for Ilumina MiSeq sequencing and phylogenetic identification and data analysis have been described in Chapter 2. It is noted that 16S rRNA sequencing experiment was performed on the five randomised representatives of each group due to the limited amount of some samples and cost-effectiveness of the analytical platform.

5.3 Results

5.3.1 Changes in pH after caloric restriction or RYGB operation

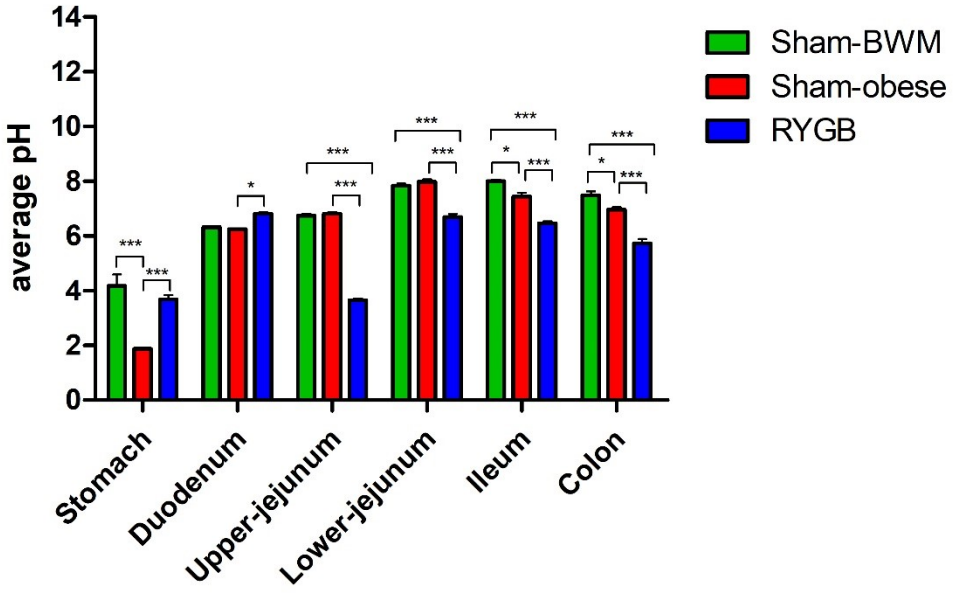


Figure 5-1. Measurement of pH in different gastrointestinal contents of sham-obese, sham-BWM and RYGB groups. Data are shown as mean ± SEM (* p < 0.05; ** p < 0.01 and *** p < 0.001) and statistical differences determined by one-way ANOVA.

Contents obtained from distal stomach (bypassed portion) of RYGB and stomach of caloric restriction groups (3.68 ± 0.15 and 4.18 ± 0.41, respectively) showed higher pH than that of sham-obese rats (1.88 ± 0.01) (Figure 5-1). However, pH of duodenal contents was similar in all groups. More interestingly, upper-jejunal pH of RYGB (3.65 ± 0.07) was much lower than sham-BWM and obese control. Lower compartments of the GI tract, including lower-jejunum, ileum and colon, demonstrated lower pH values in the RYGB animals compared with either sham-BWM or sham-obese rats.

5.3.2 Genotype-related metabolic profiles of gastric and intestinal contents of obese and lean Zucker rats

PCA and O-PLS-DA pairwise comparison models were constructed in order to visualise the metabolic fingerprints indicating the genotype-related metabolic differences, and RYGB or caloric restriction-induced changes in each luminal compartment (Table 5-1).

Table 5-1. Summary of O-PLS-DA statistical parameters for all pairwise comparison models demonstrated in Chapter 5.

GI content	Model	O-PLS-DA statistical parameter					
		R^2X		Q^2Y		Permutation P value	
		POS	NEG	POS	NEG	POS	NEG
Stomach content	Sham-lean vs. Sham-obese	49.7%	55.2%	-0.24	0.35	1	0.140
	Sham-BWM vs. Sham-obese	61.3%	**55.9%**	0.14	**0.59**	0.352	**0.014**
	RYGB vs. Sham-obese	**69.7%**	**61.5%**	**0.88**	**0.91**	**0.002**	**0.002**
	RYGB vs. Sham-BWM	**77.4%**	**74.5%**	**0.98**	**0.98**	**0.002**	**0.002**
Duodenum content	Sham-lean vs. Sham-obese	47.8%	48.9%	0.24	0.30	0.340	0.196
	Sham-BWM vs. Sham-obese	**45.4%**	**46.3%**	**0.67**	**0.58**	**0.05**	**0.022**
	RYGB vs. Sham-obese	49.3%	40.5%	<0	<0	1	0.500
	RYGB vs. Sham-BWM	49.3%	46.1%	0.18	<0	0.216	0.476
Upper-jejunum content	**Sham-lean vs. Sham-obese**	**57.0%**	63.0%	**0.60**	<0	**0.008**	0.756
	Sham-BWM vs. Sham-obese	**60.0%**	67.7%	**0.66**	<0	**0.05**	0.940
	RYGB vs. Sham-obese	**61.9%**	57.7%	**0.67**	<0	**0.008**	0.728
	RYGB vs. Sham-BWM	**60.0%**	21.4%	**0.66**	<0	**0.05**	0.846
Lower-jejunum content	**Sham-lean vs. Sham-obese**	**52.2%**	**51.1%**	**0.67**	**0.73**	**0.04**	**0.002**
	Sham-BWM vs. Sham-obese	47.9%	44.9%	<0	<0	0.644	0.512
	RYGB vs. Sham-obese	**26.6%**	**42.0%**	**0.69**	**0.77**	**0.002**	**0.002**
	RYGB vs. Sham-BWM	**43.0%**	46.2%	**0.67**	0.71	**0.001**	0.846
Ileum content	**Sham-lean vs. Sham-obese**	**54.3%**	**48.6%**	**0.71**	**0.61**	**0.014**	**0.046**
	Sham-BWM vs. Sham-obese	**49.5%**	40.0%	**0.69**	0.34	**0.034**	0.234
	RYGB vs. Sham-obese	**42.1%**	**38.4%**	**0.88**	**0.59**	**0.002**	**0.002**
	RYGB vs. Sham-BWM	**49.5%**	**38.9%**	**0.57**	**0.65**	**0.004**	**0.004**
Colon content	**Sham-lean vs. Sham-obese**	53.2%	**53.2%**	0.50	**0.50**	0.096	**0.002**
	Sham-BWM vs. Sham-obese	59.0%	**40.0%**	0.04	**0.34**	0.406	**0.002**
	RYGB vs. Sham-obese	**33.8%**	**38.4%**	**0.52**	**0.59**	**0.024**	**0.002**
	RYGB vs. Sham-BWM	**38.4%**	**38.9%**	**0.62**	**0.65**	**0.01**	**0.002**

Abbreviations: GI, Gastrointestinal; POS, Positive electrospray ionisation mode; NEG, Negative electrospray ionisation mode. Bold indicates significant statistical models.

PCA scores plots (Figure 5-2) of HILIC-MS (ESI+) data obtained from the duodenal, upper-jejunal, lower-jejunal and ileal contents showed distinct clustering between Zucker obese and lean rats along PC1 (38.2%), PC2 (18.4%), PC1 (38%) and PC1 (38.1%), respectively. A clear clustering between the two genotypes was also observed in the PCA scores plot of the HILIC-MS (ESI-) data of the lower-jejunal content along the PC1 (Figure 5-2). O-PLS-DA analysis was applied to investigate the genotype-related metabolic changes and permutation testing was used to confirm the model robustness (Table 5-1). Significant metabolic differences between Zucker obese and lean rats were observed in the upper-jejunal contents (ESI+ mode), lower-jejunal contents (ESI+ & ESI- modes), ileal content (ESI+ & ESI- modes), and colonic content (ESI- mode). Metabolic features for class discrimination were visualised in S-plots in SIMCA with the cut-off values of p(corr)>0.5 and p[1]>0.05 were used as selection criteria that were availed throughout this study. A total of 25 significantly altered features were identified, nine in ESI+ and 16 in ESI- modes, from upper-jejunum, ileum and colon contents compared between Zucker obese and lean rats (Table 5-2). In the positive ionisation mode, levels of taurine, cytosine and 5-hydroxymethyluracil in the upper-jejunum content were higher and levels of decanoylcarnitine and lysophosphatidylcholine (LysoPC) (O-18:2) were lower in obese rats compared with lean animals (Table 5-2).

Lower-jejunal content of obese Zucker rat contained lower concentrations of L-asparagine and L-tryptophan detected in the positive ionisation mode but higher levels of S-adenosylhomocysteine observed in the negative ionisation mode (Table 5-2).

In the ileal content, relative concentrations of arachidonyl-1-thio-glycerol, arachidonic acid, cholesterol sulfate, D-glucuronic acid, α-CEHC and γ-glutamylglutamic acid were found to be significantly lower, whereas the concentrations of *N1*-acetylspermidine and pantothenic acid were found to be higher in obese rats compared with lean animals. The relative concentrations of cycteinyldopa, octadecanedioic acid and pantothenic acid in

colonic contents were significantly higher in the lean animals, whereas the levels of 4-pyridoxic acid and hippuric acid were higher in obese rats (Table 5-2).

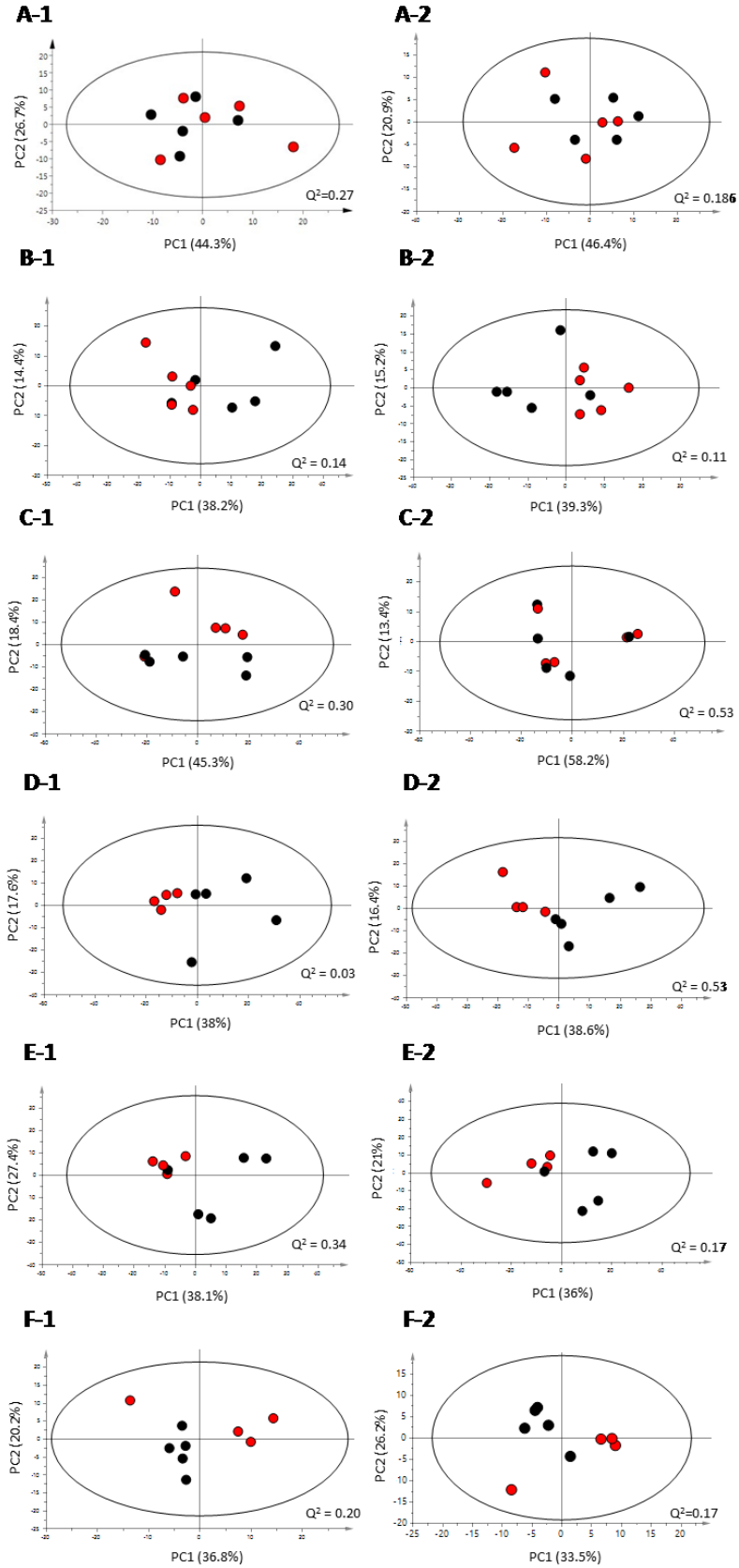


Figure 5-2. PCA scores plots of HILIC-UPLC-MS data sets of the luminal content from stomach (A), duodenum (B), upper-jejunum (C), lower-jejunum (D), ileum (E) and colon (F) of lean (black) and obese (red) Zucker rats at 3-week post-operation. Left and right panels represent positive (1) and negative (2) modes.

Table 5-2. List of metabolites found in different gastrointestinal contents obtained from pairwise O-PLS-DA analysis between Zucker obese and lean rats

Metabolite	GI Content**	LoA*	Molecular formula [Adduct]	Retention time (min)	m/z observed	m/z theoretical	Δppm	CV %
HILIC Positive Mode								
L-Asparagine	LJ[b]	2	$C_4H_8N_2O_3$ $[M+H]^+$	6.72	132.0531	132.0535	3	9
L-Tryptophan	LJ[b]	2	$C_{11}H_{12}N_2O_2$ $[M+H]^+$	5.53	204.0901	204.0899	4	14
Taurine	UJ[a]	3	$C_2H_7NO_3S$ $[M+Na]^+$	5.70	125.0144	125.1470	0	10
Cytosine	UJ[a]	2	$C_4H_5N_3O$ $[M+Na]^+$	3.88	111.0422	111.0000	3	21
5-Hydroxymethyluracil	UJ[a]	1	$C_5H_6N_2O_3$ $[M+H]^+$	5.70	142.0413	142.0378	2	11
Decanoylcarnitine	UJ[b]	1	$C_{17}H_{34}NO_4$ $[M+H]^+$	6.07	316.2216	316.2448	-1	11
lysoPC(O -18:2)	UJ[b]	1	$C_{26}H_{53}NO_6P$ $[M+H]^+$	7.07	506.2604	506.3610	0	16
Arachidonoyl-1-thio-Glycerol	I[b]	1	$C_{23}H_{38}O_3S$ $[M+NH_4]^+$	5.3402	394.246	394.3000	7	27
Arachidonic acid	I[b]	1	$C_{20}H_{31}O_2$ $[M+H]^+$	0.78	303.2350	303.2324	4	26
Cholesterol sulfate	I[b]	1	$C_{27}H_{45}O_4S$ $[M+H]^+$	2.64	465.2858	465.3039	5	27
N1-Acetylspermidine	I[a]	1	$C_{12}H_{28}N_4O$ $[M+H]^+$	8.50	187.168	187.1865	2	12
HILIC Negative Mode								
S-Adenosylhomocysteine	LJ[a]	1	$C_{14}H_{20}N_6O_5S$ $[M-H]^-$	6.41	384.1112	384.1216	3	6
Luteinizing hormone-releasing factor	I[b]	1	$C_{50}H_{70}N_{16}O_{11}$ $[M-H_2O-H]^-$	4.41	1070.5730	1,070.5400	26	22
D-Glucuronic acid	I[b]	2	$C_6H_{10}O_7$ $[M-H]^-$	6.09	194.0417	194.0430	7	3
α-CEHC	I[b]	1	$C_{16}H_{22}O_4$ $[M-H]^-$	0.83	278.1522	278.1520	1	9
γ-Glutamylglutamic acid	I[b]	1	$C_{10}H_{16}N_2O_7$ $[M-H_2O-H]^-$	0.70	276.1036	276.0960	14	9
Pantothenic Acid	I[a] / C[b]	2	$C_9H_{17}NO_5$ $[M-H]^-$	3.84	219.1100	219.1110	6	16
N_α-acetyllysine	I[a]	1	$C_8H_{16}N_2O_3$ $[M-H]^-$	6.35	188.115	188.1000	9	11
N2-Acetyl-L-ornithine	I[a]	1	$C_7H_{14}N_2O_3$ $[M-H]^-$	6.56	174.1001	174.1000	6	13
Succinic acid	I[a]	5	$C_4H_6O_4$ $[M-H]^-$	3.80	118.0274	118.0266	2	4

Glycocholic Acid	I[a]	2	$C_{26}H_{43}NO_6$ $[M+Cl]^-$	5.63	465.8241	465.3090	8	26
Cysteinyldopa	C[b]	1	$C_{12}H_{16}N_2O_6S$ $[M-H_2O-H]^-$	0.69	316.1349	316.0730	15	13
Octadecanedioic acid	C[b]	1	$C_{18}H_{34}O_4$ $[M-H]^-$	0.79	314.2446	314.2000	4	7
4-Pyridoxic acid	C[a]	1	$C_8H_9NO_4$ $[M-H]^-$	0.90	183.052	183.0530	10	7
Hippuric acid	C[a]	5	$C_9H_9NO_3$ $[M-H]^-$	5.94	179.0342	179.0580	29	14

***LoA: Level of Assignment; 1: Accurate mass matched to database, 2: Accurate mass matched to database and tandem MS spectrum matched to *in silico* fragmentation pattern, 3: Tandem MS spectrum matched to database or literature, 4: Retention time and the molecular mass matched to standard compound, 5: MS/MS spectrum matched standard compound. **GI contents involved in the analyses comprise of lower-jejunum (LJ), upper-jejunum (UJ), ileum (I) and colon (C). [a] indicates metabolite with higher intensity in obese Zucker rats, whereas [b] indicates metabolite with higher intensity in lean Zucker rats.**

5.3.3 Effects of caloric restriction on metabolic profiles of gastric and intestinal contents

HILIC-UPLC-MS data obtained from gastrointestinal contents of sham-BWM and sham-obese rats were analysed to examine the metabolic effects of caloric restriction on the luminal contents along the gastrointestinal tract. PCA scores plots of gastrointestinal contents between these two groups are shown in Figure 5-3. The gastric content of sham-BWM rats clustered together and differentiated from that of sham-obese rats along PC1 (R^2X=18.1%) in the positive ionisation mode (Figure 5-3: A-1) and along PC2 (R^2X=20%) in the negative ionisation mode (Figure 5-3: A-2). Likewise, a distinct separation of duodenal contents between sham-BWM and sham-obese rats along PC1 was observed in both ionisation modes (Figure 5-3: B-1 and B-2). However, such clear clustering between these two groups was not observed in jejunal, ileal and colonic contents (Figure 5-3: C-F).

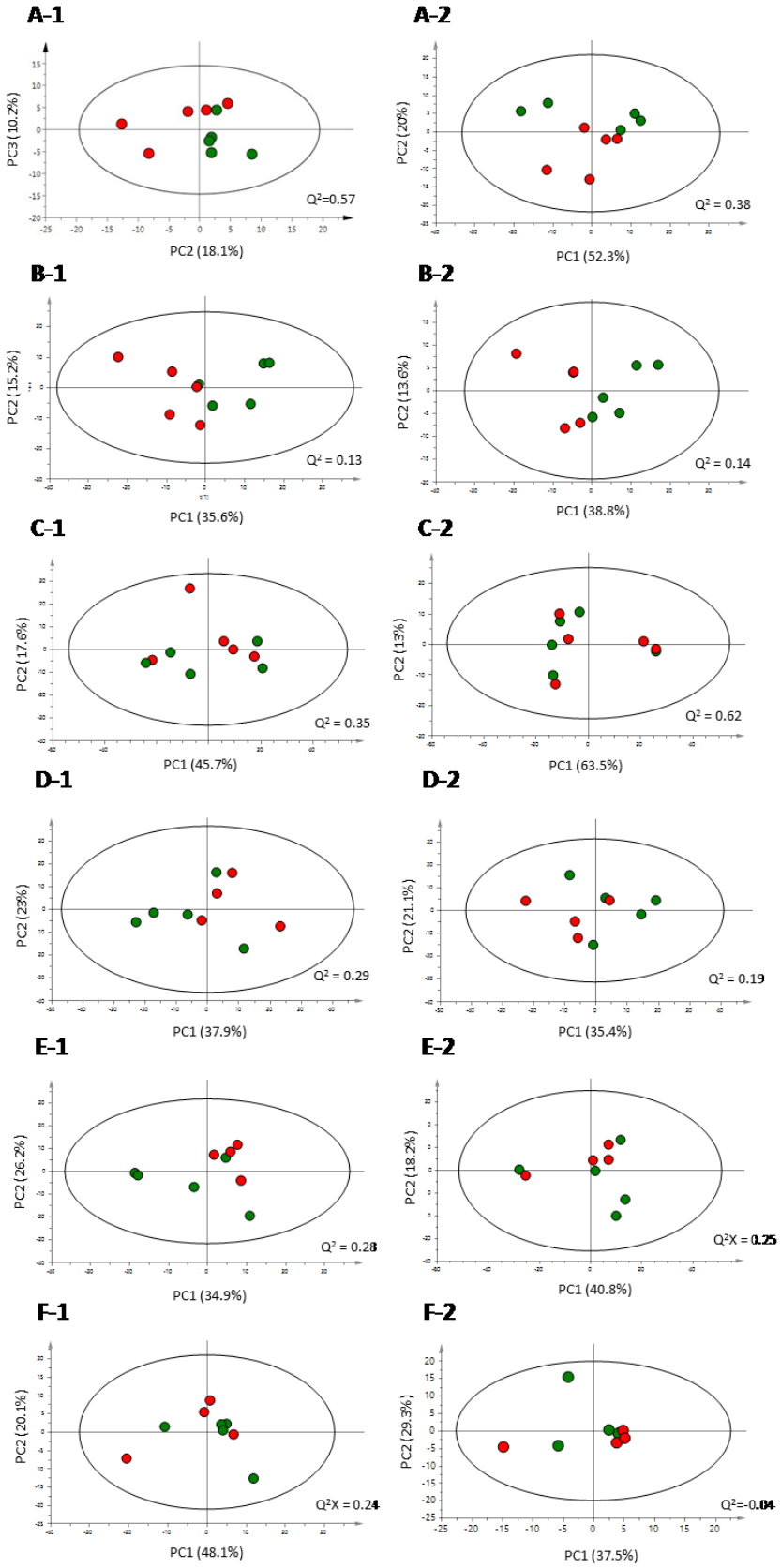


Figure 5-3. PCA scores plots of GI content data set including stomach (A), duodenum (B), upper-jejunum (C), lower-jejunum (D), ileum (E) and colon (F) contents of sham-BWM (green) and sham-obese (red) Zucker rats at 3-week post-sham-operation analysed using HILIC-UPLC-MS positive (1) and negative (2) modes.

O-PLS-DA analyses showed significant classification between the sham-obese and sham-BWM in the gastric (negative ionisation mode), duodenal (both ionisation modes), upper jejunal (positive ionisation mode), ileal (positive ionisation mode) and colonic (negative ionisation mode) contents (Table 5-1). The significantly altered features, which are related to caloric restriction, are summarised in Table 5-3. The higher relative levels of alanyl-leucine and glutathionylspermidine and lower PC(7:0/8:0) were observed in the gastric contents of the BWM rats compared with that of the obese animals. A large number of altered metabolites were found in the duodenal contents between the obese and BWM animals. For example, relative concentrations of 3-aminopropanal, homoserine lactone, cysteine, L-phenylalanine and merodesmosine were higher in sham-BWM rats compared with sham-obese rats. Sham obese rats, on the other hand, exhibited higher duodenal levels of δ-tocopherol, PS(12:0/14:1), PS(18:0/18:1), phosphatidylcholine (PC) (O-12:0/O-1:0), PC(16:0/20:3), PC(18:3/22:6), TG(17:0/18:1), PG(P-18:0/0:0), glycocholic acid and deoxycholic acid glycine conjugate in contrast to the BWM animals. In the upper jejunal content, concentrations of PS(18:2/22:2), 7-hydroxy-3-oxocholanoic acid, hypotaurine, isotricosanoic acid, cis-(homo)2aconitate, tetracosahexaenoic acid, taurine and nicotinic acid were found to be higher in the obese rats. A range of metabolites including homovanillic acid, L-furosine, butyro-betaine, *N*-acetyl-L-glutamate 5-semialdehyde, 2-aminooctanoic acid and glycyl-asparatate in the ileal contents were higher in sham-BWM contents when comparing with the obese group. Moreover, higher relative concentrations of L-furosine and lower concentrations of Austalide I were found in the colonic contents from sham-BWM rats compared with their obese counterparts (Table 5-3).

Table 5-3. List of metabolites found in different gastrointestinal contents obtained from pairwise O-PLS-DA analysis between caloric restriction-treated and obese Zucker rats

Metabolite	GI Content	LoA*	Molecular formula [Adduct]	Retention time (min)	m/z observed	m/z theoretical	Δppm	CV %
HILIC Positive Mode								
3-Aminopropanal	D[a]	3	C_3H_7NO $[M+H]^+$	6.20	73.0526	73.0528	7	6
Homoserine lactone	D[a]	1	$C_4H_7NO_2$ $[M+H]^+$	6.24	101.0482	101.0477	10	14
Cysteine	D[a]	2	$C_3H_7NO_2S$ $[M+H]^+$	5.64	121.0201	121.0197	7	7
L-Phenylalanine	D[a]	5	$C_9H_{11}NO_2$ $[M+H]^+$	5.71	165.1691	165.079	10	8
δ-Tocopherol	D[b]	1	$C_{27}H_{46}O_2$ $[M+Na]^+$	4.80	402.3523	402.3498	7	18
PC(O-12:0/O-1:0)	D[b]	1	$C_{21}H_{46}NO_6P$ $[M+NH_4]^+$	0.85	439.2911	439.3063	22	6
PS(15:0/0:0)	D[b]	1	$C_{21}H_{42}NO_9P$ $[M+H]^+$	4.78	483.2631	483.2597	8	13
PS(12:0/14:1)	D[b]	1	$C_{32}H_{60}NO_{10}P$ $[M+H]^+$	0.88	649.3854	649.3955	15	8
PC(16:0/20:3)	D[b]	1	$C_{44}H_{82}NO_8P$ $[M+H]^+$	0.86	783.5630	783.5778	10	23
PS(18:0/18:1)	D[b]	1	$C_{42}H_{80}NO_{10}P$ $[M+H]^+$	0.86	806.5641	806.5785	17	11
PC(18:3/22:6)	D[b]	1	$C_{48}H_{78}NO_8P$ $[M+H]^+$	4.97	827.5329	827.5465	5	18
TG(17:0/18:1)	D[b]	1	$C_{58}H_{110}O_6$ $[M+NH_4]^+$	5.51	902.7980	902.8302	29	29
PS(18:2/22:2)	UJ[b]	1	$C_{46}H_{82}NO_{10}P$ $[M+H]^+$	0.87	839.5590	839.5676	10	14
7-Hydroxy-3-oxocholanoic acid	UJ[b]	1	$C_{24}H_{38}O_4$ $[M+H]^+$	0.86	390.2724	390.2770	1	8
Hypotaurine	UJ[b]	2	$C_2H_7NO_2S$ $[M+H]^+$	6.36	109.0128	109.0197	9	14
Isotricosanoic acid	UJ[b]	1	$C_{23}H_{46}O_2$ $[M+H]^+$	0.86	354.3426	354.3498	3	14

cis-(homo)2aconitate	UJ[b]	1	$C_8H_{10}O_6$ [M+H]$^+$	4.27	202.0433	202.0477	10	22
Tetracosahexaenoic acid	UJ[b]	1	$C_{24}H_{36}O_2$ [M+H]$^+$	5.90	356.2680	356.2715	8	10
Taurine	UJ[b]	5	$C_2H_7NO_3S$ [M+H]$^+$	5.70	125.0122	125.0146	0	5
Nicotinic acid	UJ[b]	5	$C_6H_5NO_2$ [M+H]$^+$	4.77	123.0321	123.0320	6	12
Homovanillic acid	I[a]	1	$C_9H_{10}O_4$ [M+H]$^+$	0.72	182.0525	182.0579	1	19
L-Furosine	I[a]	1	$C_{12}H_{18}N_2O_4$ [M+H]$^+$	9.25	254.1235	254.1267	4	26
Butyrobetaine	I[a]	3	$C_7H_{16}NO_2$ [M+H]$^+$	7.76	144.1326	145.1388	1	16
N-Acetyl-L-glutamate 5-semialdehyde	I[a]	1	$C_7H_{11}NO_4$ [M+H]$^+$	7.09	173.0680	173.0688	0	15
2-Aminooctanoic acid	I[a]	1	$C_8H_{17}NO_2$ [M+H]$^+$	5.55	159.1260	159.1259	5	13
Glycyl-Aspartate	I[a]	1	$C_6H_{10}N_2O_5$ [M+H]$^+$	7.61	190.0537	190.0590	4	13
HILIC Negative Mode								
Alanyl-Leucine	S[a]	1	$C_9H_{18}N_2O_3$ [M-H]$^-$	6.46	202.1284	202.1000	2	10
Glutathionylspermidine	S[a]	1	$C_{17}H_{34}N_6O_5S$ [M-H_2O-H]$^-$	7.14	434.245	434.2311	17	9
PC(7:0/8:0)	S[b]	1	$C_{23}H_{46}NO_8P$ [M+Cl]$^-$	5.34	495.2732	495.2961	14	11
L-Phenylalanine	D[a]	5	$C_9H_{11}NO_2$ [M-H]$^-$	5.71	165.0821	165.0790	10	15
Merodesmosine	D[a]	1	$C_{18}H_{34}N_4O_6$ [M-H]$^-$	6.50	402.1660	402.2478	1	19
Glycocholic Acid	D[b]	3	$C_{26}H_{43}NO_6$ [M-H]$^-$	5.63	465.9309	465.3090	3	22
PG(P-18:0/0:0)	D[b]	1	$C_{24}H_{49}O_8P$ [M+H-H_2O]$^+$	4.94	496.3236	496.3165		17
Deoxycholic acid glycine conjugate	D[b]	1	$C_{26}H_{43}NO_5$ [M-H]$^-$	0.88	449.2174	449.3141	19	12
Austalide I	C[b]	1	$C_{27}H_{34}O_8$ [M-H]$^-$	5.22	486.2282	486.2254	8	10

L-Furosine	C[a]	1	$C_{12}H_{18}N_2O_4$ [M-H]$^-$	6.48	254.1098	254.1267	5	8

***LoA: Level of Assignment; 1: Accurate mass matched to database, 2: Accurate mass matched to database and tandem MS spectrum matched to *in silico* fragmentation pattern, 3: Tandem MS spectrum matched to database or literature, 4: Retention time and the molecular mass matched to standard compound, 5: MS/MS spectrum matched standard compound. **GI contents involved in the analyses comprise of stomach (S), duodenum (D), upper-jejunum (UJ), ileum (I) and colon (C). [a] indicates metabolite with higher intensity in sham-BWM rats, whereas [b] indicates metabolite with higher intensity in sham-obese Zucker rats.**

5.3.4 Effects of RYGB on metabolic profiles of gastric and intestinal contents

In order to investigate the effects of RYGB on metabolic profiles of gastric and intestinal contents, UPLC-MS data sets of gastrointestinal contents obtained from RYGB-operated and sham-obese rats were analysed using pairwise PCA and O-PLS-DA methods. PCA scores plots of both positive and negative ionisation modes clearly demonstrated the inherent separation in the gastric content between these two groups along the PC1 (ESI+ mode, R^2X=60.6% and ESI- mode, R^2X=55%) (Figure 5-4: A-1 and A-2). Moreover, distinct class separation was also observed in the upper-jejunal, lower-jejunal and ileal contents when comparing these two groups in the positive ionisation mode, of which the class differentiations occurred along PC1 (R^2X=47.9%), PC2 (R^2X=17.8%) and PC 2 (R^2X=19.2%), respectively (Figure 5-4: C-1, D-1 and E-1). Additionally, lower jejunal contents obtained from RYGB and sham-obese rats were significantly different and separated along PC2 (R^2X=16.7%) in the negative ionisation mode (Figure 5-4: D-2).

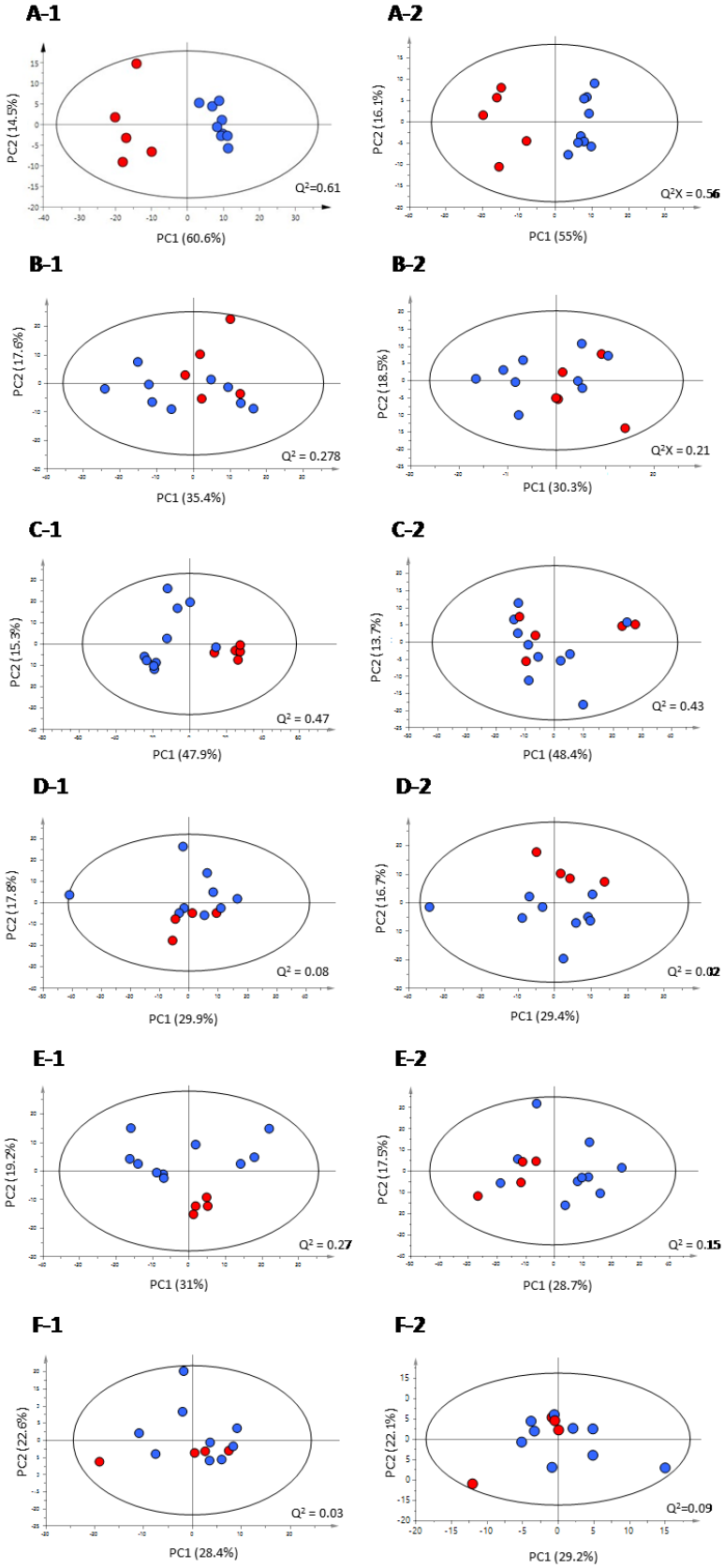


Figure 5-4. PCA scores plots of GI content data set including stomach (A), duodenum (B), upper-jejunum (C), lower-jejunum (D), ileum (E) and colon (F) contents of RYGB (blue) and sham-obese (red) Zucker rats at 3-week post- operation analysed using HILIC-UPLC-MS positive (1) and negative (2) modes.

O-PLS-DA illustrated the significantly discriminatory features between RYGB and sham-obese rats in gastric (both ionisation modes), upper-jejunal (positive ionisation mode), lower-jejunal (both ionisation modes), ileal (both ionisation modes) and colonic (both ionisation modes) contents (Table 5-4). Relative concentrations of PC(6:0/8:0), cytochalasin B and taurine are higher in the gastric content from the bypassed stomach of RYGB-operated rats compared with obese animals. In contrast, the levels of sucrose, dextrin, 1,6-kestotetraose, cysteic acid, trigonelline and 2-methylpropyl propanoate in the gastric contents were higher in the obese animals compared with RYGB group. In the upper jejunal contents, higher levels of choline and hypoxanthine, and lower levels of isoleucine, L-phenylalanine, L-arginine and sodium taurocholate were observed in RYGB-operated rats compared to obese rats. Relative concentrations of 2-piperidone was higher, whereas relative concentrations of 7-methyladenine and valyl-glutamine were lower in lower-jejunal contents of RYGB compared to its obese counterpart. In the ileal contents, RYGB animals exhibited relatively higher concentrations of dehydroabietic acid, creatine and 2-hydroxyhexadecanoic acid and relatively lower concentrations of *N*-hydroxybenzenesulfonamide, fructosamine, allantoin and ascorbate 2-sulfate compared to sham-obese rats. Relative colonic concentrations of both 3-indolepropionic acid and isoleucyl-lysine were lower in colonic contents of RYGB in comparison with obese animals.

Table 5-4. List of metabolites found in different gastrointestinal contents obtained from pairwise O-PLS-DA analysis between RYGB-treated and obese Zucker rats

Metabolite	GI Content	LoA*	Molecular formula [Adduct]	Retention time (min)	m/z observed	m/z theoretical	Δppm	CV %
HILIC Positive Mode								
Cysteic acid	S[b]	2	$C_3H_7NO_5S$ $[M+H-H2O]^+$	9.98	169.6261	169.005	11	10
Trigonelline	S[b]	4	$C_7H_7NO_2$ $[M+H]^+$	6.52	137.0472	137.0477	0	6
2-Methylpropyl propanoate	S[b]	1	$C_7H_{14}O_2$ $[M+H-H2O]^+$	5.80	130.1339	130.0994	5	17

PC(6:0/8:0)	S[a]	1	$C_{22}H_{44}NO_8P$ $[M+H-H2O]^+$	0.86	481.2827	481.2085	11	22
Cytochalasin B	S[a]	1	$C_{29}H_{37}NO_5$ $[M+H-H2O]^+$	4.44	479.2680	479.2672	7	21
Choline	UJ[a]	5	$C_5H_{13}NO$ $[M+H]^+$	5.59	104.9431	104.0997	28	9
Hypoxanthine	UJ[a]	4	$C_5H_4N_4O$ $[M+H]^+$	2.15	136.0412	136.0385	0	5
Isoleucine	UJ[b] C[a]	5	$C_6H_{13}NO_2$ $[M+H]^+$	5.80	131.0980	131.0946	14	10
L-Phenylalanine	UJ[b]	5	$C_9H_{11}NO_2$ $[M+H]^+$	5.71	165.0790	165.0790	4	3
L-Arginine	UJ[b] C[a]	5	$C_6H_{14}N_4O_2$ $[M+H]^+$	7.99	174.1131	174.1117	5	2
Sodium taurocholate	UJ[b]	3	$C_{26}H_{38}O_{12}$ $[M+NH_4]^+$	4.08	557.2396	537.2736	18	4
2-Piperidinone	LJ[a]	1	C_5H_9NO $[M+H]^+$	6.38	99.0680	99.0684	3	5
7-Methyladenine	LJ[b]	1	$C_6H_9N_5O$ $[M+H]^+$	5.26	149.0697	149.0701	0	12
Dehydroabietic acid	I[a]	1	$C_{20}H_{28}O_2$ $[M+H]^+$	0.73	300.2075	300.2089	1	17
N-hydroxybenzenesulfonamide	I[b]	1	$C_6H_7NO_3S$ $[M+H]^+$	6.08	173.1160	173.0147	0	8
Fructosamine	I[b]	1	$C_6H_{13}NO_5$ $[M+H]^+$	1.95	179.0801	179.0794	7	23
3-Indolepropionic acid	C[b]	1	$C_{11}H_{11}NO_2$ $[M+H]^+$	0.80	189.0792	189.0790	4	8
Isoleucyl-Lysine	C[b]	1	$C_{12}H_{25}N_3O_3$ $[M+H]^+$	7.98	259.1902	259.1896	4	19
HILIC Negative Mode								
Sucrose	S[b]	5	$C_{12}H_{22}O_{11}$ $[M-H]^-$	6.19	342.1161	342.1162	7	10
Dextrin	S[b]	3	$C_{18}H_{32}O_{16}$ $[M-H]^-$	6.36	504.1690	504.1690	16	26
1,6-Kestotetraose	S[b]	1	$C_{24}H_{42}O_{21}$ $[M-H]^-$	7.18	666.2220	666.5790	0	10
Taurine	S[a]	5	$C_2H_7NO_3S$ $[M-H]^-$	5.78	125.0151	125.0147	21	6
Valyl-Glutamine	LJ[b]	1	$C_{10}H_{19}N_3O_4$ $[M-H]^-$	6.26	245.0435	245.1376	1	5
Creatine	I[a]	5	$C_4H_9N_3O_2$ $[M-H]^-$	0.92	131.0670	131.0695	24	19
2-Hydroxyhexadecanoic acid	I[a]	1	$C_{16}H_{32}O_3$ $[M-H]^-$	0.75	272.2351	272.2351	3	11
Allantoin	I[b]	3	$C_4H_6N_4O_3$ $[M-H]^-$	1.50	158.0440	158.044	4	11
Ascorbate 2-sulfate	I[b]	1	$C_6H_8O_9S$ $[M-H]^-$	0.64	255.9892	255.9889	2	16

***LoA: Level of Assignment; 1: Accurate mass matched to database, 2: Accurate mass matched to database and tandem MS spectrum matched to *in silico* fragmentation pattern, 3: Tandem MS spectrum matched to database or literature, 4: Retention time and the molecular mass matched to standard compound, 5: MS/MS spectrum matched standard compound. **GI contents involved in the analyses comprise of stomach (S), upper-jejunum (UJ), lower-jejunum (LJ), ileum (I) and colon (C). [a] indicates metabolite with higher intensity in RYGB-treated rats, whereas [b] indicates metabolite with higher intensity in sham-obese Zucker rats.**

In order to further investigate the RYGB-induced but weight loss-independent metabolic responses along the gastrointestinal tract, metabolic profiles of the gastrointestinal contents collected from RYGB rats were compared with those of sham-BWM rats. PCA scores plots clearly showed the group differentiation between RYGB and sham-BWM rats in both ionisation modes along PC1 (ESI+ mode, R^2X=58.1% and ESI- mode, R^2X=52.1%) (Figure 5-5: A-1 and A-2), similar to when compared with those of sham-obese rats (Figure 5-4: A-1 and A-2). In addition, upper-jejunal content obtained from RYGB was differentiated from that of sham-BWM rats along PC1 (R^2X=45.7%) and the ileal content of the RYGB group was separated from sham-obese group along PC2 (R^2X=16.9%) in the positive ionisation mode (Figure 5-5).

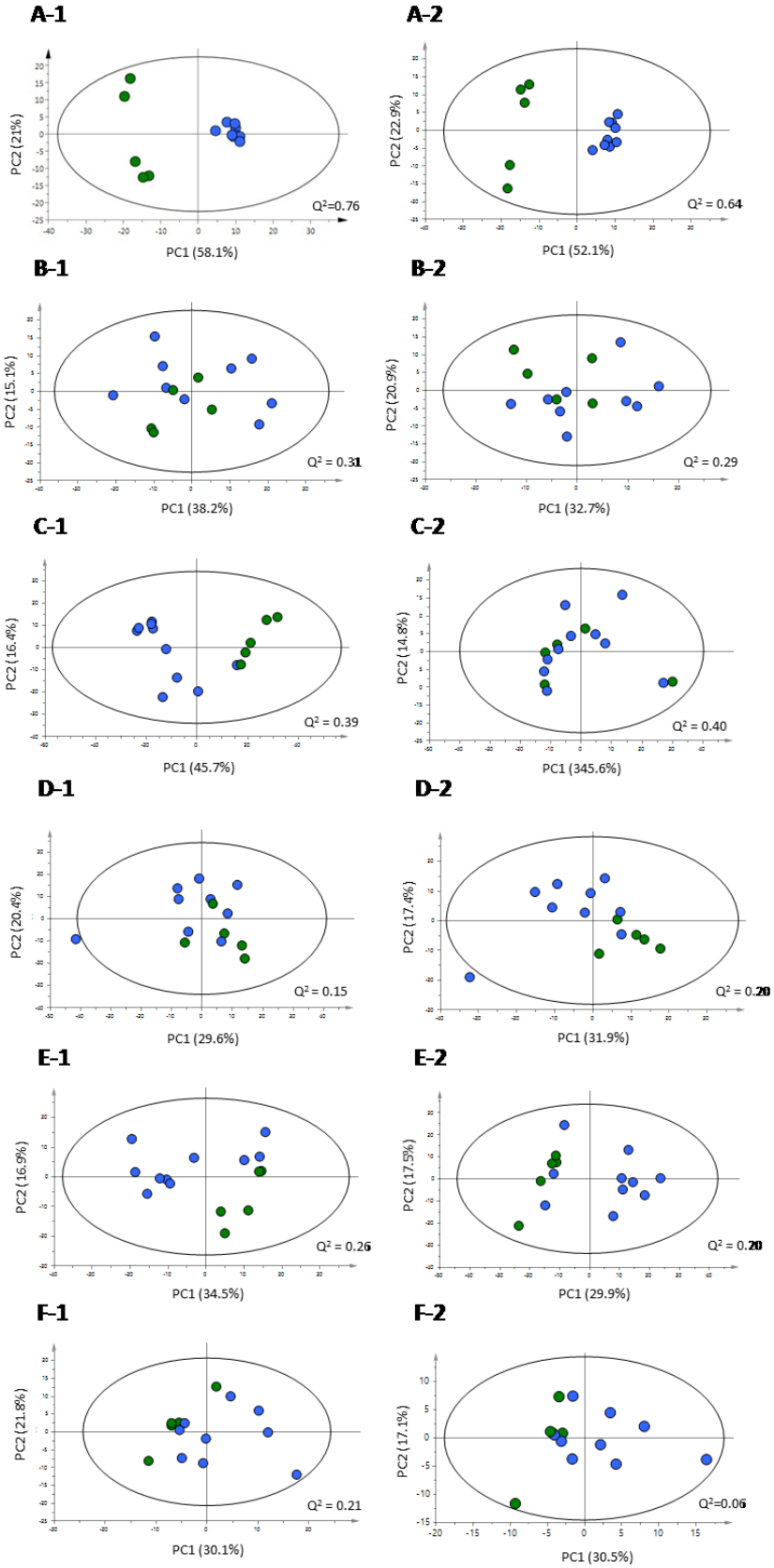


Figure 5-5. PCA scores plots of GI content data set including stomach (A), duodenum (B), upper-jejunum (C), lower-jejunum (D), ileum (E) and colon (F) contents of RYGB (blue) and sham-BWM (green) Zucker rats at 3-week post- operation analysed using HILIC-UPLC-MS positive (1) and negative (2) modes.

O-PLS-DA illustrated the significantly discriminatory features between RYGB and sham-BWM rats in gastric (both ionisation modes), upper-jejunal (ESI+), lower-jejunal (ESI+), ileal (both ionisation modes) and colonic (both ionisation modes) contents (Table 5-5). Relative concentrations of agmatine, trigonelline, levanbiose, glycogen, and dextrin were lower while relative concentrations of creatinine, nicotinamide, taurine, imidazolepropionic acid, L-carnitine, adrenaline, L-acetylcarnitine, prostaglandin H2 and PS(8:0/8:0) were higher in gastric contents of RYGB compared to sham-BWM rats. In upper-jejunal contents, RYGB animals exhibited greater relative concentrations of pantothenic acid, nicotinic acid, *N*-acetylcadaverine and isonicotinamide and lower relative concentrations of L-phenylalanine, *N*2-acetyl-L-ornithine, deoxycorticosterone and tetracosahexaenoic acid compared to caloric restriction group. Lower-jejunal contents of RYGB animals carried relatively higher concentrations of 3-methylbutyrolactone but lower concentrations of trigonelline, cytidine, 1-methyladenine and hydroxypropionylcarnitine in comparison to sham-BWM rats. Relative concentrations of 2-oxoisocaproate, tyramine-O-sulfate and L-ornithine were higher, whereas relative concentrations of β-D-glucosamine, phosphatidylinositol phosphate (PIP) (18:2/18:0) and methyl β -D-glucopyranoside were lower in ileal contents of RYGB compared with caloric restriction group. Colonic contents collected from RYGB animals demonstrated higher relative concentration of uric acid, whereas sham-BWM rats exhibited higher relative concentrations of 3-indolepropionic acid, cytosine, 4-methyoxytyramine, proline betaine and 5-phenylvaleric acid in their colonic contents compared to RYGB.

Table 5-5. List of metabolites found in different gastrointestinal contents obtained from pairwise O-PLS-DA analysis between RYGB-treated and caloric-restricted obese Zucker rats

Metabolite	GI Content	LoA*	Molecular formula [Adduct]	Retention time (min)	m/z observed	m/z theoretical	Δppm	CV %
HILIC Positive Mode								
Agmatine	S[b]	2	$C_5H_{14}N_4$ $[M+H]^+$	8.32	130.1220	130.1218	6	3
Trigonelline	S[b] LJ[b]	4	$C_7H_7NO_2$ $[M+H]^+$	6.52	137.0471	137.0477	0	6
Levanbiose	S[b]	1	$C_{12}H_{22}O_{11}$ $[M+Na]^+$	6.25	342.1161	342.1162	1	27
Creatinine	S[a]	5	$C_4H_7N_3O$ $[M+H]^+$	3.02	113.0590	113.0589	7	12
Nicotinamide	S[a]	3	$C_6H_6N_2O$ $[M+H]^+$	6.16	122.0483	122.0480	6	21
Taurine	S[a]	3	$C_2H_7NO_3S$ $[M+H]^+$	5.79	125.0141	125.0147	0	25
Imidazolepropionic acid	S[a]	1	$C_6H_8N_2O_2$ $[M+H]^+$	6.31	140.0580	140.0586	1	15
L-Carnitine	S[a]	3	$C_7H_{15}NO_3$ $[M+H]^+$	7.64	161.1051	161.1052	3	3
Adrenaline	S[a]	3	$C_9H_{13}NO_3$ $[M+H]^+$	7.64	183.0866	183.0895	10	12
L-Acetylcarnitine	S[a]	1	$C_9H_{17}NO_4$ $[M+H]^+$	7.31	203.1148	203.1158	0	20
Prostaglandin H2	S[a]	1	$C_{20}H_{32}O_5$ $[M+H]^+$	0.85	352.2230	352.2250	6	11
Pantothenic acid	UJ[a]	2	$C_9H_{17}NO_5$ $[M+H]^+$	4.26	219.1100	219.1107	0	10
Nicotinic acid	UJ[a]	5	$C_6H_5NO_2$ $[M+H]^+$	4.77	123.0321	123.0320	6	12
N-Acetylcadaverine	UJ[a]	1	$C_7H_{16}N_2O$ $[M+H]^+$	5.96	144.1261	144.1262	3	6
Isonicotinamide	UJ[a]	1	$C_6H_7N_3$ $[M+H]^+$	5.55	121.9172	121.0640	6	6
L-Phenylalanine	UJ[b]	5	$C_9H_{11}NO_2$ $[M+H]^+$	5.71	165.0792	165.0790	4	3
N2-Acetyl-L-ornithine	UJ[b]	1	$C_7H_{14}N_2O_3$ $[M+H]^+$	6.56	174.0998	174.1000	1	7
Deoxycorticosterone	UJ[b]	1	$C_{21}H_{30}O_3$ $[M+H]^+$	5.37	330.2195	330.2195	4	7
Tetracosahexaenoic acid	UJ[b]	1	$C_{24}H_{36}O_2$ $[M+H]^+$	5.90	356.2680	356.2715	8	10
Cytidine	LJ[b]	1	$C_9H_{13}N_3O_5$ $[M+H]^+$	6.48	243.0860	243.0855	5	16
1-Methyladenine	LJ[b]	1	$C_6H_7N_5$ $[M+H]^+$	5.26	149.0701	149.0701	4	12
Hydroxypropionylcarnitine	LJ[b]	1	$C_{10}H_{19}NO_5$ $[M+H]^+$	5.27	233.1272	233.1263	6	13
3-Methylbutyrolactone	LJ[a]	1	$C_5H_8O_2$ $[M+H]^+$	6.37	100.0540	100.0525	3	2

beta-D-Glucosamine	I[b]	1	$C_6H_{13}NO_5$ $[M+H]^+$	1.95	179.0800	179.0794	8	23
3-Indolepropionic acid	C[b]	1	$C_{11}H_{11}NO_2$ $[M+H]^+$	0.80	189.0791	189.079	4	8
Cytosine	C[b]	2	$C_4H_5N_3O$ $[M+H]^+$	3.83	111.0426	111.0433	4	8
4-Methoxytyramine	C[b]	1	$C_9H_{13}NO_2$ $[M+H]^+$	6.28	167.0938	167.0946	1	29
Proline betaine	C[b]	1	$C_7H_{13}NO_2$ $[M+H]^+$	6.53	143.0941	143.0946	1	6
5-Phenylvaleric acid	C[b]	1	$C_{11}H_{14}O_2$ $[M+H]^+$	3.17	178.0990	178.0994	2	13
HILIC Negative Mode								
Glycogen	S[b]	2	$C_{24}H_{42}O_{21}$ $[M-H]^-$	7.18	666.2221	666.2219	1	10
Dextrin	S[b]	3	$C_{18}H_{32}O_{16}$ $[M-H]^-$	6.36	504.1687	504.1690	2	26
Levanbiose	S[b]	1	$C_{12}H_{22}O_{11}$ $[M-H]^-$	6.19	342.1162	342.1162	3	7
PS(8:0/8:0)	S[a]	1	$C_{22}H_{42}NO_{10}P$ $[M-H]^-$	0.87	511.2590	511.2546	7	5
Taurine	S[a]	3	$C_2H_7NO_3S$ $[M-H]^-$	5.78	125.0151	125.0147	3	6
PIP(18:2/18:0)	I[b]	1	$C_{45}H_{84}O_{16}P_2$ $[M-H]^-$	5.91	942.5150	942.5235	10	11
Methyl beta-D-glucopyranoside	I[b]	1	$C_7H_{14}O_6$ $[M-H]^-$	2.91	194.0785	194.0790	4	7
2-Oxoisocaproate	I[a]	1	$C_6H_{10}O_3$ $[M-H]^-$	0.91	130.0630	130.063	6	24
Tyramine-O-sulfate	I[a]	1	$C_8H_{11}NO_4S$ $[M-H]^-$	3.44	217.0411	217.0409	3	9
L-Ornithine	I[a]	1	$C_5H_{12}N_2O_2$ $[M-H]^-$	6.98	132.0900	132.0899	5	9
Uric acid	C[a]	3	$C_5H_4N_4O_3$ $[M-H]$	4.60	168.0283	168.0283	6	16

***LoA: Level of Assignment; 1: Accurate mass matched to database, 2: Accurate mass matched to database and tandem MS spectrum matched to *in silico* fragmentation pattern, 3: Tandem MS spectrum matched to database or literature, 4: Retention time and the molecular mass matched to standard compound, 5: MS/MS spectrum matched standard compound. **GI contents involved in the analyses comprise of stomach (S), upper-jejunum (UJ), lower-jejunum (LJ), ileum (I) and colon (C). [a] indicates metabolite with higher intensity in RYGB-treated rats, whereas [b] indicates metabolite with higher intensity in sham-BWM rats.**

5.3.5 Gastrointestinal microbial shifts following RYGB surgery and caloric restriction

Bacterial community of gastrointestinal contents was characterised using 16S rRNA gene Illumina MiSeq sequencing to assess the composition of the gut bacterial community of RYGB-treated, caloric restriction-treated, and obese Zucker rats. Non-metric multidimensional scaling (NMDS) plots based on weighted UniFrac matrices revealed different gradient structures of taxonomic composition for each gastrointestinal compartment and showed the shifts of centroids (indicated by arcs) and variance of bacterial profiles of each compartment (circled areas) (Figure 5-6). Gastric bacterial profiles of RYGB was shown to carry the different centroid shift direction compared with those of sham-BWM and sham-obese rats. This phenomenon persisted in the duodenum, upper-jejunum, lower jejunum and ileum, but not in the colonic content (Figure 5-6). Furthermore, as indicated by the overlapped areas in each plot (Figure 5-6), RYGB and sham-BWM rats, to some extent, appeared to contain similar bacterial community profiles in the stomach, duodenum and colon. Despite the similar direction of centroid shift of sham-BWM and sham-obese rats in the stomach, sham-BWM animals showed the markedly higher degree of variance in the bacterial profiles compared with sham-obese group (Figure 5-6A). Obese group exhibited the smallest variance in the duodenal bacterial profiles (Figure 5-6B). Upper-jejunal bacterial community profiles of all three groups were remarkably different in both shift direction and degree of variance (Figure 5-6C). Lower-jejunal bacterial community profiles of four out of five animals in RYGB group clustered tightly with much lower variation and exhibited a different projection of centroid shift when compared with sham-BWM and sham-obese groups (Figure 5-6D). Likewise, the similar pattern was observed in the ileal bacterial profiles but with a more similar projection among the three groups (Figure 5-6E). All three groups of animals were demonstrated to contain the similar bacterial communities in their colonic contents in spite of a different direction of the shift in sham-obese group (Figure 5-6F).

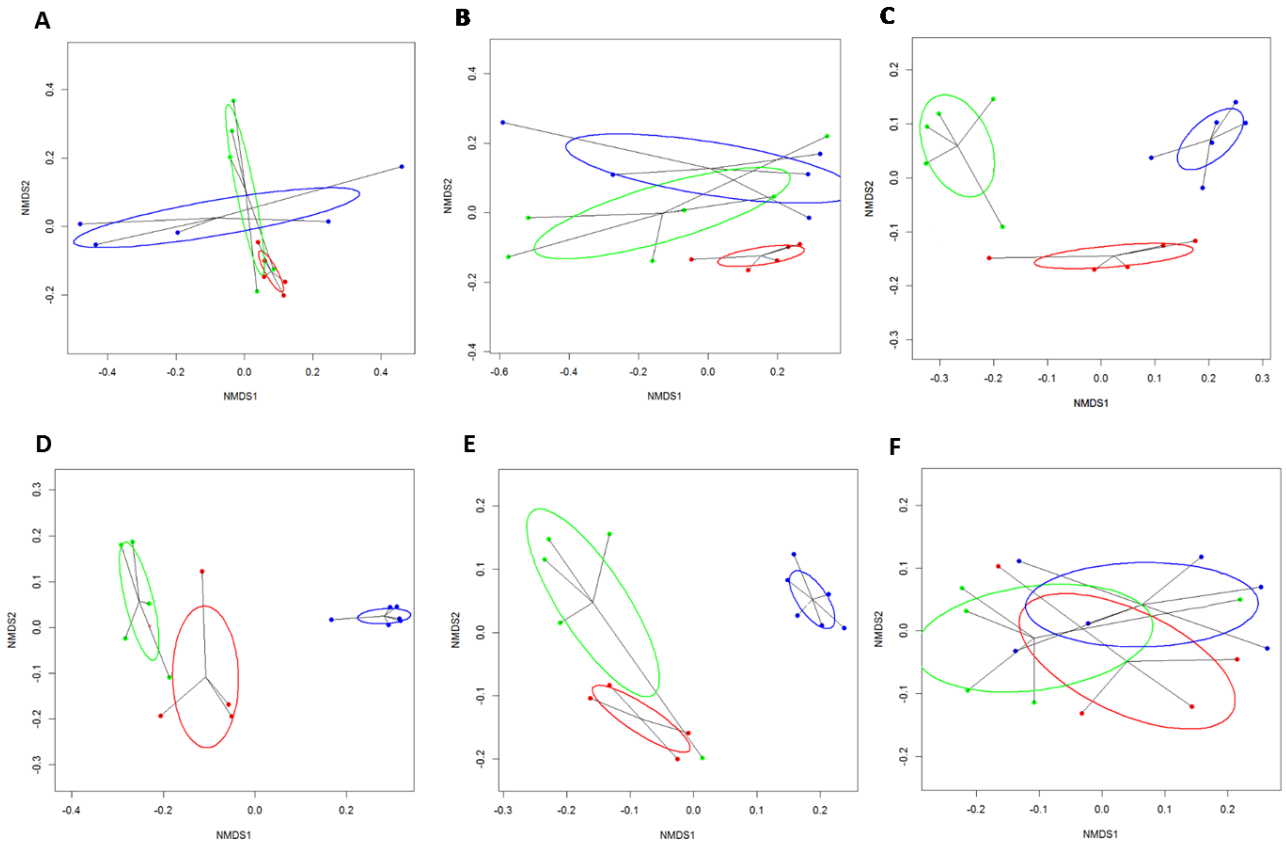


Figure 5-6. Non-metric dimensional scaling (NMDS) plots of the weighted UniFrac distances of bacterial community data obtained from different gastrointestinal contents including stomach (A), duodenum (B), upper-jejunum (C), lower-jejunum (D), ileum (E) and colon (F) contents of RYGB (blue), sham-BWM (green) and sham-obese (red) rats.

Firmicutes were the most predominant bacteria residing in the stomach of sham-obese rats with the mean relative abundance of 50.06% (Figure 5-7). Following caloric restriction treatment, the mean relative abundance of *Firmicutes* was two-fold greater compared with sham-obese control, whereas a compositional shift from *Firmicutes* to *Proteobacteria* was observed in the gastric content of RYGB animals (Figure 5-7). Sham-obese and sham-BWM rats demonstrated the similar bacterial abundance in their duodenal contents with predominant *Firmicutes* accounting for 59.09% and 64.40%, respectively. *Proteobacteria* remained highly abundant in the duodenal content from RYGB group (30.87%) (Figure 5-7). More interestingly, upper-jejunal content obtained from sham-BWM rats showed a large abundance of *Actinobacteria* (59.93%) compared with those of RYGB group (3.73%) and of sham-obese group (5.89%) (Figure 5-7). It is

also noted that bacterial composition of RYGB group was similar to that of sham-obese group with slightly small proportion of *Bacteroidetes* and *Actinobacteria* (Figure 5-7). The mean relative abundance of *Proteobacteria* remained the highest in the lower-jejunal content of RYGB (23.63%) among these three groups, whereas lower-jejunal contents of sham-obese and sham-BWM carried only 1.64% and 0.44% of *Proteobacteria*, respectively (Figure 5-7). Despite that *Firmicutes* was the most predominant phylum in all animal groups, sham-BWM group showed the highest proportion of *Firmicutes* (82.6%), followed by the sham-obese (64.49%) and RYGB (62.79%) groups (Figure 5-7). Sham-obese and sham-BWM groups demonstrated very similar bacterial composition in their ileal contents but RYGB group exhibited much greater abundance of *Proteobacteria* (23.63%) and *Bacteroidetes* (10.07%) compared with the other groups (Figure 5-7). Apart from a greater abundance of *Proteobacteria* in RYGB colonic content, all three groups of animals depicted similar degree of bacterial composition in their colonic contents (Figure 5-7), which is accordant with the NMDS plot (Figure 5-6F).

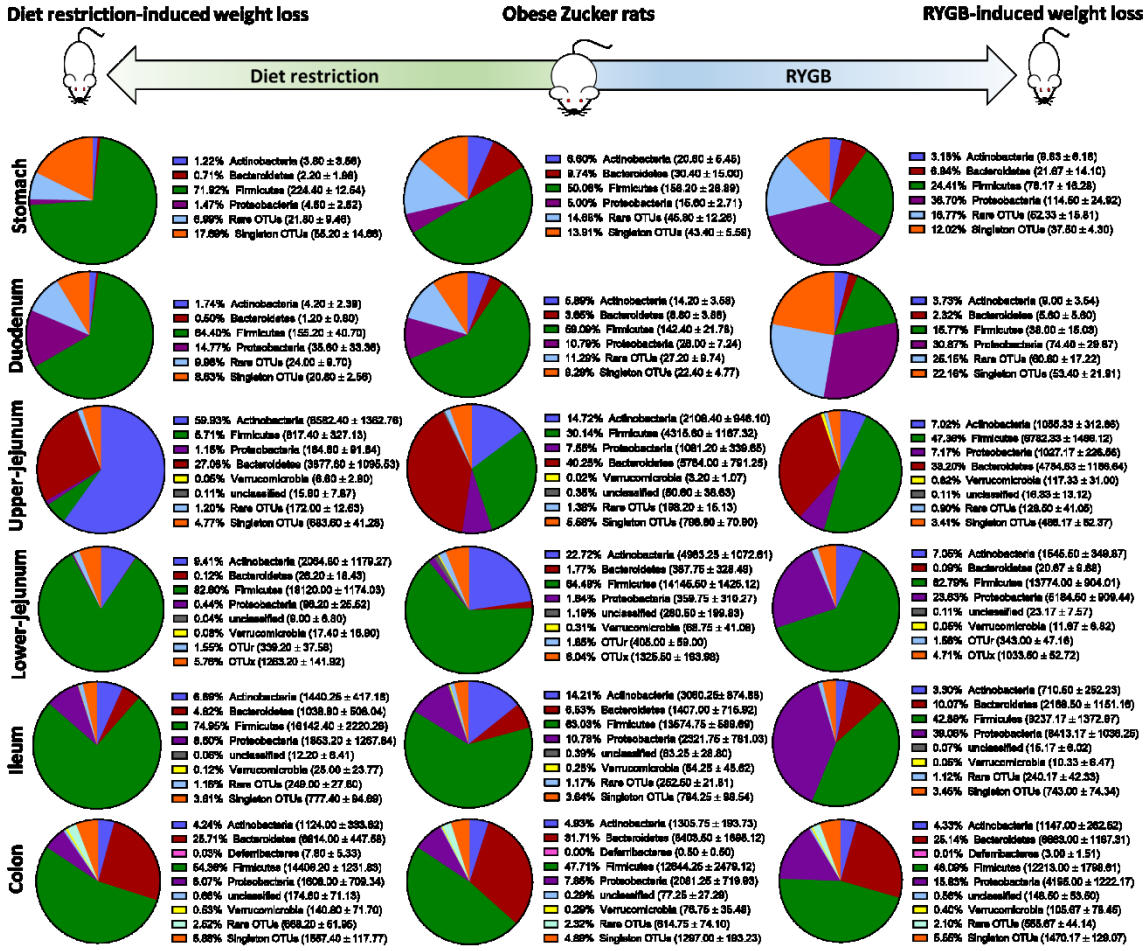


Figure 5-7. Pie charts representing the percentages of the mean relative abundances of bacteria at the phylum level in different luminal regions along the gastrointestinal tract of obese hyperinsulinemic (sham-obese), RYGB-operated (RYGB) and diet restriction-treated (sham-BWM) Zucker rats. Data was shown in percentage of relative abundance ± SD

5.3.6 Caloric restriction-induced bacterial alteration along gastrointestinal tract

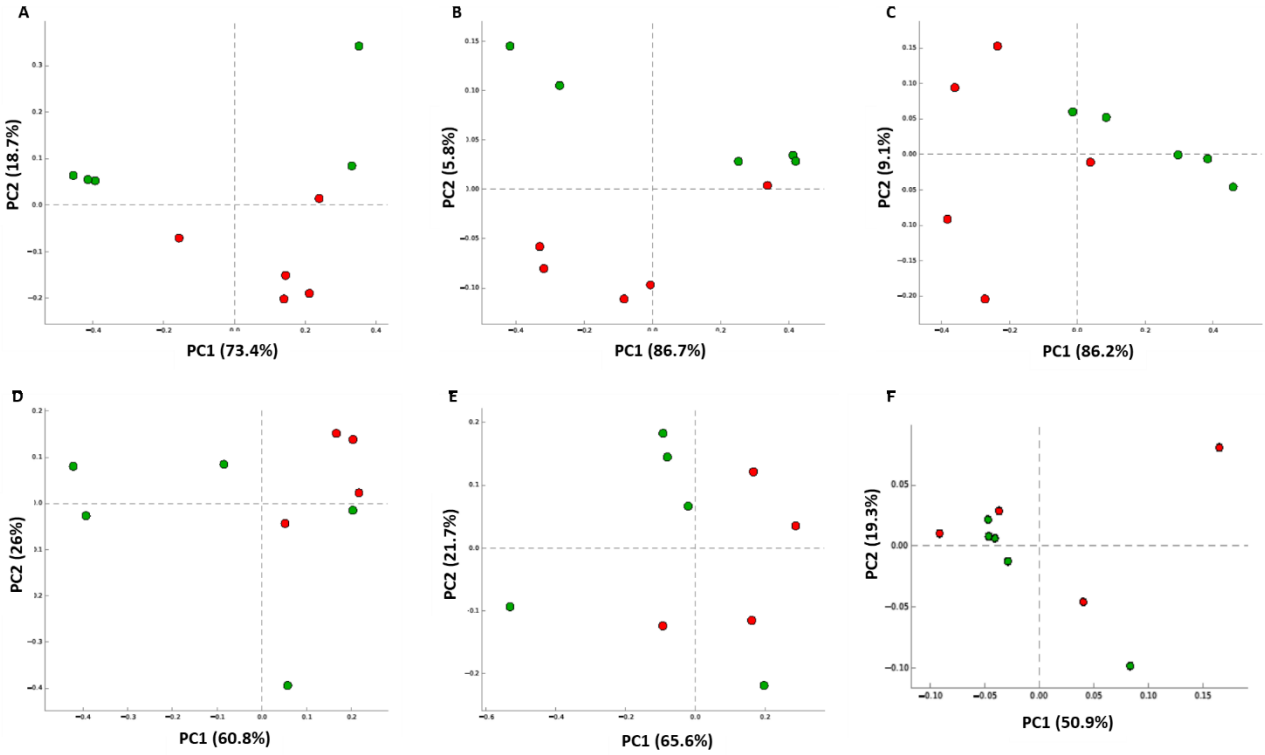


Figure 5-8. PCA scores plots of bacterial profiles from GI contents including gastric (A), duodenal (B), upper-jejunal (C), lower-jejunal (D), ileal (E) and colonic (F) contents between sham-BWM (green) and sham-obese (red) rats using 16S rRNA gene sequencing analysis at the genus level.

To further extract detailed information and visualise the significant changes in gut bacterial alteration for each gastrointestinal compartment, pairwise comparison models were constructed. Bacterial profiles of all gastrointestinal compartments of sham-BWM rats were compared with sham-obese rats in order to examine the effects of caloric restriction on the gut bacterial changes. PCA scores plots showed the group differentiation between sham-BWM and sham-obese group in bacterial profiles of stomach, duodenum and upper-jejunum determined by PC2 (18.7%), PC2 (5.8%) and PC1 (86.2%), respectively (Figure 5-8A-C). However, clear class separation between sham-BWM and sham-obese groups was not observed in lower-jejunal, ileal and colonic microbial profiles (Figure 5-8D-F).

Pairwise comparisons using two-sided non-parametric t-test with Welch's correction were conducted at the genus level. Significant differences were found in the higher relative abundance of gastric *Bifidobacterium* (P=0.04), *Lactobacillus* (P=0.03) and *Parasutterella* (P=0.01) in sham-obese compared with sham-BWM (Figure 5-9).

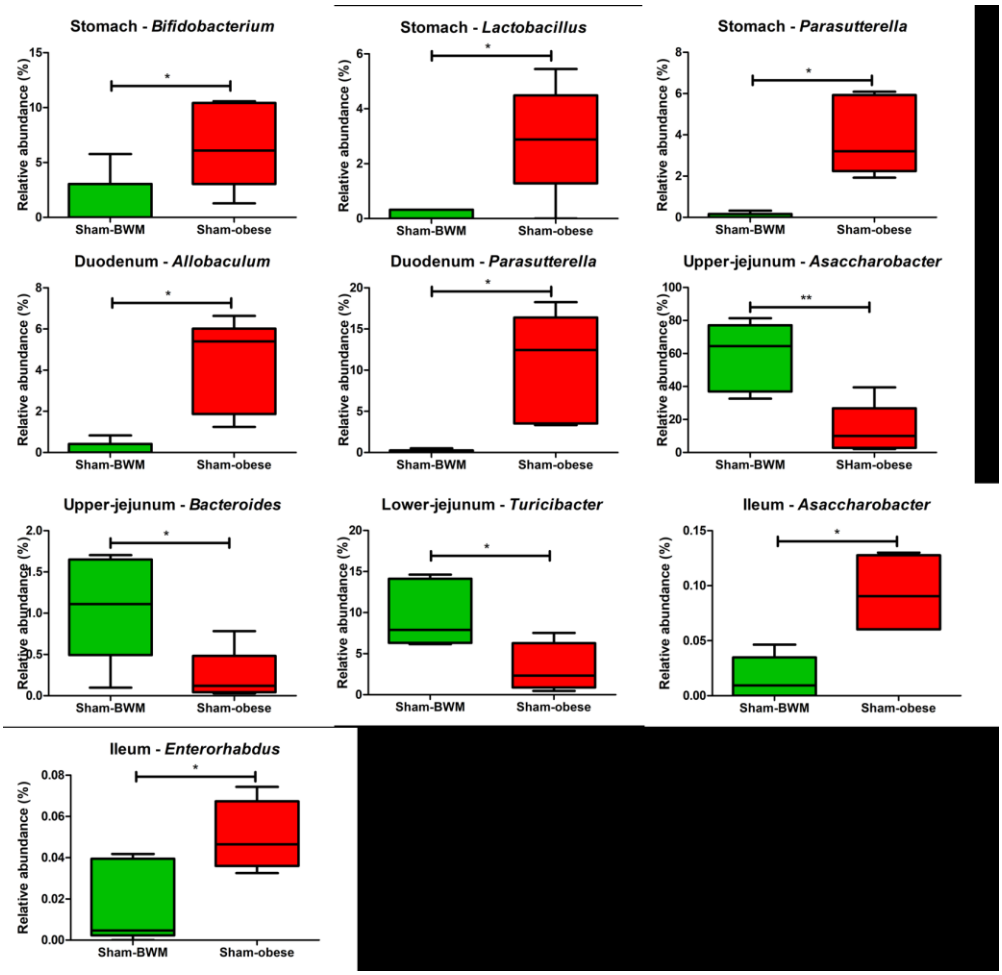


Figure 5-9. Box plots of the significantly altered gut microbiota between sham-BWM (green) and sham-obese (red) rats at the genus level. Two-sided non-parametric t-test with Welch's correction was performed. Asterisks indicate significant differences: * P<0.05 and ** P<0.01.

In addition, sham-obese rats showed higher relative abundance of duodenal *Allobaculum* (P=0.01) and *Parasutterella* (P=0.02) (Figure 5-8). Furthermore, the relative abundance of ileal *Asaccharobacter* (P=0.02) and *Enterorhabdus* (P=0.04) were shown to be greater in sham-obese group (P<0.05) compared with BWM group (Figure 5-9). On the contrary, a greater relative abundance of *Asaccharobacter* (P=0.006) and *Bacteroides* (P=0.04) in the upper-jejunal contents, together with higher relative abundance of *Turicibacter* in the lower-jejunal contents (P=0.03) was observed in sham-BWM group compared with sham-obese group (Figure 5-9).

5.3.7 Gastrointestinal bacterial shifts following RYGB operation

Class separation between RYGB and sham-obese groups was observed in the gastric and duodenal contents, determined by PC2 (24.1%) and PC1 (60.3%), respectively and more clearly seen in lower-jejunum along PC1 (58.1%) and ileum along PC1 (48.9%) (Figure 5-10).

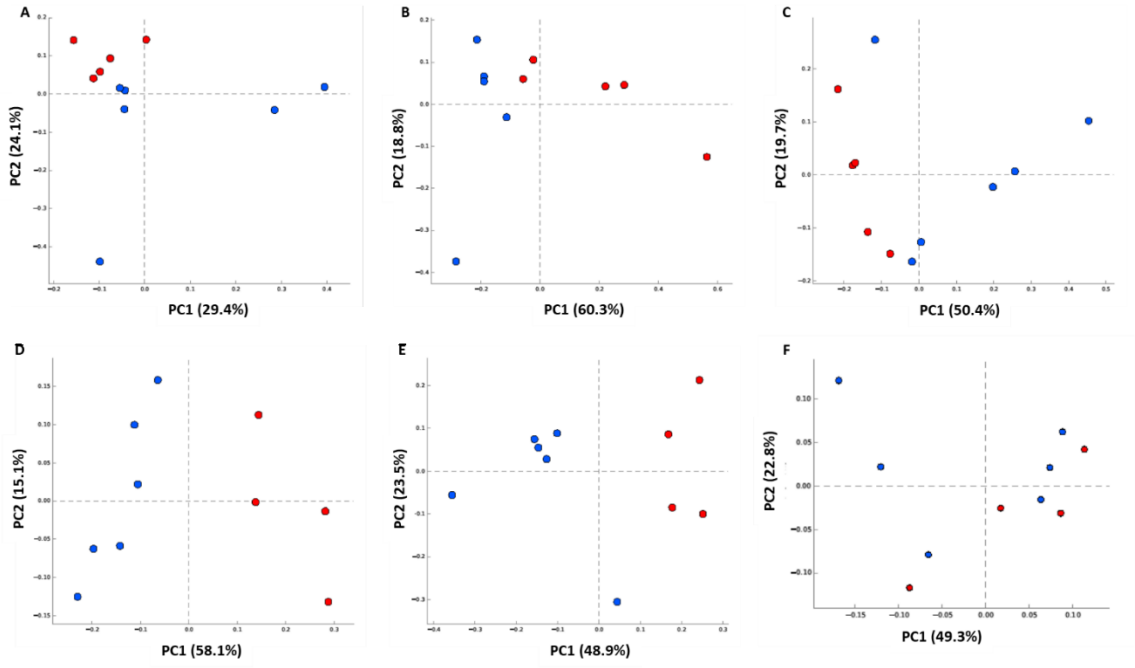


Figure 5-10. PCA scores plots of bacterial profiles from GI contents including gastric (A), duodenal (B), upper-jejunal (C), lower-jejunal (D), ileal (E) and colonic (F) contents between RYGB (blue) and sham-obese (red) rats using 16S rRNA gene sequencing analysis at the genus level.

There were two bacterial genera including *Clostridium XI* (P=0.0362) and *Lactobacillus* (0.0379) that were significantly differentiated in the gastric contents between RYGB and sham-obese rats (Figure 5-11). The relative abundance of *Allobaculum* was higher in duodenal content of sham-obese group (P=0.01), whereas duodenal content collected from RYGB contained higher relative abundance of *Escherichia* (P=0.04) (Figure 5-11). Upper-jejunal contents obtained from RYGB carried greater relative abundance of *Akkermansia* (P=0.01) and *Acinetobacter* (P=0.004), along with higher relative abundance of *Allobaculum* (P=0.002), *Clostridium XIVa* (P=0.02), *Enterococcus*

(P=0.01), *Escherichia* (P=0.003) and *Streptococcus* (P=0.02) in their lower-jejunal content (Figure 5-10). Moreover, the relative abundance of ileal *Blautia* (P=0.02), *Clostridium IV* (P=0.001), *Clostridium XI* (P= 0.03), *Clostridium XIVa* (P=0.02), *Enterococcus* (P=0.02), *Escherichia* (P=0.01) and *Streptococcus* (P=0.04) were found to be significantly higher in RYGB group (Figure 5-11). On the other hand, ileal content from sham-obese rats exhibited higher relative abundance of *Enterorhabdus* (P=0.01) (Figure 5-11).

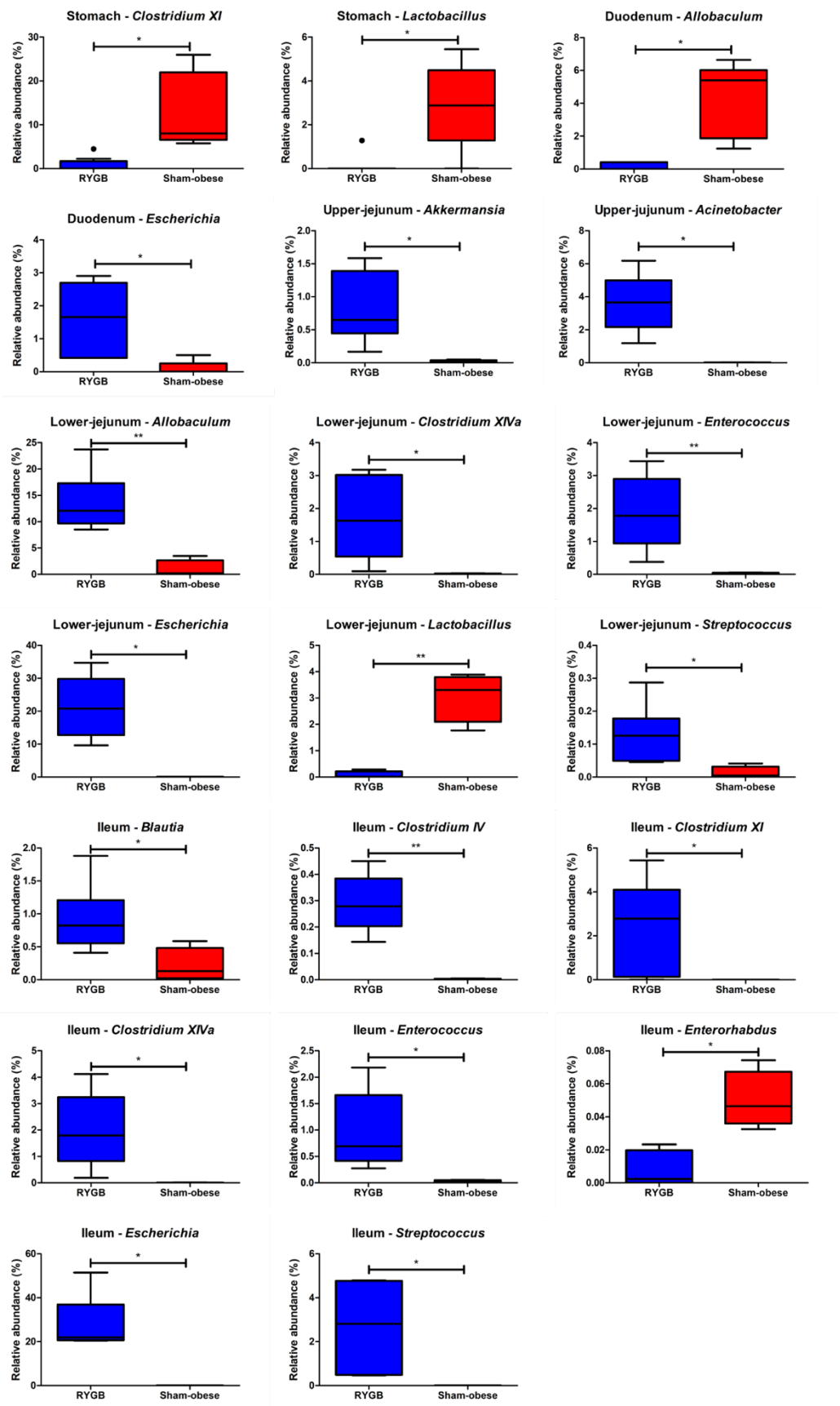


Figure 5-11. Box plots show the significantly altered gut microbiota between RYGB (blue) and sham-obese (red) rats at the genus level. Two-sided non-parametric t-test with Welch's correction was performed. Asterisks indicate significant differences: * P<0.05 and ** P<0.01.

5.3.8 Gastrointestinal bacterial differences between RYGB and caloric restriction

PCA scores plots showed the inherent separation of bacterial profiles between RYGB and sham-BWM groups in stomach, upper-jejunum, lower-jejunum and ileum determined by PC2 (22.4%), PC1 (73.7%), PC1 (69.1%) and PC1 (59.2%) (Figure 5-12).

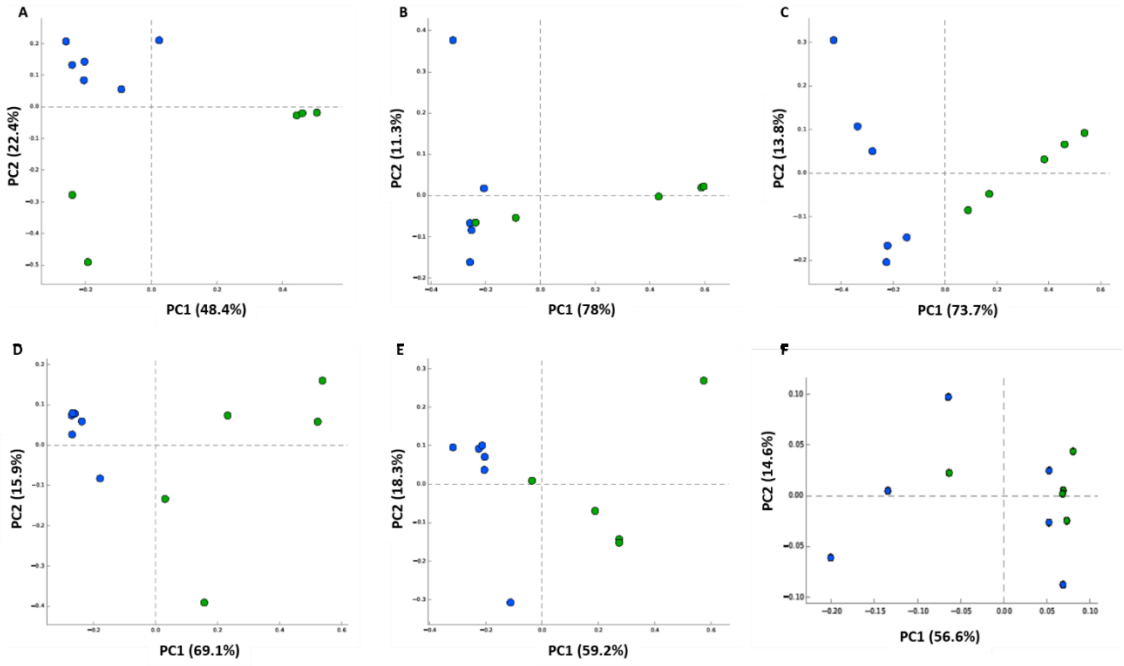


Figure 5-12. PCA scores plots of bacterial profiles from GI contents including gastric (A), duodenal (B), upper-jejunal (C), lower-jejunal (D), ileal (E) and colonic (F) contents between RYGB (blue) and sham-BWM (green) rats using 16S rRNA gene sequencing analysis at the genus level.

RYGB rats showed higher relative abundance of upper-jejunal *Acinetobacter* (P=0.005) and *Akkermansia* (P=0.01), lower-jejunal *Asaccharobacter* (P=0.004), *Blautia* (P=0.02), *Clostridium XIVa* (P=0.02), *Entrococcus* (P=0.01), *Escherichia* (P=0.003), *Olsenella* (*P*=0.01) and *Streptococcus* (P=0.03) accompanied with greater relative abundance of *Blautia* (P=0.008), *Clostridium* genera including *Clostridium IV* (P=0.001), *Clostridium XI* (P=0.04), *Clostridium XIVa* (P=0.02) and *Clostridium XVIII* (P=0.02), *Enterococcus* (P=0.0288), *Escherichia* (P=0.003) and *Streptococcus* (P=0.03) in ileal content of RYGB (Figure 5-13). However, the relative abundance of *Asaccharobacter* in the upper-jejunal content (P=0.04), *Lactobacillus* in the lower-jejunal, ileal and colonic contents (P=0.005,

P=0.005 and P=0.05, respectively), and *Prevotella* in colonic content (P=0.0442) were found to be higher in sham-BWM rats compared with RYGB rats (Figure 5-13).

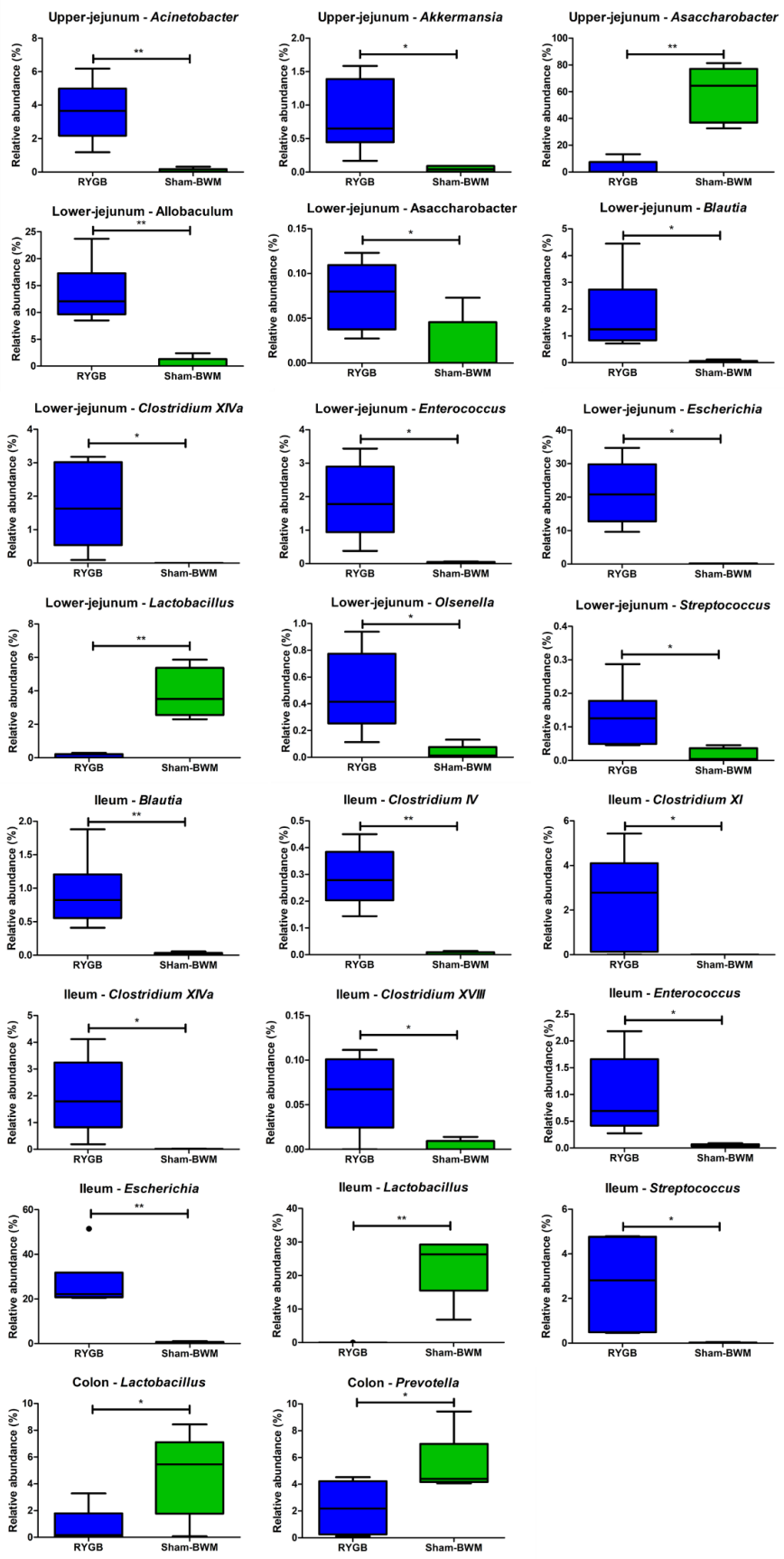
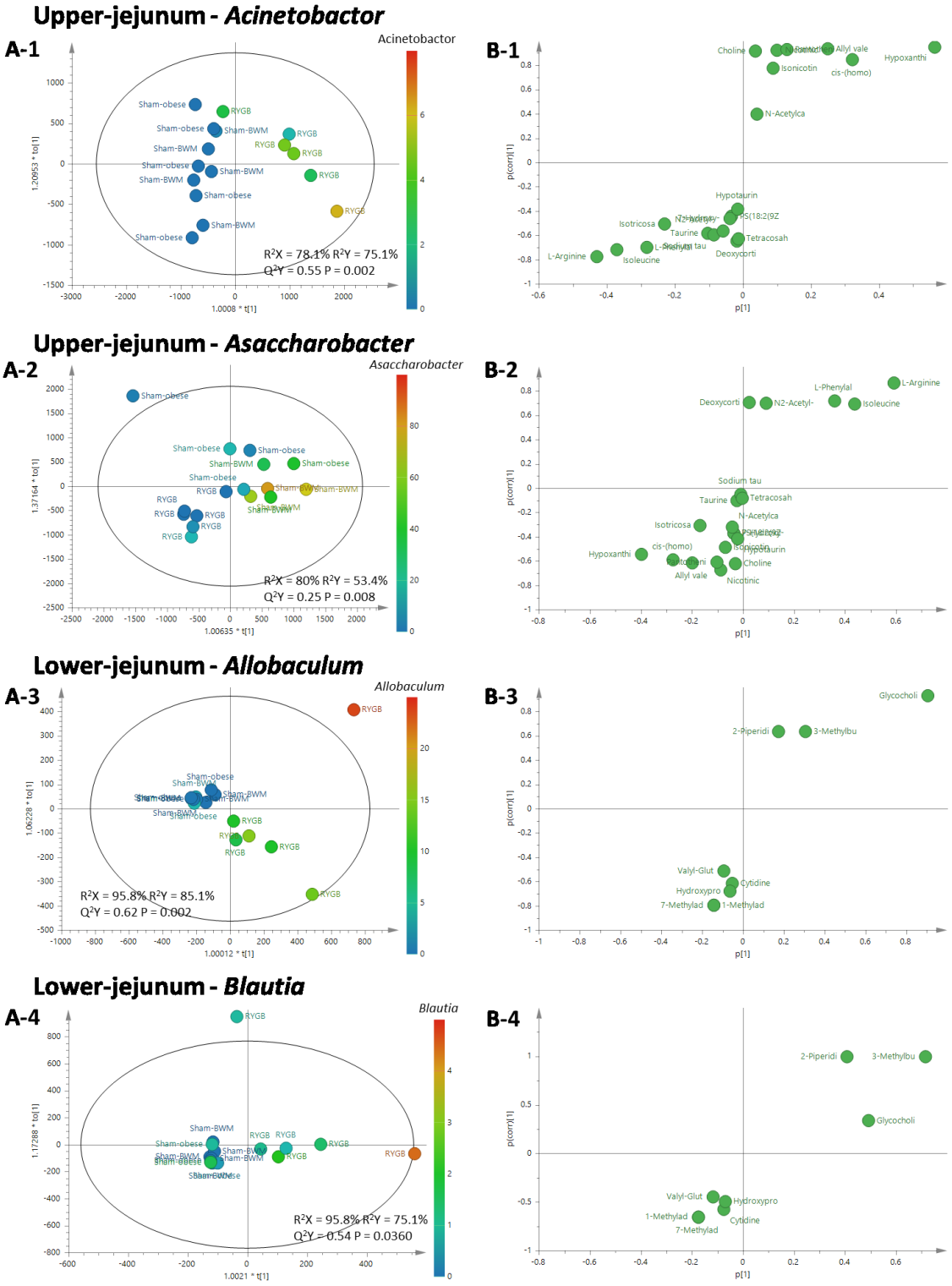
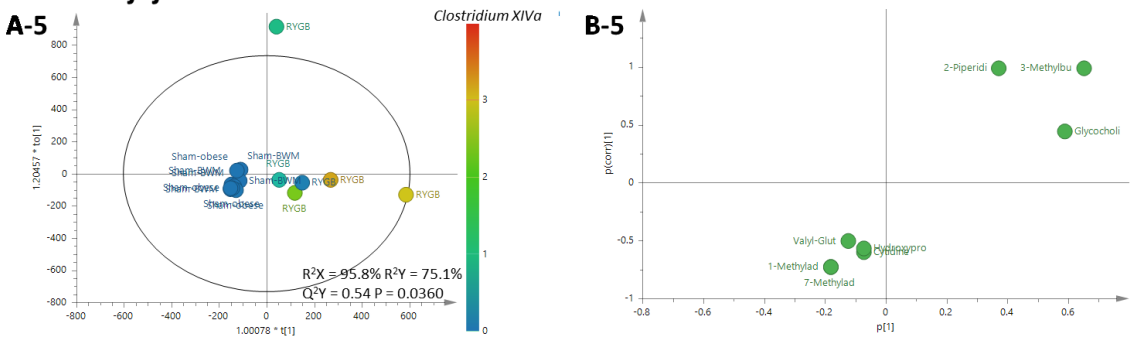


Figure 5-13. Box plots show the significantly altered gut microbiota between RYGB (blue) and sham-BWM (green) rats at genus level. Two-sided non-parametric t-test with Welch's correction was performed. Asterisks indicate significant differences: * P<0.05 and ** P<0.01.

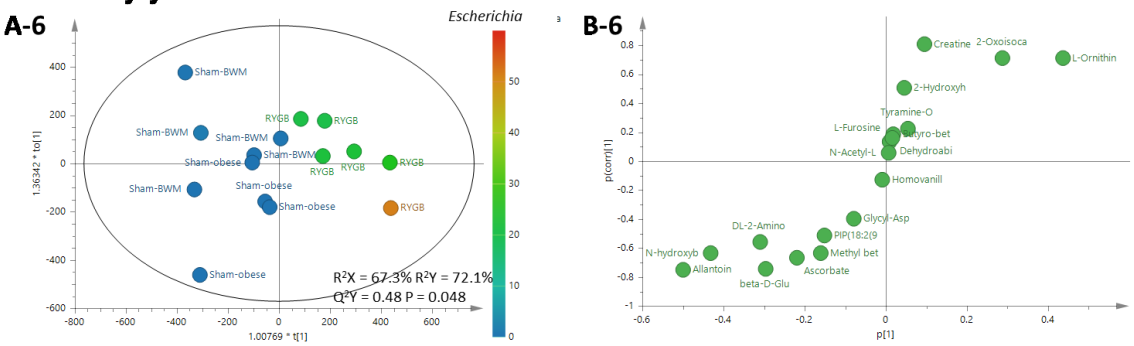
5.3.9 Correlation analysis of metabolome and microbiome data



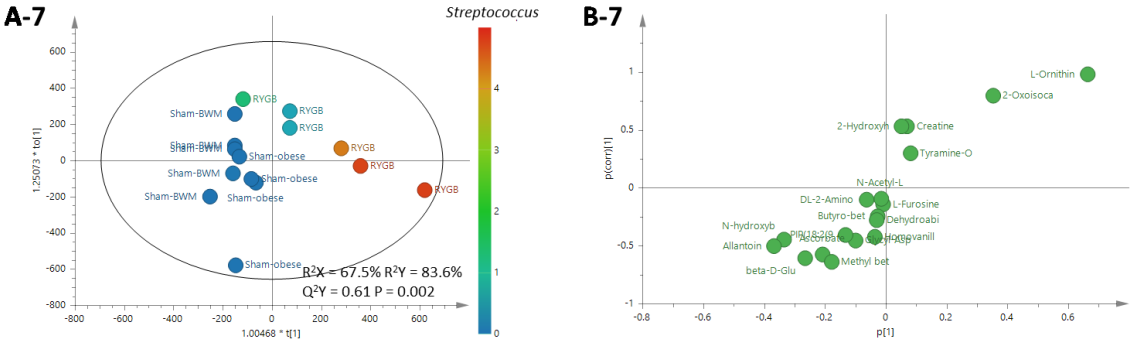
Lower-jejunum – *Clostridium XIVa*



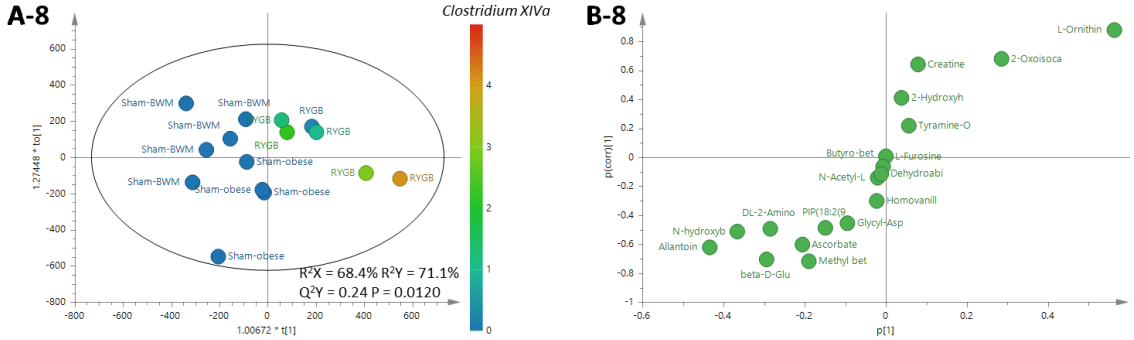
Lower-jejunum – *Escherichia*



Ileum – *Streptococcus*



Ileum – *Clostridium XIVa*



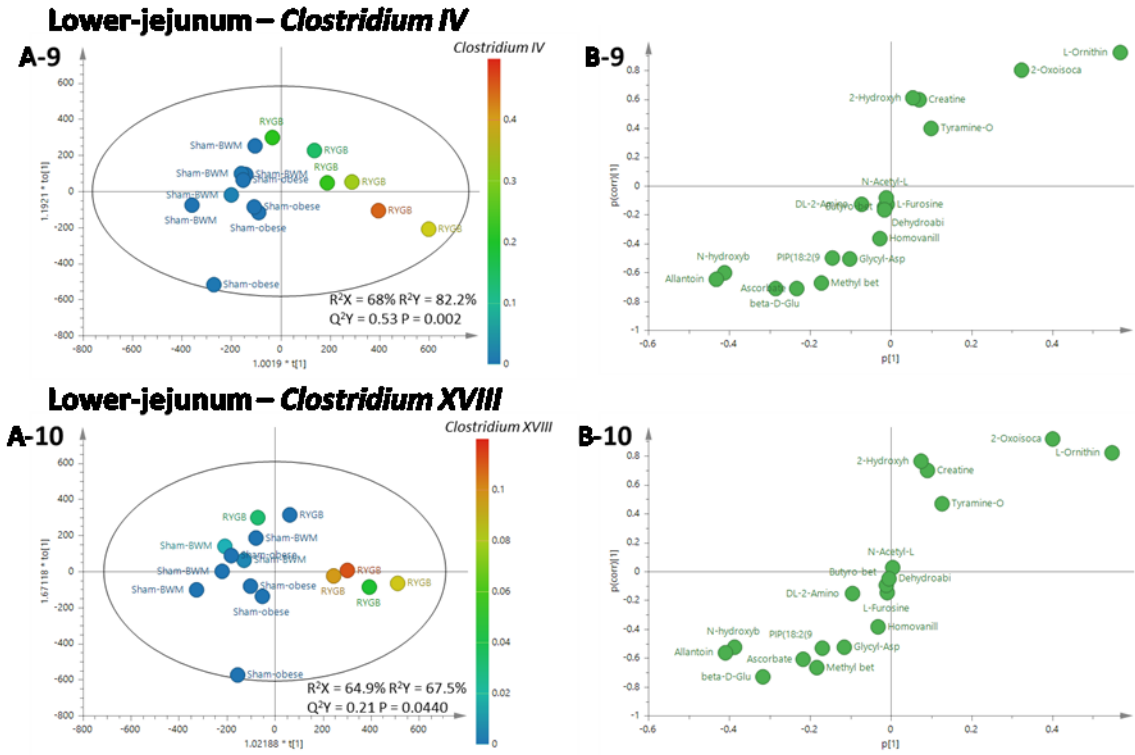


Figure 5-14. O-PLS regression analysis of the selected significantly altered metabolites detected using HILIC-UPLC-MS against discriminatory bacterial genera; A, O-PLS scores plots and B, corresponding S-line plots showing the correlated features to either increased or decreased relative abundance of bacteria.

HILIC-UPLC-MS metabolites considered discriminating factors between the two groups of pairwise comparison models in each gastrointestinal content were selected and further analysed using O-PLS approach to investigate the statistical correlation with the discriminatory bacterial genera of the true-matched sample set. Eleven valid O-PLS models (permutation P<0.05) were obtained (Figure 5-14). The results showed that *Acinetobacter* highly contained in upper-jejunal content of RYGB rats was positively correlated with hypoxanthine (R^2X=78.1%, R^2Y=75.1%, Q^2Y=0.55, permutation P=0.002) (Figure 5-14: A-1 and B-1). Furthermore, higher relative abundance of *Asaccharobacter* in upper-jejunal content was shown to be strongly associated with L-arginine but inversely correlated with hypoxanthine (R^2X=80%, R^2Y=53.4%, Q^2Y=0.25, permutation P=0.008) (Figure 5-14: A-2 and B-2). Significantly higher level of 3-methylbutyrolactone in lower-jejunal content of RYGB group was strongly correlated with increased relative abundance of *Blautia* (R^2X=95.8%, R^2Y=75.1%, Q^2Y=0.54, permutation P=0.36) and *Clostridium XIVa* (R^2X=95.8%, R^2Y=75.1%, Q^2Y=0.54,

permutation P=0.036) (Figure 5-14: A-4 – B-5). The higher relative abundance of Lower-jejunal *Allobaculum* was also found to be correlated with glycocholic acid (R^2X=95.8%, R^2Y=85.1%, Q^2Y=0.62, permutation P=0.002) (Figure 5-14: A-3 and B-3). *Escherichia* found in lower-jejunal content, together with of RYGB was additionally demonstrated to be positively associated with L-ornithine (R^2X=67.2%, R^2Y=72.1%, Q^2Y=0.48, permutation P=0.048) (Figure 5-14: A-6 and B-6). Higher levels of L-ornithine observed in RYGB were positively associated with ileal *Streptococcus* (R^2X=67.5%, R^2Y=83.6%, Q^2Y=0.61, permutation P=0.002), ileal *Costridium XIVa* (R^2X=68.4%, R^2Y=71.1%, Q^2Y=0.24, permutation P=0.012), lower-jejunal *Clostridium IV* (R^2X=68%, R^2Y=82.2%, Q^2Y=0.53, permutation P=0.002) and lower-jejunal *Clostridium XVIII* (R^2X=64.9%, R^2Y=67.5%, Q^2Y=0.21, permutation P=0.044) (Figure 5-14: A-7 – B-10).

5.4 Discussion

Gastrointestinal contents obtained from RYGB, sham-BWM and sham-obese groups were, for the first time in studying mechanisms of RYGB surgery, analysed using both HILIC-HPLC-MS and 16S rRNA gene Illumina MiSeq sequencing platforms. The results obtained from both analytical approaches provide further understanding and insights of the metabolic and microbial changes along the gastrointestinal tract, in addition to the findings of the biofluids discussed in Chapters 3 and 4.

5.4.1 An obese phenotype-related gastrointestinal metabolic and microbial fingerprints

In this study, sham-obese rats contained higher levels of taurine in the upper-jejunal contents and elevated levels of ileal *N1*-acetylspermidine, pantothenic acid and succinic acid, accompanied with higher levels of *4*-pyridoxic acid and hippuric acid in the colonic contents, compared with lean Zucker rats. It is noted that significant metabolites with the level of assignment below 3 will not be discussed due to higher uncertainty of the metabolite identification.

Taurine is one of the end products of sulphur metabolism and involved in several physiological events such as neuromodulation, osmoregulation, immunomodulation, antioxidation, retinal and cardiac function and brain development (Huang, Guo & Yuan, 2014). Taurine is thought to play an important role in the intestinal functions when present at high concentrations in the small intestine, for example, exerting a protective effect on gastric injury and colonic damage through its antioxidant properties (Son *et al.*, 1996), maintaining mucosal thickness of the small intestine and height of villus during the total parenteral nutrition (Tsuchioka, Fujiwara & Sunagawa, 2006) and maintaining normal serum concentrations of insulin-like growth factor-I (IGF-I), which promote intestinal development (Hu *et al.*, 2000; Park, Monaco & Donovan, 1999). In addition, taurine was previously shown to lower blood glucose levels and improve hyperglycaemia (Tsuchiya & Kawamata, 2017). Tsuchiya and colleagues (2017) reported that taurine could suppress the increase of hepatic portal glucose concentrations via suppression of sodium-glucose cotransporter 1 (SGLT1) activity in the rat jejunal tissue dependant on the presence of chloride ions (Tsuchiya & Kawamata, 2017). However, in this study, luminal taurine was found in relatively higher concentration that could be due to higher food intake of obese rats compared with lean rats that was previously reported in Chapter 3.

Succinic acid is a dicarboxylic acid and a component of the tricarboxylic acid (TCA) cycle (Bechthold *et al.*, 2008). In Chapter 3, it was reported that there was an elevated uptake of succinic acid and enhanced hepatic succinate metabolism in lean animals leading to decreased succinic acid availability in the gut lumen with its increased portal vein blood concentration. It is accordant with the results in this Chapter in which higher level of ileal succinic acid was observed in obese animals indicating less succinic acid uptake through portal vein. Higher ileal succinic acid indicates greater abundance of succinate in the obese animals. The increase in caecal succinate concentration was also previously reported to be significantly correlated with the abundance of *Bacteroides* (Fischbach & Sonnenburg, 2011). In this study, a larger abundance of *Bacteroides* was observed in

sham-obese Zucker rats. It is, however, noteworthy that *Prevotella* which are important succinic acid producers were not found to be correlated with the increase in succinic acid concentration in the current study. This may be due to the fact that the growth of *Prevotella* is promoted by diet enriched in dietary fibres and depleted in presence of fat (De Filippo *et al.*, 2010), whereas *Bacteroides* abundance has been associated with protein- and animal fat-rich diet (Wu *et al.*, 2011).

Hippuric acid level was also significantly higher in colonic content of sham-obese rats. It is the glycine conjugate of benzoic acid, and has long been associated with the microbial degradation of certain dietary components, hepatic function and toluene exposure, and is also commonly used as a measure of renal clearance (Lees *et al.*, 2013). Moreover, hippuric acid could be related to age progression and gender effects on metabolism in Type-2 diabetes and the changes in the profile of microbial metabolites in biological fluids can be related to the level of specific families of bacteria (Palau-Rodriguez *et al.*, 2015; Delzenne & Cani, 2011).

4-Pyridoxic acid is the catabolic product of vitamin B6 and this metabolite can be further broken down by the gut microbiota *via 4*-pyridoxic acid dehydrogenase catalysing the four electron oxidation of *4*-pyridoxic acid to 3-hydroxy-2-methylpyridine-5, 5-dicarboxylate with nicotinamide adenine dinucleotide as a cofactor (Coburn *et al.*, 2002). Previous studies showed that bacteria belonging to genus *Pseudomonas* possess *4*-pyridoxic acid dehydrogenase, hence promoting vitamin B6 oxidation (RODWELL *et al.*, 1958; Yagi, Kishore & Snell, 1983). This indicates that, in obese animals, vitamin B6 may be absorbed through enterocytes less than that in lean animals. As a result, it is metabolised by the intestinal microbiota that is evident by higher colonic concentration of *4*-pyridoxic acid in obese animals. Alternatively, it could also be due to greater nutrient flux in the gut since food intake was higher in obese animals.

5.4.2 Caloric restriction reverses metabolome and microbiome of obese Zucker rats to leaner phenotype

Obese hyperinsulinemic Zucker rats with caloric restriction showed higher concentrations of 3-aminopropanal, homoserine lactone, cysteine, L-phenylalanine, merodesmosine in duodenal content, homovanillic acid, butyrobetaine and *N*-acetyl-L-glutamate 5-semialdehyde in ileal contents, and L-furosine in both ileal and colonic contents.

3-Aminopropanal is a reactive aldehyde that has been shown to mediate progressive neuronal necrosis and glial apoptosis (Ivanova *et al.*, 2002). Higher concentration of this metabolite indicates increased activity of polyamine oxidase that catabolises polyamines (*e.g.* spermine, spermidine and putrescine) to yield 3-aminopropanal (Li *et al.*, 2003). Although polyamine metabolites are required for mammalian cell proliferation and for embryonic development, accumulation of these polyamines, especially spermine, have been shown in obese children and are related to biomarkers of oxidative/nitrosative stress, inflammation and leptin (Ishii *et al.*, 2012; Codoñer-Franch *et al.*, 2011) so that caloric restriction may play an important role in lowering polyamines as evident by higher concentration of 3-aminopropanal.

Levels of amino acids such as essential amino acid (*e.g.* phenylalanine), sulfur-containing amino acid (*e.g.* Cysteine) and alpha-amino acid (*e.g.* merodesmosine and L-furosine) were higher in sham-BWM rats. Phenylalanine is an essential amino acid and the precursor of the amino acid tyrosine and is also a precursor for catecholamines including tyramine, dopamine, epinephrine, and norepinephrine (Matthews, 2007). Cysteine is unique amongst the twenty natural amino acids as it contains thiol group that can undergo redox reactions and is also an important source of sulfur in human metabolism (Dong & Coquelet, 1980). Merodesmosine is a member of the class of compounds known as alpha amino acids and is found in animal foods (Francis, John & Thomas, 1973). Higher concentrations of these amino acids in the duodenal content of

sham-BWM rats suggest either lower amino acid absorption or enhanced production of amino acids through endogenous protein metabolism or bacterial process during caloric restriction. L-furosine, another alpha amino acid that showed its higher concentration in both ieal and colonic content of sham-BWM rats, is primarily located in the cytoplasm and can also be found extracellularly (Henle, Zehetner & Klostermeyer, 1995). Moreover, furosine, a glycation product of collagen, has been shown as a strong inverse predictor of life span in both *ad libitum* and caloric restricted mice suggesting that glucose tolerance is impaired in aging mice leading to early death or alternatively, a process responsible for decreased collagen turnover rate may be responsible for decreased removal rate of damaged cellular organelles from critical life span controlling tissues (Hamelin *et al.*, 2003). In this study, concentration of L-furosine was higher in sham-BWM rats compared with sham-obese rat indicating that early onset of caloric restriction may enhance hypercatabolic state that may result in increased carbonyl and oxidative stress to ileal and colonic epithelial cells. In addition to increased ileal and colonic concentration of furosine, significantly higher relative abundance of colonic *Oscillibacter* was observed that is consistent with the previous study by Qu *et al* (2017) demonstrating that *Oscillibacter* showed a dramatic increase with advanced glycation end products (AGEs) and reduced proximal colon transepithelial resistance in a high-fat diet group (Qu *et al.*, 2017; Lam *et al.*, 2012).

Although significant alteration of metabolome was not observed in lower-jejunal content between calorie-restricted obese Zucker rats and their obese counterparts, the presence of lower relative abundance of lower-jejunal *Turicibacter* in obese animal found in this study is in line with a previous study conducted by Everard *et al* (2014) of which they showed markedly reduced abundance of this bacterial genus in mice fed a high fat diet (Everard *et al.*, 2014). Our findings may raise the question whether this taxon might have anti-inflammatory properties.

Concentration of butyrobetaine, a highly water-soluble derivative of gamma-amino butyric acid, was increased and this metabolite can be microbially converted into L-

carnitine, then trimethylamine (TMA) and trimethylamine-*N*-oxide (TMAO), which was shown to be proatherosclerotic metabolite (Koeth *et al.*, 2014). Moreover, a previous study by Koeth *et al* (2014) demonstrated that gut microbial metabolism of butyrobetaine to TMA/TMAO, but not butyrobetaine itself directly, was associated with enhanced atherosclerosis. This is evident as mice supplemented with butyrobetaine and treated with oral antibiotics to suppress gut microbe, TMA/TMAO production did not have an increase in aortic root and atherosclerotic plaque area (Koeth *et al.*, 2014). This suggests that caloric restriction may alter the gut microbiome in the ileum, resulting in less abundance of bacteria that are capable of metabolising butyrobetaine to TMA or TMAO, hence lower risk of atherosclerosis.

5.4.3 RYGB-related effects improve gastrointestinal health of obese Zucker rats

Comparing with sham-obese rats, RYGB rats demonstrated lower concentrations of gastric trigonelline, sucrose and dextrin but higher concentrations of PC(6:0/8:0) and cytochalasin B in gastric content. Moreover, the upper-jejunal content of RYGB contained higher levels of choline, hypoxanthine with lower levels of isoleucine, L-phenylalanine, L-arginine and sodium taurocholate, and low levels of lower-jejunal 7-methyladenine. Ileal concentrations of creatine and 2-hydroxyhexadecanoic acid were increased while ileal levels of fructosamine, *N*-hydroxybenzenesulfonamide, allantoin and ascorbate-2-sulfate, together with colonic level of 3-indoleproprionic acid were markedly decreased.

Cysteic acid or 3-sulfoalanine is water-soluble and an extremely strong acidic compound that is primarily located in the mitochondria of the cells. It is a crystalline amino acid formed in the oxidation of cysteine and is also a precursor of taurine (Edgar *et al.*, 1994). Taurine is among the few naturally occurring organic sulfonic acids that is a recognized constituent of human bile and plays role in reducing oxidative stress, providing cardiomyocyte osmoregulation, and membrane stabilization (Schaffer *et al.*, 2010).

Furthermore, effect of taurine on gut microbiota could regulate the gut micro-ecology, which might be of benefit to health by inhibiting the growth of harmful bacteria (*Proteobacteria*, especially *Helicobacter* – a residential microbiota in stomach), accelerating the production of SCFA and reducing LPS concentration (Yu *et al.*, 2016). In the current study, greater concentration of taurine accompanied with lower concentration of cysteic acid may indicate the upregulated taurine production through cysteic acid decarboxylation. Despite a number of species-dependent beneficial effects of genera *Lactobacillus* and *Allobaculum* that was shown to be significantly higher in obese animals, *Clostridium* cluster XI is a pathogen-associated cluster with *C.difficile* as one of the members and it has been shown to strikingly increase in obese mice and associated with hepatocellular carcinoma development (Qiao *et al.*, 2014; Gomes, Costa & Alfenas, 2015; Hara, 2015). In the present study, RYGB has been shown to lower the relative abundance of *Clostridium* cluster XI in stomach, together with beneficial effects of greater taurine concentration suggesting the reduced risk of tumorigenesis.

Decreased concentrations of vitamin B3 metabolite (*e.g.* trigonelline) and polysaccharide metabolites (*e.g.* sucrose and dextrin) in stomach of RYGB group were observed. This could be due to the lack of food arrival in the distal stomach (bypassed gastric section).

Choline is important as a precursor of acetylcholine, as a methyl donor in various metabolic processes, and in lipid metabolism (Wells & Remy, 1965). It is also known as dietary precursors for TMA and further TMAO production by the gut microbiota (King, 1984). As higher concentration of faecal TMA in RYGB-treated rats was previously reported in Chapter 4, greater concentration of choline in upper-jejunal content, in this Chapter, indicates the rich pool of TMA precursors in post-RYGB operation.

Hypoxanthine is a naturally occurring purine derivative and a reaction intermediate in the metabolism of adenosine and in the formation of nucleic acids by the salvage pathway (Saugstad, 1975). Higher concentrations of upper-jejunal hypoxanthine in the current study, along with hepatic hypoxanthine and its urinary concentration in the previous

studies (Wu *et al.*, 2015; Narath *et al.*, 2016) might indicate the modification of nucleotide metabolism after bariatric intervention.

Lower levels of amino acids including isoleucine, phenylalanine and arginine in the upper-jejunal content post-RYGB operation may reflect the enhanced absorption of amino acids post-RYGB. Previous study shows that despite exclusion of a major part of the stomach and the mixing of gastropancreatic secretions in the distal part of jejunum, RYGB does not appear to impair protein digestion and an accelerated appearance of amino acids, derived from protein ingested was also observed (Azim & Kashyap, 2016). Accelerated protein digestion and amino acid absorption can influence the metabolic and hormonal changes that occur following RYGB. Amino acids such as leucine and phenylalanine are capable of stimulating insulin secretion from pancreatic beta-cells and GLP-1 secretion from intestine L-cells (Magkos *et al.*, 2013).

A previous study by Zhang and co-workers (2009) reported that obese and lean individuals possessed *Firmicutes* as the dominant gut bacteria, whereas post-gastric bypass individuals demonstrated the proportional increase of *Gammaproteobacteria* (Zhang *et al.*, 2009). Later in 2011, Li and colleagues further demonstrated, in a non-obese rat model, the substantial shifts of the main gut phyla towards higher abundance of *Proteobacteria*, especially *Enterobacter hormaechei* post-RYGB operation compared with sham-operated rats (Li *et al.*, 2011). In addition, a study by Liou *et al* (2015) confirmed that transfer of the gut microbiota from RYGB-treated mice to non-operated, germ-free mice resulted in weight reduction and decrease of fat mass in the recipient animals relative to recipients of microbiota induced by sham surgery (Liou *et al.*, 2013). In this study, the microbial alterations along the gastrointestinal tract in the RYGB- and caloric restriction-treated obese Zucker rat in response to obese Zucker rat control have been reported for the first time. Microbial shifts have been clearly observed following RYGB intervention as evidenced by increases in duodenal *Escherichia*, upper-jejunal *Akkermansia* and *Acinetobacter*, lower-jejunal *Allobaculum*, *Enterooccus*, *Streptococcus,* ileal *Blautia* and *Enterorhabdus*. More interestingly, *Clostridium* cluster

XIVa, IV and XI were increased along lower-jejunum and ileum. These microbial alteration in RYGB compared with obese control were mostly similar to the comparison between RYGB and sham-BWM group, with the more significant models. *Akkermansia*, especially the strain *Akkermansia muciniphila* which is a mucin-degrading bacterium and has been inversely associated with body fat mass and glucose intolerance, showed greater improvement in insulin sensitivity markers and other clinical parameters after 6-week caloric restriction in human (Dao *et al.*, 2016). However, caloric restriction performed in the obese Zucker rat model did not show the significant changes in this taxon, so this means that RYGB may exert a stronger degree of restricted calorie intake in the Zucker rats. However, *Clostridium* cluster XIVa is known for polysaccharide fermentation and butyrate-producing bacteria in the gut that results in more efficient energy extraction from diet (Jiao *et al.*, 2017). *Enterococcus* also increased in obese animals which could release bile salt hydrolase (BSH) that convert conjugated bile acids into free bile acids through deconjugation (Jiao *et al.*, 2017). *Blautia* genus was shown in high abundance in the participants with glucose intolerance even while consuming fewer carbohydrates and fat (Egshatyan *et al.*, 2016).

Acinetobacter, a genus of Gram-negative bacteria belonging to the wider class of *Gammaproteobacteria*, was directly correlated with hypoxanthine in RYGB. Wang and colleagues demonstrated that bacterial xanthine dehydrogenase from *Acinetobacter baumannii* catalyses the oxidation of hypoxanthine to xanthine and also xanthine to uric acid by an oxidative hydroxylation mechanism (Wang *et al.*, 2016). In addition, L-ornithine showed the positive correlation with several genera, for instance, *Escherichia, Clostridium* clusters IV and XVIII in lower-jejunum and *Streptococcus* and *Clostridium* cluster XIVa in ileum. Some bacteria may utilise L-ornithine as a carbon and energy source, for example, *E.coli first* decarboxylates L-ornithine to putrescine which is transaminated to gamma-aminobutyraldehyde, and oxidized to gamma-aminobutyric acid (GABA) (Shaibe, Metzer & Halpern, 1985). This is also accordant with high concentration of GABA observed in the faecal samples collected from RYGB rats.

Asaccharobacter, bacterial genus from the family of *Coriobacteriaceae* and predominantly found in sham-BWM group was positively correlated with L-arginine (Minamida *et al.*, 2008). Strains of this bacterium were unable to metabolise glucose or other carbohydrates as sole carbon sources; growth was enhanced in the presence of arginine which is the first decarboxylated to agmatine, which is hydrolysed to urea and putrescine. (Minamida *et al.*, 2008).

5.5 Summary

In the current study, RYGB has been shown to provide the health effects, evidenced by the altered metabolites that are associated with the modification of nucleotide metabolism and enhanced absorption of amino acids after bariatric intervention. In addition to the changes in metabolic profiles, RYGB showed the increases in the abundance of some bacterial genera such as duodenal Escherichia, upper-jejunal *Akkermansia* and *Acinetobacter*, lower-jejunal *Allobaculum*, *Enterooccus*, Streptococcus, ileal *Blautia* and *Enterorhabdus* and some of which had been revealed in the previous studies to provide beneficial effects on host health. Besides, caloric restriction may play an important role in lowering polyamines as evident by higher polyamine catabolism end-products and alter the gut microbiome in the ileum, resulting in less abundance of bacteria that are capable of metabolising atherosclerosis risk-related metabolites.

6. Summary and future work

6.1 Summary and general discussion

The application of an NMR spectroscopy- or mass spectrometry-based metabolic profiling in combination with 16S rRNA sequencing have been proven to assist the characterisation of host-microbial interactions at a systems biology level (Osaka *et al.*, 2017; Foschi *et al.*, 2017). Multivariate statistical data analyses have been employed in this study to aid the data analysis and visualisation, especially the identification of biomarkers and signaling molecules of host-microbial metabolic interactions. This thesis, based on a hyperinsulinemic obese Zucker rat model, has focused on understanding the obese phenotype-related metabolic fingerprints in biofluids, especially portal vein plasma which has been reported for the first time (Chapter 3), the effects of caloric restriction or RYGB surgery on the metabolic alterations in biofluids (Chapter 4), and gastrointestinal metabolic and microbial changes following caloric restriction or RYGB (Chapter 5). Distinct metabolome and microbiome alterations at the systematic level after either caloric restriction or gastric bypass have been studied and reported in this thesis.

6.1.1 Summary of animal randomisation and sham-operation

Animal randomisation: Obese Zucker rats were, in this study, randomised into three different treatment groups: sham-obese, sham-BWM and RYGB. The metabolic profiles of these three groups of rats at the pre-operation time point were compared using both unsupervised and supervised statistical analyses, and invalidity of the models indicated no significant differences between obese animals allocated into different treatment groups prior to the intervention.

Sham-operation: Sham-operation conducted in this study was proven that it does not induce the metabolic alterations in this animal model as indicated by the invalid statistical models between obese control animals at pre-sham operation and post-sham operation time points. Therefore, it can be ensured that there was no metabolic alteration as a consequence of sham-operation throughout the study.

6.1.2 Summary of energy metabolism

Enhanced lipogenesis, indicated by elevated peripheral and portal vein levels of several lipid species, was clearly observed in hyperinsulinemic obese Zucker rats compared with the lean genotype (Figure 6-1). Lipogenesis involves the conversion of acetyl-CoA, which is an intermediate in the metabolism of glucose, into fatty acid and the energy can be efficiently stored in the form of fats (Turkenkopf *et al.*, 1980). RYGB-treated obese Zucker rats, instead, showed significantly lower levels of lipids with higher urinary concentration of 3-hydroxybutyrate, which is a ketone body. These observations indicated a shift from the use of carbohydrates to fats as the main fuel of the body, resulting in ketogenesis, which has an effect on hunger suppression. However, such a metabolic event was not observed following caloric restriction.

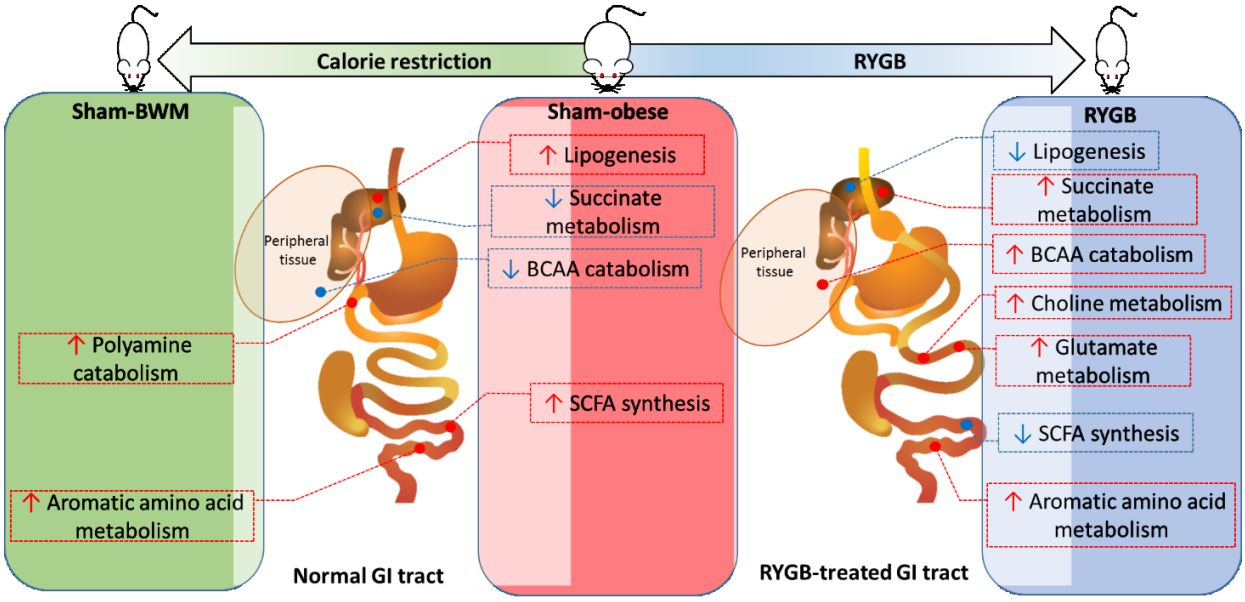


Figure 6-1. Schematic illustration of the suggested metabolic alterations based on altered metabolites found in obese, caloric restriction and RYGB groups of this study. Abbreviations: BCAA, branched-chain amino acid; GI, gastrointestinal; SCFA, short-chain fatty acid.

6.1.3 Summary of BCAA metabolism

BCAAs are considered the insulin resistance-related biomarkers and have been found in high concentrations, together with low alanine level in the obese rat suggesting a down-regulation of alanine synthesis from BCAAs. On the other hand, RYGB showed the increased catabolism of BCAAs, evidenced by higher concentrations of urinary BCAA breakdown products (*e.g.* α-ketoisovalerate), accompanied with lower concentrations of pyridoxal, a form of vitamin B6 required as cofactor to catalyze the reaction (Figure 6-1). Decreases in BCAA levels after RYGB may be predominantly caused by the gastric bypass procedure and is not due to weight loss as caloric restriction group was unable to show such metabolic shifts. Effects of RYGB on reducing BCAA levels found in this study is in line with a previous study showing that RYGB procedure promotes BCAA catabolic gene expression in adipose tissue (She *et al.*, 2007). It is, however, interesting that several studies reported

the beneficial effects of caloric restriction on glucose metabolism and reversal of insulin resistance. This suggests that caloric restriction could exert its effect on improvement of insulin resistance through other mechanisms without affecting BCAA concentrations.

6.1.4 Summary of polyamine catabolism

Polyamine biosynthesis may be upregulated as indirectly shown by the higher level of *N1*-acetylspermidine in the ileal contents of obese group, which could in turn indicate an enhanced activity of enzyme SSAT in obese rats. Although polyamine is required for cell proliferation, accumulation of polyamine has been considered as the biomarkers of oxidative/nitrosative stress and inflammation (Codoñer-Franch *et al.*, 2011). In the current study, caloric restriction induced higher levels of polyamine catabolism products (*e.g.*3-aminopropanol) in the duodenum, which may indicate an increased activity of polyamine oxidase and a lower risk of oxidative stress and inflammation.

6.1.5 Summary of gut microbiota-related metabolisms

SFCA metabolism: Obese Zucker rats showed the elevated fermentation substrate bioavailability and increased microbial non-digestible carbohydrate fermentation by the gut microbiota. Such a metabolic phenomenon was altered in RYGB-treated rats as lower concentrations of faecal propionate and acetate, potentially resulting from lower abundance of SCFA-producing bacteria such as *Lactobacillus* were observed in lower-jejunal, ileal and colonic contents of RYGB in this study (Figure 6-1). Interestingly, portal vein plasma of both RYGB and caloric restriction groups carried high level of propionate but not acetate, collectively indicating the up-regulated gluconeogenesis despite the differences in weight loss approach.

Choline metabolism: As discussed in Chapter 3, obese phenotype of the Zucker rats could be independent of microbial choline metabolism. However, RYGB procedure seems to promote microbial conversion of choline into TMA found in faeces, indicating higher abundance of TMA producers in the gut. Consistently, RYGB group showed greater abundance of *Clostridium* cluster XIVa and *Escherichia* in the lower-jejunal content (Chapter 5) and these two bacterial genera were shown to be able to produce TMA (Rath *et al.*, 2017). Therefore, microbial choline metabolism is likely to be enhanced by RYGB surgery (Figure 6-1).

Aromatic amino acid metabolism: The conversion of phenylalanine into 3-HPPA was preferred in caloric restriction and obese groups, whereas RYGB showed the enhanced conversion of phenylalanine into PAG, which could be considered as RYGB-specific metabolic route for phenylalanine metabolism (Figure 6-1). RYGB also demonstrated increased catabolism of tryptophan into indole. This microbial conversion may result from increased abundance of Gram-negative bacteria such as *Escherichia* (Li & Young, 2013). Furthermore, the conversion of tyrosine into *4*-cresyl glucuronide was also enhanced, potentially resulting from elevated abundance of bacteria belonging to the genus *Clostridium,* of which some *Clostridium* species had the ability to convert tyrosine into 4-cresol (Dawson *et al.*, 2011).

Metabolism of microbially-derived neuroactive intermediates: Higher faecal concentration of GABA in the current study suggested that RYGB procedures may alter the microenvironment to favour the growth of GABA-producing bacteria, such as *Lactobacillus* and *Bifidobacterium* in the lower-jejunum (Figure 6-1). The GI tract motility could be modulated following RYGB (Ardila-Hani & Soffer, 2011), also evidenced by greater level of

serotonin precursor (5-HTP) in this study. This suggests that RYGB could change the GI motility by increased levels of serotonin precursor.

6.1.6 Summary of hepatic succinate metabolism

Obese Zucker rat showed high ileal level and faecal excretion of succinate. In contrast, RYGB promotes the portal vein succinate uptake and possibly hepatic succinate metabolism. Together with previous findings in the decreased levels of tricarboxylic acid (TCA) cycle intermediates in urine following RYGB, these findings suggested enhanced TCA cycle activity after RYGB surgery (Li *et al.*, 2011) (Figure 6-1).

This study has systemically demonstrated for the first time the metabolic profiles of urine, portal vein and peripheral plasma, faecal water, gastrointestinal contents along with the microbial profiles of gastrointestinal contents of RYGB-, caloric restriction-treated obese Zucker rats in comparison with obese Zucker rats. As explained in Chapter 3, obese Zucker rats had distinct gut microbial metabolic activities that promote the production of SCFAs, especially acetate (Figure 3-4) which in turn enhances hepatic lipogenesis (Figure 6-1). Caloric restriction has demonstrated some metabolic changes such as increased polyamine catabolism and aromatic amino acid metabolism, providing the health benefits. Metabolic alterations induced by the RYGB surgery include the enhanced production of neuroactive metabolites, succinate metabolism, BCAA catabolism, aromatic amino acid metabolism with lower lipogenesis and SCFA production, and microbial shifts which also affect the microbial choline metabolism.

6.1.7 Implications

The findings in the current study collectively suggest that bariatric surgery, particularly RYGB is crucial for effective and sustainable weight loss and improvement of metabolic syndromes in severely co-morbid obese individuals whom lifestyle modification and pharmacotherapy are less effective. RYGB has, however, been shown to involve the production of oxidative stress-related metabolites and inflammation-related gut microbiota that may contribute to the adverse effects on health in a long-term period. The results in this thesis emphasise the need to further investigate the long-term metabolic derangements induced by the RYGB procedure and their impact on human health. Therefore, it is noteworthy that oxidative stress and inflammation should be carefully monitored throughout the follow-up appointments.

6.2 Future work

Future work should focus on the following aspects: (1) mechanisms underlining the effects on caloric restriction on improvement of insulin resistance. Although BCAAs have so far been reported to be associated with insulin resistance and it is further confirmed in this study for the role of RYGB in resolving such the metabolic condition by reducing plasma BCAA levels. However, caloric restriction-induced improvement of insulin resistance seems to be independent of lowering BCAA levels. Therefore, the impact of caloric restriction on insulin resistance and its related mechanisms should be further investigated. An experiment on nervous and hormonal regulation post-caloric restriction could be of interest to further address this question. (2) Confirmation of suggested metabolic pathways reported in this study. A great number of metabolites were observed to be altered in different biofluids and gastrointestinal contents in regards with RYGB or caloric restriction and several metabolic pathways have also been suggested. The next step would be to experimentally confirm

these metabolic changes, for example, measuring the enzyme activity that is related to the biosynthesis or biodegradation of altered metabolites in appropriate cell line or *in vivo*. (3) Validation of suggested bacterial activity. This study showed a number of changes in microbial composition after the RYGB or caloric restriction intervention. The subsequent step would be to conduct the experiments on isolating beneficial bacteria from the biofluids and gastrointestinal contents in order to study their biological functions *in vitro* and *in vivo*. This would further our understanding at both the mechanisms underlining host-microbial metabolism and the use of 'good bacteria' on microbiota transplantation to improve gut health. (4) Pro-inflammatory responses and oxidative stress status following RYGB. Several pro-inflammation- and oxidative stress-related metabolites were observed in this study. It would be interesting to experiment on host pro-inflammatory cytokines and manifestation of reactive oxygen species in biofluids and tissue samples in both animal and human population studies. This piece of information would aid the post-RYGB prognosis and preventive medicine.

References

Abdi, H. & Williams, L.J. (2010) Principal component analysis. *Wiley Interdisciplinary Reviews: Computational Statistics*. [Online]. 2 (4) pp.433–459. Available from: doi:10.1002/wics.101.

Adeghate, E. & Ponery, A.S. (2002) GABA in the endocrine pancreas: cellular localization and function in normal and diabetic rats. *Tissue & cell*. [Online] 34 (1), 1–6. Available from: doi:10.1054/tice.2002.0217.

Adeva, M.M., Calviño, J., Souto, G. & Donapetry, C. (2012) Insulin resistance and the metabolism of branched-chain amino acids in humans. *Amino Acids*. [Online]. 43 (1) pp.171–181. Available from: doi:10.1007/s00726-011-1088-7.

Afarideh, M., Behdadnia, A., Noshad, S., Mirmiranpour, H., et al. (2015) Association of peripheral 5-hydroxyindole-3-acetic acid, a serotonin derivative, with metabolic syndrome and low-grade inflammation. *Endocrine practice*. [Online] 21 (7), 711–718. Available from: doi:10.4158/EP14442.OR.

Anon (1972) Ribosomes: Roles in ribosomes. [Online] 239 (5366), 9–10. Available from: doi:10.1038/239009c0.

Ardila-Hani, a & Soffer, E.E. (2011) Review article: the impact of bariatric surgery on gastrointestinal motility. *Alimentary pharmacology & therapeutics*. [Online] 34 (8), 825–831. Available from: doi:10.1111/j.1365-2036.2011.04812.x.

Aron-Wisnewsky, J., Dore, J. & Clement, K. (2012) The importance of the gut microbiota after bariatric surgery. *Nat Rev Gastroenterol Hepatol*. [Online] 9, 590–598. Available from: doi:10.1038/nrgastro.2012.161.

Ash, C.E. & Merry, B.J. (2011) The molecular basis by which dietary restricted feeding reduces mitochondrial reactive oxygen species generation. *Mechanisms of Ageing and Development*. [Online] 132 (1–2), 43–54. Available from: doi:10.1016/j.mad.2010.12.001.

Azim, S. & Kashyap, S.R. (2016) Bariatric Surgery: Pathophysiology and Outcomes. *Endocrinology and Metabolism Clinics of North America*. [Online]. 45 (4) pp.905–921. Available from: doi:10.1016/j.ecl.2016.06.011.

Bartley, J.M., Zhou, X., Kuchel, G.A., Weinstock, G.M., et al. (2017) Impact of Age, Caloric Restriction, and Influenza Infection on Mouse Gut Microbiome: An Exploratory Study of the Role of Age-Related Microbiome Changes on Influenza Responses. *Frontiers in Immunology*. [Online] 8 (SEP). Available from: doi:10.3389/fimmu.2017.01164.

Barzilai, N., Banerjee, S., Hawkins, M., Chen, W., et al. (1998) Caloric restriction reverses hepatic insulin resistance in aging rats by decreasing visceral fat. *Journal of Clinical Investigation*. [Online] 101 (7), 1353–1361. Available from: doi:10.1172/JCI485.

Baxmann, A.C., Ahmed, M.S., Marques, N.C., Menon, V.B., et al. (2008) Influence of muscle mass and physical activity on serum and urinary creatinine and serum cystatin C. *Clin J Am Soc Nephrol*. [Online] 3, 348–354. Available from: doi:10.2215/CJN.02870707.

Bechthold, I., Bretz, K., Kabasci, S., Kopitzky, R., et al. (2008) Succinic acid: A new platform chemical for biobased polymers from renewable resources. *Chemical Engineering and Technology*. [Online]. 31 (5) pp.647–654. Available from: doi:10.1002/ceat.200800063.

Beckonert, O., Keun, H.C., Ebbels, T.M., Bundy, J., et al. (2007a) Metabolic profiling, metabolomic and metabonomic procedures for NMR spectroscopy of urine, plasma, serum and tissue extracts. *Nat Protoc*. [Online] 2, 2692–2703. Available from: doi:10.1038/nprot.2007.376.

Beckonert, O., Keun, H.C., Ebbels, T.M.D., Bundy, J., et al. (2007b) Metabolic profiling, metabolomic and metabonomic procedures for NMR spectroscopy of urine, plasma, serum and tissue extracts. *Nature protocols*. [Online] 2 (11), 2692–2703. Available from: doi:10.1038/nprot.2007.376.

Belachew, M., Legrand, M., Vincent, V., Deffechereux, T., et al. (1995) Laparoscopic Placement of Adjustable Silicone Gastric Band in the Treatment of Morbid Obesity: How to Do It. *Obesity Surgery: Including Laparoscopy and Allied Care*. [Online] 5 (1), 66–70. Available from: doi:10.1381/096089295765558196.

Bennett, S.E., Bevington, A. & Walls, J. (1992) Creatine and creatinine metabolism in uraemia. *Miner Electrolyte Metab*. [Online] 18, 192–195. Available from: http://www.ncbi.nlm.nih.gov/pubmed/1465056.

Bertrand, H.A., Lynd, F.T., Masoro, E.J. & Yu, B.P. (1980) Changes in adipose mass and cellularity through the adult life of rats fed ad libitum or a life-prolonging restricted diet. *Journals of Gerontology*. [Online] 35 (6), 827–835. Available from: doi:10.1093/geronj/35.6.827.

den Besten, G., van Eunen, K., Groen, A.K., Venema, K., et al. (2013a) The role of short-chain fatty acids in the interplay between diet, gut microbiota, and host energy metabolism. *J Lipid Res*. [Online] 54, 2325–2340. Available from: doi:10.1194/jlr.R036012.

den Besten, G., van Eunen, K., Groen, A.K., Venema, K., et al. (2013b) The role of short-chain fatty acids in the interplay between diet, gut microbiota, and host energy metabolism. *Journal of Lipid Research*. [Online] 54 (9), 2325–2340. Available from: doi:10.1194/jlr.R036012.

Booth, S.L. (2009) Roles for Vitamin K Beyond Coagulation. *Annual Review of Nutrition*. [Online] 29 (1), 89–110. Available from: doi:10.1146/annurev-nutr-080508-141217.

Bower, G., Athanasiou, T., Isla, A.M., Harling, L., et al. (2015) Bariatric surgery and nonalcoholic fatty liver disease. *Eur J Gastroenterol Hepatol*. [Online] 27, 755–768. Available from: doi:10.1097/MEG.0000000000000375.

Bowman, T.A., Ramakrishnan, S.K., Kaw, M., Lee, S.J., et al. (2010) Caloric restriction reverses hepatic insulin resistance and steatosis in rats with low aerobic capacity. *Endocrinology*. [Online] 151 (11), 5157–5164. Available from: doi:10.1210/en.2010-0176.

Buchwald, H. & Oien, D.M. (2013) Metabolic/bariatric surgery worldwide 2011. *Obesity Surgery*. [Online] 23 (4), 427–436. Available from: doi:10.1007/s11695-012-0864-0.

Byrne, C.S., Chambers, E.S., Morrison, D.J. & Frost, G. (2015) The role of short chain fatty acids in appetite regulation and energy homeostasis. *International journal of obesity (2005)*. [Online] 39 (9), 1331–1338. Available from: doi:10.1038/ijo.2015.84.

Canani, R.B., Costanzo, M. Di, Leone, L., Pedata, M., et al. (2011) Potential beneficial effects of butyrate in intestinal and extraintestinal diseases. *World Journal of Gastroenterology*. [Online] 17 (12), 1519–1528. Available from: doi:10.3748/wjg.v17.i12.1519.

Cao, S.X., Dhahbi, J.M., Mote, P.L. & Spindler, S.R. (2001) Genomic profiling of short- and long-term caloric restriction effects in the liver of aging mice. *Proceedings of the National Academy of Sciences of the United States of America*. [Online] 98 (19), 10630–10635. Available from: doi:10.1073/pnas.191313598.

Cappelli, A.P., Zoppi, C.C., Barbosa-Sampaio, H.C., Costa, J.M., et al. (2014) Taurine-induced insulin signalling improvement of obese malnourished mice is associated with redox balance and protein phosphatases activity modulation. *Liver International*. [Online] 34 (5), 771–783. Available from: doi:10.1111/liv.12291.

De Carvalho, F.G., Galan, B.S.M., Santos, P.C., Pritchett, K., et al. (2017) Taurine: A potential ergogenic aid for preventing muscle damage and protein catabolism and decreasing oxidative stress produced by endurance exercise. *Frontiers in Physiology*. [Online] 8 (SEP). Available from: doi:10.3389/fphys.2017.00710.

de Castro, N.M., Yaqoob, P., de la Fuente, M., Baeza, I., et al. (2013) Premature impairment of methylation pathway and cardiac metabolic dysfunction in fa/fa obese Zucker rats. *J Proteome Res*. [Online] 12, 1935–1945. Available from: doi:10.1021/pr400025y.

Catalano, K.J., Stefanovski, D. & Bergman, R.N. (2010) Critical role of the mesenteric depot versus other intra-abdominal adipose depots in the development of insulin resistance in young rats. *Diabetes*. [Online] 59 (6), 1416–1423. Available from: doi:10.2337/db08-0675.

Chen, Y., Palm, F., Lesch, K.P., Gerlach, M., et al. (2011) 5-hydroxyindolacetic acid (5-HIAA), a main metabolite of serotonin, is responsible for complete Freund's adjuvant-induced thermal hyperalgesia in mice. *Molecular Pain*. [Online] 7. Available from: doi:10.1186/1744-8069-7-21.

Cloarec, O., Dumas, M.E., Craig, A., Barton, R.H., et al. (2005) Statistical total correlation spectroscopy: an exploratory approach for latent biomarker identification from metabolic 1H NMR data sets. *Anal Chem*. [Online] 77, 1282–1289. Available from: doi:10.1021/ac048630x.

Coburn, S.P., Reynolds, R.D., Mahuren, J.D., Schaltenbrand, W.E., et al. (2002) Elevated plasma 4-pyridoxic acid in renal insufficiency. *American Journal of Clinical Nutrition*. 75 (1), 57–64.

Codoñer-Franch, P., Tavaŕez-Alonso, S., Murria-Estal, R., Herrera-Martiń, G., et al. (2011) Polyamines are increased in obese children and are related to markers of oxidative/nitrosative stress and angiogenesis. *Journal of Clinical Endocrinology and Metabolism*. [Online] 96 (9), 2821–2825. Available from: doi:10.1210/jc.2011-0531.

Crawford, P.A., Crowley, J.R., Sambandam, N., Muegge, B.D., et al. (2009) Regulation of myocardial ketone body metabolism by the gut microbiota during nutrient deprivation. *Proceedings of the National Academy of Sciences*. [Online] 106 (27), 11276–11281. Available from: doi:10.1073/pnas.0902366106.

Cummins, T.D., Holden, C.R., Sansbury, B.E., Gibb, A.A., et al. (2014) Metabolic remodeling of white adipose tissue in obesity. *AJP: Endocrinology and Metabolism*. [Online] 307 (3), E262–E277. Available from: doi:10.1152/ajpendo.00271.2013.

Dale, J.W., Hollingworth, G.J. & McKenna, J.M. (2011) Developments and Advances in Gastrointestinal Prokinetic Agents. *Annual Reports in Medicinal Chemistry*. [Online] 46, 135–154. Available from: doi:10.1016/B978-0-12-386009-5.00018-7.

Dao, M.C., Everard, A., Aron-Wisnewsky, J., Sokolovska, N., et al. (2016) Akkermansia muciniphila and improved metabolic health during a dietary intervention in obesity: Relationship with gut microbiome richness and ecology. *Gut*. [Online] 65 (3), 426–436. Available from: doi:10.1136/gutjnl-2014-308778.

Dashti, H.M., Mathew, T.C., Hussein, T., Asfar, S.K., et al. (2004) Long-term effects of a ketogenic diet in obese patients. *Exp Clin Cardiol*. [Online] 9, 200–205. Available from: http://www.ncbi.nlm.nih.gov/pubmed/19641727.

Davie, J.R. (2003) Inhibition of Histone Deacetylase Activity by Butyrate. *The Journal of Nutrition*. [Online] 133 (7), 2485S–2493S. Available from: doi:10.1093/jn/133.7.2485S.

Dawson, L.F., Donahue, E.H., Cartman, S.T., Barton, R.H., et al. (2011) The analysis of para-cresol production and tolerance in Clostridium difficile 027 and 012 strains. *BMC Microbiology*. [Online] 11. Available from: doi:10.1186/1471-2180-11-86.

Delaney, J., Neville, W.A., Swain, A., Miles, A., et al. (2004) Phenylacetylglycine, a putative biomarker of phospholipidosis: its origins and relevance to phospholipid accumulation using amiodarone treated rats as a model. *Biomarkers*. [Online] 9, 271–290. Available from: doi:10.1080/13547500400018570.

Delzenne, N.M. & Cani, P.D. (2011) Interaction Between Obesity and the Gut Microbiota: Relevance in Nutrition. *Annual Review of Nutrition*. [Online] 31 (1), 15–31. Available from: doi:10.1146/annurev-nutr-072610-145146.

Demigne, C., Morand, C., Levrat, M.A., Besson, C., et al. (1995) Effect of propionate on fatty acid and cholesterol synthesis and on acetate metabolism in isolated rat hepatocytes. *Br J Nutr*. [Online] 74, 209–219. Available from: http://www.ncbi.nlm.nih.gov/pubmed/7547838.

Derogar, M., Hull, M.A., Kant, P., Östlund, M., et al. (2013) Increased risk of colorectal cancer after obesity surgery. *Annals of Surgery*. [Online] 258 (6), 983–988. Available from: doi:10.1097/SLA.0b013e318288463a.

Diaz, E., Ferrandez, A., Prieto, M.A. & Garcia, J.L. (2001) Biodegradation of Aromatic Compounds by Escherichia coli. *Microbiology and Molecular Biology Reviews*. [Online] 65 (4), 523–569. Available from: doi:10.1128/MMBR.65.4.523-569.2001.

Dinan, T.G. & Cryan, J.F. (2017) The Microbiome-Gut-Brain Axis in Health and Disease. *Gastroenterology Clinics of North America*. [Online]. 46 (1) pp.77–89. Available from: doi:10.1016/j.gtc.2016.09.007.

Dona, A.C., Jimenez, B., Schafer, H., Humpfer, E., et al. (2014) Precision high-throughput proton NMR spectroscopy of human urine, serum, and plasma for large-scale metabolic phenotyping. *Anal Chem*. [Online] 86, 9887–9894. Available from: doi:10.1021/ac5025039.

Dong, L.H. & Coquelet, C. (1980) Cysteine derivatives. *Fr. Demande*. (FR2430945A2), 12 pp. Addn. to Fr. Demande 2,266,502.

Dumas, M.E., Barton, R.H., Toye, A., Cloarec, O., et al. (2006) Metabolic profiling reveals a contribution of gut microbiota to fatty liver phenotype in insulin-resistant mice. *Proc Natl Acad Sci U S A*. [Online] 103, 12511–12516. Available from: doi:10.1073/pnas.0601056103.

Eckburg, P., Bik, E., Bernstein, C., Purdom, E., et al. (2005) Diversity of the human

intestinal microbial flora. *Science*. [Online] 308 (5728), 1635. Available from: doi:10.1126/science.1110591.

Edgar, S.E., Hickman, M.A., Marsden, M.M., Morris, J.G., et al. (1994) Dietary cysteic acid serves as a precursor of taurine for cats. *The Journal of nutrition*. [Online] 124 (1), 103–109. Available from: http://www.ncbi.nlm.nih.gov/pubmed/8283286.

Egshatyan, L., Kashtanova, D., Popenko, A., Tkacheva, O., et al. (2016) Gut microbiota and diet in patients with different glucose tolerance. *Endocrine connections*. [Online] 5 (1), 1–9. Available from: doi:10.1530/EC-15-0094.

Everard, A., Lazarevic, V., Gaïa, N., Johansson, M., et al. (2014) Microbiome of prebiotic-treated mice reveals novel targets involved in host response during obesity. *ISME Journal*. [Online] 8 (10), 2116–2130. Available from: doi:10.1038/ismej.2014.45.

De Filippo, C., Cavalieri, D., Di Paola, M., Ramazzotti, M., et al. (2010) Impact of diet in shaping gut microbiota revealed by a comparative study in children from Europe and rural Africa. *Proceedings of the National Academy of Sciences of the United States of America*. [Online] 107 (33), 14691–14696. Available from: doi:10.1073/pnas.1005963107.

Fischbach, M.A. & Sonnenburg, J.L. (2011) Eating for two: How metabolism establishes interspecies interactions in the gut. *Cell Host and Microbe*. [Online]. 10 (4) pp.336–347. Available from: doi:10.1016/j.chom.2011.10.002.

Fontana, L., Meyer, T.E., Klein, S. & Holloszy, J.O. (2004) Long-term calorie restriction is highly effective in reducing the risk for atherosclerosis in humans. *Proceedings of the National Academy of Sciences of the United States of America*. [Online] 101 (17), 6659–6663. Available from: doi:10.1073/pnas.0308291101.

Foschi, C., Laghi, L., Parolin, C., Giordani, B., et al. (2017) Novel approaches for the taxonomic and metabolic characterization of lactobacilli: Integration of 16S rRNA gene sequencing with MALDI-TOF MS and 1H-NMR. *PLoS ONE*. [Online] 12 (2). Available from: doi:10.1371/journal.pone.0172483.

Foxall, P.J., Spraul, M., Farrant, R.D., Lindon, L.C., et al. (1993) 750 MHz 1H-NMR spectroscopy of human blood plasma. *J Pharm Biomed Anal*. [Online] 11, 267–276. Available from: http://www.ncbi.nlm.nih.gov/pubmed/8357863.

Francis, G., John, R. & Thomas, J. (1973) Biosynthetic pathway of desmosines in elastin. *The Biochemical journal*. [Online] 136 (1), 45–55. Available from: doi:10.1042/bj1360045.

Fujita, K., Kakuya, F. & Ito, S. (1993) Vitamin K1and K2status and faecal flora in breast fed and formula fed 1-month-old infants. *European Journal of Pediatrics*. [Online] 152 (10), 852–855. Available from: doi:10.1007/BF02073386.

Gomes, J.M.G., Costa, J.A. & Alfenas, R.C. (2015) Could the beneficial effects of dietary calcium on obesity and diabetes control be mediated by changes in intestinal microbiota and integrity? *British Journal of Nutrition*. [Online] 114 (11), 1756–1765. Available from: doi:10.1017/S0007114515003608.

Gong, Z.G., Hu, J., Wu, X. & Xu, Y.J. (2017) The Recent Developments in Sample Preparation for Mass Spectrometry-Based Metabolomics. *Critical Reviews in Analytical Chemistry*. [Online]. 47 (4) pp.325–331. Available from: doi:10.1080/10408347.2017.1289836.

Grundy, S.M. (2008) Metabolic syndrome pandemic. *Arteriosclerosis, Thrombosis, and Vascular Biology*. [Online]. 28 (4) pp.629–636. Available from: doi:10.1161/ATVBAHA.107.151092.

Hamady, M. & Knight, R. (2009) Microbial community profiling for human microbiome projects: Tools, techniques, and challenges. *Genome Res*. [Online] 19, 1141–1152. Available from: doi:10.1101/gr.085464.108.

Hambly, C., Mercer, J.G. & Speakman, J.R. (2007) Hunger Does Not Diminish Over Time in Mice Under Protracted Caloric Restriction. *Rejuvenation Research*. [Online] 10 (4), 533–542. Available from: doi:10.1089/rej.2007.0555.

Hamelin, M., Borot-Laloi, C., Friguet, B. & Bakala, H. (2003) Increased level of glycoxidation product Nε-(carboxymethyl)lysine in rat serum and urine proteins with aging: Link with glycoxidative damage accumulation in kidney. *Archives of Biochemistry and Biophysics*. [Online] 411 (2), 215–222. Available from: doi:10.1016/S0003-9861(02)00735-X.

Hara, E. (2015) Relationship between Obesity, Gut Microbiome and Hepatocellular Carcinoma Development. *Digestive diseases (Basel, Switzerland)*. [Online] 33 (3), 346–350. Available from: doi:10.1159/000371679.

Haymond, M.W. & Miles, J.M. (1982) Branched chain amino acids as a major source of alanine nitrogen in man. *Diabetes*. [Online] 31, 86–89. Available from: http://www.ncbi.nlm.nih.gov/pubmed/7152124.

Henle, T., Zehetner, G. & Klostermeyer, H. (1995) Fast and sensitive determination of furosine. *Z Lebensm Unters Forsch*. [Online] 200, 235–237. Available from: doi:10.1017/CBO9781107415324.004.

Hoffmann, E. De & Stroobant, V. (2007) *Mass Spectrometry Principles and Applications*. [Online]. Available from: doi:10.1002/9783527654703.ch11.

Holmes, E., Li, J. V, Marchesi, J.R. & Nicholson, J.K. (2012) Gut microbiota composition and activity in relation to host metabolic phenotype and disease risk. *Cell Metab*. [Online] 16, 559–564. Available from: doi:10.1016/j.cmet.2012.10.007.

Hong, S., Moreno-Navarrete, J.M., Wei, X., Kikukawa, Y., et al. (2015) Nicotinamide N-methyltransferase regulates hepatic nutrient metabolism through Sirt1 protein stabilization. *Nat Med*. [Online] 21, 887–894. Available from: doi:10.1038/nm.3882.

Hu, J.M., Rho, J.Y., Suzuki, M., Nishihara, M., et al. (2000) Effect of taurine in rat milk on the growth of offspring. *The Journal of veterinary medical science / the Japanese Society of Veterinary Science*. [Online] 62 (7), 693–698. Available from: doi:10.1292/jvms.62.693.

Huang, C., Guo, Y. & Yuan, J. (2014) Dietary taurine impairs intestinal growth and mucosal structure of broiler chickens by increasing toxic bile acid concentrations in the intestine. *Poultry Science*. [Online] 93 (6), 1475–1483. Available from: doi:10.3382/ps.2013-03533.

Hughes, R., Magee, E. a & Bingham, S. (2000) Protein degradation in the large intestine: relevance to colorectal cancer. *Current issues in intestinal microbiology*. 1, 51–58.

Huxtable, R. (1992) Pysiological Actions of Taurine. *Physiological reviews*. 72 (1), 101–163.

Ishii, I., Ikeguchi, Y., Mano, H., Wada, M., et al. (2012) Polyamine metabolism is involved

in adipogenesis of 3T3-L1 cells. *Amino Acids*. [Online] 42 (2–3), 619–626. Available from: doi:10.1007/s00726-011-1037-5.

Ito, T., Pastukh, V., Solodushko, V., Azuma, J., et al. (2009) Effect of taurine on protein kinase C isoforms: Role in Taurine's actions? In: *Advances in Experimental Medicine and Biology*. [Online]. 2009 pp. 3–11. Available from: doi:10.1007/978-0-387-75681-3_1.

Ivanova, S., Batliwalla, F., Mocco, J., Kiss, S., et al. (2002) Neuroprotection in cerebral ischemia by neutralization of 3-aminopropanal. *Proceedings of the National Academy of Sciences of the United States of America*. [Online] 99 (8), 5579–5584. Available from: doi:10.1073/pnas.082609299.

Janda, J.M. & Abbott, S.L. (2007) 16S rRNA gene sequencing for bacterial identification in the diagnostic laboratory: Pluses, perils, and pitfalls. *Journal of Clinical Microbiology*. [Online]. 45 (9) pp.2761–2764. Available from: doi:10.1128/JCM.01228-07.

Jandhyala, S.M., Talukdar, R., Subramanyam, C., Vuyyuru, H., et al. (2015) Role of the normal gut microbiota. *World Journal of Gastroenterology*. [Online] 21 (29), 8836–8847. Available from: doi:10.3748/wjg.v21.i29.8787.

Jiao, N., Baker, S.S., Nugent, C.A., Tsompana, M., et al. (2017) High-fat diet increases clostridium clusters XIVa in obese rodents. *FASEB Journal*. [Online] 31 (1 Supplement 1). Available from: http://www.fasebj.org/content/31/1_Supplement/965.9.abstract?sid=37c1a053-7fcc-4eb4-bf59-ebdca670f7e0%0Ahttp://ovidsp.ovid.com/ovidweb.cgi?T=JS&PAGE=reference&D=emex&NEWS=N&AN=616959398.

Karlsson, K.R., Ko, R. & Blomstrand, E. (2006) Branched-Chain Amino Acids : Metabolism , Physiological Function , and Application Branched-Chain Amino Acids Activate Key Enzymes in Protein Synthesis. *The Journal of Nutrition*. 136 (15), 269–273.

Khoursheed, M.A., Al-Bader, I.A., Al-Asfar, F.S., Mohammad, A.I., et al. (2011) Revision of failed bariatric procedures to Roux-en-Y gastric bypass (RYGB). *Obesity Surgery*. [Online] 21 (8), 1157–1160. Available from: doi:10.1007/s11695-010-0229-5.

Kimura, I., Inoue, D., Hirano, K. & Tsujimoto, G. (2014) The SCFA receptor GPR43 and energy metabolism. *Frontiers in Endocrinology*. [Online]. 5 (JUN). Available from: doi:10.3389/fendo.2014.00085.

Kindberg, C., Suttie, J.W., Uchida, K., Hirauchi, K., et al. (1987) Menaquinone production and utilization in germ-free rats after inoculation with specific organisms. *The Journal of nutrition*. 117 (6), 1032–1035.

King, G.M. (1984) Metabolism of trimethylamine, choline, and glycine betaine by sulfate-reducing and methanogenic bacteria in marine sediments. *Appl Environ Microbiol*. [Online] 48, 719–725. Available from: http://www.ncbi.nlm.nih.gov/pubmed/16346640.

Klein, S., Mittendorfer, B., Eagon, J.C., Patterson, B., et al. (2006) Gastric Bypass Surgery Improves Metabolic and Hepatic Abnormalities Associated With Nonalcoholic Fatty Liver Disease. *Gastroenterology*. [Online] 130 (6), 1564–1572. Available from: doi:10.1053/j.gastro.2006.01.042.

Koeth, R.A., Levison, B.S., Culley, M.K., Buffa, J.A., et al. (2014) γ-butyrobetaine is a proatherogenic intermediate in gut microbial metabolism of L-carnitine to TMAO. *Cell Metabolism*. [Online] 20 (5), 799–812. Available from:

doi:10.1016/j.cmet.2014.10.006.

Kothari, S.N., DeMaria, E.J., Sugerman, H.J., Kellum, J.M., et al. (2002) LAP-BAND failures: Conversion to gastric bypass and their preliminary outcomes. *Surgery*. [Online] 131 (6), 625–629. Available from: doi:10.1067/msy.2002.124879.

Kraus, D., Yang, Q., Kong, D., Banks, A.S., et al. (2014) Nicotinamide N-methyltransferase knockdown protects against diet-induced obesity. *Nature*. [Online] 508, 258–262. Available from: doi:10.1038/nature13198.

Kremen, A., Linner, J. & Nelson, C. (1954) An experimental evaluation of the nutritional importance of proximal and distal small intestine. *Annals of Surgery*. 140 (3), 439–447.

Kuhla, A., Hahn, S., Butschkau, A., Lange, S., et al. (2014) Lifelong caloric restriction reprograms hepatic fat metabolism in mice. *Journals of Gerontology - Series A Biological Sciences and Medical Sciences*. [Online] 69 (8), 915–922. Available from: doi:10.1093/gerona/glt160.

Kurihara, S., Kato, K., Asada, K., Kumagai, H., et al. (2010) A putrescine-inducible pathway comprising PuuE-YneI in which γ-aminobutyrate is degraded into succinate in Escherichia coli K-12. *Journal of Bacteriology*. [Online] 192 (18), 4582–4591. Available from: doi:10.1128/JB.00308-10.

Lam, Y.Y., Ha, C.W., Campbell, C.R., Mitchell, A.J., et al. (2012) Increased gut permeability and microbiota change associate with mesenteric fat inflammation and metabolic dysfunction in diet-induced obese mice. *PLoS One*. [Online] 7, e34233. Available from: doi:10.1371/journal.pone.0034233.

Lanyon, R.I. & Maxwell, B.M. (2007) Predictors of outcome after gastric bypass surgery. *Obesity Surgery*. [Online] 17 (3), 321–328. Available from: doi:10.1007/s11695-007-9059-5.

LeBlanc, J.G., Milani, C., de Giori, G.S., Sesma, F., et al. (2013) Bacteria as vitamin suppliers to their host: A gut microbiota perspective. *Current Opinion in Biotechnology*. [Online]. 24 (2) pp.160–168. Available from: doi:10.1016/j.copbio.2012.08.005.

Lees, H., Swann, J., Poucher, S.M., Nicholson, J.K., et al. (2014) Age and microenvironment outweigh genetic influence on the Zucker rat microbiome. *PLoS One*. [Online] 9, e100916. Available from: doi:10.1371/journal.pone.0100916.

Lees, H.J., Swann, J.R., Wilson, I.D., Nicholson, J.K., et al. (2013) Hippurate: The natural history of a mammalian-microbial cometabolite. *Journal of Proteome Research*. [Online] 12 (4), 1527–1546. Available from: doi:10.1021/pr300900b.

Lenz, E.M. & Wilson, I.D. (2007) Analytical strategies in metabonomics. *Journal of Proteome Research*. [Online]. 6 (2) pp.443–458. Available from: doi:10.1021/pr0605217.

Ley, R.E. (2010) Obesity and the human microbiome. *Current Opinion in Gastroenterology*. [Online]. 26 (1) pp.5–11. Available from: doi:10.1097/MOG.0b013e328333d751.

Ley, R.E., Backhed, F., Turnbaugh, P., Lozupone, C.A., et al. (2005) Obesity alters gut microbial ecology. *Proc Natl Acad Sci U S A*. [Online] 102, 11070–11075. Available from: doi:10.1073/pnas.0504978102.

Ley, R.E., Turnbaugh, P.J., Klein, S. & Gordon, J.I. (2006) Microbial ecology: human gut microbes associated with obesity. *Nature*. [Online] 444, 1022–1023. Available from: doi:10.1038/4441022a.

Li, G. & Young, K.D. (2013) Indole production by the tryptophanase TnaA in escherichia coli is determined by the amount of exogenous tryptophan. *Microbiology (United Kingdom)*. [Online] 159 (2), 402–410. Available from: doi:10.1099/mic.0.064139-0.

Li, J. V., Ashrafian, H., Bueter, M., Kinross, J., et al. (2011a) Metabolic surgery profoundly influences gut microbial - Host metabolic cross-talk. *Gut*. [Online] 60 (9), 1214–1223. Available from: doi:10.1136/gut.2010.234708.

Li, J. V, Ashrafian, H., Bueter, M., Kinross, J., et al. (2011b) Metabolic surgery profoundly influences gut microbial-host metabolic cross-talk. *Gut*. [Online] 60, 1214–1223. Available from: doi:10.1136/gut.2010.234708.

Li, J. V, Ashrafian, H., Bueter, M., Kinross, J., et al. (2011c) Metabolic surgery profoundly influences gut microbial-host metabolic cross-talk. *Gut*. [Online] 60, 1214–1223. Available from: doi:10.1136/gut.2010.234708.

Li, J. V, Reshat, R., Wu, Q., Ashrafian, H., et al. (2011d) Experimental bariatric surgery in rats generates a cytotoxic chemical environment in the gut contents. *Front Microbiol*. [Online] 2, 183. Available from: doi:10.3389/fmicb.2011.00183.

Li, W., Yuan, X.-M., Ivanova, S., Tracey, K.J., et al. (2003) 3-Aminopropanal, formed during cerebral ischaemia, is a potent lysosomotropic neurotoxin. *Biochem J*. [Online] 371 (Pt 2), 429–436. Available from: doi:10.1042/BJ20021520.

Liou, A.P., Paziuk, M., Luevano, J.M., Machineni, S., et al. (2013a) Conserved shifts in the gut microbiota due to gastric bypass reduce host weight and adiposity. *Science Translational Medicine*. [Online] 5 (178). Available from: doi:10.1126/scitranslmed.3005687.

Liou, A.P., Paziuk, M., Luevano Jr., J.M., Machineni, S., et al. (2013b) Conserved shifts in the gut microbiota due to gastric bypass reduce host weight and adiposity. *Sci Transl Med*. [Online] 5, 178ra41. Available from: doi:10.1126/scitranslmed.3005687.

Llado, I., Palou, A. & Pons, A. (1998) Hepatic glycogen and lactate handling in dietary obese rats. *Ann Nutr Metab*. [Online] 42, 181–188. Available from: http://www.ncbi.nlm.nih.gov/pubmed/9657462.

Lozupone, C., Hamady, M. & Knight, R. (2006) UniFrac--an online tool for comparing microbial community diversity in a phylogenetic context. *BMC Bioinformatics*. [Online] 7, 371. Available from: doi:10.1186/1471-2105-7-371.

Lyra, A., Lahtinen, S., Tiihonen, K. & Ouwehand, A.C. (2010) Intestinal microbiota and overweight. *Benef Microbes*. [Online] 1, 407–421. Available from: doi:10.3920/BM2010.0030.

MacLean, L.D., Rhode, B.M. & Nohr, C.W. (2000) Late outcome of isolated gastric bypass. *Annals of Surgery*. [Online] 231 (4), 524–528. Available from: doi:10.1097/00000658-200004000-00011.

MacLean, L.D., Rhode, B.M., Sampalis, J. & Forse, R.A. (1993) Results of the surgical treatment of obesity. *American journal of surgery*. 165 (1), 155-60-2.

Maggard, M.A., Shugarman, L.R., Suttorp, M., Maglione, M., et al. (2005) Meta-analysis: Surgical treatment of obesity. *Annals of Internal Medicine*. [Online]. 142 (7) pp.547–

559. Available from: doi:10.7326/0003-4819-142-7-200504050-00013.

Magkos, F., Bradley, D., Schweitzer, G.G., Finck, B.N., et al. (2013) Effect of roux-en-y gastric bypass and laparoscopic adjustable gastric banding on branched-chain amino acid metabolism. *Diabetes*. [Online] 62 (8), 2757–2761. Available from: doi:10.2337/db13-0185/-/DC1.

Malhotra, A. (2002) rRNA Structure. *eLS*.

Marihart, C.L., Brunt, A.R. & Geraci, A.A. (2014) Older adults fighting obesity with bariatric surgery: Benefits, side effects, and outcomes. *SAGE Open Medicine*. [Online] 2, 205031211453091. Available from: doi:10.1177/2050312114530917.

Markley, J.L., Brüschweiler, R., Edison, A.S., Eghbalnia, H.R., et al. (2017) The future of NMR-based metabolomics. *Current Opinion in Biotechnology*. [Online]. 43 pp.34–40. Available from: doi:10.1016/j.copbio.2016.08.001.

Mason, E.E. & Ito, C. (1969) Gastric bypass. *Annals of surgery*. [Online] 170 (3), 329–339. Available from: doi:10.1097/00000658-196909010-00003.

Masoro, E.J. (2005) Overview of caloric restriction and ageing. *Mechanisms of Ageing and Development*. [Online]. 126 (9 SPEC. ISS.) pp.913–922. Available from: doi:10.1016/j.mad.2005.03.012.

Matthews, D.E. (2007) An overview of phenylalanine and tyrosine kinetics in humans. *The Journal of nutrition*. [Online] 137 (6 Suppl 1), 1549S–1555S; discussion 1573S–1575S. Available from: doi:10.1016/j.bbi.2008.05.010.

McCay, C.M., Crowell, M.F. & Maynard, L.A. (1935) The effect of retarded growth upon the length of life span and upon the ultimate body size. *The Journal of Nutrition*. [Online] 5 (3), 63–79. DOI: Available from: doi:2520283.

McNeil, N.I. (1984) The contribution of the large intestine to energy supplies in man. *American Journal of Clinical Nutrition*. [Online] 39 (2), 338–342. Available from: doi:10.1080/19397030902947041.

Minamida, K., Ota, K., Nishimukai, M., Tanaka, M., et al. (2008) Asaccharobacter celatus gen. nov., sp. nov., isolated from rat caecum. *International Journal of Systematic and Evolutionary Microbiology*. [Online] 58 (5), 1238–1240. Available from: doi:10.1099/ijs.0.64894-0.

Minor, R.K., Chang, J.W. & de Cabo, R. (2009) Hungry for life: How the arcuate nucleus and neuropeptide Y may play a critical role in mediating the benefits of calorie restriction. *Molecular and Cellular Endocrinology*. [Online] 299 (1), 79–88. Available from: doi:10.1016/j.mce.2008.10.044.

Mitchell, G.A., Kassovska-Bratinova, S., Boukaftane, Y., Robert, M.F., et al. (1995) Medical aspects of ketone body metabolism. *Clin Invest Med*. [Online] 18, 193–216. Available from: http://www.ncbi.nlm.nih.gov/pubmed/7554586.

Monte, S. V, Caruana, J.A., Ghanim, H., Sia, C.L., et al. (2012) Reduction in endotoxemia, oxidative and inflammatory stress, and insulin resistance after Roux-en-Y gastric bypass surgery in patients with morbid obesity and type 2 diabetes mellitus. *Surgery*. [Online] 151, 587–593. Available from: doi:10.1016/j.surg.2011.09.038.

Morton, G.J., Meek, T.H. & Schwartz, M.W. (2014) Neurobiology of food intake in health and disease. *Nat Rev Neurosci*. [Online] 15, 367–378. Available from: doi:10.1038/nrn3745.

Mulat, D.G. & Feilberg, A. (2015) GC/MS method for determining carbon isotope enrichment and concentration of underivatized short-chain fatty acids by direct aqueous solution injection of biogas digester samples. *Talanta*. [Online] 143, 56–63. Available from: doi:10.1016/j.talanta.2015.04.065.

Murakami, S. (2015) Role of taurine in the pathogenesis of obesity. *Molecular Nutrition and Food Research*. [Online]. 59 (7) pp.1353–1363. Available from: doi:10.1002/mnfr.201500067.

Mutch, C.A., Funatsu, N., Monuki, E.S. & Chenn, A. (2009) Beta-catenin signaling levels in progenitors influence the laminar cell fates of projection neurons. *J Neurosci*. [Online] 29, 13710–13719. Available from: doi:10.1523/JNEUROSCI.3022-09.2009.

Myers, P.A. & Zatman, L.J. (1971) The metabolism of trimethylamine N-oxide by Bacillus PM6. *Biochem J*. [Online] 121, 10P. Available from: http://www.ncbi.nlm.nih.gov/pubmed/5116524.

Narath, S.H., Mautner, S.I., Svehlikova, E., Schultes, B., et al. (2016) An untargeted metabolomics approach to characterize short-term and long-term metabolic changes after bariatric surgery. *PLoS ONE*. [Online] 11 (9). Available from: doi:10.1371/journal.pone.0161425.

Nehlig, A. (2004) Brain uptake and metabolism of ketone bodies in animal models. *Prostaglandins Leukotrienes and Essential Fatty Acids*. [Online]. 70 (3) pp.265–275. Available from: doi:10.1016/j.plefa.2003.07.006.

Newgard, C.B., An, J., Bain, J.R., Muehlbauer, M.J., et al. (2009) A branched-chain amino acid-related metabolic signature that differentiates obese and lean humans and contributes to insulin resistance. *Cell Metab*. [Online] 9, 311–326. Available from: doi:10.1016/j.cmet.2009.02.002.

Nicholson, J.K., Holmes, E., Kinross, J., Burcelin, R., et al. (2012) Host-gut microbiota metabolic interactions. *Science*. [Online] 336, 1262–1267. Available from: doi:10.1126/science.1223813.

Nicholson, J.K. & Lindon, J.C. (2008) Systems biology: Metabonomics. *Nature*. [Online]. 455 (7216) pp.1054–1056. Available from: doi:10.1038/4551054a.

Nicholson, J.K., Lindon, J.C. & Holmes, E. (1999) 'Metabonomics': Understanding the metabolic responses of living systems to pathophysiological stimuli via multivariate statistical analysis of biological NMR spectroscopic data. *Xenobiotica*. [Online]. 29 (11) pp.1181–1189. Available from: doi:10.1080/004982599238047.

Nicholson, J.K., O'Flynn, M.P., Sadler, P.J., Macleod, A.F., et al. (1984) Proton-nuclear-magnetic-resonance studies of serum, plasma and urine from fasting normal and diabetic subjects. *The Biochemical journal*. [Online] 217 (2), 365–375. Available from: doi:10.1042/bj2170365.

Nzakizwanayo, J., Dedi, C., Standen, G., Macfarlane, W.M., et al. (2015) Escherichia coli Nissle 1917 enhances bioavailability of serotonin in gut tissues through modulation of synthesis and clearance. *Scientific Reports*. [Online] 5. Available from: doi:10.1038/srep17324.

O'Brien, P. et al (2003) Lap-band: outcomes and results. *Journal of laparoendoscopic & advanced surgical techniques*. [Online] 13 (4), 265–270. Available from: doi:10.1089/109264203322333593.

O'Mahony, S.M., Clarke, G., Borre, Y.E., Dinan, T.G., et al. (2015) Serotonin, tryptophan metabolism and the brain-gut-microbiome axis. *Behavioural Brain Research*. [Online]. 277 pp.32–48. Available from: doi:10.1016/j.bbr.2014.07.027.

Oana, F., Takeda, H., Hayakawa, K., Matsuzawa, A., et al. (2005) Physiological difference between obese (fa/fa) Zucker rats and lean Zucker rats concerning adiponectin. *Metabolism: Clinical and Experimental*. [Online] 54 (8), 995–1001. Available from: doi:10.1016/j.metabol.2005.02.016.

Okafor, P.N., Lien, C., Bairdain, S., Simonson, D.C., et al. (2015) Effect of vagotomy during Roux-en-Y gastric bypass surgery on weight loss outcomes. *Obesity Research and Clinical Practice*. [Online] 9 (3), 274–280. Available from: doi:10.1016/j.orcp.2014.09.005.

Osaka, T., Moriyama, E., Arai, S., Date, Y., et al. (2017) Meta-analysis of fecal microbiota and metabolites in experimental colitic mice during the inflammatory and healing phases. *Nutrients*. [Online] 9 (12). Available from: doi:10.3390/nu9121329.

Palau-Rodriguez, M., Tulipani, S., Queipo-Ortuï¿½o, M.I., Urpi-Sarda, M., et al. (2015) Metabolomic insights into the intricate gut microbial-host interaction in the development of obesity and type 2 diabetes. *Frontiers in Microbiology*. [Online]. 6 (OCT). Available from: doi:10.3389/fmicb.2015.01151.

Park, Y.K., Monaco, M.H. & Donovan, S.M. (1999) Enteral insulin-like growth factor-I augments intestinal disaccharidase activity in piglets receiving total parenteral nutrition. *Journal of Pediatric Gastroenterology and Nutrition*. [Online] 29 (2), 198–206. Available from: doi:10.1097/00005176-199908000-00018.

Peters, B.A., Hall, M.N., Liu, X., Neugut, Y.D., et al. (2014) Creatinine, arsenic metabolism, and renal function in an arsenic-exposed population in Bangladesh. *PLoS One*. [Online] 9, e113760. Available from: doi:10.1371/journal.pone.0113760.

Phypers and Pierce, J.M., B. (2006) Lactate Physiology in Health and Disease. *Oxford J*. 6, 128–132.

Poesen, R., Evenepoel, P., de Loor, H., Kuypers, D., et al. (2016) Metabolism, protein binding, and renal clearance of microbiota-derived p-cresol in patients with CKD. *Clinical Journal of the American Society of Nephrology*. [Online] 11 (7), 1136–1144. Available from: doi:10.2215/CJN.00160116.

Pories, W.J., Swanson, M.S., MacDonald, K.G., Long, S.B., et al. (1995) Who would have thought it? An operation proves to be the most effective therapy for adult-onset diabetes mellitus. In: *Annals of Surgery*. [Online]. 1995 pp. 339–352. Available from: doi:10.1097/00000658-199509000-00011.

Qiao, Y., Sun, J., Xie, Z., Shi, Y., et al. (2014) Propensity to high-fat diet-induced obesity in mice is associated with the indigenous opportunistic bacteria on the interior of Peyer's patches. *J Clin Biochem Nutr*. [Online] 55, 120–128. Available from: doi:10.3164/jcbn.14-38.

Qu, W., Yuan, X., Zhao, J., Zhang, Y., et al. (2017) Dietary advanced glycation end products modify gut microbial composition and partially increase colon permeability in rats. *Molecular Nutrition and Food Research*. [Online] 61 (10). Available from: doi:10.1002/mnfr.201700118.

Ramautar, R., Somsen, G.W. & de Jong, G.J. (2009) CE-MS in metabolomics. *Electrophoresis*. [Online]. 30 (1) pp.276–291. Available from:

doi:10.1002/elps.200800512.

Rapin, A., Pattaroni, C., Marsland, B.J. & Harris, N.L. (2017) Microbiota Analysis Using an Illumina MiSeq Platform to Sequence 16S rRNA Genes. In: *Current Protocols in Mouse Biology*. [Online]. pp. 100–129. Available from: doi:10.1002/cpmo.29.

Rath, S., Heidrich, B., Pieper, D.H. & Vital, M. (2017) Uncovering the trimethylamine-producing bacteria of the human gut microbiota. *Microbiome*. [Online] 5, 54. Available from: doi:10.1186/s40168-017-0271-9.

Reichardt, N., Duncan, S.H., Young, P., Belenguer, A., et al. (2014) Phylogenetic distribution of three pathways for propionate production within the human gut microbiota. *ISME J*. [Online] 8, 1323–1335. Available from: doi:10.1038/ismej.2014.14.

Remely, M., Aumueller, E., Jahn, D., Hippe, B., et al. (2014) Microbiota and epigenetic regulation of inflammatory mediators in type 2 diabetes and obesity. *Benef Microbes*. [Online] 5, 33–43. Available from: doi:10.3920/BM2013.006.

Ridlon, J.M., Kang, D.J. & Hylemon, P.B. (2006) Bile salt biotransformations by human intestinal bacteria. *J Lipid Res*. [Online] 47, 241–259. Available from: doi:10.1194/jlr.R500013-JLR200.

Riederer, M., Erwa, W., Zimmermann, R., Frank, S., et al. (2009) Adipose tissue as a source of nicotinamide N-methyltransferase and homocysteine. *Atherosclerosis*. [Online] 204, 412–417. Available from: doi:10.1016/j.atherosclerosis.2008.09.015.

Robillard, K.R., Bone, D.B.J. & Hammond, J.R. (2008) Hypoxanthine uptake and release by equilibrative nucleoside transporter 2 (ENT2) of rat microvascular endothelial cells. *Microvascular Research*. [Online] 75 (3), 351–357. Available from: doi:10.1016/j.mvr.2007.10.002.

RODWELL, V.W., VOLCANI, B.E., IKAWA, M. & SNELL, E.E. (1958) Bacterial oxidation of vitamin B6. I. Isopyridoxal and 5-pyridoxic acid. *The Journal of biological chemistry*. 233 (6), 1548–1554.

Ruiz, A., Cerdó, T., Jáuregui, R., Pieper, D.H., et al. (2017) One-year calorie restriction impacts gut microbial composition but not its metabolic performance in obese adolescents. *Environmental Microbiology*. [Online] 19 (4), 1536–1551. Available from: doi:10.1111/1462-2920.13713.

Saha, J.R., Butler, V.P., Neu, H.C. & Lindenbaum, J. (1983) Digoxin-inactivating bacteria: identification in human gut flora. *Science (New York, N.Y.)*. 220 (4594), 325–327.

Sanz, A., Caro, P. & Barja, G. (2004) Protein restriction without strong caloric restriction decreases mitochondrial oxygen radical production and oxidative DNA damage in rat liver. *Journal of Bioenergetics and Biomembranes*. [Online] 36 (6), 545–552. Available from: doi:10.1007/s10863-004-9001-7.

Saugstad, O.D. (1975) Hypoxanthine as a measurement of hypoxia. *Pediatric Research*. [Online] 9 (4), 158–161. Available from: doi:10.1203/00006450-197504000-00002.

Schaffer, S.W., Ju Jong, C., Kc, R. & Azuma, J. (2010) Physiological roles of taurine in heart and muscle. In: *Journal of Biomedical Science*. [Online]. 2010 p. Available from: doi:10.1186/1423-0127-17-S1-S2.

Schauer, P.R., Ikramuddin, S., Gourash, W., Ramanathan, R., et al. (2000) Outcomes after laparoscopic Roux-en-Y gastric bypass for morbid obesity. *Annals of surgery*.

[Online] 232 (4), 515–529. Available from: doi:10.1097/00000658-200010000-00007.

Schmidt, J.B., Pedersen, S.D., Gregersen, N.T., Vestergaard, L., et al. (2013) Effects of RYGB on energy expenditure, appetite and glycaemic control: a randomized controlled clinical trial. *International Journal of Obesity*. [Online] (August), 1–10. Available from: doi:10.1038/ijo.2015.162.

Selkrig, J., Wong, P., Zhang, X. & Pettersson, S. (2014) Metabolic tinkering by the gut microbiome. *Gut Microbes*. [Online] 5 (3), 369–380. Available from: doi:10.4161/gmic.28681.

Sender, R., Fuchs, S. & Milo, R. (2016) Revised Estimates for the Number of Human and Bacteria Cells in the Body. *PLoS Biology*. [Online] 14 (8). Available from: doi:10.1371/journal.pbio.1002533.

Ser, K.H., Lee, W.J., Lee, Y.C., Chen, J.C., et al. (2010) Experience in laparoscopic sleeve gastrectomy for morbidly obese Taiwanese: Staple-line reinforcement is important for preventing leakage. *Surgical Endoscopy and Other Interventional Techniques*. [Online] 24 (9), 2253–2259. Available from: doi:10.1007/s00464-010-0945-x.

Serkova, N.J., Jackman, M., Brown, J.L., Liu, T., et al. (2006) Metabolic profiling of livers and blood from obese Zucker rats. *J Hepatol*. [Online] 44, 956–962. Available from: doi:10.1016/j.jhep.2005.07.009.

Seyfried, F., Li, J. V, Miras, A.D., Cluny, N.L., et al. (2013) Urinary phenotyping indicates weight loss-independent metabolic effects of Roux-en-Y gastric bypass in mice. *J Proteome Res*. [Online] 12, 1245–1253. Available from: doi:10.1021/pr300909v.

Shah, N., Tang, H., Doak, T.G. & Ye, Y. (2011) Comparing bacterial communities inferred from 16S rRNA gene sequencing and shotgun metagenomics. *Pac Symp Biocomput*. [Online] 165–176. Available from: doi:10.1142/9789814335058.

Shaibe, E., Metzer, E. & Halpern, Y.S. (1985) Metabolic pathway for the utilization of L-arginine, L-ornithine, agmatine, and putrescine as nitrogen sources in Escherichia coli K-12. *Journal of Bacteriology*. 163 (3), 933–937.

She, P., Van Horn, C., Reid, T., Hutson, S.M., et al. (2007) Obesity-related elevations in plasma leucine are associated with alterations in enzymes involved in branched-chain amino acid metabolism. *Am J Physiol Endocrinol Metab*. [Online] 293, E1552-63. Available from: doi:10.1152/ajpendo.00134.2007.

Shimizu, H., Hirose, Y., Goto, S., Nishijima, F., et al. (2012) Indoxyl sulfate enhances angiotensin II signaling through upregulation of epidermal growth factor receptor expression in vascular smooth muscle cells. *Life Sciences*. [Online] 91 (5–6), 172–177. Available from: doi:10.1016/j.lfs.2012.06.033.

Shin, N.-R., Lee, J.-C., Lee, H.-Y., Kim, M.-S., et al. (2014) An increase in the *Akkermansia* spp. population induced by metformin treatment improves glucose homeostasis in diet-induced obese mice. *Gut*. [Online] 63 (5), 727–735. Available from: doi:10.1136/gutjnl-2012-303839.

Sjöström, L., Narbro, K., Sjöström, C.D., Karason, K., et al. (2007) Effects of Bariatric Surgery on Mortality in Swedish Obese Subjects. *New England Journal of Medicine*. [Online] 357 (8), 741–752. Available from: doi:10.1056/NEJMoa066254.

Smith, E.A. & Macfarlane, G.T. (1996) Enumeration of human colonic bacteria producing

phenolic and indolic compounds: effects of pH, carbohydrate availability and retention time on dissimilatory aromatic amino acid metabolism. *Journal of Applied Bacteriology*. [Online] 81 (3), 288–302. Available from: doi:10.1111/j.1365-2672.1996.tb04331.x.

Son, M., Kim, H.K., Kim, W.B., Yang, J., et al. (1996) Protective effect of taurine on indomethacin-induced gastric mucosal injury. *Archives of Pharmacal Research*. [Online] 19 (2), 85–90. Available from: http://www.scopus.com/inward/record.url?eid=2-s2.0-0030438554&partnerID=40&md5=e4d7fe86c6dd6223f5e0433d8fa3b923.

Speakman, J.R. & Mitchell, S.E. (2011) Caloric restriction. *Molecular Aspects of Medicine*. [Online]. 32 (3) pp.159–221. Available from: doi:10.1016/j.mam.2011.07.001.

Suter, M., Donadini, A., Romy, S., Demartines, N., et al. (2011) Laparoscopic Roux-En-Y gastric bypass: Significant long-term weight loss, improvement of obesity-related comorbidities and quality of life. *Annals of Surgery*. [Online] 254 (2), 267–273. Available from: doi:10.1097/SLA.0b013e3182263b66.

Tang, Y., Chen, Y., Jiang, H., Robbins, G.T., et al. (2011) G-protein-coupled receptor for short-chain fatty acids suppresses colon cancer. *International Journal of Cancer*. [Online] 128 (4), 847–856. Available from: doi:10.1002/ijc.25638.

Teufel, R., Mascaraque, V., Ismail, W., Voss, M., et al. (2010) Bacterial phenylalanine and phenylacetate catabolic pathway revealed. *Proceedings of the National Academy of Sciences*. [Online] 107 (32), 14390–14395. Available from: doi:10.1073/pnas.1005399107.

Trammell, S.A. & Brenner, C. (2015) NNMT: A Bad Actor in Fat Makes Good in Liver. *Cell Metab*. [Online] 22, 200–201. Available from: doi:10.1016/j.cmet.2015.07.017.

Trelles, N. & Gagner, M. (2007) Sleeve Gastrectomy. *Operative Techniques in General Surgery*. [Online] 9 (3), 123–131. Available from: doi:10.1053/j.optechgensurg.2007.09.001.

Trygg, J. & Wold, S. (2002) Orthogonal projections to latent structures (O-PLS). *Journal of Chemometrics*. [Online] 16 (3), 119–128. Available from: doi:10.1002/cem.695.

Tsuchioka, T., Fujiwara, T. & Sunagawa, M. (2006) Effects of glutamic acid and taurine on total parenteral nutrition. *Journal of Pediatric Surgery*. [Online] 41 (9), 1566–1572. Available from: doi:10.1016/j.jpedsurg.2006.05.021.

Tsuchiya, Y. & Kawamata, K. (2017) Effects of taurine on plasma glucose concentration and active glucose transport in the small intestine. *Animal Science Journal*. [Online] 88 (11), 1763–1767. Available from: doi:10.1111/asj.12829.

Turkenkopf, I.J., Olsen, J.L., Moray, L., Greenwood, M.R., et al. (1980) Hepatic lipogenesis in the preobese Zucker rat. *Proc Soc Exp Biol Med*. [Online] 164, 530–533. Available from: http://www.ncbi.nlm.nih.gov/pubmed/6106202.

Turnbaugh, P.J., Ley, R.E., Mahowald, M.A., Magrini, V., et al. (2006) An obesity-associated gut microbiome with increased capacity for energy harvest. *Nature*. [Online] 444, 1027–1031. Available from: doi:10.1038/nature05414.

Ueno, H. (2000) Enzymatic and structural aspects on glutamate decarboxylase. *Journal of Molecular Catalysis - B Enzymatic*. [Online]. 10 (1–3) pp.67–79. Available from: doi:10.1016/S1381-1177(00)00114-4.

Unger, R.H. (1997) How obesity causes diabetes in Zucker diabetic fatty rats. *Trends in Endocrinology and Metabolism*. [Online]. 8 (7) pp.276–282. Available from: doi:10.1016/S1043-2760(97)00094-5.

Vella, M. & Galloway, D.J. (2003) Laparoscopic adjustable gastric banding for severe obesity. *Obesity Surgery*. [Online]. 13 (4) pp.642–648. Available from: doi:10.1381/096089203322190899.

Verbrugghe, A., Hesta, M., Daminet, S., Polis, I., et al. (2012) Propionate absorbed from the colon acts as gluconeogenic substrate in a strict carnivore, the domestic cat (Felis catus). *Journal of Animal Physiology and Animal Nutrition*. [Online] 96 (6), 1054–1064. Available from: doi:10.1111/j.1439-0396.2011.01220.x.

Vernia, P., Caprilli, R., Latella, G., Barbetti, F., et al. (1988) Fecal lactate and ulcerative colitis. *Gastroenterology*. [Online] 95, 1564–1568. Available from: http://www.ncbi.nlm.nih.gov/pubmed/3181680.

Vinaixa, M., Samino, S., Saez, I., Duran, J., et al. (2012) A guideline to univariate statistical analysis for LC/MS-based untargeted metabolomics-derived data. *Metabolites*. [Online]. 2 (4) pp.775–795. Available from: doi:10.3390/metabo2040775.

Waldram, A., Holmes, E., Wang, Y., Rantalainen, M., et al. (2009) Top-down systems biology modeling of host metabotype-microbiome associations in obese rodents. *J Proteome Res*. [Online] 8, 2361–2375. Available from: doi:10.1021/pr8009885.

Wang, C.-H., Zhao, T.-X., Li, M., Zhang, C., et al. (2016) Characterization of a novel Acinetobacter baumannii xanthine dehydrogenase expressed in Escherichia coli. *Biotechnology letters*. [Online] 38 (2), 337–344. Available from: doi:10.1007/s10529-015-1986-y.

Want, E.J., Masson, P., Michopoulos, F., Wilson, I.D., et al. (2013) Global metabolic profiling of animal and human tissues via UPLC-MS. *Nature Protocols*. [Online] 8 (1), 17–32. Available from: doi:10.1038/nprot.2012.135.

Wells, I.C. & Remy, C.N. (1965) Choline metabolism in normal and choline-deficient rats of different ages. *Arch Biochem Biophys*. [Online] 112, 201–206. Available from: http://www.ncbi.nlm.nih.gov/pubmed/5865117.

Wijekoon, E.P., Skinner, C., Brosnan, M.E. & Brosnan, J.T. (2004) Amino acid metabolism in the Zucker diabetic fatty rat: effects of insulin resistance and of type 2 diabetes. *Can J Physiol Pharmacol*. [Online] 82, 506–514. Available from: doi:10.1139/y04-067.

Wijeyesekera, A., Clarke, P.A., Bictash, M., Brown, I.J., et al. (2012) Quantitative UPLC-MS/MS analysis of the gut microbial co-metabolites phenylacetylglutamine, 4-cresyl sulphate and hippurate in human urine: INTERMAP Study. *Anal Methods*. [Online] 4, 65–72. Available from: doi:10.1039/C1AY05427A.

Wilson, I.D. & Nicholson, J.K. (2009) The role of gut microbiota in drug response. *Curr Pharm Des*. [Online] 15 (13), 1519–1523. Available from: doi:10.2174/138161209788168173.

Wishart, D.S. (2008) Quantitative metabolomics using NMR. *TrAC - Trends in Analytical Chemistry*. [Online] 27 (3), 228–237. Available from: doi:10.1016/j.trac.2007.12.001.

Wishart, D.S., Feunang, Y.D., Marcu, A., Guo, A.C., et al. (2018) HMDB 4.0: The human metabolome database for 2018. *Nucleic Acids Research*. [Online] 46 (D1), D608–D617. Available from: doi:10.1093/nar/gkx1089.

World Health Organization (2014) Constitution of the world health organization. *Basic Documents*. [Online]. (Forty-eighth edition) pp.1–19. Available from: doi:12571729.

Worley, B. & Powers, R. (2012) Multivariate Analysis in Metabolomics. *Current Metabolomics*. [Online] 1 (1), 92–107. Available from: doi:10.2174/2213235X11301010092.

Wu, G.D., Chen, J., Hoffmann, C., Bittinger, K., et al. (2011) Linking long-term dietary patterns with gut microbial enterotypes. *Science*. [Online] 334 (6052), 105–108. Available from: doi:10.1126/science.1208344.

Wu, Q., Li, J. V, Seyfried, F., le Roux, C.W., et al. (2015) Metabolic phenotype-microRNA data fusion analysis of the systemic consequences of Roux-en-Y gastric bypass surgery. *Int J Obes (Lond)*. [Online] 39, 1126–1134. Available from: doi:10.1038/ijo.2015.33.

Yagi, T., Kishore, G.M. & Snell, E.E. (1983) The bacterial oxidation of vitamin B6. 4-Pyridoxic acid dehydrogenase: a membrane-bound enzyme from Pseudomonas MA-1. *Journal of Biological Chemistry*. 258 (15), 9419–9425.

Yano, J.M., Yu, K., Donaldson, G.P., Shastri, G.G., et al. (2015) Indigenous bacteria from the gut microbiota regulate host serotonin biosynthesis. *Cell*. [Online] 161 (2), 264–276. Available from: doi:10.1016/j.cell.2015.02.047.

Yin, P., Lehmann, R. & Xu, G. (2015) Effects of pre-analytical processes on blood samples used in metabolomics studies. *Analytical and Bioanalytical Chemistry*. [Online] 407 (17). Available from: doi:10.1007/s00216-015-8565-x.

Yokoyama, M.T. & Carlson, J.R. (1979) Microbial metabolites of tryptophan in the intestinal tract with special reference to skatole. *Am J Clin Nutr*. [Online] 32, 173–178. Available from: http://www.ncbi.nlm.nih.gov/pubmed/367144.

Yong Chan, E.C., Mal, M. & Pasikanti, K.K. (2012) Metabonomics. In: *Gas Chromatography*. [Online]. pp. 545–562. Available from: doi:10.1016/B978-0-12-385540-4.00024-9.

Yu, H., Guo, Z., Shen, S. & Shan, W. (2016) Effects of taurine on gut microbiota and metabolism in mice. *Amino Acids*. [Online] 48 (7), 1601–1617. Available from: doi:10.1007/s00726-016-2219-y.

Yuan, H., Chen, Y., Zhang, H., Jiang, S., et al. (2006) Improved bioproduction of short-chain fatty acids (SCFAs) from excess sludge under alkaline conditions. *Environmental Science and Technology*. [Online] 40 (6), 2025–2029. Available from: doi:10.1021/es052252b.

Zambell, K.L., Fitch, M.D. & Fleming, S.E. (2003) Acetate and butyrate are the major substrates for de novo lipogenesis in rat colonic epithelial cells. *J Nutr*. [Online] 133, 3509–3515. Available from: http://www.ncbi.nlm.nih.gov/pubmed/14608066.

Zhang, C., Rexrode, K.M., van Dam, R.M., Li, T.Y., et al. (2008a) Abdominal obesity and the risk of all-cause, cardiovascular, and cancer mortality: sixteen years of follow-up in US women. *Circulation*. [Online] 117, 1658–1667. Available from: doi:10.1161/CIRCULATIONAHA.107.739714.

Zhang, H., DiBaise, J.K., Zuccolo, A., Kudrna, D., et al. (2009) Human gut microbiota in obesity and after gastric bypass. *Proceedings of the National Academy of Sciences of the United States of America*. [Online] 106 (7), 2365–2370. Available from:

doi:10.1073/pnas.0812600106.

Zhang, Y., Yang, Y., Shi, W.Y., Cai, J.T., et al. (2008b) [Study of the bacterial community structure of microbiota in bacterial vaginosis using amplified ribosomal DNA restriction analysis]. *Nan Fang Yi Ke Da Xue Xue Bao*. [Online] 28, 1626–1629,1633. Available from: http://www.ncbi.nlm.nih.gov/pubmed/18819883.

Zhao, L., Gao, H., Lian, F., Liu, X., et al. (2011) (1)H-NMR-based metabonomic analysis of metabolic profiling in diabetic nephropathy rats induced by streptozotocin. *Am J Physiol Renal Physiol*. [Online] 300, F947-56. Available from: doi:10.1152/ajprenal.00551.2010.

Zhao, L.C., Zhang, X.D., Liao, S.X., Wang, H.Y., et al. (2010) A metabonomic comparison of urinary changes in Zucker and GK rats. *Journal of Biomedicine and Biotechnology*. [Online] 2010. Available from: doi:10.1155/2010/431894.

Appendix I

Published paper 1:

Systemic Characterization of an Obese Phenotype in the Zucker Rat Model Defining Metabolic Axes of Energy Metabolism and Host−Microbial Interactions

Jutarop Phetcharaburanin, Hannah Lees, Julian R. Marchesi, Jeremy K. Nicholson, Elaine Holmes, Florian Seyfried, and Jia V. Li. *Journal of Proteome Research* 2016 *15* (6), 1897-1906 DOI: 10.1021/acs.jproteome.6b00090

Appendix II

Published paper 2:

Optimized Sample Handling Strategy for Metabolic Profiling of Human Feces

Jasmine Gratton, Jutarop Phetcharaburanin, Benjamin H. Mullish, Horace R. T. Williams, Mark Thursz, Jeremy K. Nicholson, Elaine Holmes, Julian R. Marchesi, and Jia V. Li.

Analytical Chemistry **2016** *88* (9), 4661-4668 DOI: 10.1021/acs.analchem.5b04159

Appendix III

Under peer-review manuscript 1 (manuscript not included):

Phenotyping change in appetite regulation and body composition following equivalent weight loss induced by low-calorie diet and Roux-en-Y gastric bypass, a preliminary randomised controlled trial

Jeanne H Bottin, Elizabeth L Thomas, Julie A Fitzpatrick, Jia V Li, Jutarop Phetcharaburanin, Elaine Holmes, Bolanle Balogun, Krishna Moorthy, Paul R Bech, Mohammed A Ghatei5, Gareth A Wallis, Jimmy D Bell, Anthony R Leeds, Gary S Frost.

Submitted to International Journal of Obesity